Autonomous Fluid Flow on Supramolecular Interfaces: A Step towards Powerless Microfluidic Device

Mujeeb Alam

A thesis submitted for the partial fulfilment of the
Degree of Doctor of Philosophy

Institute of Nano Science and Technology
Knowledge City, Sector 81, SAS Nagar 140306, Punjab, India.

Indian Institute of Science Education and Research Mohali
Knowledge City, Sector 81, SAS Nagar, Manauli PO, Mohali 140306, Punjab, India.

October 2022

Dedicated to

my beloved family and

teachers

Declaration

The work presented in this thesis has been carried out by me under the guidance of Dr. Debabrata Patra at the Institute of Nano Science and Technology (INST), Mohali. This work has not been submitted in part or in full for a degree, a diploma, or a fellowship to any other university or institute. Whenever contributions of others are involved, every effort is made to indicate this clearly, with due acknowledgement of collaborative research and discussions. This thesis is a bonafide record of original work done by me and all sources listed within have been detailed in the bibliography.

Mujeeb Alam

In my capacity as the supervisor of the candidate's thesis work, I certify that the above statements by the candidate are true to the best of my knowledge.

Prof. Debabrata Patra
Scientist F
Institute of Nano Science and Technology, Mohali

Acknowledgements

First of all, I bow in reverence to ***ALLAH****,* ***The AL ALEEM****.* ***The Almighty****,* ***the Most Beneficent and the Merciful****, creator of the universe for providing enough patience, courage, and zeal that enabled me to accomplish my Ph.D. thesis work.*

The work presented in this thesis would not have been possible without the support and guidance that I received from many people. Towards the submission of this work, I would take this opportunity to extend my sincere gratitude and appreciation to all those who made this Ph.D. thesis possible.

Foremost, I wholeheartedly thank my supervisor, ***Prof. Debabrata Patra****, Senior Scientist, Institute of Nano Science and Technology, Mohali, Punjab, India. A man with a passion for science with a "never say die" mindset. His strong academic and research expertise, as well as his genuine and honest interest in my work, assisted me in developing a clear vision of the study that would be conducted for my thesis. Discussions with him assisted me in overcoming obstacles in my profession and establishing the zeal for the never-ending pursuit of knowledge. His constant supervision in developing a scientific attitude during my Ph.D. studies at INST is beyond words. I consider myself lucky to be his second Ph.D. student because the vast knowledge I gained from him throughout my stay will shape my future endeavours. His advice, incredible support, and inspiration helped me throughout the research and writing of this thesis. I take this opportunity to express my heartfelt thanks to him for being my Ph.D. supervisor.*

I would like to thank the INST for providing a very hospitable environment, infrastructure facility and resources. Here, I found not only a dynamic research environment to accomplish my research work, but also good people.

I highly acknowledge my doctoral committee members, ***Prof. Asish Pal*** *and* ***Prof. Prakash P. Neelakandan****, for their valuable suggestions for improving my research work and their continuous support.*

I am thankful to all the Directors of INST (the founder director, the ex-officiating director, and the present director), and the esteemed Faculty of INST for the guidance and affectionate conversation during my tenure. I want to express my deepest gratitude to ***Dr. Sangeeta Roy****, who has always motivated me during this course of time.*

I wish to acknowledge the research fellowship provided by the Department of Science and Technology, India, and INST Mohali, which makes it possible for me to carry out related research activities and finish this thesis.

I would also like to extend my gratitude to ***Prof. Naveen Tiwari****, Indian Institute of Technology, Kanpur, India for providing us theoretical support.*

I am grateful to the INST family for providing me with a safe working environment. Thanks to the staff members for assisting us in obtaining necessary logistics as soon as possible. I also want to thank the non-administrative staff who have always been willing to help us. I would also want to thank the DST, Government of India, for giving me with a fellowship for my Ph.D. period. I would also like to thank IISER Mohali and CIAB Mohali for providing the required infrastructure during this time.

I am lucky enough to have worked with amazing people in our lab. I would like to use this opportunity to thank all of my lab members: ***Dr. Rohit****,* ***Arshdeep****,* ***Chinmayee, Dr. Rekha, Devender, Reek, Anvi, Mohit*** *who have always supported and motivated me that helped me to explore myself. I would also like to thank our intern students:* ***Vighnesh, Ayan, Sanjana, Sudip*** *with whom I have wonderful memories during my tenure.*

Friends deserve special attention since without their encouragement and support, this little piece of work would not have been completed. My deepest gratitude to ***Dr. Safdar, Aakriti, Rimple, Gurpreet, Tanmay*** *for their continuous help and support. My heartiest regards go to* ***Vianni, Ankush, Gaurav, Avinash, Shikha, Manju, Kuljeet, Khushbu.*** *My special Thanks to* ***Rizwan, Ariz, Aiman, Imran, Anas, Shamik, Dr. Zaidi, Dr. Vipul, Dr. Akmal*** *for their moral support and encouragement. I'm also grateful to the wonderful people at INST who deserve to be acknowledged. The list is endless, but mentioning a few are* ***Dr. Harsimran, Dr. Ashmeet, Dr. Pooja, Dr. Vijay, Chirag, Sourav, Annu, Jyoti, Hemant, Prodipto, Krishna, Venu, Dr. Nandan, Dr. Ravi, Dr. Pushpendra, Dr. Jijo, Dr. Neha, Arpana, Mithiliesh,***

Neethu, Zinnia, Hari, Varun*. Special regards for my brother's* ***Dr. Bilal, Dr. Naimat, Dr. Anas, Dr. Khalid, Dr. Arif, Dr. Selim, Dr. Zubair, Dr. Riyaj, Dr. Rejaul, Dr. Atikur, Nadim, Raihan, Naushad, Farhan, Kashif, Aaqib, Aneesh, Shumile, Afshan, Rose, Ayyub, Muhammad, Saad*** *for their unconditional care and support.*

Now I would like to write about the people who are most important in my life: ***my family****. It was only because of their love and support that I was able to get here, and it has given me enormous confidence and bravery to never give up in life. My profound thanks go to my* ***parents*** *and* ***grandparents*** *for believing in me and providing the environment so that I can achieve my goals. Their patience and sacrifice will be an inspiration to me for the rest of my life. My father's beliefs about being honest, sincere, and disciplined in one's job have always been a guiding force in my life. As taught by my mother, love and respect for others have allowed me to receive the same from others. They have always made certain that I got the greatest possible prospect at every stage. My family always went out of their way to make me happy and raise my morale whenever I was down or feeling down so that I could work properly.*

At last, I again bow in reverence to ***ALLAH*** *and his most beloved* ***Prophet*** *(PBUH) for giving me this life, full of blessings and knowledge. I pray to* ***ALLAH, "The AR RASHEED"*** *to keep guiding and enriching me with knowledge so that I can dedicate my life to the cause of humanity.*

Mujeeb Alam

ABBREVIATIONS

α-/β-/γ-CD	α-/β-/γ- Cyclodextrin
P[5]A	Pillar[5]arene
P[6]A	Pillar[6]arene
CT	Charge transfer
LbL	Layer-by-layer
L/D-Trp	L-/D-Tryptophan
o-/p-NP	o-/p- Nitrophenol
PAA	Polyacrylic acid
PEI	Polyethylenimine
PEI-β-CD	β-Cyclodextrin grafted polyethylenimine
p-TsCl	para-Toluenesulfonyl chloride
AdA	Adamantylamine hydrochloride
FcA	Ferrocenecarboxylic acid
Ts-O-β-CD	Mono-6-(p-tolyl sulfonyl)-β-CD
BzI	Benzimidazole
PEG	Polyethylene glycol
RhB	Rhodamine B
PDMS	Polydimethylsiloxane
DMSO	Dimethyl sulfoxide
HDMI	Hexamethylene diisocyanate
$BF_3.(OC_2H_5)$	Boron trifluoride diethyl etherate

DS	Degree of substitution
MV	Methyl viologen
BL	Bilayer
M_w	Molecular weight
DBTDL	Dibutylin dilaurate
DMF	Dimethyl formamide
FTIR	Fourier transform infrared spectroscopy
AFM	Atomic force microscopy
NMR	Nuclear magnetic resonance
UV-Vis	Ultra violet-visible spectroscopy
ITC	Isothermal titration calorimetry
CLSM	Confocal laser scanning microscopy

ABSTRACT

Flow control is at the core of a microfluidic device and plays an important role in unit operations. Non-mechanical nano and microfluidic devices that operate without an external power source and can be customized to individual demands define the next generation of smart devices. Due to their promise of combining various features with high throughput and low sample amounts, microfluidic devices have gained substantial attention in both academic and industrial research, particularly for microfluidic applications. We have shown that supramolecular interfaces (such as host functionalized films and gels) were used as scaffolds to devise the pumps which drive fluid flow in the presence of any guest molecule that initiates the "host-guest" molecular recognition. The utilisation of non-covalent interaction-based reactions to construct a self-powered micropump provides specificity, sensitivity, and selectivity while removing a significant barrier in microfluidics: the requirement for external pressure-driven pumps to push fluids through devices. The fluid velocities achieved in these systems are directly proportional to the concentration of the component that triggers "host-guest" molecular recognition.

The micropumps made from these noncovalent building blocks will open up new avenues in designing dynamic systems for applications ranging from single-use diagnostics to microanalysis. However, fluid flow generated from supramolecular interactions has mainly remained unexplored, and further research is needed to have a thorough grasp of the fundamental principles of actuation and the parameters that determine the output of the micropump, as well as experimental analysis of some of their possible applications. This work highlights all of the studies conducted with self-powered micropumps, from the invention of the micropump design to the efforts made in understanding the "host-guest" based pump concept as a whole. Self-powered supramolecular micropumps could potentially provide a solution for a powerless microfluidic device where the fluid flow can be manipulated by modulating noncovalent interactions. In our first approach, we attempted to fabricate thin film-based micropumps by depositing β-cyclodextrin ("host") functionalized polymer on a glass slide via LbL assembly. These supramolecular micropumps turned on fluid flow upon the addition of "guest" molecules to the multilayer films. The flow velocity was tuned by the concentration of the "guest" molecules as well as the number of "host" layers inside the multilayer films. The numerical modeling uncovers that the solutal buoyancy originated from "host-guest" complexations is primarily responsible for the fluid flow. In view of potential application in self-powered devices, the micropump was integrated into the microfluidic device to show molecular and colloidal transport over long distances. In the next work, a valveless micropump was designed via dynamic supramolecular interaction between β-cyclodextrin (β-CD) and benzimidazole (BzI). It shows flow reversal in response to the pH change. An L-shaped microchannel was used to demonstrate the flow reversibility over long distances. In another approach, again we have developed thin film-based micropumps by depositing β-cyclodextrin (“host”) functionalized polymer and pillar[5]arene on a glass slide, which can be utilized to recognize isomers of tryptophan and nitrophenol, respectively. When "guest" molecules were added, these supramolecular micropumps activated fluid flow, and the difference in fluid velocity of “guest” molecules was further used for their recognition. Such a device could aid in the development of new recognition techniques and lead to a better understanding of chiral and molecular recognition in biological systems. Finally, we explored the self-sorting behaviour of pillar[n]arenes (pillar[5]arenes and pillar[6]arenes) on a substrate based on a principle of geometrical complementarity by shape using a macroscopic fluid-flow strategy.

Overall, this work demonstrated the designing of a self-powered supramolecular microfluidic device that utilises different supramolecular interfaces to trigger fluid flow. The recognition of different molecules using fluid flow can pave the way for the development of point-of-care devices for the detection of drugs, insecticides, and physiologically relevant compounds.

Table of Contents

Chapter 1: Supramolecular Micropumps as Powerless Microfluidic Devices: An Introduction

1.1 General Overview and Scope of Microfluidic Devices…………………………………………......1

1.2 Motion at a Small Scale……………………………………………………………………………3

1.3 Self-powered Micropumps: Next Generation Device…………………………………………….6

1.4 Introduction of Supramolecular Chemistry……………………………………………………....8

  1.4.1 History of Supramolecular Chemistry…………………………………………………….8

  1.4.2 Supramolecular Chemistry: An Overview……………………………………………......9

1.5 Host-Guest Chemistry………………………………………………………...............................11

1.6 Self-Assembly…………………………………………………………………………………….11

1.7 Supramolecular Interactions……………………………………………………………………...12

  1.7.1 Ionic and dipolar interactions……………………………………………………………....12

  1.7.2 Hydrogen Bonding………………………………………………............................…...13

  1.7.3 π-Interactions…………………………………………………...................................…...14

  1.7.4 van der Waals Interactions……………………………………………………………….....15

  1.7.5 Hydrophobic Effects……………………………………………………………………........16

1.8 Macrocyclic Hosts…………………………………………………………………………………......17

  1.8.1 Chemistry of Cyclodextrins…………………………………………………………………......18

    1.8.1.1 Host-guest properties of β-CDs…………………………………………………….....20

  1.8.2 Chemistry of Pillar[n]arenes…………………………………………………………….....21

    1.8.2.1 Host-guest properties of Pillar[n]arenes………………………..........................22

1.9 Autonomous Fluid Flow on Supramolecular Interfaces using Host-Guest Interactions: Supramolecular Micropumps for Regulating Fluid-Flow…………………………………………….....23

1.10 Dissertation Overview………………………………………………………………………….....26

1.11 References…………………………………………………………………………………………......28

Chapter 2: Polymer Multilayer Films Triggers Autonomous Fluid Flow and Power Microfluidic Devices

2.1 Introduction…………………………………………………………………............................35

2.2 Results and Discussions……………………………………………………………………….....36

  2.2.1 Deposition of Multilayer Film…………………………………………………………….36

2.2.2 Guest-Induced Micropump Study……………………………………………………………38

2.2.3 Pumping Mechanism…………………………………………………………………………39

2.2.4 Effects of Number of BLs and "Guest" Concentration on Fluid Velocity…...........43

2.2.5 Temporal Variations in Pumping……………………………………………………………44

2.2.6 Reusability of Supramolecular Micropump……………………………………………….45

2.2.7 Autonomous Fluid Flow in Microchannels………………………………………………..46

2.3 Conclusions……………………………………………………………………………………….50

2.4 Experimental Section……………………………………………………………………………51

2.4.1 Reagents and Materials……………………………………………………………………51

2.4.2 Characterization…………………………………………………………………..................51

2.4.3 Synthesis of PEI-β-CD…………………………………………………………………….52

2.4.3.1 Synthesis of Mono-6-(p-Tolylsulfonyl)-β-Cyclodextrin (Ts-O-β-CD)………52

2.4.3.2 Synthesis of PEI-β-CD……………………………………………………………54

2.4.4 Synthesis of Ferrocenecarboxylic Acid…………………………………………………..55

2.4.5 Substrate……………………………………………………………………………………….57

2.4.6 Pattern of Multilayer Film and Tracking the Fluid Flow……………………………..57

2.4.7 Fabrication of Microfluidic Device…………………………………………………………57

2.4.8 Isothermal Titration Calorimetry……………………………………………….................58

2.5 References……………………………………………………………………………………….58

Chapter 3: pH Responsive Supramolecular Micropump Regulate Reversal Flow

3.1 Introduction……………………………………………………………………………………….61

3.2 Results and Discussions………………………………………………………………………..62

3.2.1 Guest Induced Micropump Study……………………………………………………………62

3.2.2 Mechanism of Fluid Pumping………………………………………………………………63

3.2.3 pH Responsive Behaviour of Micropump…………………………………………………..64

3.2.4 Effect of Concentration and pH on "Host-Guest" Assembly and Disassembly........65

3.2.5 Temporal Change in Pumping of "Host-Guest" Assembly and Disassembly………67

3.2.6 Flow Reversal in Complicated Microchannel……………………………………………..67

3.3 Conclusions……………………………………………………………………………………….69

3.4 Experimental Section……………………………………………………………………………69

3.4.1 Reagents and Materials……………………………………………………………………69

3.4.2 Characterization……………………………………………………………………………69

3.4.3 Synthesis of β-cyclodextrin-Polyethylene Glycol (β-CD-PEG) Gel………………….69

3.4.4 Isothermal Titration Calorimetry……………………………………………………………71
3.4.5 UV-Vis Study of BzI soaked β-CD gel………………………………………………………72
3.5 References…………………………………………………………………………………….72

Chapter 4: Macroscopic Discrimination of Isomers on Supramolecular Interfaces by Autonomous Fluid Flow

4.1 Introduction……………………………………………………………………………………75
4.2 Results and discussions……………………………………………………………………….76
4.2.1 Fabrication of Supramolecular Interface and Discrimination of Chiral Isomers…76
4.2.2 Investigation of "Host-Guest" Complexation…………………………………………..79
4.2.3 Competitive Binding Effects on Pumping Velocity……………………………………81
4.2.4 Theoretical Investigation of Density Driven Flow……………………………………..82
4.2.5. Temporal Changes in Pumping…………………………………………………………..85
4.2.6. Recognition of Nitrophenol Isomers by Pillar[5]arene Multilayer Films………..85
4.2.7. Investigation of "Host-Guest" Complexation…………………………………………87
4.3 Conclusions…………………………………………………………………………………….88
4.4 Experimental Section………………………………………………………………………….88
4.4.1 Reagents and Materials………………………………………………………………….88
4.4.2 Characterization……………………………………………………………………………89
4.4.3 Synthesis of PEI-β-CD…………………………………………………………………….89
4.4.3.1 Synthesis of Mono-6-(p-Tolylsulfonyl)-β-Cyclodextrin (Ts-O-β-CD)………89
4.4.3.2 Synthesis of PEI-β-CD…………………………………………………………….90
4.4.4 Synthesis of Cationic pillar[5]arene (CP[5]A)…………………………………………92
4.4.4.1 Synthesis of 1……………………………………………………………………….92
4.4.4.2 Synthesis of 2……………………………………………………………………….92
4.4.4.3 Synthesis of 3……………………………………………………………………….93
4.4.5 Substrate…………………………………………………………………………………….93
4.4.6 Multilayer Film Pattern and Tracking Fluid Flow……………………………………..94
4.4.7 Fabrication of Multilayer Film……………………………………………………………95
4.4.8 Isothermal Titration Calorimetry (ITC)…………………………………………………95
4.5 References……………………………………………………………………………………..96

Chapter 5: Cavity Shape Dependent Self-Sorting of Pillar[n]arenes via Macroscopic Fluid Flow

5.1 Introduction……………………………………………………………………………………99
5.2 Results and Discussions………………………………………………………………………100
  5.2.1 Fabrication of Multilayer Films……………………………………………………………100
  5.2.2 Self-Sorting on a Surface (Fluid-Pumping Study)………………………………………101
  5.2.3 Effects of Substrate Concentration on Fluid Velocity……………………………………103
  5.2.4 Self-Sorting Analysis by UV-Vis Absorption Spectra……………………………………105
  5.2.5 Effect of Adding Guest Molecule on Fluid Pumping………………………………………107
  5.2.6 Self-Sorting in Microchannel…………………………………………………………………108
5.3 Conclusions…………………………………………………………………………………………109
5.4 Experimental Section……………………………………………………………………………109
  5.4.1 Reagents and Materials……………………………………………………………………109
  5.4.2 Characterization……………………………………………………………………………110
  5.4.3 Synthesis of Pillar[n]arenes………………………………………………………………110
    5.4.3.1 Synthesis of Cationic Pillar[5]arene (CP[5]A)…………………………………………110
      5.4.3.1.1 Synthesis of 1……………………………………………………………………110
      5.4.3.1.2 Synthesis of 2……………………………………………………………………111
      5.4.3.1.3 Synthesis of 3……………………………………………………………………111
    5.4.3.2 Synthesis of Cationic Pillar[6]arene (CP[6]A)…………………………………………112
      5.4.3.2.1 Synthesis of 4……………………………………………………………………112
      5.4.3.2.2 Synthesis of 5……………………………………………………………………112
    5.4.3.3 Synthesis of Anionic Pillar[5]arene (AP[5]A)…………………………………………113
      5.4.3.3.1 Synthesis of 6……………………………………………………………………113
      5.4.3.3.2 Synthesis of 7……………………………………………………………………114
      5.4.3.3.3 Synthesis of 8……………………………………………………………………114
    5.4.3.4 Synthesis of Anionic Pillar[6]arene (AP[6]A)…………………………………………115
      5.4.3.4.1 Synthesis of 9……………………………………………………………………115
      5.4.3.4.2 Synthesis of 10…………………………………………………………………115
  5.4.4 Substrate……………………………………………………………………………………116
  5.4.5 Multilayer Film Pattern and Fluid Flow Tracking…………………………………………116
5.5 References…………………………………………………………………………………………117

List of Figures

Chapter 1: Supramolecular Micropumps as Powerless Microfluidic Devices: An Introduction

Figure 1.1: *Schematic of Au/Pt nanowires and the reactions leading to self-electrophoresis………………………………………………………………………………………….4*

Figure 1.2: *Schematic of Ag/Au micropumps and the reactions involved in their pumping mechanism…………………………………………………………………………………………….5*

Figure 1.3: *Schematic concept of molecular, supramolecular and to organised assemblies……………………………………………………………………………………………….10*

Figure 1.4: *Schematic concept of the "host-guest" complexation from the molecular to the supramolecular scale…………………………………………………………………………………….11*

Figure 1.5: *A simple example of self-assembly: the DNA double-helix……………………….12*

Figure 1.6: *Examples of dipole and ionic interactions………………………………………..…13*

Figure 1.7: *A visual representation of H-bonding with DNA base pairs………………………14*

Figure 1.8: *The two types of π- interactions: (a) face-to-face, (b) edge-to-face………………15*

Figure 1.9: *Top and (b) side views of the layered structure of graphite, held together by face-to-face π-interactions………………………………………………………………………………….15*

Figure 1.10: *The enthalpic hydrophobic effect is caused by the expulsion of water molecules from a hydrophobic cavity…………………………………………………………………………………16*

Figure 1.11: *The entropic hydrophobic effect is caused by two organic molecules forming a hole in an aqueous phase - one hole is more stable than two………………………………………17*

Figure 1.12: *Macrocyclic compounds- (a) crown ether, (b) calixarene, (c) porphyrin, (d) cucurbituril, (e) pillararene and (f) cyclodextrin…………………………………………………….18*

Figure 1.13: *Chemical structure and molecular shape of cyclodextrins……………………….20*

Figure 1.14: *Chemical structure and molecular shape of pillar[n]arenes…………………….21*

Figure 1.15: *Examples of supramolecular interfaces……………………………………………….23*

Figure 1.16: *Schematic of multifunctional interface responding under external stimuli…….24*

Figure 1.17: *Schematic of layer-by-layer assembly process for fabricating multilayer film…….25*

Figure 1.18: *Dissertation Overview…………………………………………………………………...28*

Chapter 2: Polymer Multilayer Films Triggers Autonomous Fluid Flow and Power Microfluidic Devices

Figure 2.1: *Schematic of layer layer (LbL) assembly using PAA and PEI-β-CD polymer pairs. (b) Thickness profile of polymer multilayer film grown on silicon wafer………………36*

Figure 2.2: *Thickness measurement using AFM (a) 1 BL (b) 2 BLs (c) 4 BLs (d) 6 BLs, and (e) 8 BLs…………………………………………………………………………………………37*

Figure 2.3. Tracer particles trajectories: *Directional flow in presence of (a) AdA, (b) FcA, and no flow in (c) and (d)………………………………………………………………………….....38*

Figure 2.4: *Schematic of fluid pumping as a result of "host-guest" complex formation…….39*

Figure 2.5: *Isothermal titration calorimetry (ITC) isotherm of (a) 1-AdA (5 mM) with b-CD (100 mM) and (b) FcA (20 mM) with b-CD (1 mM) at 25 °C………………………………………40*

Figure 2.6: *(a) Domain, and (b) Mesh used in the numerical study……………………………42*

Figure 2.7: *(a). Velocity contour and streamlines for 1mM AdA at t=1 min.* $k_r = 9x10^{-08}s^{-1}$, $\gamma = 4x0^{-03}s^{-1}$, *(b). Velocity contour and streamlines for 1mM AdA at t=9 min.* $k_r = 9x10^{-08}s^{-1}$, $\gamma = 4x10^{-03}s^{-1}$*…………………………………………………………………………………………….....43*

Figure 2.8: *Tracer velocity with (a) varying number of BLs for AdA (1 mM) and FcA (1 mM), and (b) varying concentration of AdA@2BL film and FcA@2BL film…………………………44*

Figure 2.9: *The temporal variation of fluid pumping in case of (a) AdA, (b) FcA at 1mM, and (c) AdA, (d) FcA at 10mM…………………………………………………………………………....45*

Figure 2.10: *The demonstration of reusable micropump in presence of (a) AdA, and (b) FcA…………………………………………………………………………………………………....46*

Figure 2.11: *(a) Schematic representation of a channel to demonstrate dye release over long distances (20.4 mm), (b) variation of dye release at different distances from the host film with and without the addition of a competitive guest (AdA), (c) schematic representation of a channel to demonstrate the capability of moving particles over long distances (8.4 mm) and around corners, and (d) tracer velocity of moving particles at the different junctions of the L-shaped chamber……………………………………………………………………………………….....47*

Figure 2.12: *CLSM images demonstrating the release of dye after addition of AdA (1mM) showing dye intensity at different points away from the coating (a) 0.3 mm, (b) 4.5 mm, (c) 11 mm, (d) 14 mm, and (e) 17 mm.………………………………………………………………………48*

Figure 2.13: *CLMS images demonstrating the release of dye after addition of aqueous solution without any competitive guest showing dye intensity at different points (a) 0.3 mm, (b) 4.5 mm, (c) 11 mm, (d) 14 mm, and (e) 17 mm….………………………………………………….49*

Figure 2.14: *Synthesis of cyclodextrin functionalized polyethyleneimine (PEI-β-CD)………52*

Figure 2.15: *400 MHz 1H NMR spectra of (a) Tosyl-β-CD in DMSO-d_6……………….......53*

Figure 2.16. *Electrospray ionization mass spectrum of Tosyl- β-CD………………………….....53*

Figure 2.17: *400 MHz ^{1}H NMR spectra of PEI-β-CD in D_2O…………………………………......54*

Figure 2.18: *FTIR spectra of β-CD, PEI, and β -CD-PEI………………………………………….55*

Figure 2.19: *Synthesis of ferrocenecarboxylic acid………………………………………………55*

Figure 2.20: *^{1}H NMR spectra of 2-chlorobenzoyl in $CDCl_3$……………………………………….56*

Figure 2.21: *400MHz ^{1}H NMR spectra of ferrocenecarboxylic acid in DMSO-d_6…………......56*

Chapter 3: pH Responsive Supramolecular Micropump Regulate Reversal Flow

Figure 3.1: *Schematic of fluid flow reversal caused by the ''host–guest'' assembly and disassembly between b-CD and BzI…………………………………………………………………62*

Figure 3.2. *Tracer particles trajectories: directional flow as a result of "host-guest" recognition between BzI and β-CD, and (b) no flow in the presence of water……………......63*

Figure 3.3: *Isothermal Titration Calorimetry (ITC) isotherm of BzI (10mM) with β-CD (200 µM) at 25°C……………………………………………………………………………………….63*

Figure 3.4. *(a) Reverse fluid flow in an upside-down configuration of micropump chamber, and (b) absorption spectra of β-CD-PEG gel pre-assembled with BzI………………………64*

Figure 3.5. *(a) Reverse fluid flow as a result of "host-guest" disassembly, (b) no directional fluid flow in the presence of water (pH<5), and (c) Isothermal Titration Calorimetry (ITC) isotherm of β-CD (150 µM) pre-soaked with BzI (50mM) at 25°C……………………………......65*

Figure 3.6: *Absorption spectra of β-CD-PEG gel pre-assembled with Bzi on addition of acidic water at (a) pH3, (b) pH4, (c) pH5, and (d) with time at pH3, pH4, pH5……………......66*

Figure 3.7: *(a) Tracer velocity with varying concentrations of Bzi; (b) tracer velocity with varying pH values with the addition of the acidic solution (pH = 6) to the pre-soaked b-CD-PEG/Bzi gel (10 mM)…………………………………………………………………………….66*

Figure 3.8: *(a) The temporal variation of fluid pumping for the addition of BzI (''host–guest'' assembly); and on the addition of an acidic solution (pH<6) to the pre-soaked b-CD-PEG/BzI gel (''host–guest'' disassembly, 10 mM); (b) spatial changes in the fluid pumping velocity after addition of BzI (''host–guest'' assembly) ……………………………………….67*

Figure 3.9: *(a) Schematic representation of a channel to demonstrate the capability of moving particles over long distances (12.2 mm) and around corners; (b) tracer velocity for assembly and disassembly in the L-shaped chamber……………………………………………......69*

Figure 3.10: *(a) End-capping process of PEG with HDMI, (b) Reaction among the end-capped PEG with isocyanate groups and the β-CD, together with an idealized outline of the structure of the gel……………………………………………………………………………………..70*

Figure 3.11: *FTIR Spectra of PEG, β-CD, and a β-CD-PEG gel………………………………71*

Chapter 4: Macroscopic Discrimination of Isomers on Supramolecular Interfaces by Autonomous Fluid Flow

Figure 4.1: *(a) Schematic of layer layer (LbL) assembly using PAA and PEI-β-CD, (b) Thickness profile of the polymer multilayer film grown on a silicon wafer (dry state)………77*

Figure 4.2. *(a) Schematic of fluid pumping as a result of "host-guest" complex formation, (b) Variation of fluid pumping velocity with concentration, (b) directional flow as a result of "host-guest" recognition between (b) L-Trp and β-CD, and (c) D-Trp and β-CD……………78*

Figure 4.3. *No flow on injecting (a) water with PAA/PEI-β-CD film, and (b) Trp with PAA/PEI film. (c) variation of fluid pumping velocity with concentration……………………..78*

Figure 4.4: *Isothermal Titration Calorimetry (ITC) isotherm of (a) L-Trp (20 mM), and (b) D-Trp with β-CD (250µM) at 25 °C………………………………………………………………79*

Figure 4.5. *400 MHz ^{1}HNMR spectra of β-CD with L-Trp. The concentration for each component was 5 mM……………………………………………………………………………………80*

Figure 4.6. *400 MHz ^{1}HNMR spectra of β-CD with D-Trp. The concentration for each component was 5 mM……………………………………………………………………………………80*

Figure 4.7: *(a) Tracer velocity of competitive binding between L-Trp and D-Trp. (b) directional flow on injecting L-Trp, and (c) no flow on injecting D-Trp……………………….81*

Figure 4.8: *(a) Domain, and (b) Mesh used in the numerical study……………………………83*

Figure 4.9: *(a) Velocity contour and streamlines for 40 mM L-Trp at t=1 minute. The arrows indicate the direction of the flow, (b) Velocity contour and streamlines for 40 mM L-Trp at t=11 minutes. The arrows indicate the direction of the flow……………………………………........84*

Figure 4.10: *The temporal variation of fluid pumping in case of (a) L-Trp (1mM), (b) D-Trp (10mM)…………………………………………………………………………………………….85*

Figure 4.11: *(a) Schematic of layer layer (LbL) assembly using PAA and PEI-β-CD……....86*

Figure 4.12. *(a) Tracer particles trajectories: Directional flow for p-NP, (b) no flow for o-NP, and (c) Variation of fluid pumping velocity of isomers of nitrophenol at 1mM…………86*

Figure 13: *400 MHz ^{1}H NMR spectra of (a) p-NP, CP[5]A + p-NP, and CP[5]A. The concentration for each component was 10 mM………......………………………………………87*

Figure 14: *400 MHz ^{1}H NMR spectra of (a) o-NP, CP[5]A + o-NP, and CP[5]A. The concentration for each component was 10 mM.………..………………………………………88*

Figure 4.15: *Synthesis of cyclodextrin functionalized polyethyleneimine (PEI-β-CD)………90*

Figure 4.16: *400 MHz 1H NMR spectra Tosyl-β-CD in DMSO-d_6……………………………..91*

Figure 4.17: *400 MHz 1H NMR spectra Tosyl-β-CD in DMSO-d_6……………………………..91*

Figure 4.18: *Synthesis of cationic Pillar[5]arene (CP[5]A)…………………………………….92*

Figure 4.19: *400 MHz ^{1}H NMR spectra 1 in $CDCl_3$…………………………………………......93*

Figure 4.20: *400 MHz ^{1}H NMR spectra 2 in $CDCl_3$…………………………………………......94*

Figure 4.21: *400 MHz ^{1}H NMR spectra 3 in D_2O……………………………………………......94*

Chapter 5: Cavity Shape Dependent Self-Sorting of Pillar[n]arenes via Macroscopic Fluid Flow

Figure 5.1: *Schematic of layer layer (LbL) assembly using cationic and anionic P[n]As...101*

Figure 5.2: *Schematic of fluid pumping as a result of self-sorting for (a) ionic pillar[5]arene, and (b) ionic pillar[6]arene, (c) directional flow as a result of self-sorting between same shape and oppositely charged pillar[n]arenes, and (d) no flow as a result of no self-sorting between different shape and oppositely charged pillar[n]arenes………………………………..102*

Figure 5.3: *Tracer velocity for (a) $(AP[5]A/CP[5]A)_{5BLs}$, (b) $(CP[5]A/AP[5]A)_{5BLs}$, (C) $(AP[6]A/CP[6]A)_{5BLs}$, and (d) $(CP[5]A/AP[5]A)_{5BLs}$ film in the presence of their corresponding substrates (AP[5]A, CP[5]A, AP[6]A, and CP[6]A)………………………….103*

Figure 5.4: *(a) Tracer velocity with varying concentration of corresponding substrate (a) $(AP[5]A/CP[5]A)_{5BLs}$ with AP[5]A, $(CP[5]A/AP[5]A)_{5.5BLs}$ with CP[5]A, $(AP[6]A/CP[6]A)_{5BLs}$ with AP[6]A, and $(CP[6]A/AP[6]A)_{5.5BLs}$ with CP[6]A……………….104*

Figure 5.5: *Tracer velocity on adding mixture of (AP[5]A+AP[6]A) and (CP[5]A+C[6]A) solution (6mM) to the corresponding multilayer films…………………………………………..105*

Figure 5.6: *UV-vis absorption spectra of the film obtained by consecutive adsorption of (a) AP[5]A and CP[5]A, (b) AP[6]A and CP[6]A (c) cationic and anionic P[5]As (dotted line), and (b) cationic and anionic P[6]As (solid line)…………………………………………......106*

Figure 5.7: *UV-vis absorption spectra of the film obtained from the consecutive adsorption of (a) AP[5]A and CP[6]A, and (b) AP[6]A and CP[5]A………………………………………107*

Figure 5.8: *Schematic representation of a channel to demonstrate self-sorting over long distances………………………………………………………………………………………….108*

Figure 5.9: *Synthesis of cationic Pillar[5]arene (CP[5]A)…………………………………...…110*

Figure 5.10: *400 MHz ^{1}H NMR spectra 3 in D_2O………………………………………………….110*

Figure 5.11: *Synthesis of cationic Pillar[6]arene (CP[6]A)…………………………………..112*

Figure 5.12: *400 MHz ^{1}H NMR spectra 5 in D_2O……………………………………………….113*

Figure 5.13: *Synthesis of anionic Pillar[5]arene (CP[5]A)……………………………………113*

Figure 5.14: *400 MHz ^{1}H NMR spectra 8 in DMSO-d_6………………………………….……114*

Figure 5.15: *Synthesis of anionic Pillar[6]arene (AP[6]A)……………………………………115*

Figure 5.16: *400 MHz ^{1}H NMR spectra 10 in DMSO-d_6……………………………………….116*

List of Tables

Table 2.1: *Values of k and γ (effective rate parameters) used in the calculations of various cases of AdA and FcA molecule*……………………………………………………………………......43

Table 4.1: *Values of k and γ (effective rate parameters) used in the calculations of various cases of L-Trp and D-Trp molecule*…………………………………………………………………84

Table 5.1: *Tracer particles velocity at different junctions of microchannel*…………………….109

List of Publications……………………….………………………………………………………119

Workshop and Conferences Attended………………………………………………………………121

Permissions from Journals for reuse of content in Thesis……………………………………......122

Chapter 1

Supramolecular Micropumps as Powerless Microfluidic Devices: An Introduction

1.1 General Overview and Scope of Microfluidic Devices

For decades, we have imagined a world where excellent new technologies contribute to making our everyday lives more accessible (e.g., driverless cars, faster and smaller data processors, smart home appliances and houses), while also working to improve our quality of life by providing improved health diagnostics, treatments, and preventative measures. While we are well on the way to making advanced technology, equal improvements in the field of single-use diagnosis and microanalysis are more complicated. Scientific efforts in the field of nanotechnology are gradually shifting toward developing technologies/devices that are more effective, less harmful and autonomous, inspired from natural behaviours and processes. One of the driving motivations behind the development of micro/nanofluidics is the scaling down of a complete laboratory operating system on a single chip. The majority of the research has been on encouraging micro- and nanostructures to deform, rotate, and repeatedly move over well-defined molecular-scale distances.[1] The ultimate objective in this field is to create identical characteristics using smaller, more efficient devices. In this context, microfluidics can provide a diverse toolset for designing autonomous lab-on-chip devices for potential applications from industries to the health sector.

Microfluidics is an emerging field of research that deals with the manipulation of small volumes of fluids at the microscale level in small confinements such as microchannels. Flow control is the basis of a microfluidic device and performs an essential part in unit operations.[2] Microfluidic technologies provide a range of useful capabilities, including the possibility to utilize minimal amounts of samples and reagents to perform detections and separations with good precision and sensitivity, as well as low cost, quick analysis times, and small analytical device footprints.[3] Microfluidics also provides new and unique features for controlling molecule concentrations in space and time. It has many applications, including protein crystallisation,[4] separation in mass spectroscopy,[5] biological analysis,[6] microchip cooling[7] and drug delivery.[8] The branch of microfluidics can lead to a major revolution because of the introduction of lab-on-chip devices, which are predicted to bring an upheaval in the world of technology and scientific research.[9,10]

Most microfluidics promising applications and limitations require microscale fluid flows, which differ significantly from macroscale hydrodynamics. For example, in microfluidic environments, the Reynolds number (ratio of inertial forces to viscous forces) is typically very small, indicating that viscous forces predominate at these scales and flows are laminar in nature. Furthermore, as indicated by the Peclet number, diffusion plays a considerably more pivotal role in mass transfer in microfluidic channels. In microfluidics, high surface area-to-volume ratios and considerable surface tension are key barriers that significantly increase hydrodynamic drag.[10,11] These factors invariably result in operational issues regarding how to drive fluid flow in microchannels effectively, conveniently, and controllably. On the other hand, the incorporation of several components in a small chip, presents a major and fundamental obstacle to the generation of lab-on-a-chip devices. Pumps, which drive the fluid flow in such devices, must also be miniaturized. As a result, in constructing nano/micro devices, it is necessary to physically construct a dimensionally efficient device, and understand how to appropriately combine materials and characteristics to make it effective under the specified environmental factors. Innovative designs of micropumping systems that overcome the challenges mentioned above are thus urgently required.

Recent research advancements have not only achieved good management of the issues, as mentioned earlier. Still, they have also presented the prospect of developing microscopic devices that can work without the assistance of an external power source.[12–15] This method has been used to construct chemical and biosensors, drug delivery devices, and cargo transport mechanisms, taking advantage of various mechanisms of motion in these automated systems as an outcome of chemical energy inputs.[16] Supramolecular interfaces can be utilised in these devices to power fluid and particle motion, providing a control mechanism for the system's behaviour in situ. This novel method of powering motion at smaller dimensions opens up unlimited possibilities for constructing self-powered nano/micro- scale devices that require minimum resources, minimal to no energy inputs, and possibly more cost-effective designs. Supramolecular interact moieties were widely used for various applications, including sensing, imaging, the manufacture of hybrid polymers, the activation and deactivation of deoxyribonucleic acid (DNA)-nanoreactors, and nanodevices.[17–20] Considering the specificity of supramolecular interactions, their ability to work in crowded environments and under varying conditions, the broad range of stimuli that may be employed for their activation, and using them to fabricate nano/micro devices appears to be a possible next step.[21–23] Supramolecular interfaces not only function effectively and controllably, but they can also work as micropumps, utilising the energy generated from the surrounding chemical reaction.[24,25] We investigated the autonomous fluid flow on supramolecular interfaces to power microfluidic devices, which can address the limitations of previously developed micro scale devices.

1.2 Motion at a Small Scale

Science is catching up to Hollywood's imagination over five decades later. We have seen in films and television shows like "Fantastic Voyage," "Ant-Man," and "The Magic School Bus" how the benefits of being able to repair, assemble, or disassemble items on a tiny scale are highlighted in a conversational and fun way, without neglecting the problems that it may include. The concept of developing microscopic artificial machines or prototypes capable of performing a task in a precise and regulated manner is not new. Recent advancements in artificial nano/microscale devices may contribute to the Fantastic Voyage concept of repairing, assembling or disassembling things on a small scale. In that case, it will impact how scientific challenges are tackled, as there is a growing interest in understanding processes at a small scale, particularly by imitating those already present in nature.

Motors and machines are so ubiquitous in our lives that it's difficult to fathom a world without them. It is reasonable to assume that machines driven by water, wind, electricity, and fuel played a significant part in the evolution of civilization, allowing humans to live on a scale that would not be conceivable without them. Motors and machines are now found in practically every area of modern technology. On the other hand, biological motors and machines are essential components of every living cell and organism. Chemically driven nanomotors in the cell carry out protein synthesis, DNA replication, ATP generation, cell division, and motility.[26] Despite the fact that designed motors and machines are familiar to humankind and nanomotors are common in biology, and the notions have only recently begun to meet in the construction of synthetic nano- and micromachines.[27] Making operational motors on the nano- and micrometer length scales is difficult, not only because the fabrication of structurally complicated items of this size is challenging but also because of the conventional macroscopic concepts of powering them do not scale down successfully.[28] Since its discovery in 2004, synthetic motors and machines that are propelled by self-generated gradients have sparked a lot of attention and research. Nature has unquestionably taken the lead in terms of regulated processes, arrangement, and motion. Motor proteins like kinesin, myosin, and dynein, for example, move with considerable speed control and directionality across tracks, requiring input from energy-rich components like adenosine triphosphate (ATP) to power activities like cell division, cargo transit inside the cell, and muscle contraction. Flagellar motors, found in many bacteria and sperm cells, are another example of small-scale mobility powered by potential energy by electrochemical gradients.[29] In nature, energy conversion can be employed to regulate other motion-based processes, such as changes in outer hair cell length regulated by prestin, a motor protein newly found in the cochlea that transforms voltage inputs into force.[30] Most active research in the field of nanotechnology is inspired by these sorts of highly regulated systems and mechanisms, especially because of the inherent desire to construct nano and micromachines that behave like their biological counterparts but with greater environmental stability.[31] Among the several artificial motors and machines reported to date, those powered by catalytic processes are the most similar to biological motors and pumps.

In 2004, Paxton et al. provided one of the first examples of self-propelled nanomotors powered by chemical reactions. The system was built on bimetallic nanowires that moved when exposed to hydrogen peroxide (H_2O_2).[32,33] These nanowires were made up of a gold (Au) and a platinum (Pt) component, and their movement was caused by the catalytic decomposition of H_2O_2, with H_2O_2 oxidation at the Pt end and H_2O_2 reduction at the Au end, as shown in Figure 1.1. Because of the ion flow on the surface, the nanowires migrated forward with the Pt end oriented toward the Au end, following the electron flux in the bimetallic structure.[33] The nanowires moved autonomously in solution in response to a local

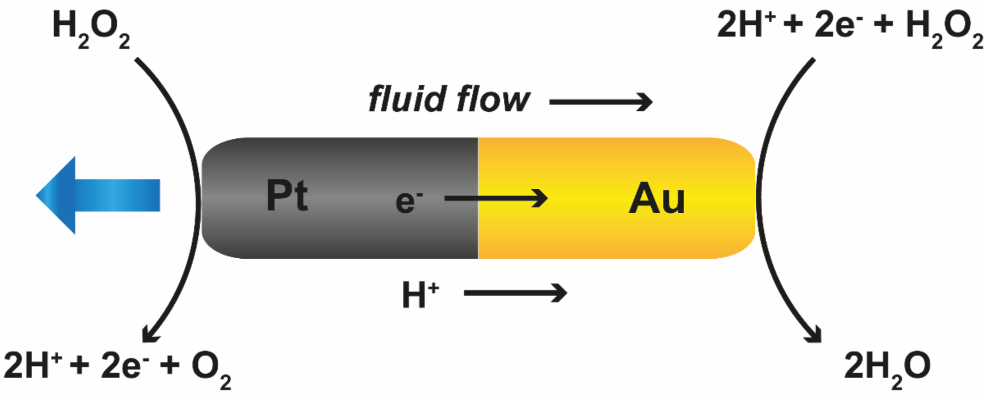

Figure 1.1. Schematic of Au/Pt nanowires and the reactions leading to self-electrophoresis. H_2O_2 is oxidised to produce protons in solution and electrons at the Pt end of the wire. The protons and electrons are subsequently consumed by reducing H_2O_2 on the Au end. The resultant ion flow causes the particle to move relative to the fluid, driving it toward the platinum end in relation to the stationary fluid.

electrochemical gradient formed by the rods itself, which was termed "self-electrophoresis." Making operational motors on the nano- and micrometer length scales is difficult, not only because of the fabricating structurally complicated items of this size is challenging but also due to the conventional macroscopic concepts of powering them do not scale down successfully [34].[34] Since its discovery in 2004, synthetic motors and machines that are propelled by self-generated gradients have sparked a lot of attention and research.

Since then, several new autonomous micro and nanomotor systems have been created,[35] including the construction of bi-metallic micropumps driven by the same operational principle that drives motion in bi-metallic nanowires.[36] In this example, silver (Ag) discs were designed onto Au surfaces to produce the two-step decomposition of H_2O_2, similar to the bi-metallic nanowires, but instead of Pt, Au was utilised as the anode (oxidation electrode) of the reaction, and Ag as the cathode.[36] Kline et al. demonstrated that fluid motion

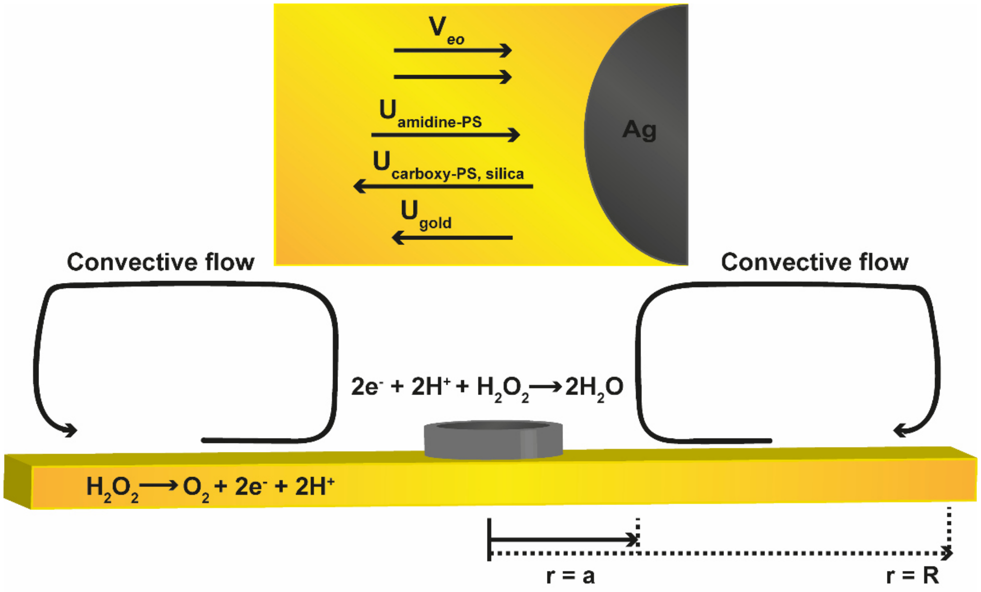

Figure 1.2. Schematic of Ag/Au micropumps and the reactions involved in their pumping mechanism. Protons (H^+) generated by oxidation of H_2O_2 migrate from the anode (gold) to the cathode (silver, center), generating an electroosmotic flow (v_{eo}). This flow creates a convection roll that sweep tracer particles inward along the gold surface. The convection roll extends from r = a (near the silver) to r = R. Positively charged tracer particles (see inset) experience an additional electrophoretic force (due to local electric fields created by the H^+ gradient in solution) towards the direction of the silver patch ($U_{amidine\text{-}PS}$). Negatively charged particles (inset) experience an electrophoretic force in the opposite direction, which results in circular patterns around the silver patches ($U_{carboxy\text{-}PS,\ silica}$). The motion of gold rods was also studied, but as they are less “negative” than the other tracers used, they experience only a small outward electrophoretic force, and are swept inward by the dominant electroosmotic flow, circulating in a tight convection roll near the silver patch.

can be induced by anchoring a catalyst to a surface, owing to the creation of chemical gradients. Convection drives overall fluid movement in the Au/Ag micropumps because a proton gradient along the Au surface sweeps fluid layers in close contact with it towards the Ag discs (inward motion) as shown in Figure 2. Fluid in the upper layers of the closed system will move away from the Ag discs due to fluid continuity (outward motion). Colloidal transport was achieved using a combination of convection and the phoretic motion of charged tracers in bulk in response to local electric fields induced by ion gradients.[36] The ability of these bimetallic micropumps to accomplish fluid motion at tiny scales represents the advent of a new class of non-mechanical micropumps that can function independently and whose fluid output can be manipulated in situ.

1.3 Supramolecular Micropumps: Next Generation Device

Micropumps are devices capable of handling small volumes of fluids at a programmable rate (micrometer/seconds) in small confinements such as microchannels.[37] Pumping, mixing, and transporting fluids on a tiny scale are now required for the microfluidics miniaturization of traditional research equipment.[38] Micropumps offer numerous applications like ink-jet printing, medicine administration and biochemical sensing, fluid conveyance on a single chip, and even remotely driven self-propelled devices that utilize microscale pumps.[27,37,39–42] However, most micropumps require an electrical power supply to function, which adds to the device's complexity and limits its incorporation with lab-on-a-chip systems. Two different approaches for designing micropumps have been developed:

1) Those controlled by external sources (non-autonomous pumps): At the nano and microscale, external fields, particularly electric[43–45] and magnetic fields,[46–49] have been employed to propel motors. In most cases, the external field is generated by a macroscopic source and applies the same forces on all of the motors in the sample at the same time. Because field lines generally govern the trajectories of motors driven by magnetic and electric fields, the motion produced is usually not autonomous. The magnetic motors reported by Dreyfus et al., which employ a random magnetic force to create a whiplike motion of a flagellar tail, are a striking exception.[50] Ibele demonstrated in 2012 that externally delivered ultrasonic energy could cause metal micro-rods to move autonomously.[51] The scattering of acoustic energy in this system causes a local pressure difference along the axis of the rod, resulting in autonomous motion. 2) Pumps that switch on automatically when exposed to a certain chemical signal and do not need to be turned off (autonomous pumps): Nano- and

micromotors moving autonomously can be described by a trajectory that is independent of other motors. Each motor moves as if it has its own notion of where it wants to go. This usually necessitates the motors converting fuel or some form of excitation energy (light, sound, etc.) locally rather than being pushed in a particular direction by an external field, for example, fluid pumping triggered by light through electrochemical reactions.[52] Usually, chemically powered nano- and micromotors are autonomous. Their independence comes from the fact that each motor is a miniature engine capable of converting chemical to mechanical energy.

The high viscosity of fluids dominates at low Reynolds numbers, making fluid pumping at the microscale challenging.[50] External sources, such as electrical,[53] electrochemical,[54] and thermal principles,[55] have previously been shown to be capable of inducing fluid motion. Reactions on the surfaces of microfluidic pumps will provide an elegant method of pumping fluid without using external pumps or sources. For the next generation of smart micro- and nanoscale devices, non-mechanical micropumps that offer precise control over fluid flow without an external power source and can turn on in response to particular analytes in solution are required. Autonomous components, such as chemical actuators and even autonomous microfluidic control based on H_2O_2 decomposition, have also been reported in previous reports.[33,36,56–58] More self-powered chemical micropumps have recently been designed, inspired by ubiquitous biological and chemical pumps such as sodium-potassium pumps on cell membranes. They can autonomously convert chemical energy stored in the surrounding environment into fluid pumping. These chemical pumps are similar to conventional micropumps, which use a pressure gradient or electromagnetic fields, even though they appear to use distinct mechanisms. Chemical micropumps often take advantage of local solute gradients created by chemical reactions to transform chemical energy into a fluid driving force.[16] Self-powered chemical micropumps differ from externally powered micropumps in how they can sense and respond to one or more external stimuli, have simple structures, do not require external control systems, are easy to miniaturize, and can be integrated into microfluidic devices. The benefit of not requiring an electrical source of power is important for pump miniaturization. Hence, these chemical micropumps bring up new and interesting possibilities for controlling flow in microfluidic systems, which shows promise in the future development of lab-on-a-chip.[27,39,40]

Non-mechanical nano/micropumps that can turn on in response to specific analytes in solution and give excellent control over fluid flow in complicated channels without an external power source are required. Hence, these pumps can be adapted to individual demands and represent the next generation of smart micro- and nanoscale devices. Previous studies have reported such autonomous components based on different fuels for e.g., hydrogen peroxide decomposition (H_2O_2).[59] H_2O_2 is a harmful fuel that impedes the practical use of micropumps in the biomedical area while also causing environmental problems. Due to this, the majority of such systems lack biocompatibility, which is essential for the construction of nano/micro devices with a view to potential applications for point-of-care devices. Efforts to build alternative forms of micropumps driven by different fuels, other actuation mechanisms, and using different pump designs are numerous.[59–61] One solution to this problem might be the non-electrolyte density-driven mechanisms developed to power micropumps based on supramolecular interactions. A micropump's ability to induce fluid flow is a distinguishing feature that makes it more attractive for a mass movement in a liquid environment. Furthermore, the solute in a solution has the most significant influence on the pumping velocity of a micropump. As a result, it has the potential to be employed as a motion-based sensing device for analyte detection. Pumping behaviour is important for a micropump, and it is preferable to manipulate it in a controlled manner. Controlled pumping behaviour can encourage the development of more sophisticated micropumps along with the generation of novel functionalities for numerous applications. However, designing and developing a micropump to control the pumping direction has always been complicated and challenging. Many researchers are working on manufacturing systems designed to control fluid direction. The micropumps constructed from the noncovalent building blocks will open up new avenues for developing dynamic systems, and the flow can be controlled remotely by manipulating the noncovalent interactions. Fluid flow resulting from supramolecular interactions has so far mainly remained unexplored in the area of microfluidics, and further research is needed to build a new paradigm while keeping the interacting supramolecular specificity. Therefore, self-powered micropumps based on supramolecular interactions represent an excellent choice for controlling fluid direction.

1.4 Introduction of Supramolecular Chemistry

1.4.1 History of Supramolecular Chemistry

Supramolecular chemistry comes from two features of molecular recognition: enzyme catalysis and non-covalent interactions between molecules. This molecular recognition depends upon three concepts:

1. Emil Fischer discovered in 1894 that binding must be selective as part of his research on enzyme receptor–substrate binding. The guest has a geometric size or shape

complementarity to the receptor or host, which he defined as a lock and key concept of steric fit.[62,63] This concept serves as the basis for molecular recognition, or a host's ability to distinguish between a variety of different guests.

2. Paul Ehrlich expanded on this in 1906 when he found that molecules do not act unless they bind, 'Corpora non agunt nisi fixata,' and so created the idea of a biological receptor.[64,65] The fact that selective binding requires mutual attraction between the host and the guest.
3. This is essentially a generalisation of Alfred Werner's 1893 coordination chemistry theory, in which it stated that noncovalent interactions were the cause of carboxylic acid dimer formation in the gas phase, while Pauling reported hydrogen bonding in 1939.[66]

These three notions originated mostly independently of one another, and it would be many years before the many domains in which they were conceived coalesced to become the highly interdisciplinary area of supramolecular chemistry. Pedersen and Lehn reported on the molecular recognition characteristics of crown ethers and cryptands in 1967, and Cram reported on cavitands in 1973, for which they shared the Nobel Prize in chemistry in 1987. According to them, the chemistry of molecular assemblies and intermolecular bonds has been classified as supramolecular chemistry.[67–69] This is more commonly referred to as "chemistry beyond the molecule."

1.4.2 Supramolecular Chemistry: An Overview

Supramolecular chemistry was originally defined as the non-covalent interaction between a "host" and a "guest" molecule, which highlights the structural and functional relationship between molecular and supramolecular chemistry.[70] Supramolecular chemistry is the phenomenon that occurs in the building of molecules or complexes by combining two or more chemical species, and it was first proposed in the context of biological structures.[71] It can be expanded to include terms like "inclusion phenomena," "host–guest chemistry," and "molecular recognition", collaborations across many fields of research in chemistry, physics, and biology resulted in the strengthening of the supramolecular chemistry idea, which now extends to the study of life at the molecular level.[72] The study of biological concepts such as enzymatic processes, the core dogma of cell transcription and translation of the genetic code, the connection of biomolecules, and signal induction by neurotransmitters all need an understanding of diverse molecular interactions.[64] Modern supramolecular chemistry research includes host-guest systems, molecular devices and machineries, molecular recognition, socalled "self-processes" like self-assembly and self-organisation, and interactions with the development of complex matter and nanochemistry. Developing devices to explore molecular interactions begins with an understanding of ligand binding and substrate, then progresses to supramolecular assemblies, and lastly to organised biomolecules or complexes that make up the device.[72]

Supramolecular chemistry is a broad discipline that draws on many different fields, such as organic and inorganic chemistry, to synthesize the precursors for a supramolecule. To understand the features of supramolecular systems, physical chemistry is used, along with computer modelling, to understand complicated supramolecular behaviour. Understanding supramolecular concepts can contribute to the explanation of many biological molecular interactions in biological chemistry, and a certain level of technical understanding is necessary to employ supramolecular systems in the real world, such as in the creation of nanotechnological devices.[66] Figure 1.3 depicts a schematic of the molecular, supramolecular, and organised assembly concepts.

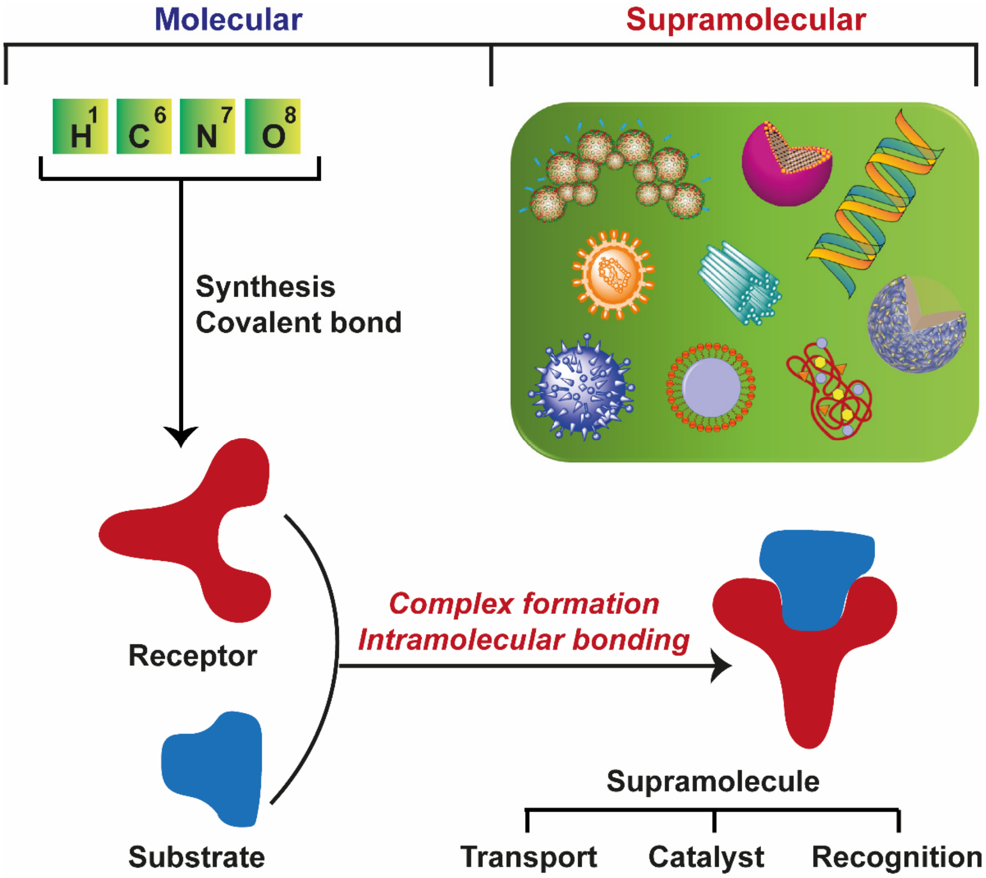

Figure 1.3. Schematic concept of molecular, supramolecular and to organised assemblies.

1.5 "Host-Guest" Chemistry

Complementary interactions are essential for the development of supramolecular structures. These can be accomplished by manipulating the structure of molecules at the molecular level such that the effects are reflected in their form. Therefore, shape complementarities determine supramolecular interactions. The essential intermolecular interactions, such as ion-dipole, dipole-dipole, and hydrogen-bonding, are directionally dependent. Furthermore, the van der Waals and hydrophobic forces that enable supramolecular stability depend on the close proximity of interacting groups. When one molecule is considerably bigger than another and can encapsulate it, the bigger molecule is considered as the "host", while the smaller molecule is considered as the "guest", which is wrapped by the host. As identified by Fischer and Koshland, enzymes are the finest examples of complementarity in nature.[62,66] In this context, a molecule (the "host") binds to another molecule (the "guest") to form a "host–guest" complex or supermolecule. A simplified illustration of the host-guest interaction is depicted in Figure 1.4, in which four binding sites of the host bind to a guest in the centre.

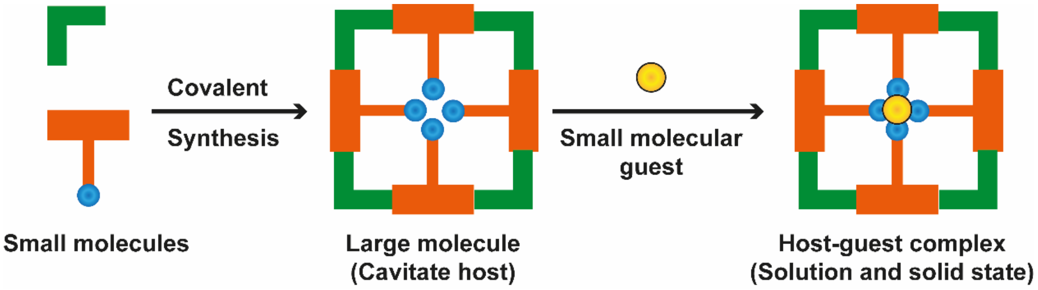

Figure 1.4. Schematic concept of the "host-guest" complexation from the molecular to the supramolecular scale.

1.6 Self-Assembly

Self-assembly is the spontaneous and reversible formation of a bigger, non-covalently bound aggregate from more than one component. This broad definition has expanded over the years to cover many parts of biochemistry and nanotechnology that use the core principles of rigorous chemical self-assembly, although with minor changes. These diverse domains have blended into one another, resulting in the exchange of concepts and terminology, and the development of a broad range of work currently known as "self-assembly".[71] In certain conditions, very simple molecules with complementary functions can connect to produce more complex supramolecular species held together only by non-covalent interactions. The DNA double-helix, depicted in Figure 1.5, is a basic example of self-assembly, where two complementary single strands of DNA are wrapped by hydrogen bonding and - stacking in a self-assembly process.[73] To create a thermodynamically stable DNA complex, the single strands recognise one other. Protein folding and viral assembly are two further biomolecular examples of self-assembly.[71]

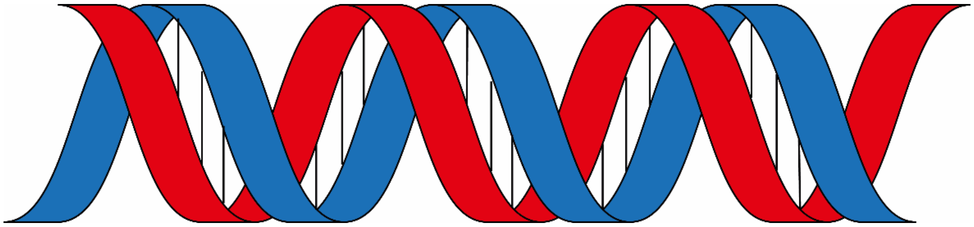

Figure 1.5. A simple example of self-assembly: the DNA double-helix.

1.7 Supramolecular Interactions

In general, non-covalent bonding interactions are the focus of supramolecular chemistry. The term "non-covalent" refers to a broad range of attractive and repulsive forces. Supramolecular chemists try to control and organize the intermolecular interaction pattern defined by Lehn in order to make materials with unique structures and characteristics. Intermolecular bonds occur in a wide range of shapes and sizes that are employed to construct supramolecular species with distinct functions.[66,71]

Non-covalent interactions hold supramolecular complexes together. Non-covalent interactions are much weaker than covalent interactions, ranging from around 150 kJ mol^{-1} to 450 kJ mol^{-1} for single bonds. Non-covalent interactions have dispersion forces ranging from 2 kJ mol^{-1} to 300 kJ mol^{-1} for interionic interactions.[74] However, when these interactions are used cooperatively, a stable supramolecular complex can be formed. Dipole and ionic interactions, inter- and intramolecular interactions, hydrogen bonds, cation-, van der Waals-, and hydrophobic interactions are all examples of non-covalent bonding.

1.7.1 Ionic and Dipolar Interactions

The coulombic attraction between opposite charges categorises ionic and dipolar interactions into three types: (i) ion–ion interactions, (ii) ion–dipole interactions, and (iii) dipole–dipole interactions. The strongest interactions are ion–ion; their energies are comparable to those of stronger covalent bonds. These interactions can happen in either direction because they are non-directional.[28] Ion–dipole and dipole–dipole interactions, on the other hand, feature orientation-dependent elements that necessitate two entities being aligned in the best direction for interactions. Because of the increased rigidity of directional interactions, only mutually complementary entities can form aggregates, while non-directional interactions can stabilise a broad range of molecular pairs. The strength of these directed interactions is governed by the species involved. The species involved determines the strength of these focused interactions. Non-directional interactions stabilise many molecular pairings in ion-dipole and dipole-dipole interactions. Ion–dipole interactions have an energy value of 50–200 kJ mole^{-1}. The energy of dipole–dipole interaction varies between 5 and 50 kJ mol^{-1}. The strength of ion-dipole interactions is more than dipole-dipole interactions because ions have a greater charge density than dipoles.[71] Ionic interactions, particularly in enzyme-substrate interactions, are significant in understanding aspects that influence high binding affinities. Charge–charge interactions and hydrogen-bond rearrangements are important in the folding and unfolding of these biological systems.[66,74]

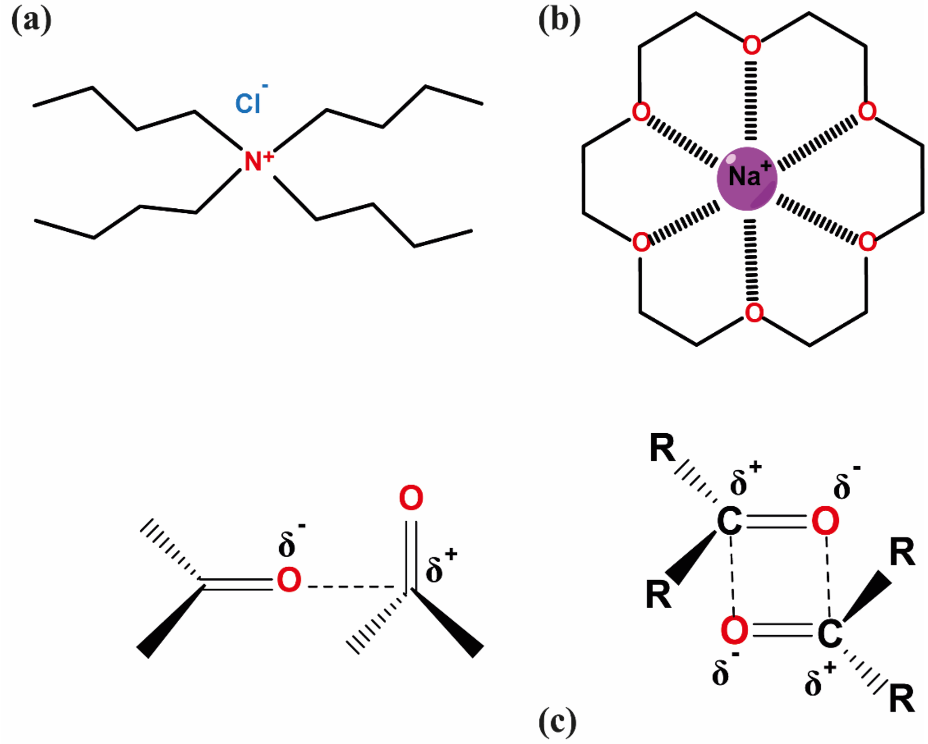

Figure 1. 6. Examples of dipole and ionic interactions.

1.7.2 Hydrogen Bonding

A hydrogen bond is a type of dipole–dipole interaction in which a hydrogen atom bonded to an electronegative atom attracts a dipole on a nearby molecule or functional group. A heteroatomic interaction is generated due to the hydrogen bond formations. In neutral molecules, hydrogen-bond strengths range from 4 to 120 kJ mol-1 and are proportional to the distance between the two interacting atoms, which is usually in the range of 1.2 A^0 to 3.2 A^0. The hydrogen bond is considered as the most important non-covalent interaction in supramolecular architecture design due to its strength and a high degree of directionality. The orientation of hydrogen bonding is important, implying that the strongest hydrogen bonds occur when atoms are aligned at an angle of 180^0 to one another. Hydrogen-bonds can have bond angles ranging from 180° to 90°, depending on how the strong bonds are.

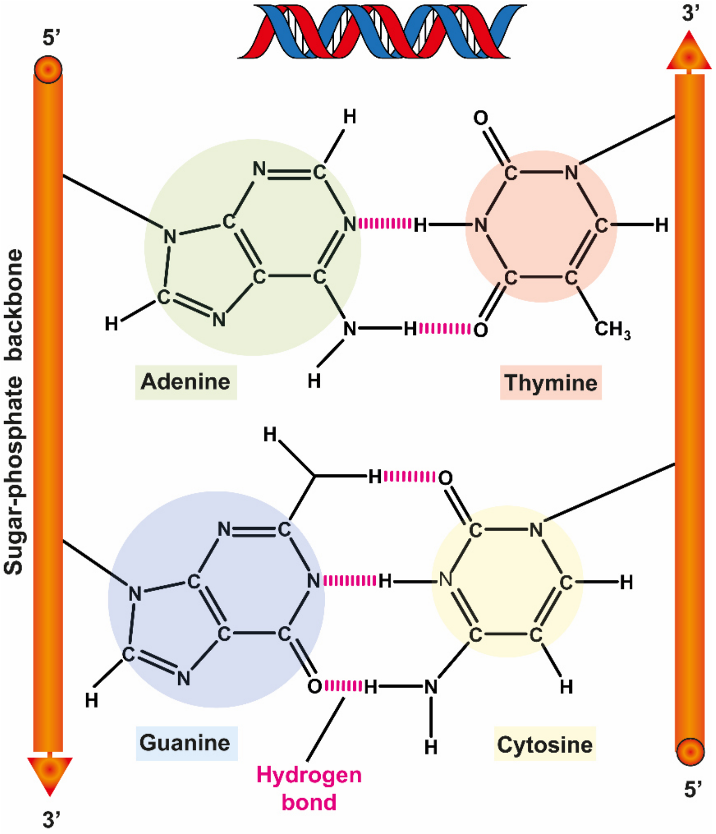

Figure 1.7. A visual representation of H-bonding with DNA base pairs.

1.7.3 π-Interactions

In supramolecular systems, there are two types of π-interactions: (i) cation-π interactions and (ii) π-π interactions. Cation-intermolecular interactions in the aromatic systemare among the strongest non-covalent intermolecular interactions, with values ranging from 60 to 160 kJmol^{-1}. Cation binding studies using cyclophane hosts have been used to study models that explain electrostatic organisation from both sides of the plane of the aromatic ring in cation-interactions. Face-to-face and edge-to-face interactions occur between parallel ring-systems separated by approximately 3.5 A^0, and the interaction occurs between one ring's centre and another's corner (Figure 1.8), and edge-to-face interactions occur when a hydrogen atom from one ring interacts with the core of another ring in a perpendicular orientation (Figure 1.9). These π-π interactions are caused by the attraction between the negatively charged π-electron cloud of one conjugated system and the positively charged sigma-framework of an adjacent molecule.[75]

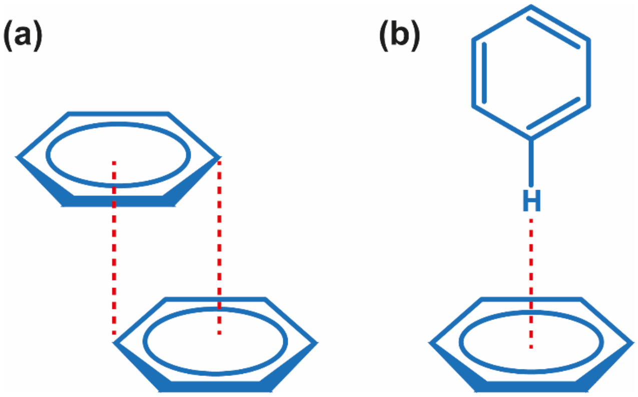

Figure 1.8. The two types of π- interactions: (a) face-to-face, (b) edge-to-face.

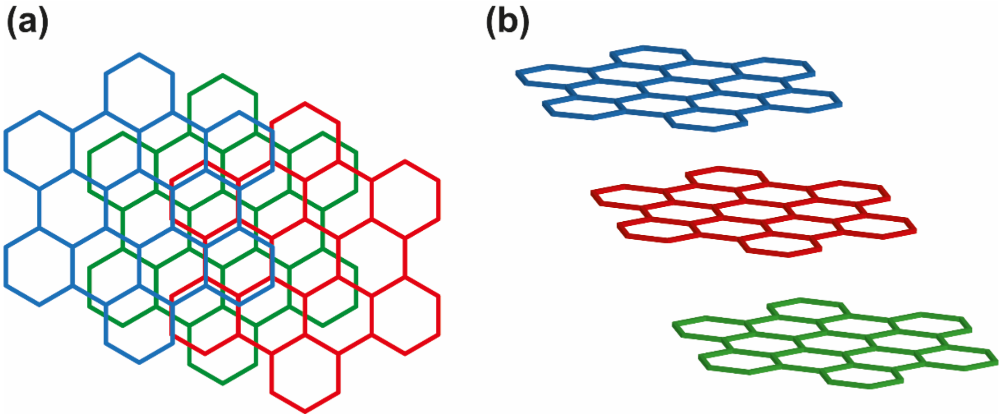

Figure 1.9. (a) Top and (b) side views of the layered structure of graphite, held together by face-to-face π-interactions.

1.7.4 Van der Waals Interactions

Van der Waals interactions are caused by variations in electron distributions between species that are close to one another. Van der Waals interactions are non-directional and result from the non-permanent polarisation of electron clouds.[76] The polarisation effect is caused by an electron cloud adjacent to non-polar atoms or groups. When the van der Waals interacting atoms are close together, their fluctuations may align, resulting in an attractive force. As a result, the force generated is greatly influenced by intermolecular and intramolecular distances. The interaction strength decreases as r_6 increases, where r is the internuclear distance.[74] Van der Waals interactions are the most important interactions between alkyl chains in a number of isomers. When the carbon atom counts are even, the interactions in the chain are disrupted because the alkyl groups in the chains are unable to form a van der Waals interacting environment.[77] Disruption of these interactions generates an odd-even phenomenon in calamitic liquid crystals with long alkyl chain substituents.

1.7.5 Hydrophobic Effects

The removal of non-polar groups from an aqueous solution result in hydrophobic effects. Water molecules bind strongly with each other or other polar groups or molecules, making this arrangement more energetically favourable. Hydrophobic interactions are important in specific supramolecular chemistry, such as the binding of organic molecules in water by cyclophanes and cyclodextrins. Hydrophobic effects have two energy components: an enthalpic hydrophobic effect and an entropic hydrophobic effect.

Enthalpic hydrophobic interactions occur when a guest replaces the water inside a cavity. Water in such systems interacts weakly with the hydrophobic cavity of the host molecule, and the energy in the system is high; therefore this occurs commonly. Once a guest has substituted the water, then the former water guest interacts with the bulk solvent outside the cavity and lowers the energy (Figure 1.10). This process also includes an entropic component, because the formerly ordered water inside the cavity becomes disordered as it leaves. The process's favourability increases as entropy increases. Entropic hydrophobic interactions occur when two or more organic molecules in an aqueous solution assemble to form a supramolecular complex that generates a hole in the water (Figure 1.10). As the total free energy of the system decreases, there is less disruption (one hole in the aqueous phase instead of multiple holes) resulting in an entropic gain.

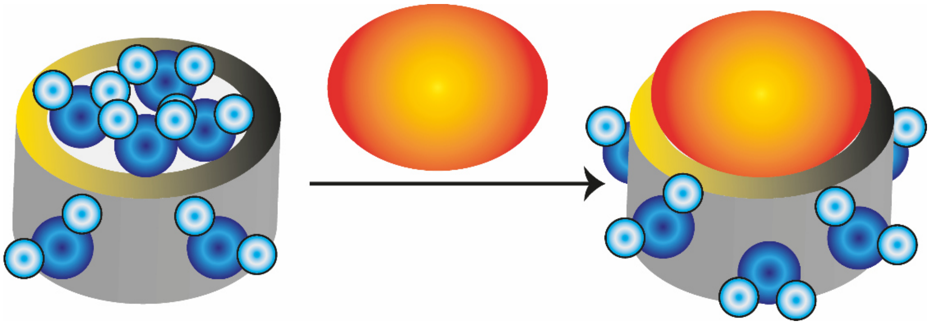

Figure 1.10. The enthalpic hydrophobic effect is caused by the expulsion of water molecules from a hydrophobic cavity.

The enthalpic hydrophobic effect is caused by the stabilisation of water molecules which are forced out of a host cavity when a guest is bound. Because host cavities are frequently hydrophobic, intracavity water does not interact strongly with the host walls and has a large energy content. When released into the bulk solvent, it is stabilised on interactions with other water molecules. The presence of two molecules (usually organic) in solution (host and guest) causes two "holes" in the framework of bulk water, resulting in the entropic hydrophobic effect. When the host molecule combines with a guest molecule to form a complex, the solvent structure is less disrupted, resulting in an entropic gain (as a result of which overall free energy is decreased). In Figure 1.11, the procedure is depicted schematically.

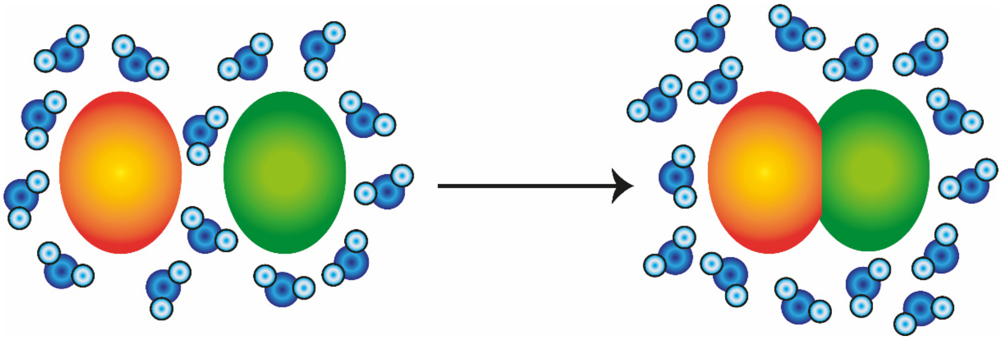

Figure 1.11. The entropic hydrophobic effect is caused by two organic molecules forming a hole in an aqueous phase - one hole is more stable than two.

1.8 Macrocyclic Hosts

Macrocyclic molecules play an important role in supramolecular chemistry because of their specified structure, nanoscale size, and molecular selectivity.[78] As a result, designing and synthesising new macrocyclic host molecules is still a hot topic. Crown ethers,[79–81] cylodextrins,[82] cucurbiturils,[83] calixarenes,[84–86] pillararenes,[87] and their structurally related scaffolds[88–90] are some of the successful examples. Crown ethers, calixarenes, porphyrins, pillararenes, cucurbiturils, and cyclodextrins can be made from simple starting materials such as alkyl ethers, phenols, hydroquinone, pyrroles, glycolurils, or glucose (Figure 1.12).[91] The shapes and characteristics of macrocyclic molecules are different.[92] Many supramolecules have been synthesised and investigated as artificial biomolecules with biomimetic architectures and functionalities using these macrocycles.[93]

Crown ethers, a new macrocyclic with intriguing binding properties, were first discovered by Pederson in 1967,[69] after Dandridge's discovery of phthalocyanines in the 1920s.[94] Pillararene was discovered by Tomoki Ogoshi in 2008.[95] Cucurbiturils were synthesised for the first time in 1905,[96] Pellagrin discovered metacyclophanes in 1899, and Villers discovered cyclodextrins in 1891. Baeyer's study of phenol-formaldehyde chemistry in the 1870s and 1880s led to the discovery of macrocyclic calixarenes, resorcinarenes, and calixpyrroles.[94]

The shape and properties of macrocyclic hosts determine the function of supramolecular compounds. Cyclodextrins, for example, are natural, water-soluble, nontoxic, and commercially accessible and have been employed as supramolecular hosts for biological applications. Both the rims of these macrocycles contain reactive hydroxyl groups. The gel formed by the hydroxyl crosslinking groups that lead to the formation of polyrotaxanes is an example of a supramolecular substance made from cyclodextrins.[97]

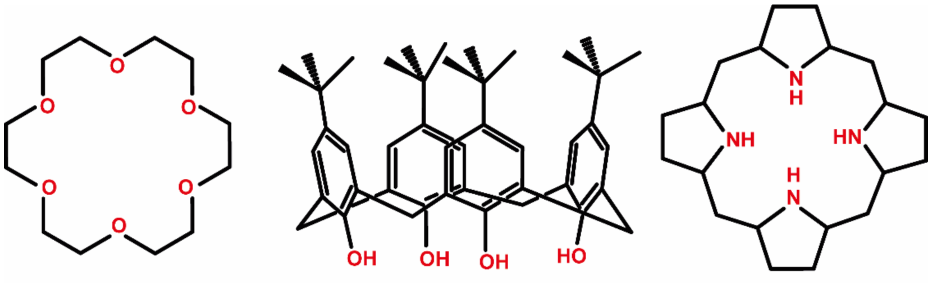

(a) Crown ether (b) Calixarene (c) Porphyrin

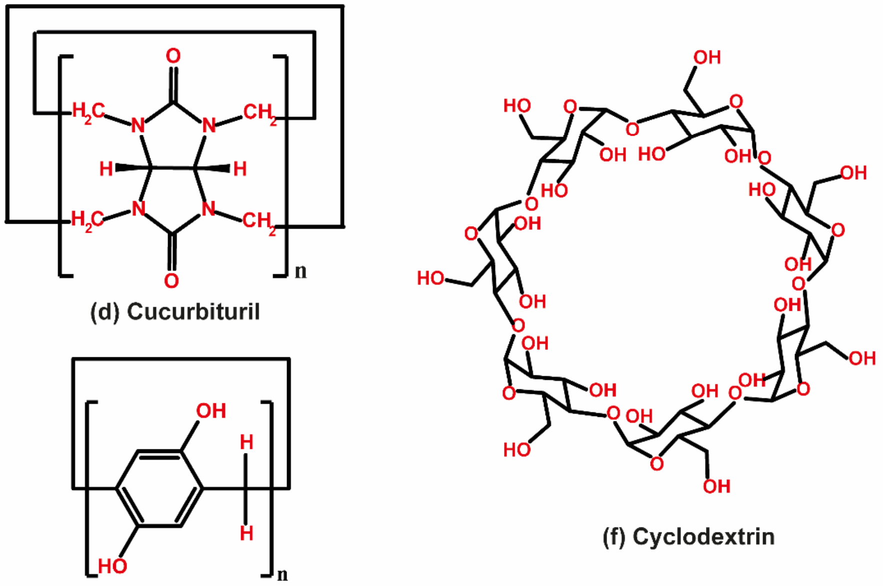

(d) Cucurbituril

(f) Cyclodextrin

(e) Pillararene

Figure 1.12. Macrocyclic compounds- (a) crown ether, (b) calixarene, (c) porphyrin, (d) cucurbituril, (e) pillararene and (f) cyclodextrin**.**

1.8.1 Chemistry of Cyclodextrins

Nowadays, it is impossible to picture a world without cyclodextrins. Inadvertently, everyone employs cyclodextrins (CDs) in their everyday lives as invisible constituents of ordinary food items, as well as in a variety of cosmetic and toiletry products, fabrics, and as enabling excipients in various types of medicinal treatments. Villiers, a French chemist, discovered magnificent crystals in alcohol waste left over from the synthesis of dextrins from starch using an impure bacterial culture in the late 19th century. The chemical composition and several chemical properties of the unknown crystals were determined by Villiers. Schardinger, who identified and described the Bacillus macerans bacterium strain responsible for CD synthesis in the early 20th century, is another notable person in CD science. He also completed a number of CD experiments, earning him the title of "Founder of CD Chemistry".[98]

There have been several studies of macrocyclic molecules, however their synthesis frequently entails multiple steps, low yields, and purifying challenges. The chemistry of cyclodextrins has become a focus of research due to its non-toxic nature, large scale production at very cheapest rate is sustainable, and they have previously shown to be efficient agents in a variety of applications.[98–105] CDs were first used in the pharmaceutical and food industries in the 1980s, even though they had been around for 120 years. They were first synthesised in a very pure form in 1984, significantly lowering prices and contributing positively to their development, particularly that of β-CD (about 10,000 tonnes produced annually at an average bulk price at around 5 USD per kg).[98] CDs are derived from the enzymatic decomposition of starch, among the most essential polysaccharides. Cyclodextrins are cyclic oligosaccharides composed of six to eight D-glucopyranoside units joined together by a 1,4 glycosidic bond [106, 107].[106,107] α-cyclodextrin (α-CD), β-cyclodextrin (β-CD), and γ-cyclodextrin (γ-CD), which have six, seven, and eight glucopyranoside units, respectively, are the three most significant members of the cyclodextrin family.[81,82] α-, β-, and γ-CDs, as well as their higher homologues, are truncated cone-shaped molecules with a 7.9-depth hollow tapering cavity. Most commonly used cyclodextrins have top and bottom cavity dimensions of 4.7 and 5.3 A^0 for α-cyclodextrin, 6.0 and 6.5 A^0 for β-CD, and 7.5 and 8.3 A^0 for γ-cyclodextrin (Figure 1.13).[106–108]

β-CD possesses various advantages over other macrocyclic hosts, including the availability and cost of production, the flexibility to be functionalized with desired functional groups to increase its water solubility using inexpensive chemicals, easy recrystallization, and high yields.[109] β-CDs have two distinct faces, referred to as the primary and secondary faces, similar to the upper and lower rims of calixarenes. The primary hydroxyl groups are located on the primary face, which is the narrow end of the torus. The -CH_2OH groups are on the wider secondary face. The six-membered D-glucopyranoside rings are connected edge to edge, with all of their faces directed inwards toward a central hydrophobic cavity. It is well-known appealing host molecules that can encapsulate a variety of organic guest molecule in its hydrophobic cavity by supramolecular assembly.

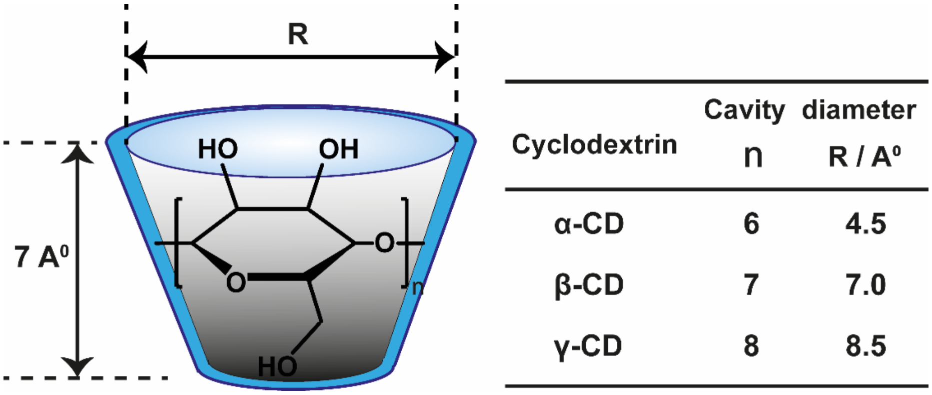

Cyclodextrin	Cavity n	diameter R / A⁰
α-CD	6	4.5
β-CD	7	7.0
γ-CD	8	8.5

Figure 1.13. Chemical structure and molecular shape of cyclodextrins.

1.8.1.1 Host-Guest Properties of β-CDs

β-CD is considered as a promising candidate for studying host-guest interactions because of its well-defined core cavity.[110] The exceptional encapsulation properties result in a "host-guest" interaction that can change and improve the physical, chemical, and/or biological aspects of the guest molecule. The most likely mechanism of binding is for the less polar portion of the guest molecule to be inserted into the cavity, while the more polar and often charged part of the guest is exposed to the bulk solvent just outside the cavity's wider opening. Inclusion complexation of guest molecules by β-CD in aqueous solutions causes a significant rearrangement and expulsion of the water molecules that were previously solvated to both the β-CD and the guest molecules, in addition to the releasing of water molecules from the cavity into the bulk water. Although van der Waals and hydrophobic interactions are thought to be the most prominent factors in binding, hydrogen bonding and steric effects also play an essential role.[106,107,111,112]

Complexation processes involving β-CD are essential in the development of drug delivery systems, as well as the separation and food industries.[113–115] These reactions can also be employed as models for learning about generic inclusion phenomena and enzyme-substrate interactions. Systematic research has been done on different types of compounds that can be included in β-CD. β-CDs can encapsulate a wide range of guests, including hydrocarbons, cyclohexane derivatives, aliphatic alcohols, diols, amines and acids, amino acids, sugars, phenols, aromatic amines, oligopeptides, azo compounds, naphthalene derivatives and other aromatic compounds, and numerous drugs are among the compounds covered.[106,107,116–118] The hydrophobic and van der Waals interactions between the inner surface of the β-CD ring and the mainly hydrophobic guests stabilise the ensuing CD inclusion complexes. External stimuli such as pH, redox changes, metal cations, changes in solvent, temperature differences, and light exposure all affect these host–guest interactions.[104,105]

1.8.2 Chemistry of Pillar[n]arenes

Developing and manufacturing new macrocyclic host molecules is always interesting because of their significance in supramolecular chemistry. Cyclodextrins, crown ethers, calixarenes, cucurbiturils, and their structurally related scaffolds are effective examples. A novel family of [1_n]paracyclophanes is now gaining popularity, having a similar composition but distinct structural properties.[119,120] Following Ogoshi's first report in 2008, pillar[n]arene chemistry has become a significant focus.[95] They exhibit pillar-shaped architectures and are highly symmetrical structures. In this novel family of macrocyclic compounds, hydroquinone units are linked at para positions by methylene bridges. The current nomenclature uses the term pillar[n]arene, with [n] denoting the number of aromatic rings in the macrocycle. Pillar[n]arenes (n = 5, 6, 7) offer few more advantages over typical hosts: can be made using inexpensive chemicals, re-crystallized readily, and produced in large quantities. P[5]As has a cavity size of around 5.5 A^0 similar to the size of α-CD cavity. While P[6]As has the cavity size of 6.7 A^0, which is comparable to β-cyclodextrin and cucurbit[6]uril. P[n]As can have a

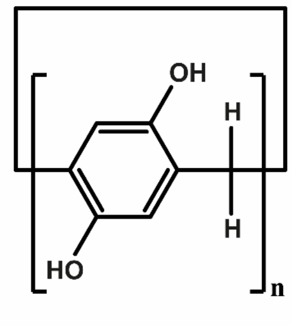

Pillar[n]arenes	Cavity	Size
P[n]A	n	A^0
P[5]A	5	4.7
P[6]A	6	6.5

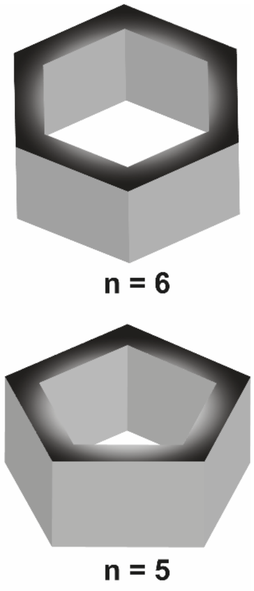

Figure 1.14. Chemical structure and molecular shape of pillar[n]arenes.

possibility of many substituents like 10 functional groups for P[5]As and 12 for P[6]As (Figure 1.14). So, this molecule can be functionalized for specific positions with the kind of group influencing their solubility by using a variety of organic synthesis methods.[97]

1.8.2.1 Host-Guest Properties of Pillar[n]arenes

Pillar[n]arenes exhibit good “host-guest” characteristics and planar chirality due to its simple structure. A number of interactions can be used to form stable "host-guest” complexes. Physical interactions such as coordination interactions between unpaired electrons and empty electron orbitals, electrostatic interactions between cationic and anionic groups, and charge-transfer (CT) interactions between electron donors and acceptors are all classified in terms of magnitude. When and hydrogen-bonding, van der Waals and π/π interactions occur in isolation, including OH/N, NH/N, CH/N, OH/O, NH/O, CH/O, CH/π, NH/π, OH/π interactions, are considered as weak physical interactions. On the other hand, in some cases, a combination of these weak physical interactions can effectively promote host guest complexation processes. All the physical interactions described above can contribute to the “host-guest” complexation of pillar[n]arenes because a range of functional groups can be implanted on the rim of pillar[n]arenes to offer adequate reactive sites for a range of guests.[121–125]

Many chemical and biological processes, including fluid actuation, matter transportation, and energy transduction, biotransformation begin with interfacial molecular recognition. Different external stimuli at interfaces strongly affect these dynamic processes in many systems.[132,133] As a result, the incorporation of various “host-guest” chemistries into surface engineering is an essential step toward the development of multifunctional interfaces with efficient stimulus responsiveness (Figure 16). It demonstrates good compatibility in imitating the complex molecular-recognition systems seen in nature, which are adaptable to environmental changes.[134–136]

In comparison to the above-mentioned usual “host” molecules, pillar[n]arenes (n = 5, 6, 7) have some advantages. First, in comparison to calixarenes and crown ethers, they are very symmetrical and rigid, allowing for selective “guest” binding. Second, unlike cucurbiturils, they are simple to functionalize with various substituents on all of the benzene rings or selectively on one or two, allowing them to modify their “host-guest” binding capacities. Third, they are highly soluble in organic solvents, making them useful additives to water-soluble cucurbiturils and cyclodextrins with similar cavity sizes.[122,123] These properties, along with their rigid electron-rich cavity, make them ideal hosts for electron-deficient guests or other neutral molecules such viologen derivatives, n-hexane, n-octyltrimethyl ammonium, alkanediamines, (bis)- imidazolium cations, and neutral bis(imidazole) derivatives.[126–130] Pillararenes with good “host-guest” characteristics may also self-assemble, allowing them to be used to make (pseudo)rotaxanes or poly(pseudo)rotaxanes, artificial transmembrane proton channels, supramolecular dimers or polymers, fluorescence sensors, and other useful materials.[122,123] As a result, this novel type of host has received a lot of attention since its introduction and has also been explored.

1.9 Autonomous Fluid Flow on Supramolecular Interfaces using Host-Guest Interactions: Supramolecular Micropumps for Regulating Fluid-Flow

The goal of “host-guest” chemistry is to examine the selective interactions of “host” and “guest” molecules. A “host” molecule is usually a molecule with a large cavity volume. “Guests” often have a complimentary shape and interact with the host, allowing for selection between the “host” and the “guest”, which is known as molecular recognition. Molecular recognition involves various noncovalent interactions such as hydrogen bonding, electrostatics, van der Waals, and hydrophobic interactions. “Host-guest” chemistry can considerably increase selectivity because of recognition-directed interactions between “host” and “guest” molecules. Furthermore, using different “host-guest” chemistry, functional geometries, and the activation of supramolecular assemblies in molecular systems can be modulated effectively. In general, “host-guest” chemistry can provide unique perspectives on

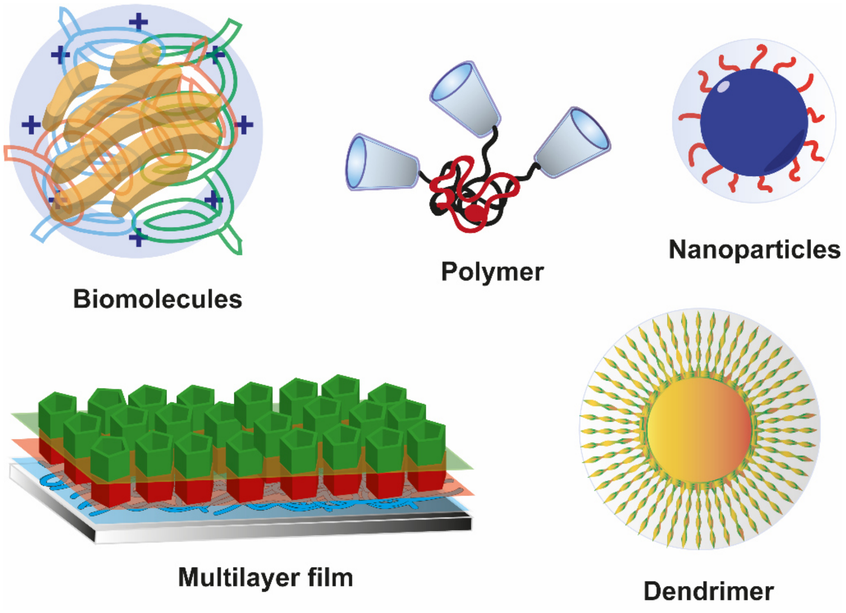

Figure 1.15. Examples of supramolecular interfaces.

the advancement of conventional fields and has numerous possibilities ranging from biomimetics to the production of programmable and controlled engineering of supramolecular soft materials such as biomolecules, polymeric materials, nanoparticles, multilayer films, dendrimers (Figure 1.15).[131]

Many chemical and biological processes, including fluid actuation, matter transportation, and energy transduction, biotransformation begin with interfacial molecular recognition. These dynamic processes in many systems are strongly affected by different external stimuli at interfaces.[132,133] As a result, the incorporation of various "host-guest" chemistries into surface engineering is an essential step toward the development of multifunctional interfaces with efficient stimulus responsiveness as shown in Figure 1.16. It demonstrates good compatibility in imitating the complex molecular-recognition systems seen in nature, which are adaptable to environmental changes.[134–136]

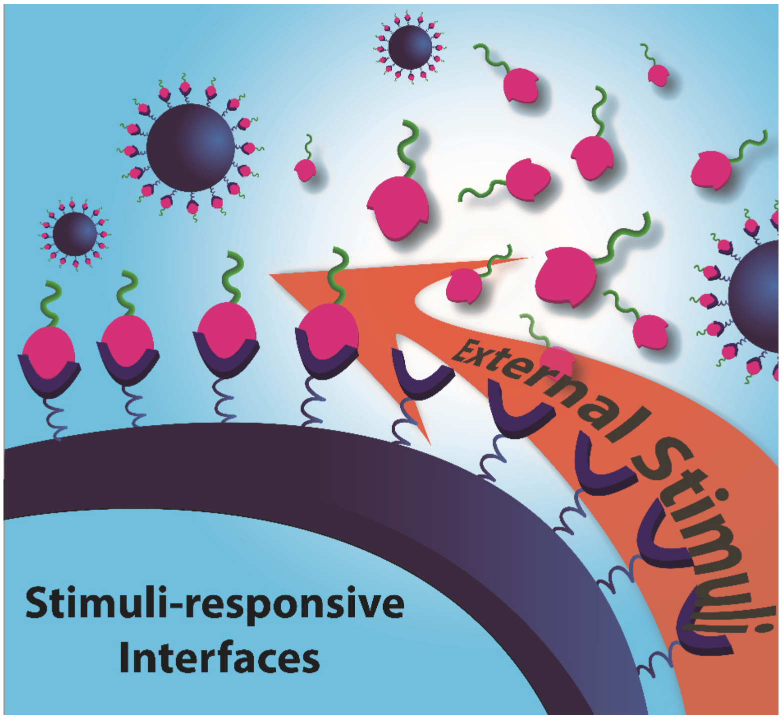

Figure 1.16. Schematic of multifunctional interface responding under external stimuli.

In our work, the host functionalized films and gels were used as interfaces to devise the micropumps that drive fluid flow in the presence of any molecule that initiates the "host-guest" recognition. Incorporating supramolecular actuators into a microfluidic device without sacrificing device geometry and performance is not always possible and would necessitate a strategy that could build the assembly on substrates of any composition and morphology.

Layer-by-layer (LbL) assembly can be a promising method for the construction of structured and functional thin films. This is because of the fact that the assembly process possesses faster film growth, conformal coating, aqueous dipping conditions, and substrate independence. In this regard, cyclodextrins functionalised polymers and pillar[n]arene derivatives have been immobilised on substrates via Layer-by-layer (LbL) deposition method to form host-functionalized multilayer films to examine the autonomous fluid flow at interfaces. Upon addition of guest molecules into the chamber, these supramolecular micropumps regulated the fluid flow in a concentration-dependent manner. Therefore, they act as self-powered platforms that integrate sensing with on-demand fluid pumping.

LbL assembly deposition is the most versatile method used for fabricating multilayer films owing to its simplicity and adaptability.[137–140] The LbL method involves the alternate dipping of the substrate into different solutions with an intermediate step of rinsing and drying (Figure 1.17). Intermolecular interactions such as hydrogen bonding, electrostatic, van der Waals forces, and charge transfer interactions are the main driving forces for the fabrication of multilayer films. These interactions can be used to incorporate various noncovalent interact moieties into multilayer films that can trigger autonomous fluid flow at the interfaces. Our work focuses only on the “host-guest” interaction to show the pumping behaviour of the self-powered micropumps. The actuation of fluid can be effectively regulated using “host-guest” chemistry, and the detection of various guests by multilayer films occurs through their host-functionalized groups. One of the most active and novel areas of supramolecular chemistry is the construction of a self-powered supramolecular micropump, which utilise the forces involved in a complex formation to trigger a fluid flow that can be observed by the observer. It is also important to consider that while many

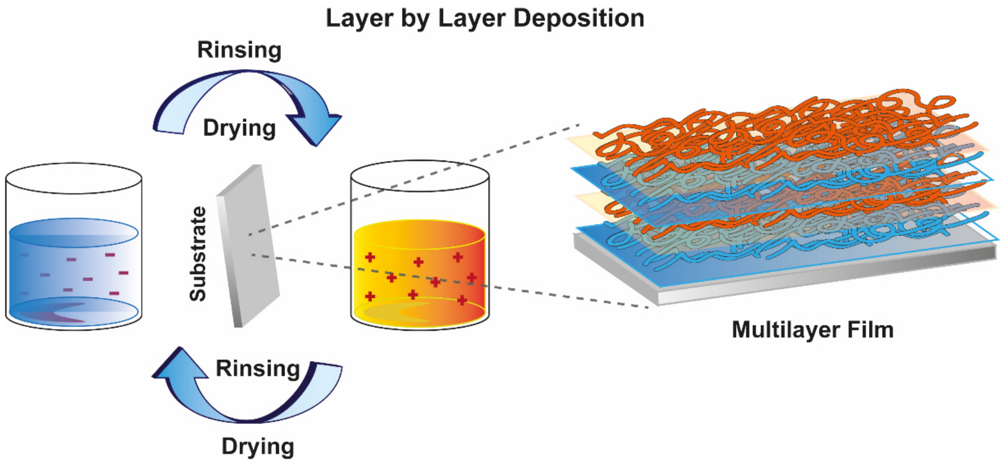

Figure 1.17. Schematic of layer-by-layer assembly process for fabricating multilayer film.

molecular devices perform well in solution, they can create challenges when transferred to solid surfaces. Therefore, creating multifunctional “host-guest” containing surfaces that perform just as well at an interface as in a solution remains a significant challenge. Also, the devices should ideally work without an external energy source and allow control over flow rates proportional to the concentration of a particular reagent (analyte) present in the fluid at various interfaces. The utilisation of a self-powered micropump based on “host-guest” molecular recognition provides a perfect solution while removing a significant barrier to utilizing supramolecular interfaces in solution and other challenges. The “host-guest” interactions at interfaces also eliminate the requirement of external power to push fluids and integrate sensing in a single microfluidic device. Therefore, these self-powered supramolecular micropumps could provide a solution for powerless microfluidic devices in which fluid flow can be controlled by modulating noncovalent interactions.

1.10 Dissertation Overview

This thesis work focuses on how supramolecular interfaces trigger an autonomous fluid flow in the presence of any substrate that initiates the molecular recognition between “host” and “guest” molecules. This work also highlighted all the studies conducted with self-powered supramolecular pumps, from the design of the micropump to the efforts made in understanding the “host-guest” based pump concept as a whole. Recent research on self-powered micropumps has piqued the curiosity of many in lab-on-a-chip microfluidics. These systems can transfer chemical energy to fluid motion without using any physical actuators or external power sources. These pumps can be miniaturised and readily incorporated into a microfluidic device. In this context, fluid flow driven by supramolecular interactions can provide a diverse toolset for designing responsive systems, opening up the opportunity to develop powerless “lab on chip” devices for potential applications ranging from single-use diagnostics to microanalysis. The fluid flow in these systems can be regulated by modulating noncovalent interactions, and can be employed as point-of-care devices.

In chapter 2, we successfully developed a versatile method for designing non-mechanical, self-powered supramolecular micropumps based on “host-guest” molecular recognition. A layer-by-layer assembly of β-cyclodextrin ("host") functionalized polymer on a glass slide was used to develop thin film-based micropumps. When "guest" molecules were introduced to the multilayer films, these supramolecular micropumps triggered fluid flow. The flow velocity was controlled by the concentration of "guest" molecules and the number of "host" layers inside the multilayer films. The numerical modeling reveals that the fluid flow is predominantly caused by solutal buoyancy induced by "host-guest" complexations. To demonstrate the molecular and colloidal transport over extended distances in self-powered systems, the micropump was incorporated into the microfluidic device for potential application in self-powered devices.

In chapter 3, a pH-responsive self-powered micropump was fabricated based on “host-guest” molecular recognition. The dynamic supramolecular interaction of beta-cyclodextrin (β-CD) with benzimidazole led to the fabrication of a valveless micropump (BzI). In reaction to a pH change, it shows flow reversal. An L-shaped microchannel was utilised to demonstrate flow reversibility over large distances. This macroscopic flow reversibility has the potential to unlock new opportunities in lab-on-a-chip applications.

The most important domains of supramolecular chemistry have always been molecular recognition based on macrocyclic host molecules. Most commonly used macrocyclic hosts like cyclodextrins (CDs), and pillararenes (P[n]As), have been shown to be an effective choice for quick and accurate recognition of isomers due to their nontoxicity, low cost, high transparency, and versatile chemical and physical properties. **In chapter 4**, we accomplished fluid-flow-based chiral and structural isomer recognition of tryptophan (Trp) and nitrophenol (NP) isomers using β-CD modified polymer and P[5]A multilayer films, respectively. The "host" component of film recognises isomers through selective "host-guest" interaction. With the addition of "guest" molecules, these supramolecular micropumps triggered fluid flow, which was primarily driven by solutal buoyancy induced by "host-guest" molecular recognition. The difference in fluid flow of guest molecules was based on the solutal buoyancy and thermodynamic parameters of particular “host-guest” pairs which were then used to recognize the isomers. These devices can be assisted in the development of novel recognition techniques and lead to a better understanding of chiral and molecular recognition in chemical and biological systems.

Finally, **Chapter 5** illustrated the flow-based self-sorting of pillar[5,6]arenes by using a concept of geometrical complementarity by shape. To develop the micropump, a multilayer thin film composed of anionic pillar[5,6]arenes and cationic pillar[5,6]arenes was fabricated by layer-by-layer (LbL) deposition technique. Fluid flow toward layers produced from oppositely charged pillar[5]arenes was seen in ionic pillar[5]arenes but not in ionic pillar[6]arenes. Similarly, in the reverse combination, ionic pillar[6]arenes exhibit fluid flow toward layers made of oppositely charged pillar[6]arenes, but not in ionic pillar[5]arenes.

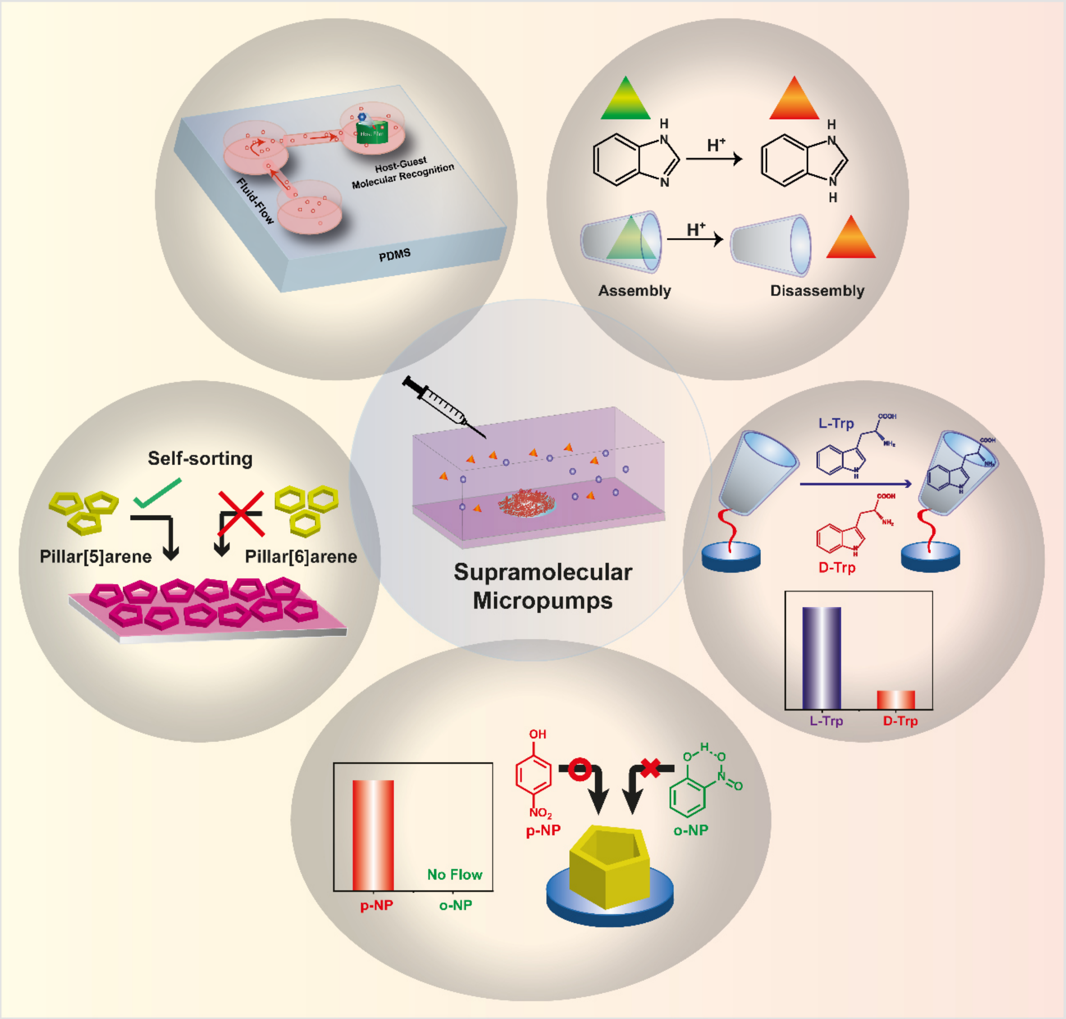

Figure 1.18. Dissertaion Overview

1.11 References

1. K. Ren, J. Zhou and H. Wu, *Acc. Chem. Res.*, 2013, **46**, 2396–2406.
2. G. A. Ozin, I. Manners, S. Fournier-Bidoz and A. Arsenault, *Adv. Mater.*, 2005, **17**, 3011–3018.
3. A. Ramachandran and J. G. Santiago, *Chem. Rev.*, 2022, **122**, 12904–12976.
4. B. Zheng, L. S. Roach and R. F. Ismagilov, *J Am Chem Soc*, 2003, **125**, 11170–11171.
5. R. S. Ramsey and J. M. Ramsey, *Anal. Chem.*, 1997, **69**, 1174–1178.
6. E. K. Sackmann, A. L. Fulton and D. J. Beebe, *Nature*, 2014, **507**, 181–189.
7. V. Singhal and S. V. Garimella, *Sens. Actuator A Phys.*, 2007, **134**, 650–659.
8. L. Y. Yeo, H.-C. Chang, P. P. Y. Chan and J. R. Friend, *Small*, 2011, **7**, 12–48.

9. P. Abgrall, V. Conedera, H. Camon, A.-M. Gue and N.-T. Nguyen, *Electrophoresis*, 2007, **28**, 4539–4551.

10. T. A. Franke and A. Wixforth, *ChemPhysChem*, 2008, **9**, 2140–2156.

11. D. J. Beebe, G. A. Mensing and G. M. Walker, *Annu Rev Biomed Eng*, 2002, **4**, 261–286.

12. J. Wang and K. M. Manesh, *Small*, 2010, **6**, 338–345.

13. A. Credi, *Angewandte Chemie International Edition*, 2014, **53**, 4274–4275.

14. S. Sánchez and M. Pumera, *Chem Asian J.*, 2009, **4**, 1402–1410.

15. T. Mirkovic, N. S. Zacharia, G. D. Scholes and G. A. Ozin, *Small*, 2010, **6**, 159–167.

16. C. Zhou, H. Zhang, Z. Li and W. Wang, *Lab Chip*, 2016, **16**, 1797–1811.

17. K. Ariga, Q. Ji, T. Mori, M. Naito, Y. Yamauchi, H. Abe and J. P. Hill, *Chem. Soc. Rev.*, 2013, **42**, 6322–6345.

18. E. Del Grosso, A.-M. Dallaire, A. Vallée-Bélisle and F. Ricci, *Nano Lett.*, 2015, **15**, 8407–8411.

19. G. Seo, Y. Jeong and Y. Kim, *ACS Materials Lett.*, 2022, **4**, 1214–1226.

20. H. Aramoto, M. Osaki, S. Konishi, C. Ueda, Y. Kobayashi, Y. Takashima, A. Harada and H. Yamaguchi, *Chemical Science*, 2020, **11**, 4322–4331.

21. S. Konishi, Y. Kashiwagi, G. Watanabe, M. Osaki, T. Katashima, O. Urakawa, T. Inoue, H. Yamaguchi, A. Harada and Y. Takashima, *Polym. Chem.*, 2020, **11**, 6811–6820.

22. G. Sinawang, M. Osaki, Y. Takashima, H. Yamaguchi and A. Harada, *Polym J*, 2020, **52**, 839–859.

23. G. Sinawang, M. Osaki, Y. Takashima, H. Yamaguchi and A. Harada, *Chem. Commun.*, 2020, **56**, 4381–4395.

24. D. A. Wilson, B. de Nijs, A. van Blaaderen, R. J. M. Nolte and J. C. M. van Hest, *Nanoscale*, 2013, **5**, 1315–1318.

25. Y. Tu, F. Peng, J. M. Heuvelmans, S. Liu, R. J. M. Nolte and D. A. Wilson, *Angew. Chem.*, 2019, **131**, 8779–8783.

26. L. K. E. A. Abdelmohsen, F. Peng, Y. Tu and D. A. Wilson, *J. Mater. Chem. B*, 2014, **2**, 2395–2408.

27. W. Wang, W. Duan, S. Ahmed, T. E. Mallouk and A. Sen, *Nano Today*, 2013, **8**, 531–554.

28. W. F. Paxton, S. Sundararajan, T. E. Mallouk and A. Sen, *Angew. Chem. Int. Ed.*, 2006, **45**, 5420–5429.

29. L. K. Lee, M. A. Ginsburg, C. Crovace, M. Donohoe and D. Stock, *Nature*, 2010, **466**, 996–1000.

30. P. Dallos and B. Fakler, *Nat Rev Mol Cell Biol*, 2002, **3**, 104–111.

31. W. R. Browne and B. L. Feringa, in *Nanosci. Technol.*, Co-Published with Macmillan Publishers Ltd, UK, 2009, 79–89.

32. W. F. Paxton, K. C. Kistler, C. C. Olmeda, A. Sen, S. K. St. Angelo, Y. Cao, T. E. Mallouk, P. E. Lammert and V. H. Crespi, *J. Am. Chem. Soc.*, 2004, **126**, 13424–13431.

33. W. F. Paxton, P. T. Baker, T. R. Kline, Y. Wang, T. E. Mallouk and A. Sen, *J. Am. Chem. Soc.*, 2006, **128**, 14881–14888.

34. P. Díez, B. E.-F. de Ávila, D. E. Ramírez-Herrera, R. Villalonga and J. Wang, *Nanoscale*, 2017, **9**, 14307–14311.

35. Y. Mei, A. A. Solovev, S. Sanchez and O. G. Schmidt, *Chem. Soc. Rev.*, 2011, **40**, 2109–2119.

36. T. R. Kline, W. F. Paxton, Y. Wang, D. Velegol, T. E. Mallouk and A. Sen, *J. Am. Chem. Soc.*, 2005, **127**, 17150–17151.

37. S. Mohith, P. N. Karanth and S. M. Kulkarni, *Mechatronics*, 2019, **60**, 34–55.

38. P. Yager, T. Edwards, E. Fu, K. Helton, K. Nelson, M. R. Tam and B. H. Weigl, *Nature*, 2006, **442**, 412–418.

39. D. Patra, S. Sengupta, W. Duan, H. Zhang, R. Pavlick and A. Sen, *Nanoscale*, 2013, **5**, 1273–1283.

40. W. Duan, W. Wang, S. Das, V. Yadav, T. E. Mallouk and A. Sen, *Annu Rev Anal Chem*, 2015, **8**, 311–333.

41. J. Khandurina, T. E. McKnight, S. C. Jacobson, L. C. Waters, R. S. Foote and J. M. Ramsey, *Anal. Chem.*, 2000, **72**, 2995–3000.

42. L. Zhang, J.-M. Koo, L. Jiang, M. Asheghi, K. E. Goodson, J. G. Santiago and T. W. Kenny, *J Microelectromech Syst.*, 2002, **11**, 12–19.

43. P. Calvo-Marzal, S. Sattayasamitsathit, S. Balasubramanian, J. R. Windmiller, C. Dao and J. Wang, *Chem. Commun.*, 2010, **46**, 1623–1624.

44. S. Tai Chang, E. Beaumont, D. N. Petsev and O. D. Velev, *Lab on a Chip*, 2008, **8**, 117–124.

45. G. Loget and A. Kuhn, *Nat Commun*, 2011, **2**, 535.

46. R. Dreyfus, J. Baudry, M. L. Roper, M. Fermigier, H. A. Stone and J. Bibette, *Nature*, 2005, **437**, 862–865.

47. W. Gao, S. Sattayasamitsathit, K. M. Manesh, D. Weihs and J. Wang, *J. Am. Chem. Soc.*, 2010, **132**, 14403–14405.

48. A. Ghosh and P. Fischer, *Nano Lett.*, 2009, **9**, 2243–2245.

49. S. Tottori, L. Zhang, F. Qiu, K. K. Krawczyk, A. Franco-Obregón and B. J. Nelson, *Adv. Mater.*, 2012, **24**, 811–816.
50. E. M. Purcell, *Am. J. Phys.*, 1977, **45**, 3–11.
51. M. Ibele, T. E. Mallouk and A. Sen, *Angew. Chem. Int. Ed.*, 2009, **121**, 3358–3362.
52. M. J. Esplandiu, A. Afshar Farniya and A. Bachtold, *ACS Nano*, 2015, **9**, 11234–11240.
53. M. W. J. Prins, W. J. J. Welters and J. W. Weekamp, *Science*, 2001, **291**, 277–280.
54. B. S. Gallardo, V. K. Gupta, F. D. Eagerton, L. I. Jong, V. S. Craig, R. R. Shah and N. L. Abbott, *Science*, 1999, **283**, 57–60.
55. D. E. Kataoka and S. M. Troian, *Nature*, 1999, **402**, 794–797.
56. T. R. Kline, J. Iwata, P. E. Lammert, T. E. Mallouk, A. Sen and D. Velegol, *J. Phys. Chem. B*, 2006, **110**, 24513–24521.
57. S. Subramanian and J. M. Catchmark, *J. Phys. Chem. C*, 2007, **111**, 11959–11964.
58. M. E. Ibele, Y. Wang, T. R. Kline, T. E. Mallouk and A. Sen, *J. Am. Chem. Soc.*, 2007, **129**, 7762–7763.
59. J. J. McDermott, A. Kar, M. Daher, S. Klara, G. Wang, A. Sen and D. Velegol, *Langmuir*, 2012, **28**, 15491–15497.
60. V. Yadav, H. Zhang, R. Pavlick and A. Sen, *J. Am. Chem. Soc.*, 2012, **134**, 15688–15691.
61. H. Zhang, K. Yeung, J. S. Robbins, R. A. Pavlick, M. Wu, R. Liu, A. Sen and S. T. Phillips, *Angew. Chem. Int. Ed.*, 2012, **124**, 2450–2454.
62. J. A. Thoma and D. E. Koshland, *J. Am. Chem. Soc.*, 1960, **82**, 3329–3333.
63. J.-M. Lehn, *Pharm. Acta Helv.*, 1995, **69**, 205–211.
64. P. Ehrlich, *The relations existing between chemical constitution, distribution and pharmacological action.*, John Wiley & Sons Ltd, New York, 1906.
65. A. J. Green, *Aust. J. Chem.*, 2002, **55**, 183–186.
66. P. J. Cragg, *Supramolecular Chemistry: From Biological Inspiration to Biomedical Applications*, Springer Science & Business Media, 2010.
67. J.-M. Lehn, *Angew. Chem. Int. Ed.*, 1988, **27**, 89–112.
68. J. M. Lehn, in *Chemistry for the Welfare of Mankind*, eds. T. Tsuruta, K. Tamaru, Y. Tamai, N. Takahashi, Y. Kitano and E. Echigoya, Pergamon, 1979, 871–892.
69. C. J. Pedersen, *J. Am. Chem. Soc.*, 1967, **89**, 7017-7036.
70. J. W. Steed and J. L. Atwood, *Supramolecular Chemistry*, John Wiley & Sons, 2022.
71 .J. W. Steed, D. R. Turner and K. J. Wallace, *Core Concepts in Supramolecular Chemistry and Nanochemistry*, John Wiley & Sons, 2007.

72. F. J. M. Hoeben, P. Jonkheijm, E. W. Meijer and A. P. H. J. Schenning, *Chem. Rev.*, 2005, **105**, 1491–1546.

73. J. Šponer, J. Florián, P. Hobza and J. Leszczynski, *J. Biomol. Struct.*, 1996, **13**, 827–833.

74. J. M. Lehn, *Science*, , DOI:10.1126/science.8511582.

75. J. M. Lehn, , J. P. Sauvage, J. Simon, R. Ziessel, C. Piccinnileopardi, G. Germain, J. P. Declercq, and M. Vanmeerssche, *Nouv. J. Chem*., 1983, **7**, 413–420.

76. S. J. Rowan, S. J. Cantrill, G. R. L. Cousins, J. K. M. Sanders and J. F. Stoddart, *Angew. Chem. Int. Ed.*, 2002, **41**, 898–952.

77. L. Trembleau and J. Rebek, *Science*, 2003, **301**, 1219–1220.

78. D. Phlip, *Adv. Mater.*, 1996, **8**, 866–868.

79. K. E. Krakowiak, J. S. Bradshaw and D. J. Zamecka-Krakowiak, *Chem. Rev.* 1989, **89**, 929–972.

80. J. S. Bradshaw and R. M. Izatt, *Acc. Chem. Res.*, 1997, **30**, 338–345.

81. G. W. Gokel, W. M. Leevy and M. E. Weber, *Chem. Rev.*, 2004, **104**, 2723–2750.

82. A. Harada, A. Hashidzume, H. Yamaguchi and Y. Takashima, *Chem. Rev.*, 2009, **109**, 5974–6023.

83. A. C. Bhasikuttan, H. Pal and J. Mohanty, *Chem. Commun.*, 2011, **47**, 9959–9971.

84. L. Baldini, A. Casnati, F. Sansone and R. Ungaro, *Chem. Soc. Rev.*, 2007, **36**, 254–266.

85. C. D. Gutsche, *Calixarenes: An Introduction*, 2nd Ed., Royal Society of Chemistry, Cambridge U.K., 2008.

86. E. Botana, E. Da Silva, J. Benet-Buchholz, P. Ballester and J. de Mendoza, *Angew. Chem. Int. Ed.*, 2007, **46**, 198–201.

87. M. Xue, Y. Yang, X. Chi, Z. Zhang and F. Huang, *Acc. Chem. Res.*, 2012, **45**, 1294–1308.

88. N. Morohashi, F. Narumi, N. Iki, T. Hattori and S. Miyano, *Chem. Rev.*, 2006, **106**, 5291–5316.

89. W. Maes and W. Dehaen, *Chem. Soc. Rev.*, 2008, **37**, 2393–2402.

90. M.-X. Wang, *Acc. Chem. Res.*, 2012, **45**, 182–195.

91. R. Kothur, B. Patel and P. Cragg, *ScienceJet*.

92. Y. Ma, Z. Zhang, X. Ji, C. Han, J. He, Z. Abliz, W. Chen and F. Huang, *Eur. J. Org. Chem.*, 2011, **2011**, 5331–5335.

93. P. J. Cragg and K. Sharma, *Chem. Soc. Rev.*, 2012, **41**, 597–607.

94. A. Dandridge and H. Drescher, *GB patent*, **322169**.

95. T. Ogoshi, S. Kanai, S. Fujinami, T. Yamagishi and Y. Nakamoto, *J. Am. Chem. Soc.*, 2008, **130**, 5022–5023.
96. J. Lagona, P. Mukhopadhyay, S. Chakrabarti and L. Isaacs, *Angew. Chem. Int. Ed.*, 2005, **44**, 4844–4870.
97. K. Uekama, F. Hirayama and T. Irie, *Chem. Rev.*, 1998, **98**, 2045–2076.
98. S. V. Kurkov and T. Loftsson, *Int. J. Pharm.*, 2013, **453**, 167–180.
99. L. F. Villalobos, T. Huang and K.-V. Peinemann, *Adv. Mater.*, 2017, **29**, 1606641.
100. J. Liu, D. Hua, Y. Zhang, S. Japip and T.-S. Chung, *Adv. Mater.*, 2018, **30**, 1705933.
101. A. Alsbaiee, B. J. Smith, L. Xiao, Y. Ling, D. E. Helbling and W. R. Dichtel, *Nature*, 2016, **529**, 190–194.
102. A. Heydari, F. Doostan, H. Khoshnood and H. Sheibani, *RSC Adv.*, 2016, **6**, 33267–33278.
103. L. Leclercq and V. Nardello-Rataj, *Eur. J. Pharm. Sci.*, 2016, **82**, 126–137.
104. X. Ji, M. Ahmed, L. Long, N. M. Khashab, F. Huang and J. L. Sessler, *Chem. Soc. Rev.*, 2019, **48**, 2682–2697.
105. E. Zhang, J. Shi, L. Xiao, Q. Zhang, M. Lu, B. Nan, K. Wu and M. Lu, *Polym. Chem.*, 2021, **12**, 831–842.
106. S. A. Nepogodiev and J. F. Stoddart, *Chem. Rev.*, 1998, **98**, 1959–1976.
107. G. Crini, *Chem. Rev.*, 2014, **114**, 10940–10975.
108. S. Li and W. C. Purdy, *Chem. Rev*. 1992, *92*, 1457-1490
109. M. V. Rekharsky and Y. Inoue, *Chem Rev*, 1998, **98**, 1875–1918.
110. M. L. Bender and M. Komiyama, in *Cyclodextrin Chemistry*, Springer-Verlag: Berlin, Heidelberg, 1978, 28–32.
111. J.-M. Lehn, *Angew. Chem. Int. Ed.*, 1990, **29**, 1304–1319.
112. R. Periasamy, *J. Carbohydr. Chem.*, 2021, **40**, 135–155.
113. B. Tian, S. Hua and J. Liu, *Carbohydr. Polym.*, 2020, **232**, 115805.
114. B. Tian and J. Liu, *New J. Chem.*, 2020, **44**, 9137–9148.
115. O. Adeoye and H. Cabral-Marques, *Int. J. Pharm.*, 2017, **531**, 521–531.
116. Y. Wei, H. Li, H. Hao, Y. Chen, C. Dong and G. Wang, *Polym. Chem.*, 2014, **6**, 591–598.
117. M. N. Roy, D. Ekka, S. Saha and M. C. Roy, *RSC Adv.*, 2014, **4**, 42383–42390.
118. C. Liu, J. Lian, Q. Liu, C. Xu and B. Li, *Anal. Methods*, 2016, **8**, 5794–5800.
119. N. L. Strutt, H. Zhang, S. T. Schneebeli and J. F. Stoddart, *Acc. Chem. Res.*, 2014, **47**, 2631–2642.

120. G. W. Gribble and C. F. Nutaitis, *Tetrahedron Lett.*, 1985, **26**, 6023–6026.
121. T. Ogoshi, T. Yamagishi and Y. Nakamoto, *Chem. Rev.*, 2016, **116**, 7937–8002.
122. M. Xue, Y. Yang, X. Chi, Z. Zhang and F. Huang, *Acc. Chem. Res.*, 2012, **45**, 1294–1308.
123. T. Ogoshi and T. Yamagishi, *Chem. Commun.*, 2014, **50**, 4776–4787.
124. C. Li, *Chem. Commun.*, 2014, **50**, 12420–12433.
125. Y. Kou, H. Tao, D. Cao, Z. Fu, D. Schollmeyer and H. Meier, *Eur. J. Org. Chem.*, 2010, **2010**, 6464–6470.
126. D. Cao, Y. Kou, J. Liang, Z. Chen, L. Wang and H. Meier, *Angew. Chem. Int. Ed.*, 2009, **48**, 9721–9723.
127. X. Shu, S. Chen, J. Li, Z. Chen, L. Weng, X. Jia and C. Li, *Chem. Commun.*, 2012, **48**, 2967–2969.
128. C. Han, F. Ma, Z. Zhang, B. Xia, Y. Yu and F. Huang, *Org. Lett.*, 2010, **12**, 4360–4363.
129. T. Ogoshi, M. Hashizume, T. Yamagishi and Y. Nakamoto, *Chem. Commun.*, 2010, **46**, 3708–3710.
130. T. Ogoshi, K. Kitajima, T. Aoki, T. Yamagishi and Y. Nakamoto, *J. Phys. Chem. Lett.*, 2010, **1**, 817–821.
131. X. Zhang and D. G. Whitten, *Langmuir*, 2011, **27**, 1245–1245.
132. E. Cabane, X. Zhang, K. Langowska, C. G. Palivan and W. Meier, *Biointerphases*, 2012, **7**, 9.
133. P. M. Mendes, *Chem. Soc. Rev.*, 2008, **37**, 2512–2529.
134. I. Hwang, K. Baek, M. Jung, Y. Kim, K. M. Park, D.-W. Lee, N. Selvapalam and K. Kim, *J. Am. Chem. Soc.*, 2007, **129**, 4170–4171.
135. R. de la Rica and H. Matsui, *Chem. Soc. Rev.*, 2010, **39**, 3499–3509.
136. Y.-W. Yang, Y.-L. Sun and N. Song, *Acc. Chem. Res.*, 2014, **47**, 1950–1960.
137. P. T. Hammond, *Adv. Mater.*, 2004, **16**, 1271–1293.
138. X. Y. Ling, I. Y. Phang, W. Maijenburg, H. Schönherr, D. N. Reinhoudt, G. J. Vancso and J. Huskens, *Angew. Chem. Int. Ed.*, 2009, **48**, 983–987.
139. X. Y. Ling, I. Y. Phang, H. Schönherr, D. N. Reinhoudt, G. J. Vancso and J. Huskens, *Small*, 2009, **5**, 1428–1435.
140. C. Jiang, S. Markutsya and V. V. Tsukruk, *Adv. Mater.*, 2004, **16**, 157–161.

Chapter 2

Polymer Multilayer Films Triggers Autonomous Fluid Flow and Power Microfluidic Devices

2.1 Introduction

Flow control is at the heart of a microfluidic device and plays an important role in executing unit operations.[1-3] Using this technology, pressure-driven micropumps are the key players for accurately manipulating the fluid flow.[4,5] However, interfacing microfluidics with fluid-control systems introduce complexity to the systems and decreases their portability for practical implementation. Several approaches have been investigated to find an alternate pumping mechanism that does not require a mechanical actuator and power source. The examples include unconventional approaches like capillary fluid flow[6-8] or stimuli-responsive actuators.[9–13] In most cases, the complex design of these devices makes them inaccessible for general use. Recent research on self-powered micropumps has attracted a great deal of interest in lab-on-a-chip microfluidics. These systems can convert chemical energy to fluid movement, and thus do not require any physical actuator or external power source.[14–20] As a result, the miniaturization of these pumps is highly feasible, and the assembly can be easily integrated into the microfluidic device. In this context, fluid flow triggered by supramolecular interactions can provide a versatile toolkit for constructing responsive systems.[21,22] The micropumps assembled from these noncovalent building blocks will offer new possibilities for creating dynamic systems, and the flow can be remotely manipulated via modulating the non-covalent interactions. However, fluid flow originating from supramolecular interactions has so far remained largely unexplored, and attention is needed to establish a new paradigm while retaining the interfacing supramolecular specificity.

The integration of supramolecular actuators into a microfluidic device without compromising the device geometry and function is not always easy, and would require an approach that can construct the assembly on substrates of any composition and topology. Layer-by-layer (LbL) assembly could be a realistic starting point for fabricating structured and functional thin films, as the assembly process exhibits faster film growth, aqueous dipping conditions, conformal coating, and substrate independence.[23–26] Moreover, the number of layers and layer sequences can be tuned by changing the sequence of the adsorption process. Through judicious choice of building blocks, the supramolecular motifs can easily be integrated into these multilayer thin films.

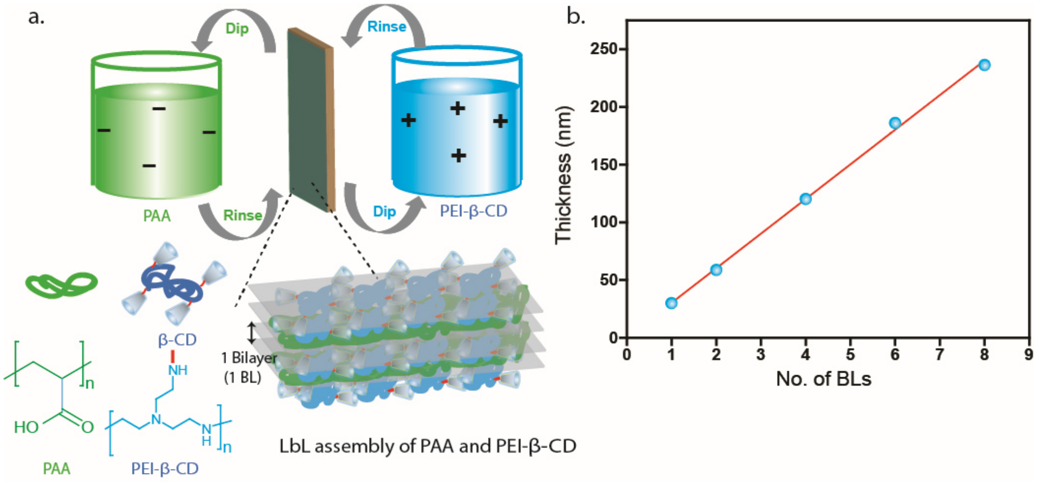

Figure 2.1. (a) Schematic of layer-by-layer (LbL) assembly using PAA and PEI-β-CD polymer pairs. (b) Thickness profile of polymer multilayer film grown on silicon wafer.

Adopting the LbL approach, herein we have fabricated a multilayer thin-film scaffold comprised of a β-cyclodextrin (‘host’) functionality to investigate the autonomous fluid flow. These supramolecular micropumps turned on the fluid flow upon addition of ‘guest’ molecules into the chamber in a concentration-dependent manner. Numerical modeling suggests that the flow is originated primarily due to the solutal buoyancy caused by the density difference between the reactants and products. Later, we show that the fluid velocity of the pumps can be tuned by varying the number of bilayers (BLs) as well as the concentration of the added guest molecules. The pumps showed a temporal variation of the fluid flow as the host binding sites are gradually occupied by the guest molecules during the reaction. These pumps assembled from supramolecular motifs are re-usable because of the inherent dynamic nature of non-covalent interactions. Finally, we demonstrate that the multilayer pump scaffold can be incorporated into a microfluidic device to regulate molecular transport and colloid transport directionally, overcoming Brownian motion.

2.2 Results and Discussions

2.2.1 Deposition of Multilayer Film

The host functionalized polymer, i.e., β-CD grafted branched polyethyleneimine (PEI-β-CD), was synthesized according to a literature report[27] and the degree of β-CD substitution was 7.91% as estimated via ^{1}H NMR spectroscopy (see experimental section for synthesis).

PEI-β-CD and polyacrylic acid (PAA) were used as the polyelectrolyte pair to fabricate the multilayer films, and the growth of the films was primarily governed by electrostatic interactions between the pairs when deposited via LbL assembly (Figure 2.1a). In a typical coating process, a cleaned substrate was initially treated with a primer solution (1 wt% branched PEI solution; pH 10) for 5 minutes and then the primer-coated substrate was alternately dipped into the solution of PAA (0.2 wt%, pH 4) and PEI-β-CD (0.1 wt%, pH 8) for 5 minutes each. The substrate was thoroughly rinsed and dried after every deposition step. Once the first bilayer (BL; the combination of one positive and one negative layer) had been constructed, additional layers were deposited using a one-minute dipping time and the procedure was repeated until the desired number of BLs was achieved. The PEI-β-CD containing film was initially grown on a silicon wafer and the thickness was measured in a dry state using atomic force microscopy (AFM) (Figure 2.2). The thickness profile in Figure 2.1b shows that the multilayer film grew linearly.

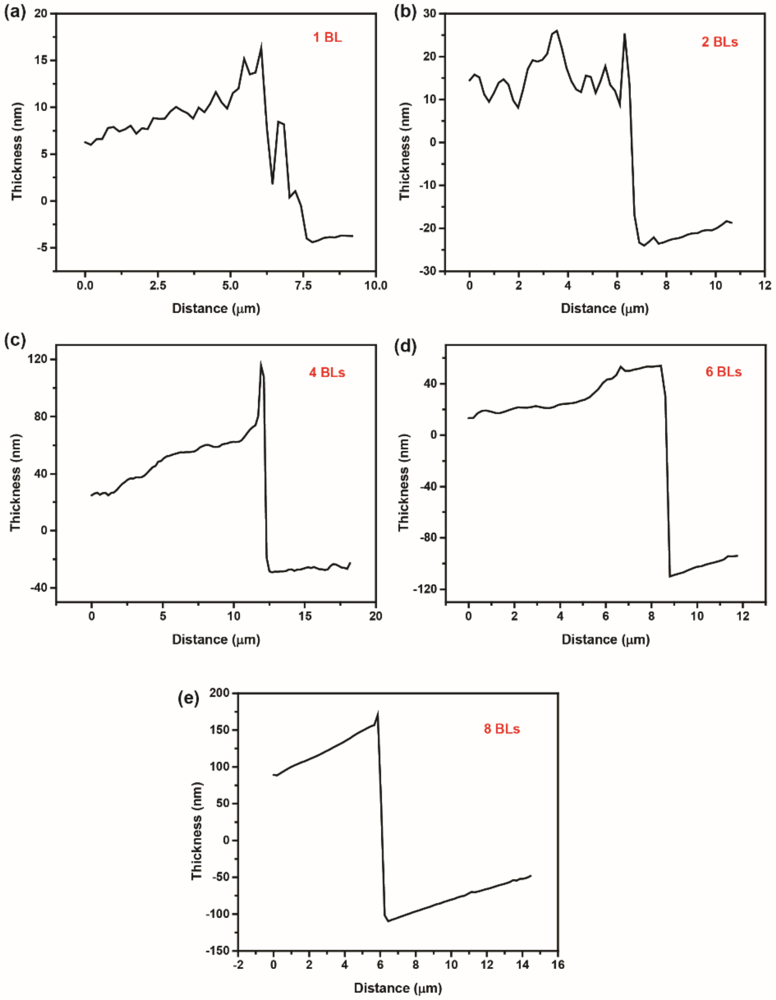

Figure 2.2. Thickness measurement using AFM (a) 1 BL (b) 2 BLs (c) 4 BLs (d) 6 BLs, and (e) 8 BLs.

2.2.2 Guest-Induced Micropump Study

The micropump was constructed by depositing the multilayer film in a circular pattern (4.6 mm diameter) on the middle of a glass slide. Next, an imaging chamber (l =1cm, b=1cm, h=1.8 mm) was placed on top of the polymeric coating to seal the pump chamber, and thus a closed chamber was created. The fluid-pumping behaviour of the β-CD-functionalized films was analyzed using two very well studied guest molecules: (i) 1- adamantylamine hydrochloride (AdA; pH 6); and (ii) ferrocenecarboxylic acid (FcA; pH 9; see experimental section for synthesis). Upon injection of the guest molecules with the tracer particles into the chamber, an inward motion of the tracer particles towards the coating was observed when viewed at the bottom layer as shown in the snapshots of videos (Figure 2.3a and b). Two control experiments were performed to verify our experimental results. First, the host multilayer film was treated with DI water at pH 6 and pH 9, the working pH values for the fluid flow studies. No flow was observed, confirming that the change in pH did not contribute to the fluid flow (Figure 2.3c). In another experiment, a $(PEI/PAA)_{2BL}$ film pattern was constructed on the glass slide without incorporating the host functionality in the film. The introduction of guest molecules into this micropump chamber did not result in any fluid movement (Figure 2.3d). This indicates that the flow could possibly originate due to host–guest molecular recognition between β-CD and the guest molecules (Figure 2.4).

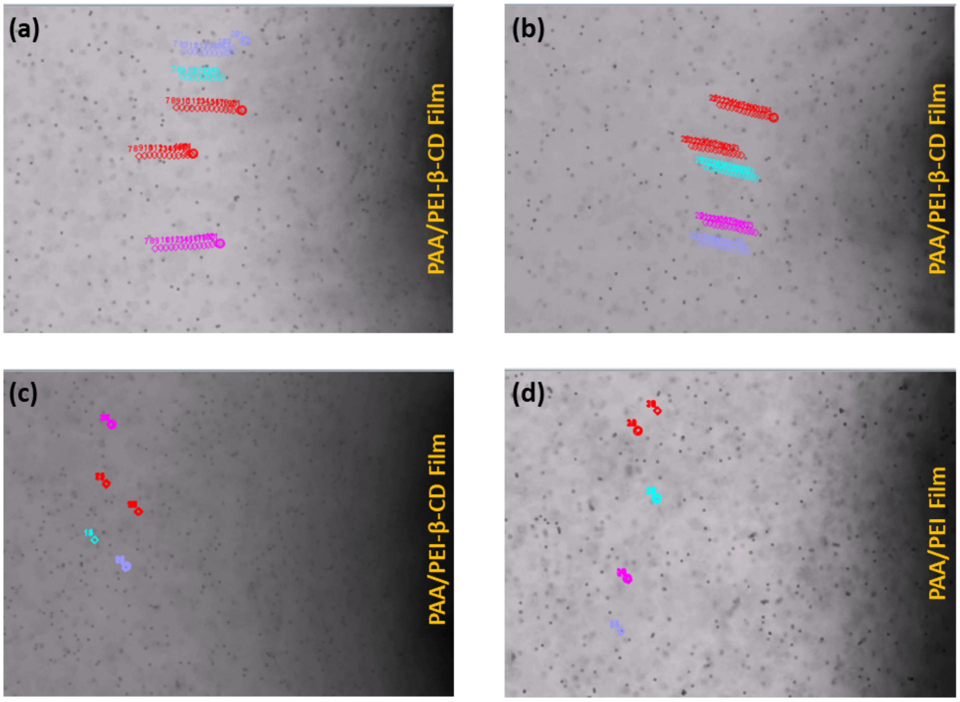

Figure 2.3. Tracer particles trajectories: Directional flow in presence of (a) AdA, (b) FcA, and no flow in control experiments (c) and (d).

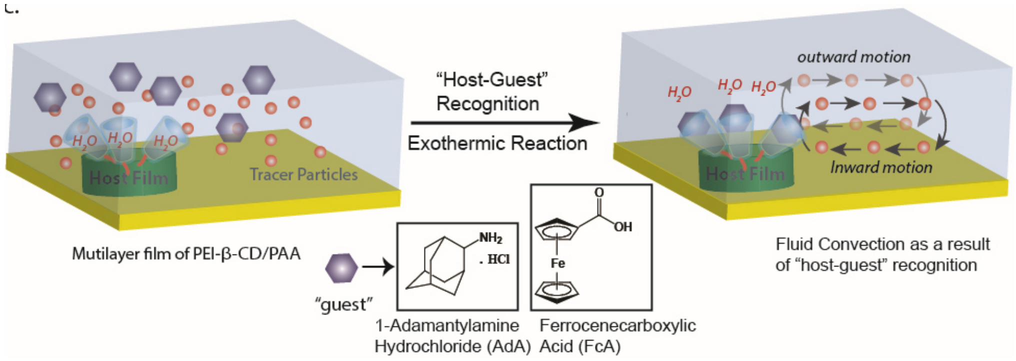

Figure 2.4. Schematic of fluid pumping as a result of "host-guest" complex formation.

2.2.3 Pumping Mechanism

β-CD is capable of forming an inclusion complex with the hydrophobic guest molecules inside their hydrophobic cavities.[28] This 'hydrophobic–hydrophobic' interaction and enthalpy-driven displacement of high-energy water molecules are the major driving forces for this type of host–guest molecular recognition. To investigate the thermodynamics of the host–guest complex, isothermal titration calorimetry (ITC) experiments were performed at 298 K. The non-linear regression fit yielded a complete set of thermodynamic parameters (K_a, ΔG, ΔH, -TΔS) for the formation of host–guest complexes as shown in Figure 2.5a and b. These showed that both AdA and FcA formed a 1:1 inclusion complex with β-CD, and the binding constant of the β-CD–AdA complex (8.4×10^3 M^{-1}) was higher than the β-CD–FcA complex (1.25×10^3 M^{-1}). This implies that β-CD forms a more stable complex with AdA than with FcA. From figure 2.5a and b, it is quite evident that the host–guest complexation is exothermic in nature and ΔH for the β-CD–AdA complex was -24.15±1.59 $kJmol^{-1}$, which is higher than for the β-CD–FcA complex (ΔH = -17.22±0.54 $kJmol^{-1}$). Based on these data, our first assumption was that thermal buoyancy may cause a density-driven flow around the polymer multilayer film, as reported earlier.[29] However, the previous reports of self-powered micropumps suggested that a combination of thermal and solutal buoyancy played a role in the density-driven flow.[30] To confirm the density-driven flow, the micropump chamber was inverted so that the direction of gravity was reversed relative to the pump orientation. The fluid-flow direction was reversed as expected, i.e., the flow was away from the pattern when observed at the bottom layer, confirming the density driven flow. To gain a deeper insight into the solutal and thermal buoyancy of the pumping speed, numerical modeling was performed. The direction and approximate amplitude of the observed pumping were previously thought to be satisfactorily explained via thermal processes, but the results of the numerical modeling suggested the hypothesis that the

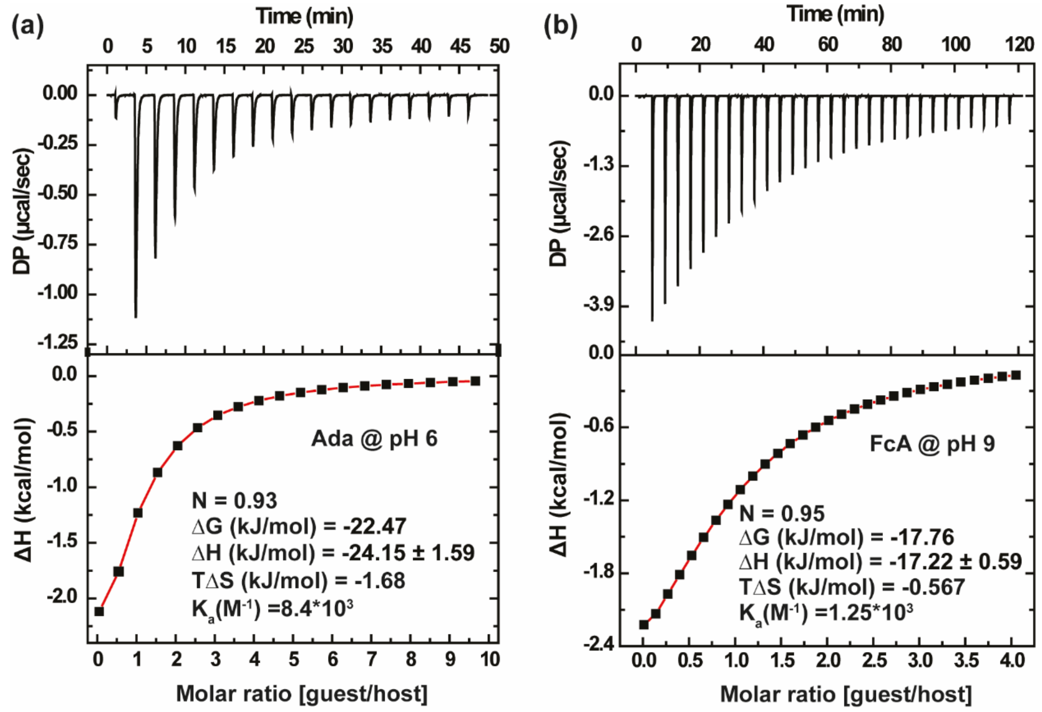

Figure 2.5. Isothermal titration calorimetry (ITC) isotherm of (a) 1-AdA (5 mM) with β-CD (100 mM) and (b) FcA (20 mM) with β-CD (1 mM) at 25 °C.

observed fluid flows were primarily driven by solutal buoyancy. To simplify the model, we considered a 2-dimensional axisymmetric geometry, where the circular patch (reaction zone) was sitting at the centre. We developed a model for the fluid flow using the Boussinesq approximation, where the density variation was assumed to affect the gravity term only. The momentum balance to compute the local fluid velocity, u, is given by

$$\rho_0\left(\frac{\partial \boldsymbol{u}}{\partial t}+\boldsymbol{u}\cdot\nabla\boldsymbol{u}\right) = -\nabla P + \mu\nabla^2\boldsymbol{u} + \rho_0 g\beta_T\left(T-T_{ref}\right)\boldsymbol{e_z} - \rho_0 g\beta_c(c-c_0)\boldsymbol{e_z} \text{ ………(1)}$$

where ρ_0 is the density at the reference temperature T_{ref} and the initial concentration c_0 of the solute in the water. The local concentration and temperature in the fluid are given by c, and T, and P denotes the local pressure. The equation took into account both the thermal and the solutal buoyancy effects, with β_T and β_c as the expansion coefficients due to temperature and concentration, respectively. No-slip condition was imposed at all the solid surfaces in the geometry.

The above equation, along with the continuity equation for an incompressible fluid, $\nabla\cdot\boldsymbol{u}=0$, governs the fluid flow. Due to the presence of the buoyancy terms in the above equation, it was strongly coupled to the energy transport equation,

$$\rho_0 C_p\left(\frac{\partial T}{\partial t}+\boldsymbol{u}\cdot\nabla T\right) = k_{th}\nabla^2 T \text{ ………….. (2)}$$

and the solutal transport equation,

$$\frac{\partial c}{\partial t} + \boldsymbol{u} \cdot \nabla c = D_i \nabla^2 c \ldots\ldots\ldots\ldots\ldots\ldots\ldots (3)$$

In the above equation, C_p was the specific heat of the fluid and k_{th} was the thermal conductivity, and both were considered to be constant. All the boundaries of the domain were no flux surfaces, except the patch region where the solute was consumed, and heat was generated due to exothermic "host-guest" reaction. The bulk diffusivity of the guest molecule in water, D_i , was assumed to be O (10^{-7} m^2/s). At the patch, the boundary condition for the consumption of guest molecule was

$$-D_i \boldsymbol{n} \cdot \nabla c = -k_r c e^{-\gamma t}$$

It indicated that the molecule diffused from the bulk was consumed at the surface, where $\boldsymbol{n}$ was the unit normal vector of the surface. The apparent rate constant k_r for the surface reaction included the resistance due to the polymer layer. The exponentially decaying term accounted for the fact that as the "guest" molecules occupied the cavity sites of β-CD, the probability of finding a favorable site decreased over time. This form of the surface reaction has been proposed based on the experimental observations. The value of γ seemed to depend weakly on the initial concentration of the "guest" molecule. It was because the probability of an unoccupied site decreased faster as the guest molecules occupied the cavity of β-CD. Also, the apparent rate constant k_r decreased with an increase in the initial concentration, possibly due to the steric hindrance at the polymeric layer. It may also be affected by the orientation of the "guest" molecule with respect to the cavity of β-CD. If the orientation is such that the insertion is not favored, then k_r can achieve a really low value leading to a smaller peak velocity.

The thermal condition at the patch was

$$-k_{th} \boldsymbol{n} \cdot \nabla \mathrm{T} = (-k_r c e^{-\gamma t}) \Delta H_{rxn}$$

As discussed in a previous study,[31-33] the solutal buoyancy contribution dominated the thermal buoyancy. A scaling analysis for the system considered in the present study indicated that the ratio of the Rayleigh numbers is

$$\frac{Ra_T}{Ra_s} = \frac{\beta_T \Delta H_{rxn}/\alpha}{\beta_s C_p \rho_0 / D} \sim O(10^{-3})$$

again indicating the negligible contribution from thermal buoyancy to the flow velocity. The enthalpy values presented earlier were used to estimate the order of magnitudes of ΔH_{rxn}. The change in density with concentration is simply given by, $\beta_s = M_w$ (molecular weight of the molecule), for example, for AdA $\beta_s = M_w = 187$ gmol^{-1}, and for FcA it is $\beta_s = M_w$=230 gmol^{-1}. We ran a few simulations with both the thermal and solutal buoyancy effects and confirmed that the presence of the thermal buoyancy in the model, though took more computational time, did not affect the velocity.

Figure 2.7 represents the contours of the x-component of the velocity vector along with the streamlines. The closed streamlines indicate recirculating flow inside the chamber. As indicated by the legend, the flow is along the positive x-axis in the upper and reverses direction in the lower half. The velocity magnitude was reduced with time as seen by comparing flow field at t = 1 min (Figure 2.7a) and t = 9min (Figure 2.7b) for 1 mM AdA. Table 2.1 denotes the effective rate parameters for the "guest" molecules used. Slightly lower values of k_r for FcA indicate its lower affinity as compared to AdA for the host site supporting the competitive binding effect hypothesis, although more systematic experimental

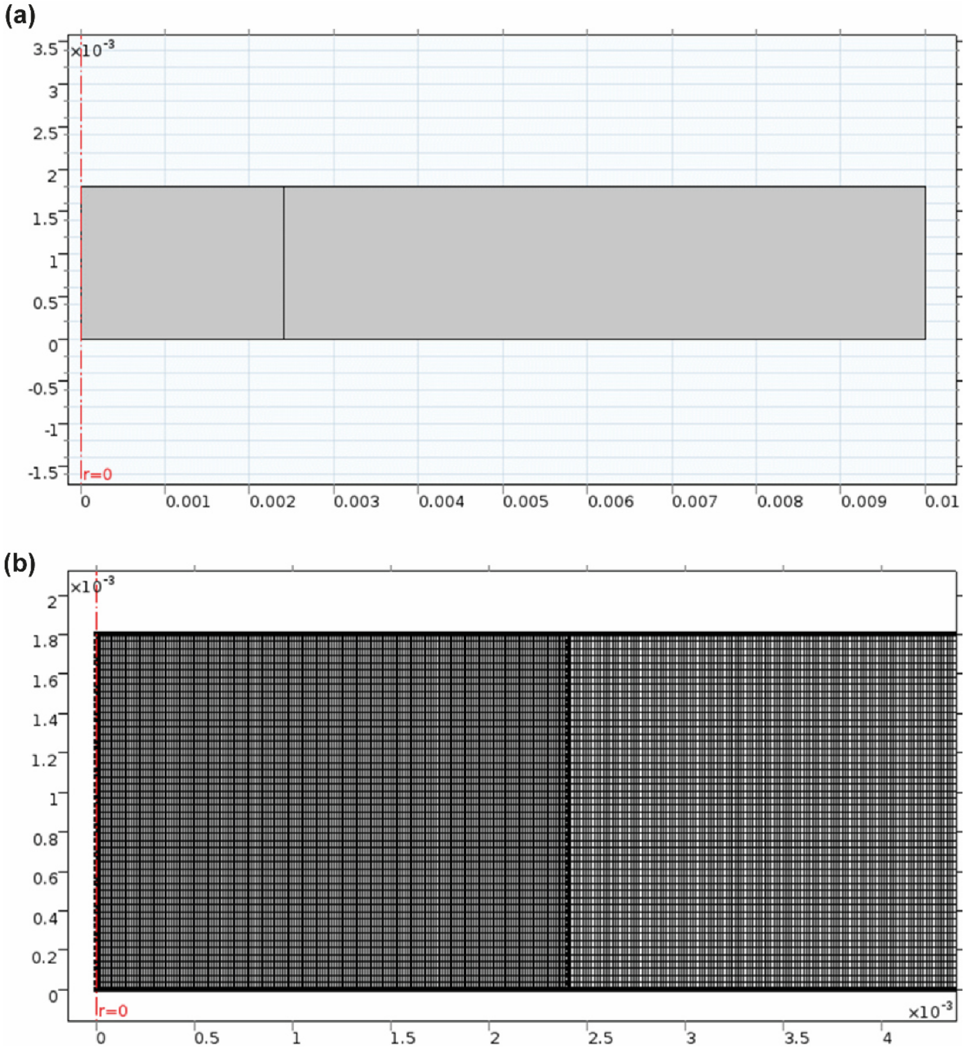

Figure 2.6. (a) Domain, and (b) Mesh used in the numerical study.

and theoretical studies are needed to affirm this observation and will be pursued in future work. The geometry is shown in figure 2.6. The model is axisymmetric with height of 1.8mm, width of 10 mm. The patch exists between center and r = 2.4mm. A mesh sensitivity test was done and a uniform mesh consisting of 50x1000 grids was found sufficient for the computations. Linear elements were used in the finite element method employed to solve the system of equations numerically.

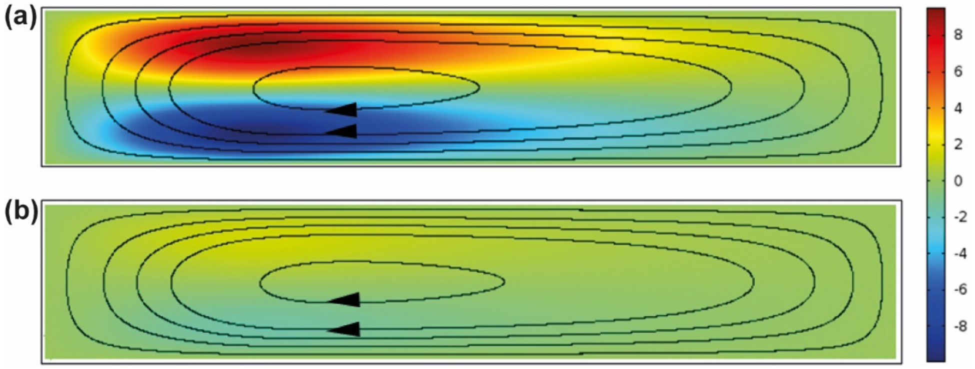

Figure 2.7. (a) Velocity contour and streamlines for 1mM AdA at t=1 min. k_r = 9x10^{-08}s^{-1}, γ = 4x0^{-03}s^{-1}, (b). Velocity contour and streamlines for 1mM AdA at t=9 min. k_r = 9x10^{-08}s^{-1}, γ = 4x10^{-03}s^{-1}.

Conc (mM)	**k_r (m/s)** **AdA**	 **FcA**	**γ (s^{-1})**
0.01	5x10^{-06}	3x10^{-06}	0.004
0.1	8x10^{-07}	5x10^{-07}	0.004
1	9x10^{-08}	7x10^{-08}	0.004
10	1.5x10^{-08}	1x10^{-08}	0.007

Table 2.1. Values of k_r and γ (effective rate parameters) used in the calculation of various cases of AdA and FcA molecules. g values are the same for AdA and FcA.

2.2.4 Effects of Number of BLs and the Guest Concentration on Fluid Velocity

To demonstrate the variation of fluid velocity with number of BLs, five sets of "host" multilayer films (1BL, 2BLs, 4BLs, 6BLs and 8 BLs) were constructed and the study was carried with a fixed concentration of "guest" molecules (1 mM). With increasing the number of BLs, the population of "host" binding sites inside the multilayer film increased. As a result, the greater number of "host- guest" complexation occurred upon addition of "guest" molecules to the multilayer film. It directly influenced the solutal buoyancy which in turn increased the tracer velocity. Figure 2.8a showed that the tracer velocity increases in both cases with the increasing number of BLs as expected. In case of AdA, 1 BL film showed a tracer velocity of 7.40±0.22 µm/s whereas the velocity raised up to 11.37±0.39 µm/s for 8 BLs. Similar trend was observed for FcA i.e., the velocity was 5.45±0.34 µm/s for 1 BL and increased up to 8.71±0.23 µm/s for 8 BLs.

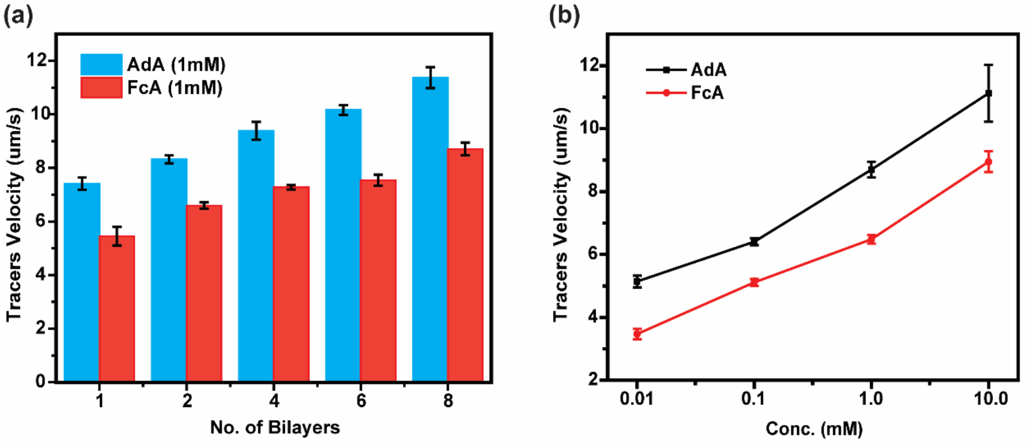

Figure 2.8. Tracer velocity with (a) varying number of BLs for AdA (1 mM) and FcA (1 mM), and (b) varying concentration of AdA@2BL film and FcA@2BL film.

Next, we were curious to know the effect of "guest" concentration on fluid velocity. We anticipated that the pumping velocity will increase with increasing the "guest" concentration as it will cause more density change in the fluid upon "host-guest" complexation. The hypothesis was examined using a 2 BLs film and the pumping behaviour was studied using four different concentrations (0.01mM, 0.1mM, 1mM and 10mM) of "guest" molecules. The plots shown in Figure 2.8b suggested that the pumping velocity increased with increasing "guest" concentration ranging from 5.14±0.18 µm/s (0.01 mM) to 11.12±0.90 µm/s (10 mM) for AdA and from 3.46±0.16 µm/s (0.01 mM) to 8.94±0.33 µm/s (10 mM) for FcA. The higher fluid velocity was the result of solutal buoyancy produced by "host-guest" complex formation with higher "guest" concentration. It is important to mention that at any given "guest" concentration, the tracer velocity was consistently higher for AdA than FcA which was attributed to the lower affinity of FcA as compared to AdA for the "host" binding site.

2.2.5 Temporal Variations in Pumping

It is expected that the "host" binding sites inside the multilayer films will be gradually occupied by "guest" molecules over time, hence it will influence the rate of the reaction which in turn will influence the tracer velocity. The temporal variation of fluid velocity was investigated using a 2 BLs film and the tracer velocity was tracked for 20 minutes at an interval of 2 minutes after injecting 1 mM "guest" to the micropump chamber. Figure 2.9a and 2.9b revealed that the velocity decreased from 8.34±0.10 μm/s (1 min) to 0.56±0.07 μm/s (17 mins) for AdA and from 6.59±0.11 μm/s (1 min) to 0.28±0.10 μm/s (17 mins) for FcA. The fluid movement came to a complete halt after 20 minutes in both cases. When 10 mM "guest" solution was added to the chamber, the fluid pumping stopped after 10 mins implying faster reaction rate at higher "guest" concentration as shown in Figure 2.9c and 2.9d. The experiment results shown in Figure 2.9 are in good agreement with the results obtained from theoretical modeling.

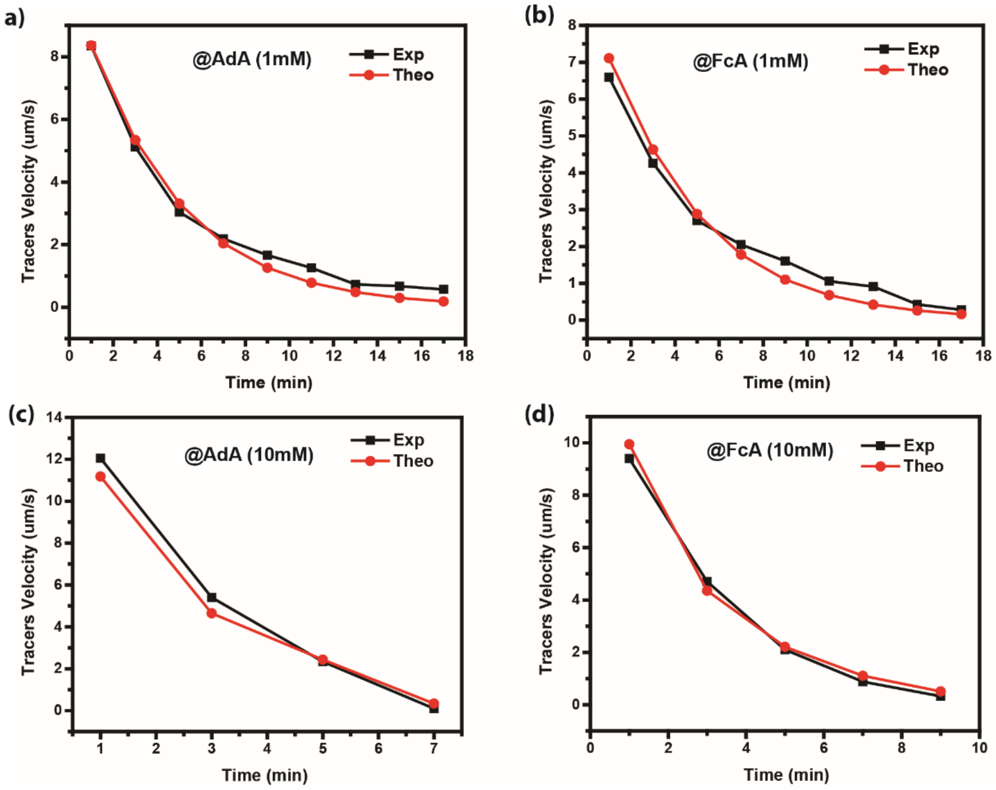

Figure 2.9. The temporal variation of fluid pumping in case of (a) AdA, (b) FcA at 1mM, and (c) AdA, (d) FcA at 10mM

2.2.6 Reusability of Supramolecular Micropump

The reversible and dynamic nature of supramolecular chemistry opens up an opportunity to design rechargeable micropump.[34, 35] As observed earlier, the fluid flow was stopped as soon as the "host" binding sites were completely occupied by "guest" molecules. To regenerate the "host" sites, it is necessary to disrupt the existing "host-guest" interactions. Previous studies have shown that the addition of organic solvents (ethanol or methanol) to the "host-guest" complex was able to displace the primary substrate from the "host" cavity as the solvent decreased the hydrophobic driving force.[36-38] In line with this hypothesis, we performed the reusability test using a 2BLs film with 1mM “guest” concentration. AdA triggered micropump showed a maximum velocity of 8.08±0.31 μm/s whereas the velocity for FcA triggered pump was 6.38±0.12 μm/s as shown in Figure 2.10a and 2.10b. The fluid flow was stopped in both cases after 20 minutes as the “host” binding sites were saturated with “guest” molecules. In order to revive the pumps, 2BLs films were soaked in ethanol for 5 minutes and were dried under a nitrogen stream for 2 minutes. This process leads to disruption of existing “host-guest” interaction leaving the “host” sites available for further binding. The recharged multilayer films were again sealed with an imaging chamber followed by addition of “guest” molecules. In both cases, the fluid flow was turned on and the maximum velocity reached 90% percent of the previous cycle. The cycle was repeated 3rd time showing a significant recovery of the fluid velocity (85 % of the first cycle). The pumping velocity of the recharged micropump was slightly less than the previous cycles because the organic solvent could not diffuse into the multilayer film during washing resulting in partial regeneration of “host” binding sites.

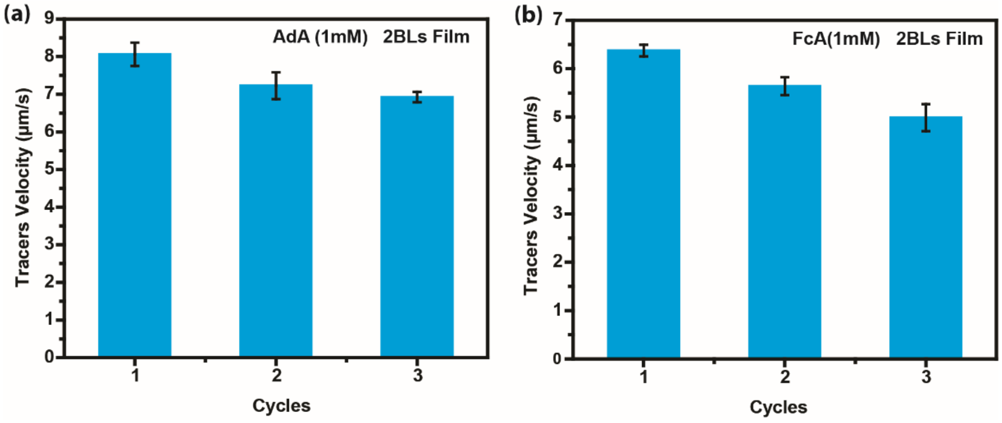

Figure 2.10. The demonstration of reusable micropump in presence of (a) AdA, and (b) FcA.

2.2.7 Autonomous Fluid Flow in Microchannels

Conventional microfluidic actuation involves complex operation and requires an external power source which restricts their usage in point-of-care systems. Supramolecular micropumps can potentially provide a solution for powerless microfluidics that can control the fluid flow by modulating noncovalent interactions. Here, we extended the reach of these autonomous pumps by exploring “host-guest” molecular recognition approach to transfer fluids over long distances across the microchannels. The objective of using this type of channel was to analyze the fluid flow through the inlet and outlet of the channel (Figure

2.11a). Rhodamine B (RhB) was used as a model dye to monitor the molecular transport that release from the "host" multilayer film. Here, we have used the competitive binding effect between "host-guest" pairs which is quite common in "host-guest" systems, and it depends on the binding constant of a particular "host-guest" pair.[39] "Guest" molecules with higher binding constant tends to occupy the cavity of β-CD molecules and it could potentially replace the pre-existing "guest" molecules with a lower binding constant. According to previous reports, AdA has a higher binding affinity for β-CD (8.4 x 10^3 M^{-1}) than the RhB (3.4 x 10^3 M^{-1}).[40,41] To demonstrate the fluid flow inside the microchannel, the "host" multilayer film was soaked in RhB (1 mM) for 30 minutes. The physically trapped and excess "guest" molecules were removed by washing with water and then dried with nitrogen stream before usage.

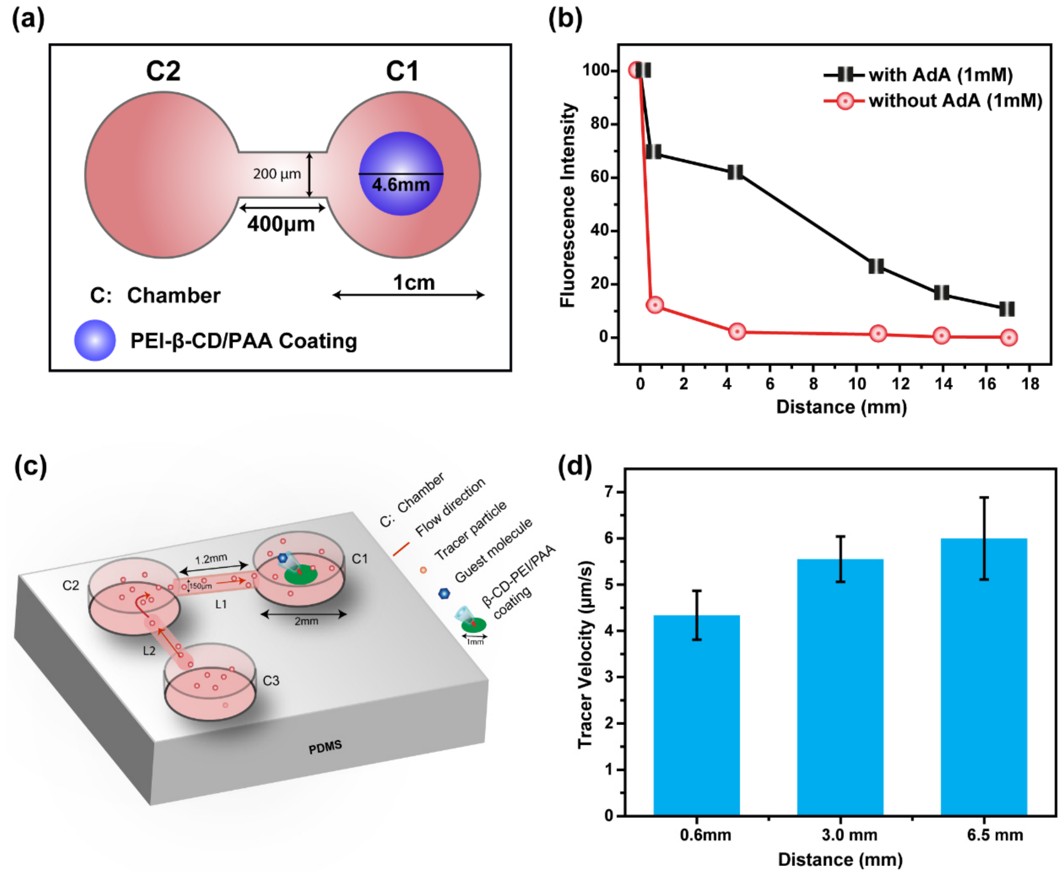

Figure 2.11. (a) Schematic representation of a channel to demonstrate dye release over long distances (20.4 mm), (b) variation of dye release at different distances from the host film with and without the addition of a competitive guest (AdA), (c) schematic representation of a channel to demonstrate the capability of moving particles over long distances (8.4 mm) and around corners, and (d) tracer velocity of moving particles at the different junctions of the L-shaped chamber.

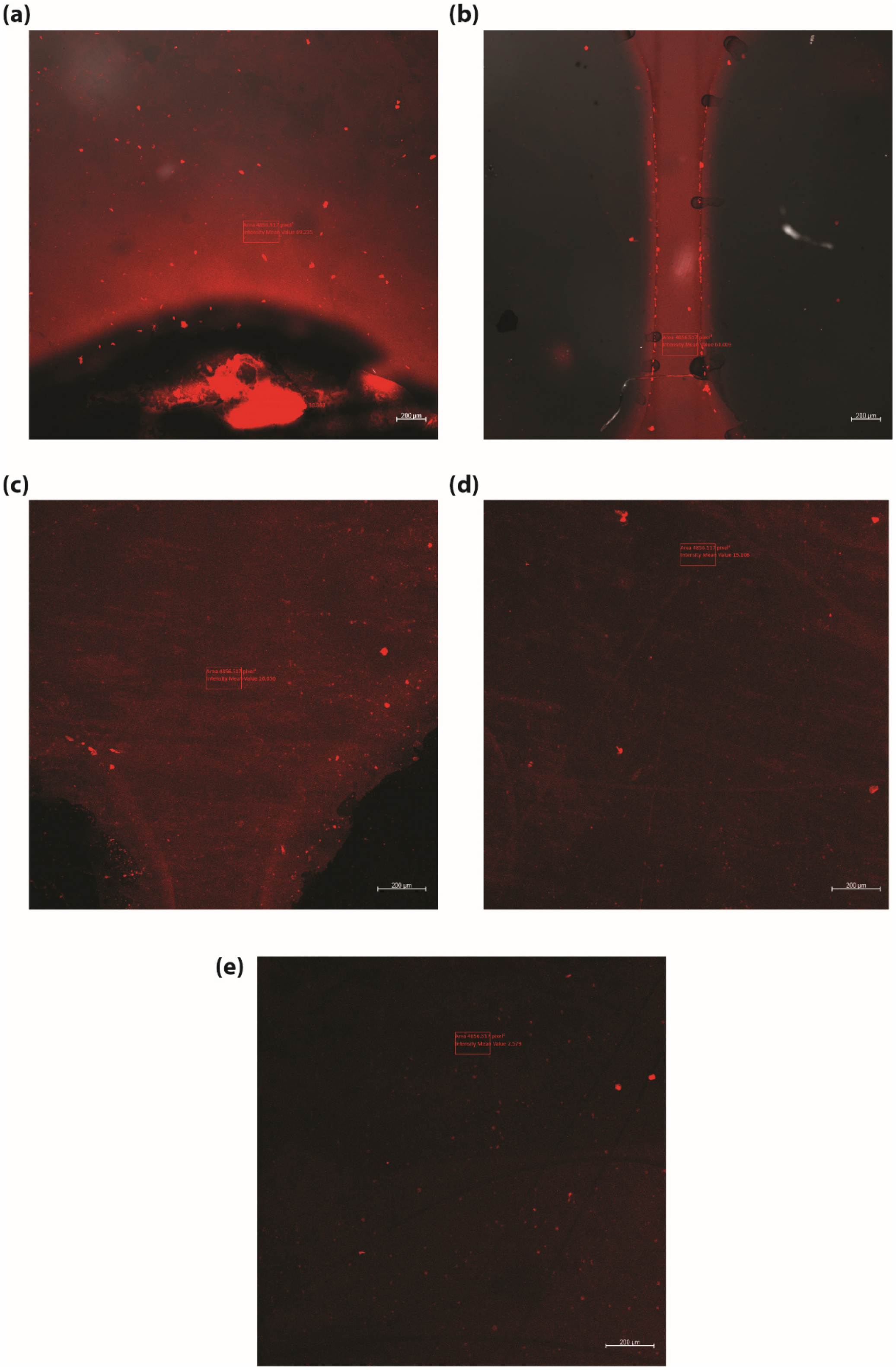

Figure 2.12. CLSM images demonstrating the release of dye after addition of AdA (1mM) showing dye intensity at different points away from the coating (a) 0.3 mm, (b) 4.5 mm, (c) 11 mm, (d) 14 mm, and (e) 17 mm.

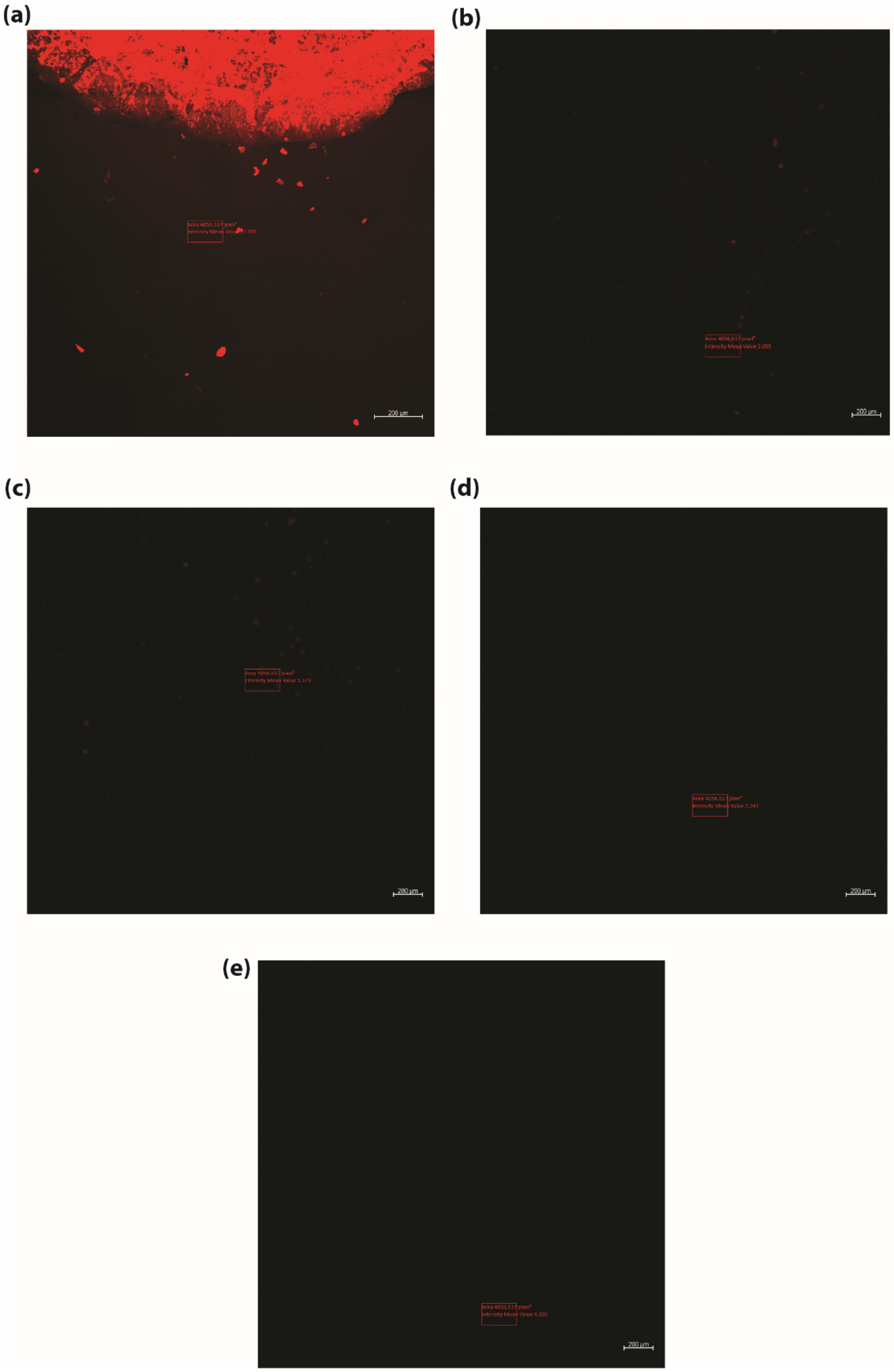

Figure 2.13. CLMS images demonstrating the release of dye after addition of aqueous solution without any competitive guest showing dye intensity at different points (a) 0.3 mm, (b) 4.5 mm, (c) 11 mm, (d) 14 mm, and (e) 17 mm.

To show the dye release, a dumbbell shaped microchannel fabricated by soft lithography was placed on the pre-soaked "host" multilayer film. The PDMS channel was made up of two 1-cm-diameter circular chambers (C1, and C2) connected by 400-μm-long, 200-μm deep connectors. Next, on injection of an aqueous solution of AdA into the chamber, the release of dye was observed under confocal laser scanning microscope (CLSM) by measuring the fluorescence intensity at different point away from the "host" multilayer film. It was observed that the dye molecules were transported from C1 chamber to C2 chamber in 5 mins and the intensity of dye decreased with distance from the "host" multilayer film as shown in Figure 2.11b and Figure 2.12. In control experiment, very negligible amount of dye release was observed without addition of competitive "guest" molecules as shown in Figure 2.11b and 2.13.

As a subsequent approach, a complex channel was designed to test colloid transport around the corners and through the inlet/outlet of the channel. For this, an L-shaped microchannel was constructed using soft lithography and the channel was made of three circular chambers (2 mm diameter; C1, C2, and C3) that were joined by connectors (L1 and L2) measuring 1.2 mm in length and 150 mm in depth. In this experiment, chamber C1 of the L-shaped channel was placed on top of a previously grown 2 BLs "host" multilayer film so that the fluid can flow across C2 and C3 chambers of the microchannel (Figure 2.11c). When the chamber was filled with "guest" solution (10mM AdA) containing polystyrene particles, the movement of particles through the entire channel (8.4 mm) was observed. The inward fluid flow that originated in chamber C1 was creating an inward fluid flux both in chamber C2 and C3. The motion in chamber C2 revealed inward flow from C3 through the inlet and outward flow towards C1 through the outlet. The velocity of the particles was 5.99±0.88 μm/s at the junction of C1-L1 connector channel and was reduced from 5.54±0.49 μm/s to 4.33±0.52 μm/s at the junctions of C2-L2 and C3-L2 connector channels respectively (Figure 2.11d). This spatial reduction of fluid velocity was due to the weaker solutal gradient from the source multilayer film as discussed earlier. The pumping ability over long distances and around the corners opens the possibility of developing microfluidic devices with complex channel architectures and complicated tasks.

2.3 Conclusions

In summary, we have successfully demonstrated a versatile approach to design non-mechanical, self-powered supramolecular micropumps based on "host–guest" molecular recognition. These micropumps were fabricated via layer-by-layer (LbL) deposition of β-CD-based host polymers, and the fluid flow was turned on after the addition of guest molecules to the multilayer films. Numerical modeling supports a buoyancy-driven pumping mechanism based on density differences between the reactants and products. The pumping velocity was adjusted by tuning the number of bilayers as well as varying the guest concentration. The thin-film based micropump was integrated into the microchannel and showed chemically powered fluid transport. This work will open a new avenue in chemically powered microfluidics for applications from single-use diagnostics to microanalysis.

2.4 Experimental Section

2.4.1 Reagents and Materials

1-Adamantylamine hydrochloride and β-CD were purchased from TCI Chemicals. Branched polyethyleneimine (bPEI; 25 kDa), polyacrylic acid (PAA; 100 kDa, 35 wt%), p-toluenesulfonyl chloride (TsCl), ferrocene, anhydrous aluminum chloride, chlorobenzoyl chloride, rhodamine B, and sulfate latex particles (5 mm in diameter), deuterated solvents (D_2O, dmso-d_6) were obtained from Sigma-Aldrich. Potassium tert-butoxide was purchased from Sisco Research Laboratories. Dimethyl sulfoxide (DMSO), dichloromethane, magnesium sulfate, hydrochloric acid and sodium hydroxide were purchased from Merck. 1,2 Dimethoxyethane was purchased from Spectrochem. DC/GEN/184 SYLGARD (PDMS Elastomer KIT) was purchased from Kevin Electrochem. Millipore water (18.2 MO cm at 25 1C) was used in all experiments.

2.4.2 Characterization

The chemical structure of tosyl-β-CD, PEI-β-CD, 2-chlorobenzoyl ferrocene and ferrocenecarboxylic acid was characterized via ^1H nuclear magnetic resonance (^1H NMR) spectra using a 400 MHz Bruker AvanceII instrument, with D_2O, DMSO-d_6, and $CDCl_3$ as the solvents. The synthesised PEI-β-CD was also characterized via FTIR spectroscopy using a Thermo Scientific instrument. The grafting level of CD was calculated according to the ^1H NMR spectrum based on proton integration. The thickness of the polymeric host multilayer film was characterized using atomic force microscopy (AFM) in the dry state. Isothermal titration calorimetric measurements were performed using a Malvern MicroCal PEAQ-ITC instrument. Videos were recorded using an inverted optical microscope (OLYMPUS IX73) with an X-Cite 120 LED Boost, via a 10X objective (CPLN10XPH), where excitation light was focused on the sample. Emission light was captured by the objective, passed through interference filters and eventually recorded at 15 frames per second using a high-resolution coloured cooled camera (DP74). Videos were recorded using the DP74 camera connected to an optical microscope at 10X. To measure the fluid-pumping velocity in each experiment, 20 tracer particles were tracked for a 30 second time interval using Tracker software (Motion Analysis Software). The dye release study was performed using a confocal laser scanning microscope (CLSM; LSM 880 NLO, Carl Zeiss, Germany) at a magnification of 5X.

2.4.3 Synthesis of PEI-β-CD

PEI-β-CD acid was synthesized according to the following two-step reaction as shown in Figure 2.14.

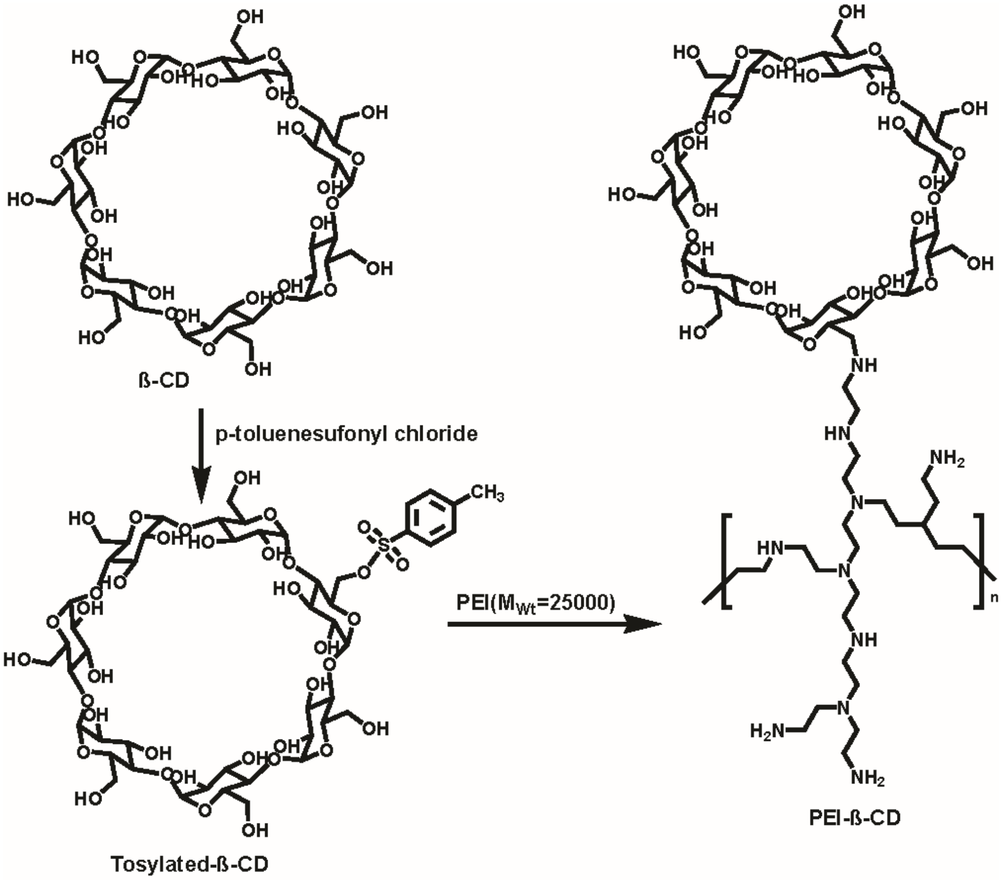

Figure 2.14. Synthesis of cyclodextrin functionalized polyethyleneimine (PEI-β-CD).

2.4.3.1 Synthesis of Mono-6-(p-Tolylsulfonyl)-β-Cyclodextrin (Ts-*O*-β-CD).

6-*O*-Ts-β-CD was prepared according to reported method[42] with little modification as shown in figure 12. 25g of β-CD was suspended in 209 mL of water and 2.73 g of NaOH in 8.75 mL of water was added dropwise to the previous solution. The suspension turned to be homogeneous. The solution was immersed into an ice-water bath, and then 6.3 g of TsCl in

12.5 mL of acetonitrile was dripped slowly. White precipitation was occurred immediately and the solution was further stirred for 2 h at 25°C. Later the suspension was cooled overnight at 4°C. Through suction filtration, the resulting precipitate was retrieved and recrystallized 3 times from hot water. The product was vacuum-dried at 50°C. Yield: 20%. ^{1}H NMR (DMSO-d_6) δ: 2.44 (s, 3H, CH_3), 3.41-3.74 (m, H-3,5,6) overlap with HOD, 4.21-4.53 (m, 6H, C6-OH), 4.80 (s, 7H, H-1 of CD), 7.43-7.77 (dd, 4H, aromatic tosyl) (Figure 2.15). m/z (ESI): calculated 1311.18; found 1311.29 $[M + Na]^+$ (Figure 2.16).

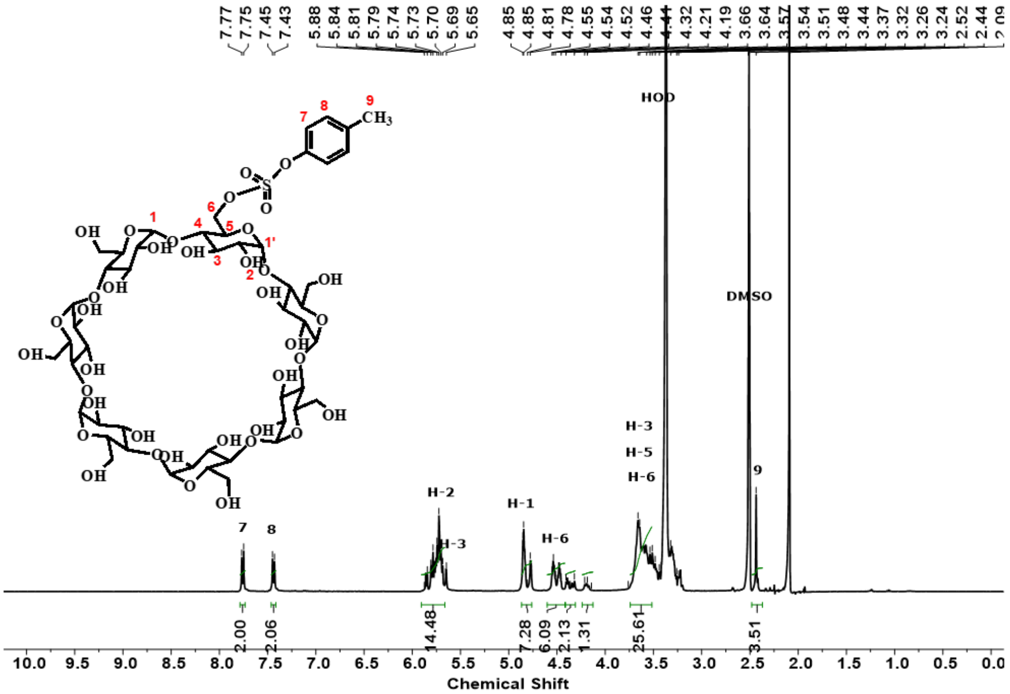

Figure 2.15. 400 MHz ^{1}H NMR spectra of Tosyl-β-CD in DMSO-d_6.

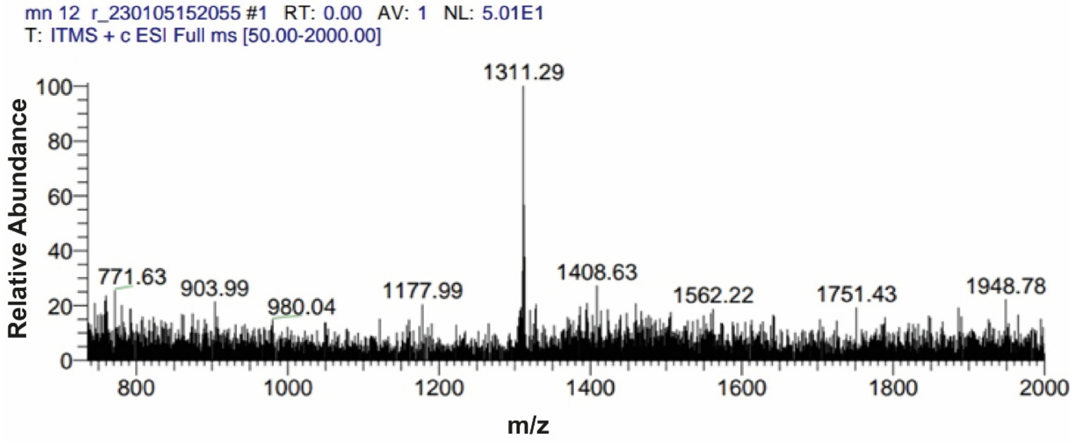

Figure 2.16. Electrospray ionization mass spectrum of Tosyl- β-CD.

2.4.3.2 Synthesis of PEI-β-CD

PEI-β-CD was prepared according to the reported procedure.[43] The procedure is shown in Figure S1. Briefly, 0.5 g of PEI in 20 ml dimethyl sulfoxide (DMSO) was reacted with 3.8 g of 6-*O*-Ts-β-CD prepared as described above. The solution was stirred in a nitrogen environment at 70°C for 3 days. After that, the product was dialyzed in water for 3 days with a MWCO 12kDa membrane. After dialysis, PEI-β-CD was obtained by freeze-drying. Yield: 35% The β-CD grafting level per PEI chain was analyzed by ^{1}H NMR (D_2O) is approximately 7.91%. δ: 4.99 (s,7H, H(e) of CD), 3.81 (m, 28H, H(a), H(c), H(f) of CD), 3.58 (m, 14H, H(b) and H(d) of CD), 2.33-2.76 (m, 78, methylene of $-CH_2CH_2$-) (Figure 2.17). From the integrated area of (S1) of H1 of β-CD and the integrated peak area (S2) of PEI from 2.76 to 2.33, the degree of β-CD substitution (DS) to PEI was calculated according to the following formula[44] : **DS= (S1/7)/ [(S2-S1)/4]**

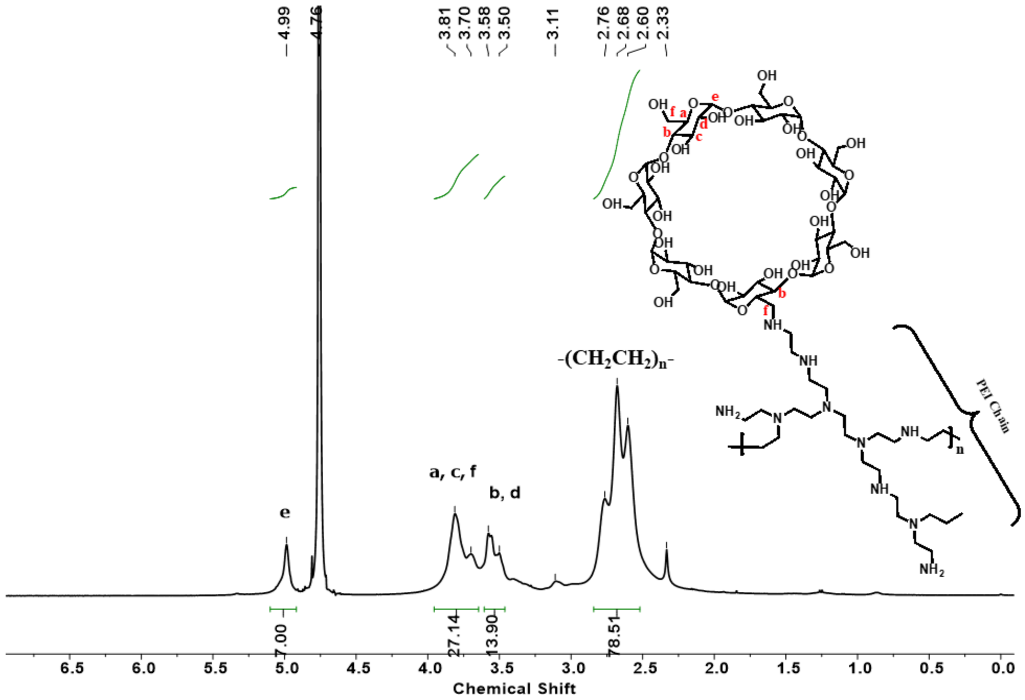

Figure 2.17. 400 MHz ^{1}H NMR spectra of PEI-β-CD in D_2O.

The distinctive adsorption peaks of β-CD are at 1030 cm^{-1} (C–O stretching vibration involving ether linkage in glucose unit), 944 cm^{-1} (skeletal vibration involving α-1,4 linkage), 756 cm^{-1} (ring breathing vibration), and 577 cm^{-1} (pyranose ring vibration) in the FTIR spectrum. The four adsorption bands mentioned above appeared at the corresponding positions in the β-CD PEI spectra but were absent in the PEI spectrum, confirming that β-CD had been covalently grafted onto PEI as shown in Figure 2.18.

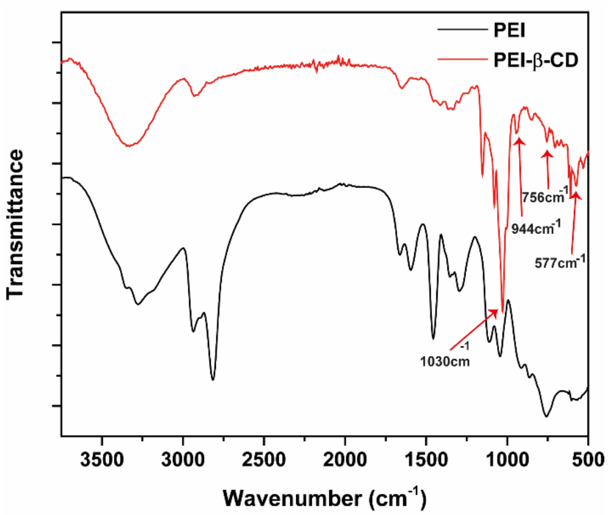

Figure 2.18. FTIR spectra of β-CD, PEI, and β -CD-PEI.

2.4.4 Synthesis of Ferrocenecarboxylic Acid

Ferrocenecarboxylic acid was synthesized according to the following two-step reaction (Figure 2.19) and characterized by ^{1}H NMR with $CDCl_3$ and DMSO-d_6 as the solvents (Figure 2.20 and 2.21).[45]

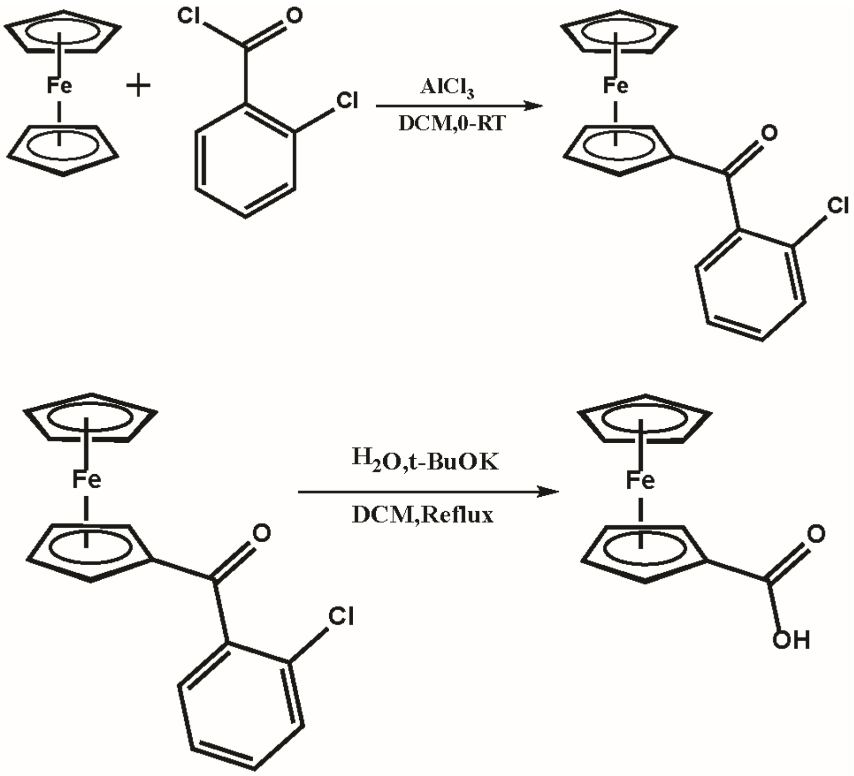

Figure 2.19. Synthesis of ferrocenecarboxylic acid.

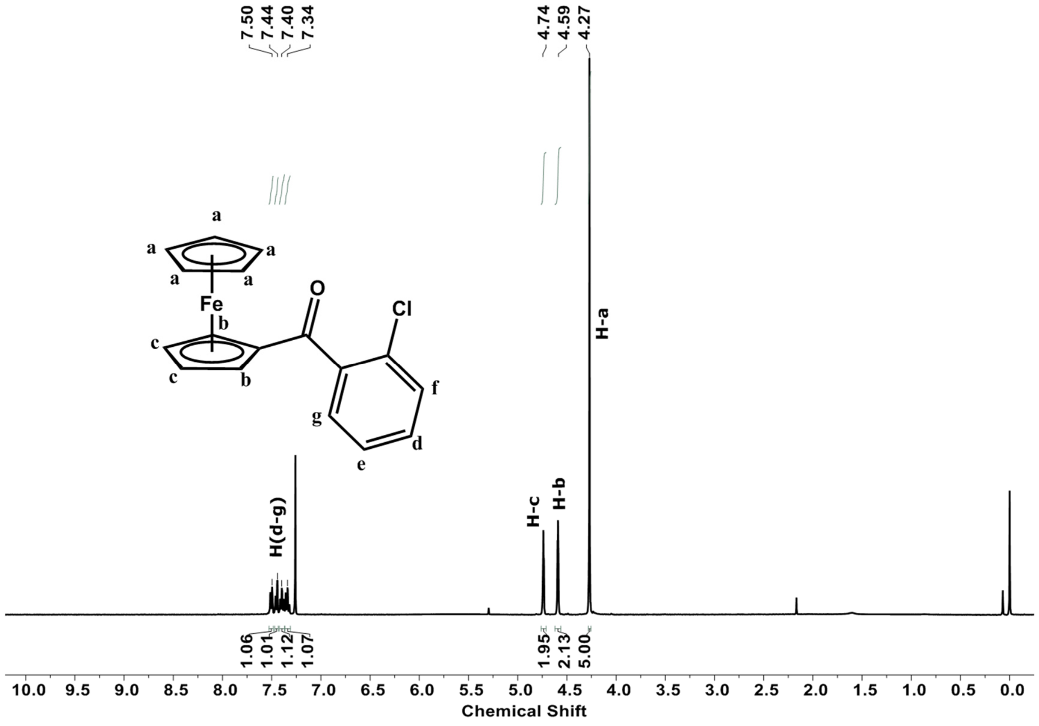

Figure 2.20. ^{1}H NMR spectra of 2-chlorobenzoyl ferrocene in $CDCl_3$.

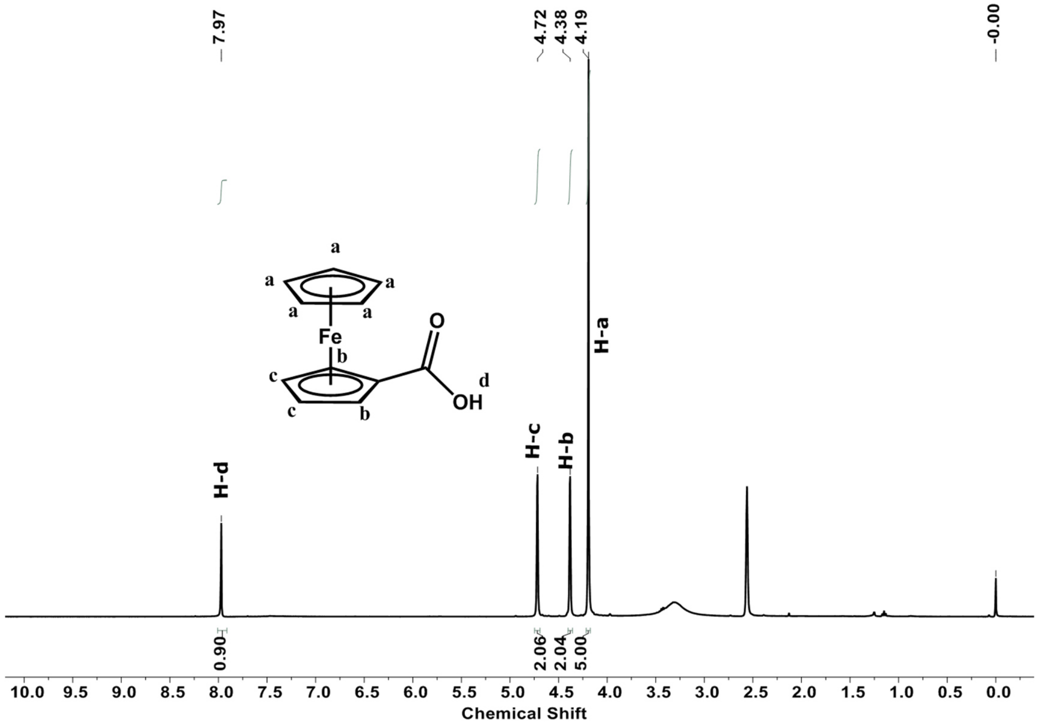

Figure 2.21. 400MHz ^{1}H NMR spectra of ferrocenecarboxylic acid in DMSO-d_6.

2.4.5 Substrate

Glass slides and silicon wafers were used as a substrate to fabricate the multilayer films. Silicon wafers were used as a substrate for measuring the thickness of the film. The PDMS elastomer was prepared by combining Sylgard 184 in a ratio of 10:1 by weight of oligomeric base to curing agent and casting onto a plastic Petri plate. The prepolymer PDMS was allowed to settle for 2 hours in a convection oven at 70°C. All glass slides and silicon wafers were cleaned using piranha solution for 45 min, and then rinsed with DI water before deposition. *Beware! Piranha solution responds violently to organic materials and requires careful handling*.

2.4.6 Pattern of Multilayer Film and Tracking the Fluid Flow

Initially a thin layer of PDMS sheet containing a small circular opening of 4.6 mm diameter in the middle was created and it was placed on the glass surface in such a way that the circular opening stayed in the middle of the slide. The same slide was used as a substrate for subsequent LbL deposition for the desired number of cycles. Since LbL deposition results in conformal coating, the entire slide was coated with the polymer film. After achieving the preferred number of bilayers, the PDMS sheet was peeled away to reveal the film pattern leaving the covered area uncoated. The surface was thoroughly washed with water followed by a jet of nitrogen gas. Next, the pattern was covered by an air-tight imaging chamber (l = 1 cm, b = 1 cm, h = 1.8 mm) and an aqueous suspension of guest molecules along with 5-mm-diameter neutral charged non-interacting polystyrene particles (tracer particles) were injected into the chamber. The entire set up was examined using an optical microscope and videos were captured for further analysis using the Tracker software. The flow velocity was measured based on analysis of the motion of the tracer particles that were imaged using digital cameras, which is the standard measurement technique in fluid dynamics research. To measure the fluid pumping velocity in each experiment, 20 tracer particles were tracked for a 30 second time interval using the Tracker software.

2.4.7 Fabrication of Microfluidic Device

Microfluidic channels were manufactured by soft lithography.[46] First, the master framework was designed using CleWin software. Next, a photoresist SU-8 2100 was then spin-coated on a 4 x 4 silicone wafer, and the pattern was transferred to the wafers using maskless photolithography (Durham Magneto Optics Maskless MicroWriter ML3). A further step is to dip the surface into the developer followed by rinsing with 2-propanol. Later the patterned surface was baked for 2 mins to stabilize the structure. Next, PDMS 184 SYLGARD was poured onto the wafer with a curing agent at a ratio of 10:1(w / w) and degassed in a vacuum desiccator until the trapped air bubbles were released. The device was put in an oven for 1 hour at 60°C. When dried, the microchannels formed on the PDMS mold were removed from the wafer and was punctured with a 2 mm diameter biopsy punch. Then, as prepared channel was used to demonstrate the powerless fluid flow through microchannel.

2.4.8 Isothermal Titration Calorimetry

Thermodynamic parameters for 1-AdA-β-CD and FcA-β-CD complexation in solution were carried out by isothermal titration calorimetry by using Malvern MicroCal PEAQ-ITC in aqueous at 25.0 ° C with a constant rate of 200rpm at different pH. The 5.0 mM Ada-NH_2-HCl (pH 6) solution in the syringe has been titrated into the 100 μM β-CD in the calorimeter cell involved 19 sequential 2 μL injections at a time interval of 150. For Fc-COOH, the solution of 20.0 mM Fc-COOH (pH 9) in the syringe was titrated into the solutions of 1.0 mM β-CD in the calorimeter cell involved 30 sequential 1.3 μL injections at a time interval of 200 s. All control experiments were performed by using the same injections into aqueous under same conditions (for the heat of dilution).

Note: The permission has been granted by authors and corresponding author of the published paper prior to its adoption in the present thesis. The publication associated with this work is:

Mujeeb Alam, Arshdeep Kaur Gill, Rohit Varshney, Chirag Miglani, Naveen Tiwari and Debabrata Patra. Polymer multilayer films regulate macroscopic fluid flow and power microfluidic devices via supramolecular interactions. ***Soft Matter***, 2022, **18**, 5605-5614.

2.5 References

1. C. Zhou, H. Zhang, Z. Li and W. Wang, *Lab Chip*, 2016, **16**, 1797–1811.
2. G. A. Ozin, I. Manners, S. Fournier-Bidoz and A. Arsenault, *Adv. Mater.*, 2005, **17**, 3011 3018.
3. H. Wang and M. Pumera, *Chem. Rev.*, 2015, **115**, 8704–8735.
4. B. D. Iverson and S. V. Garimella, *Microfluid. Nanofluid.*, 2008, **5**, 145–174.
5. X. Wang, D. Zhao, D. T. T. Phan, J. Liu, X. Chen, B. Yang, C. C. W. Hughes, W. Zhang and A. P. Lee, *Lab Chip*, 2018, **18**, 2167–2177.

6. A. Piovesan, T. Van De Looverbosch, P. Verboven, C. Achille, C. A. Parra-Cabrera, E. Boller, Y. Cheng, R. Ameloot and B. Nicolaı¨, *Lab Chip*, 2020, **25**, 1961–1974.
7. V. T. Upaassana, S. Ghosh, A. Milleman, T. Nguyen and C. H. Ahn, *Lab Chip*, 2020, **20**, 1961–1974.
8. C. Zhang, D. Xing and Y. Li, *Biotechnol. Adv.*, 2007, **25**, 483–514.
9. L. Dong and H. Jiang, *Soft Matter*, 2007, **3**, 1223–1230.
10. G. Sinawang, M. Osaki, Y. Takashima, H. Yamaguchi and A. Harada, *Polym. J.*, 2020, 1–21.
11. C. Li, A. Iscen, L. C. Palmer, G. C. Schatz and S. I. Stupp, *J. Am. Chem. Soc.*, 2020, **18**, 8447–8453.
12. I. Altinbasak, M. Arslan, R. Sanyal and A. Sanyal, *Polym. Chem.*, 2020, **11**, 7603–7624.
13. G. Wu, S. Sun, X. Zhu, Z. Ma, Y. Zhang and N. Bao, *Angew. Chem., Int. Ed.*, 2022, **61**, e202115559.
14. S. Sa´nchez, L. Soler and J. Katuri, Angew. *Chem., Int. Ed.*, 2015, **54**, 1414–1444.
15. W. Wang, T.-Y. Chiang, D. Velegol and T. E. Mallouk, *J. Am. Chem. Soc.*, 2013, **135**, 10557–10565.
16. X. Lin, T. Si, Z. Wu and Q. He, *Phys. Chem. Chem. Phys.*, 2017, **19**, 23606–23613.
17. S. Sengupta, M. E. Ibele and A. Sen, *Angew. Chem., Int. Ed.*, 2012, **51**, 8434–8445.
18. H. Zhang, K. Yeung, J. S. Robbins, R. A. Pavlick, M. Wu, R. Liu, A. Sen and S. T. Phillips, *Angew. Chem., Int. Ed.*, 2012, **51**, 2400–2404.
19. A. A. Farniya, M. J. Esplandiu, D. Reguera and A. Bachtold, *Phys. Rev. Lett.*, 2013, **111**, 168301.
20. L. Liu, Y. Dong, Y. Sun, M. Liu, Y. Su, H. Zhang and B. Dong, *Nano Res.*, 2016, **9**, 1310–1318.
21. Y. Tu, F. Peng, J. M. Heuvelmans, S. Liu, R. J. Nolte and D. A. Wilson, *Angew. Chem.*, 2019, **131**, 8779–8783.
22. M. Cheng, D. Zhang, S. Zhang, Z. Wang and F. Shi, *CCS Chem*, 2019, **1**, 148–155.
23. P. Bertrand, A. Jonas, A. Laschewsky and R. Legras, *Macromol. Rapid Commun.*, 2000, **21**, 319–348.
24. P. T. Hammond, *Adv. Mater.*, 2004, **16**, 1271–1293.
25. Y. Wang, A. S. Angelatos and F. Caruso, *Chem. Mater.*, 2008, **20**, 848–858.
26. A. K. Gill, Sk Riyajuddin, M. Alam, K. Ghosh and D. Patra, *Eur. Polym. J.*, 2020, **124**, 109455.

27. J. Nakvinda, B. Gruner, D. Gabel, W. M. Nau and K. I. Assaf, *Chem. – Eur. J.*, 2018, **49**, 12970–12975.
28. S. H. Pun, N. C. Bellocq, A. Liu, G. Jensen, T. Machemer, E. Quijano, T. Schluep, S. Wen, H. Engler and J. Heidel, *Bioconjugate Chem.*, 2004, **15**, 831–840.
29. R. Varshney, M. Alam, C. Agashe, R. Joseph and D. Patra, *Chem. Commun.*, 2020, **56**, 9248–9287.
30. A. K. Gill, R. Varshney, M. Alam, C. Agashe and D. Patra, *ACS Appl. Bio. Mater.*, 2021, **4**, 6203–6208.
31. K. Gentile, S. Maiti, A. Brink, B. Rallabandi, H. A. Stone and A. Sen, *Langmuir*, 2020, **36**, 7948–7955.
32. I. O. Rivera, H. Shum, A. Agarwal, A. Sen and A. C. Balazs, *Proc. Natl. Acad. Sci. U. S. A.*, 2016, 10, 2585–2590.
33. B. M. Tansi, R. K. Manna, O. E. Shklyaev, M. L. Peris, A. C. Balazs and A. Sen, *ACS Appl. Mater. Interfaces*, 2021, **13**, 6870–6878.
34. J.-M. Lehn, *Chem. Soc. Rev.*, 2007, **36**, 151–160.
35. D. Patra, H. Zhang, S. Sengupta and A. Sen, *ACS Nano*, 2013, **7**, 7674–7679.
36. D. Shetty, I. Jahovic, J. Raya, Z. Asfari, J.-C. Olsen and A. Trabolsi, *ACS Appl. Mater. Interfaces*, 2018, **10**, 2976–2981.
37. A. Alsbaiee, B. J. Smith, L. Xiao, Y. Ling, D. E. Helbling and W. R. Dichtel, *Nature*, 2016, **529**, 190–194.
38. Y.-L. Kang, J. Zhang, G. Wu, M.-X. Zhang, S.-C. Chen and Y.- Z. Wang, *ACS Sustainable Chem. Eng.*, 2018, **6**, 11783–11792.
39. F. Chandra, K. Pal and A. L. Koner, *Chemistry Select*, 2016, **19**, 6156–6159.
40. M. V. Rekharsky and Y. Inoue, *Chem. Rev.*, 1998, **98**, 1875–1917.
41. S. Panagiotakis, E. Saridakis, M. Malanga, I. M. Mavridis and K. Yannakopoulou, *Chem. – Asian J.*, 2021, **16**, 1–11.
42. R. C. Petter, J. S. Salek, C. T. Sikorski, G. Kumaravel, F. T. Lin, *J. Am. Chem. Soc.*, 1990, **112**, 3860–3868.
43. S. H. Pun, N. C. Bellocq, A. Liu, G. Jensen, T. Machemer, E. Quijano, T. Schluep, S. Wen, H. Engler, J. Heidel, *Bioconjugate chem.*, 2004, **15**, 831-840.
44. X. J. Han, Z.-Q. Dong, M.-M. Fan, Y. Liu, J.-H. Li, Y.-F. Wang, Q.-J. Yuan, B.-J. Li, S. Zhang, *Macromol. Rapid. Commun.*, 2012, **33**, 1055-1060.
45. P. C. Reeves, *Org. Synth.*, 1977, **56**, 28.
46. J. Wan, *Polymers*, 2012, **4**, 1084–1108.

Chapter 3

pH Responsive Supramolecular Micropump Regulate Reversal Flow

3.1 Introduction

Programmable fluid flow is an essential prerequisite for fabricating lab-on-a-chip devices.[1–4] Conventional approaches actuate fluids in several ways such as electrostatically,[5] pneumatically,[6] thermopneumatically,[7] and electromagnetically.[8] Intricate construction and requirement of external power sources make these systems ineffective for routine usage. In recent years, self-powered micropumps that do not use any mechanical actuators for flow generation have shown great promises due to their simplistic design, easy operation protocol and on-demand miniaturization.[9–12] Pioneer work by Sen et al.[13–16] have shown that surface-immobilized catalysts can harness chemical energy to create directional fluid flow in the presence of specific fuels. Later, we[17] and others[18] developed catalyst-free micropumps using supramolecular motifs, and the fluid flow was triggered by ‘‘host–guest’’ molecular recognition. The exothermic nature of the ‘‘host–guest’’ assembly was the key to generate a density gradient that was responsible for the thermal convective flow.[17] In all cases the fluid flow was unidirectional, i.e., the fluid moves either towards the micropumps or away from these microscale engines. For the fabrication of next generation point-of-care devices, it is important to create a platform where the flow direction can be switched on demand without using a mechanical valve. This area of self-powered microfluidic technology has not been realized so far. The reversible and dynamic nature of supramolecular interactions may play a pivotal role to create such dynamic platforms for regulating the valveless fluid flow.[19–23] Most importantly, the supramolecular functionalities can be integrated into the microfluidic device, where the fluid flow will be modulated by noncovalent interactions.

In view of developing the valveless flow reversal, herein, we have designed pH responsive supramolecular micropumps using ‘‘host–guest’’ molecular recognition between β-cyclodextrin (β-CD) and benzimidazole (BzI). The soft gel-based micropump triggered autonomous fluid flow due to the ‘‘host–guest’’ assembly; however, the flow direction was reversed under acidic conditions as a result of the ‘‘host–guest’’ disassembly. To demonstrate the practical utility, these gel-based micropumps were placed inside a complex microchannel and it showed pH responsive flow switching over long distances.

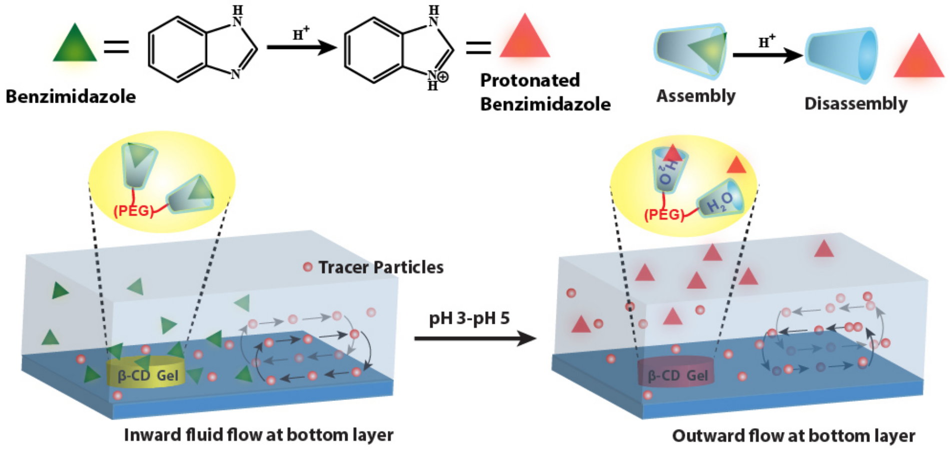

Figure 3.1. Schematic of fluid flow reversal caused by the ‘‘host–guest’’ assembly and disassembly between β-CD and BzI.

3.2 Results and Discussions

3.2.1 Guest Induced Micropump Study

To examine the feasibility of pH-responsive supramolecular micropumps, a β-CD-based scaffold was used as the ‘‘host’’ binding site and benzimidazole was used as the ‘‘guest’’ molecule. Usually, in neutral aqueous solutions, non-polar BzI enters the hydrophobic cavity of β-CD and forms a 1:1 inclusion complex due to hydrophobic interactions. However, in an acidic environment, BzI gets protonated and the binding constant between BzI and β-CD drastically reduces.[24–26] It leads to the disassembly of the supramolecular complex (Figure 3.1). In line with this observation, we synthesized a β-CD-PEG gel as a ‘‘host’’ scaffold for the micropump (see experimental section). To demonstrate the pumping activity, a small piece of the β-CD-PEG gel (1 mm x 1mm x 1 mm) was placed on the middle of a glass slide, and the gel piece was covered with an imaging chamber (l = 1 cm, b = 1 cm, and h = 1.8 mm). The ‘‘guest’’ solution was prepared by mixing BzI in an aqueous solution (1 mM; pH = 7) along with tracer particles (5 mm diameter). The solution mixture was injected into the chamber by syringe, and the entire set up was placed under a microscope to study the motion of the tracer particles. The tracer particles showed an inward motion with a velocity of 2.15±0.59 μms^{-1} towards the gel when observed at the bottom layer (450 mm above the surface) as shown in Figure 3.1 (see also Figure 3.2a). Simultaneously, an outward motion away from the gel was also observed when viewed at the top layer, and this entire process resulted in a convective flow inside the closed chamber. In a control experiment, an aqueous suspension of tracer particles was injected into the chamber containing the ‘‘host’’ gel. No directional motion was observed confirming that the ‘‘host–guest’’ assembly was the key to trigger the fluid flow (Figure 3.2b).

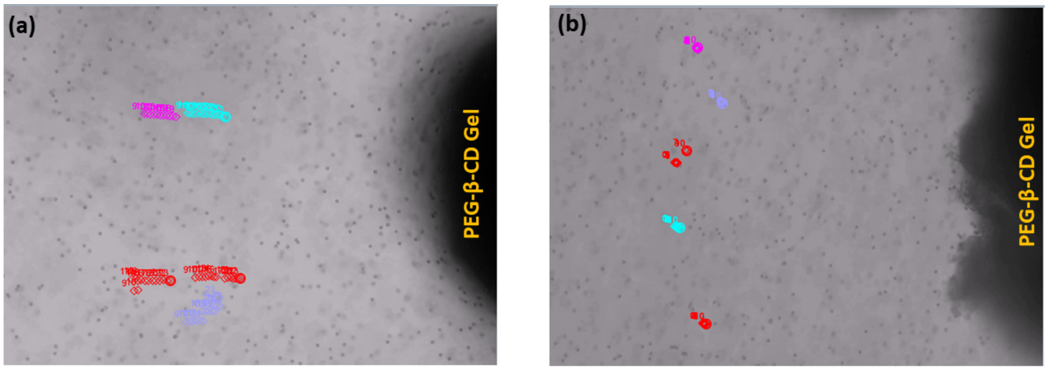

Figure 3.2. Tracer particles trajectories: directional flow as a result of “host-guest” recognition between BzI and β-CD, and (b) no flow in the presence of water.

3.2.2 Mechanism of Fluid Pumping

The formation of the inclusion complex between β-CD and benzimidazole is an enthalpy driven process, and the fluid flow is the result of thermal buoyancy produced by the heat released during ‘‘host–guest’’ recognition. An isothermal titration calorimetry (ITC)

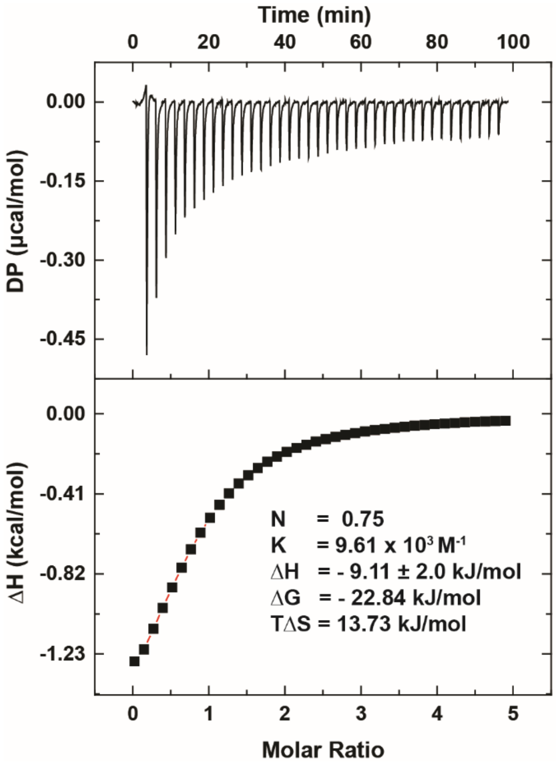

Figure 3.3. Isothermal Titration Calorimetry (ITC) isotherm of BzI (10mM) with β-CD (200 µM) at 25°C.

study was performed to investigate the thermodynamic parameters involved in this recognition process. It showed that the ‘‘host–guest’’ complex was thermodynamically stable with a binding constant of 9.61×10^3 M^{-1} and the heat released per complexation was -9.11±2.0 kJ mol^{-1} (Figure 3.3). As previously described, thermal buoyancy may generate a density-driven flow around the gel. On the other hand, our recent work on self-powered micropumps suggested that solutal buoyancy played a role in the density-driven flow.[27] To confirm that the density driven flow arises from solutal buoyancy, the micropump chamber was inverted such that the direction of gravity was reversed according to the position of the pump. In this case, the fluid flow direction was reversed as predicted, i.e., the flow was away from the edge of the gel when observed at the bottom layer (Figure 3.4a). It confirmed the density-driven flow of these supramolecular pumps. The “host-guest” assembly of β-CD-PEG gel and BzI was confirmed with the help of UV-Visible spectroscopy where a small piece of “host-guest” assembled gel was placed between two quartz slides and the absorbance of the gel demonstrated a characteristic absorption of benzimidazole (Figure 3.4b).

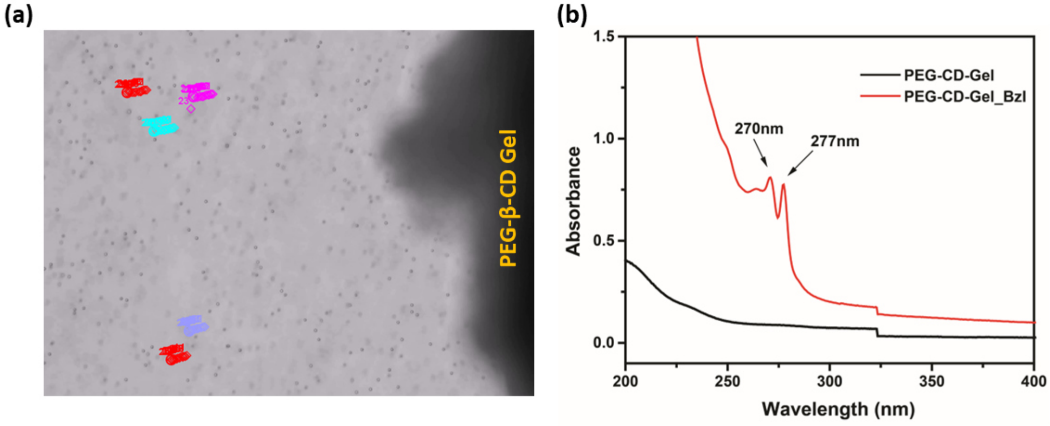

Figure 3.4. (a) Reverse flow in an upside-down configuration of micropump chamber, and (b) absorption spectra of β-CD-PEG gel pre-assembled with BzI.

3.2.3 pH Responsive Behaviour of Micropump

To demonstrate the pH responsive behaviour of the micropump, a small piece of the β-CD-PEG gel pre-soaked with BzI was placed on a glass slide, and the pump chamber was fabricated as discussed earlier. Upon injecting the acidic water (pH 3) into the chamber, a reverse flow of tracer particles was observed, i.e., the tracer particles were moving away from the gel when observed at the bottom layer of the glass slide (Figure 3.5a), and the fluid velocity was 3.18±0.20 μms^{-1}. This is due to the disassembly of the ‘‘host–guest’’ complex upon the protonation of BzI proton. The ITC study showed that the disassembly is an endothermic process (Figure 3.5c), which created the flow in the opposite direction compared to prior observation. As a control experiment, the tracer particles at pH 3 were injected into the β-CD-PEG gel chamber. It was observed that the tracer particles were moving very slowly towards the gel at a velocity of 0.59 μms^{-1} (Figure 3.5b). This inward motion possibly arises from the expansion of the gel due to change in the ionic strength of the medium. This was further concluded by UV-Visible spectroscopy where a small piece of the gel pre-soaked with ‘‘guest’’ molecules was placed inside a cuvette, and the solution pH was maintained at three different values 3, 4, and 5. This resulted in the release of BzI from the β-CD cavity, later confirmed by the absorbance at 277 nm (Figure 3.6a, b, c, d).

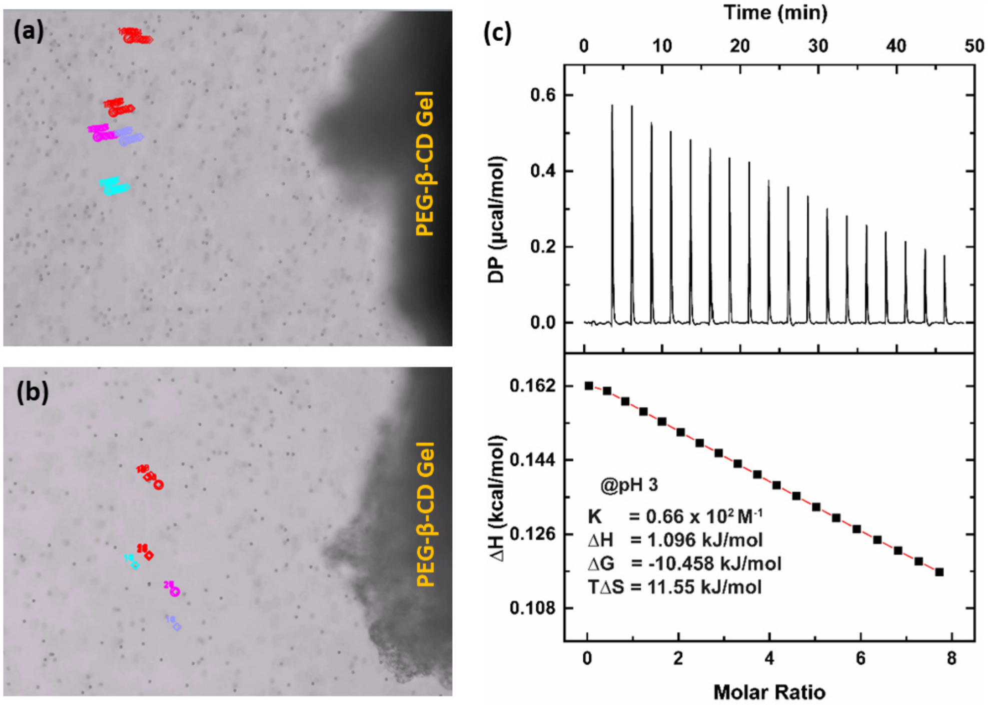

Figure 3.5. (a) Reverse flow as a result of “host-guest” disassembly, (b) no flow in the presence of water (pH<5), and (c) Isothermal Titration Calorimetry (ITC) isotherm of β-CD (150 μM) pre-soaked with BzI (50mM) at 25°C.

3.2.4 Effect of Concentration and pH on “Host-Guest” Assembly and Disassembly

The effect of ‘‘guest’’ concentration on tracer velocity was studied using three different concentrations of BzI (1 mM, 10 mM, and 20 mM). As the ‘‘guest’’ concentration increases, it produces a greater number of ‘‘host–guest’’ complexes, which corresponds to higher density change. It directly contributes to the solutal buoyancy, hence the fluid velocity. As shown in Figure 3.7a, the velocity increased linearly with the increase in the ‘‘guest’’ concentration varying from 2.15±0.59 μms^{-1} (1 mM) to 10.11±1.27 μms^{-1} (20 mM). Similarly, to investigate the role of pH in fluid pumping, the experiment was performed at

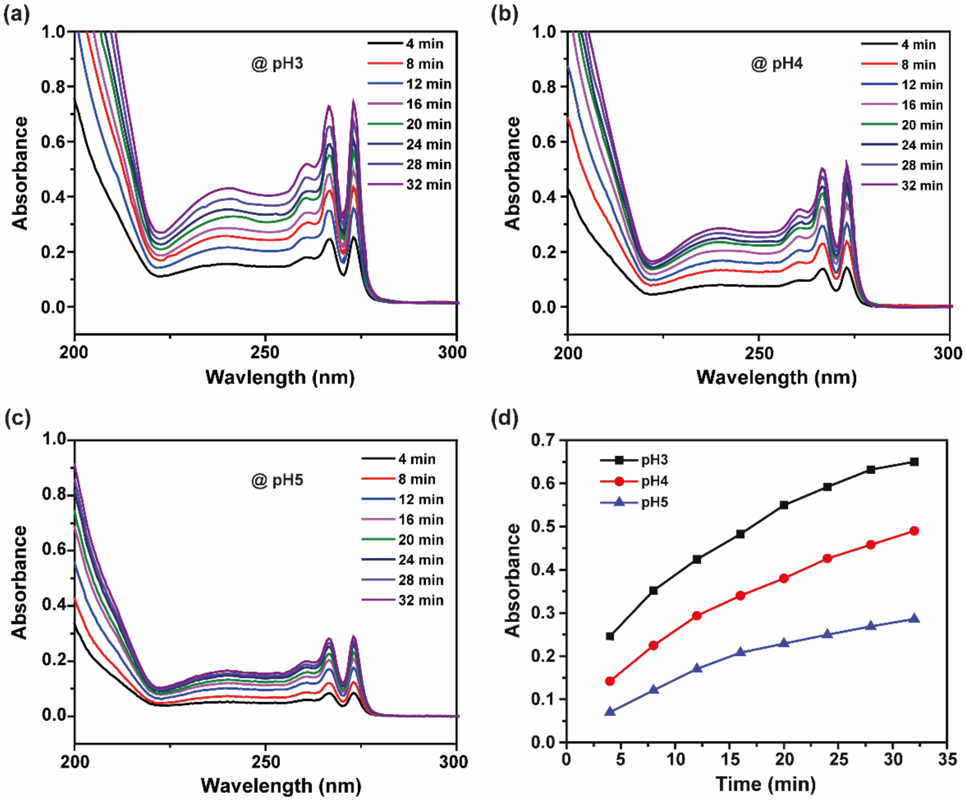

Figure 3.6. Absorption spectra of β-CD-PEG gel pre-assembled with BzI on addition of acidic water at (a) pH3, (b) pH4, (c) pH5, and (d) with time at pH3, pH4, pH5.

three different pH values, i.e., pH 3, pH 4 and pH 5 (Figure 3.7b). As discussed earlier, lowering pH will protonate the BzI proton, which resulted in the dissolution of the ‘‘host–guest’’ complex (Figure 3.6). Figure 3.7b shows the decreasing trend of the tracer velocity with the increase in pH values, i.e., from 3.14±0.54 μms^{-1} (pH 3) to 1.52±0.23 μms^{-1} (pH 5). This suggested that the release rate of BzI from the β-CD cavity was greatly enhanced at lower pH values possibly due to the higher degree of protonation of BzI protons.

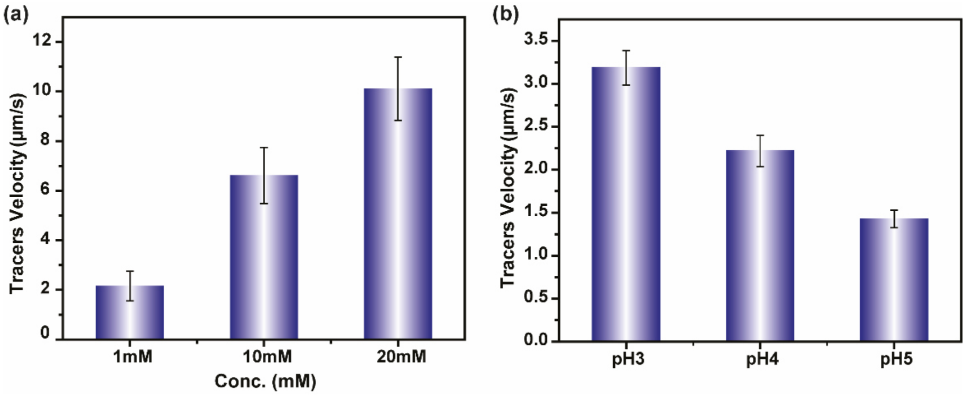

Figure 3.7. (a) Tracer velocity with varying (a) concentrations of Bzi; (b) pH values with the addition of the acidic solution (pH<6) to the pre-soaked β-CD-PEG/Bzi gel (10 mM).

3.2.5 Temporal Change in Pumping of “Host-Guest” Assembly and Disassembly

Next, the temporal change in the fluid velocity was examined during the ‘‘host–guest’’ assembly with 10 mM BzI solution over a period of 40 min. It was observed that the fluid velocity decreased from 6.56±0.54 μms^{-1} in 1min to 1.00±0.16 μms^{-1} after 40 min, as shown in Figure 3.8(a). As the ‘‘host’’ binding sites were progressively occupied by the ‘‘guest’’ molecules, the rate of reaction decreased and thereby slowed down the pumping velocity over the passage of time. Similar trends were observed when the experiment was performed in the acidic condition at pH 3. The pumping velocity decreased from 3.18±0.20 μms^{-1} in 1min to 0.71±0.13 μms^{-1} after 40 min, as represented in the Figure 3.8(a). The deduction in speed occurred due to the gradual decomplexation of the assembly over time. The spatial distribution of the fluid velocity was also investigated after the addition of 10 mM BzI to the pump chamber, and the pumping velocity was measured at fixed distances from gel edge with an interval of 1000 mm. The total distance covered for this experiment was 4000 mm. Figure 3.8(b) shows that the pumping velocity decreases over long distances from 6.32 ±0.23 μms^{-1} (1000 mm) to 3.30±0.24 μms^{-1} (4000 mm) due to the weakening of the thermal gradient away from the reaction epicentre.

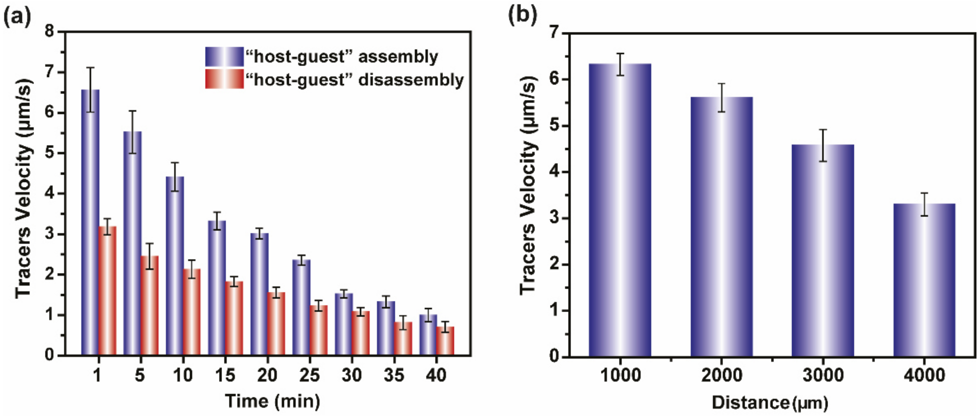

Figure 3.8. (a) The temporal variation of fluid pumping for the addition of BzI (‘‘host–guest’’ assembly); and on the addition of an acidic solution (pH<6) to the pre-soaked b-CD-PEG/BzI gel (‘‘host–guest’’ disassembly, 10 mM); (b) spatial changes in the fluid pumping velocity after addition of BzI (‘‘host–guest’’ assembly).

3.2.6 Flow Reversal in Complicated Microchannel

To demonstrate flow reversal over long distance, an L-shaped channel was fabricated. The channel was consisted of three circular chambers of 3 mm diameter (C1, C2 and C3) and those chambers were connected through 1.6 mm long and 200 mm depth connectors termed as L1 and L2 (Figure 3.9a). A small piece of the β-CD-PEG gel was kept on the glass slide, and it was covered with the L-shaped channel in such a way that the gel was placed in chamber C1. After the addition of 10 mM BzI solution to the chamber, an inward fluid flow was observed from chamber C3 to chamber C1 through chamber C2. It implied that the flow was initiated at chamber C1 near the gel edge but was able to transfer the fluid across the channel. The tracer's velocity was calculated at the connector tubes and the velocity was 6.61±0.86 μms^{-1}in L1 connector and 5.40±0.74 μms^{-1} in L2 connector. The decrease in the tracer velocity was expected as the distance from the reaction centre to connector increases. The reversible flow was demonstrated in a similar fashion, where a BzI soaked β-CD-PEG gel was placed inside C1 chamber. Upon the injection of an acidic solution (pH 3) to the chamber, an outward flow from chamber C1 to chamber C3 via chamber C2 was observed. The estimated tracer velocity was 3.36±0.66 μms^{-1}in L1 connector and 2.29±0.27 μms^{-1}in L2 connector (Figure 3.9b).

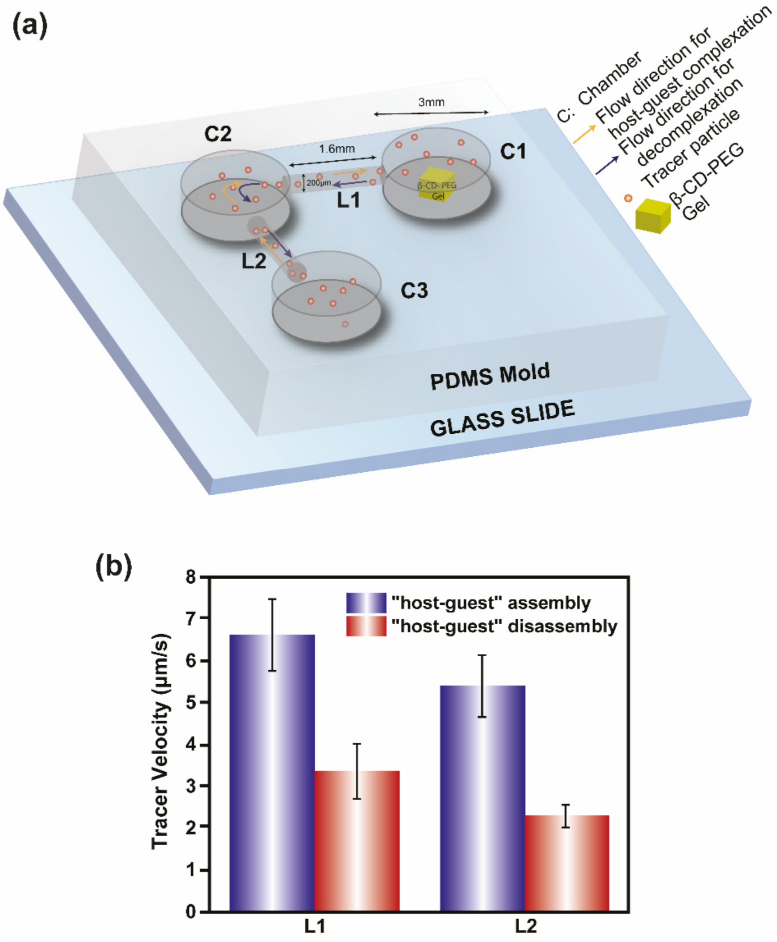

Figure 3.9. (a) Schematic representation of a channel to demonstrate the capability of moving particles over long distances (12.2 mm) and around corners; (b) tracer velocity for assembly and disassembly in the L-shaped chamber.

3.3 Conclusions

In summary, a chemically powered pH-responsive micropump was successfully demonstrated based on ‘‘host–guest’’ molecular recognition. The fluid flow direction was altered by changing the pH of the solution. These valveless miniature micropumps were easily integrated into the microchannel to manipulate the fluid flow. This macroscopic flow reversibility can open a new avenue in lab-on-a-chip applications.

3.4 Experimental Section

3.4.1 Reagents and materials

β-Cyclodextrin (β-CD), Hexamethylene diisocyanate (HDMI), and dibutyltin dilaurate (DBTDL) were purchased from TCI chemicals. Benzimidazole and Sulfate latex particles (5µm in diameter) were purchased ed from Sigma-Aldrich. Dimethyl Formamide (DMF), hydrochloric acid, and sodium hydroxide were obtained from Merck. DC/GEN/184 SYLGARD (PDMS Elastomer KIT) was purchased from Kevin Electrochem. Millipore water (18.2 MΩ•cm at 25 °C) was used in all experiments.

3.4.2 Characterization

The synthesized β-CD-PEG gel was characterized by FTIR using Thermo Scientific. Isothermal titration Calorimetric measurements were carried by Malvern MicroCal PEAQ-ITC. The UV-vis spectrophotometer (UV-2600 ultraviolet-visible spectrophotometer SHIMADZU) was used to measure the absorption of the host-guest complexation. Videos were recorded using an inverted optical microscope (OLYMPUS IX73) with a X-Cite 120 LED Boost, via a 10X objective (CPLN10XPH), excitation light was focused on the sample. Emission light was captured by the objective, passed through interference filters, and eventually recorded at 15 frames per second by a high resolution colored cooled camera (DP74). Using this DP74 camera connected to an optical microscope, videos were recorded. For each experiment, 30 tracer particles were monitored for a time interval of 15 seconds using the Tracker software (Motion Analysis Software) to calculate the fluid-pumping velocity.

3.4.3 Synthesis of β-Cyclodextrin-Polyethylene Glycol (β-CD-PEG) Gel

The β-CD-PEG- gel was prepared according to the following two step reaction as shown in Figure 3.10.[28]

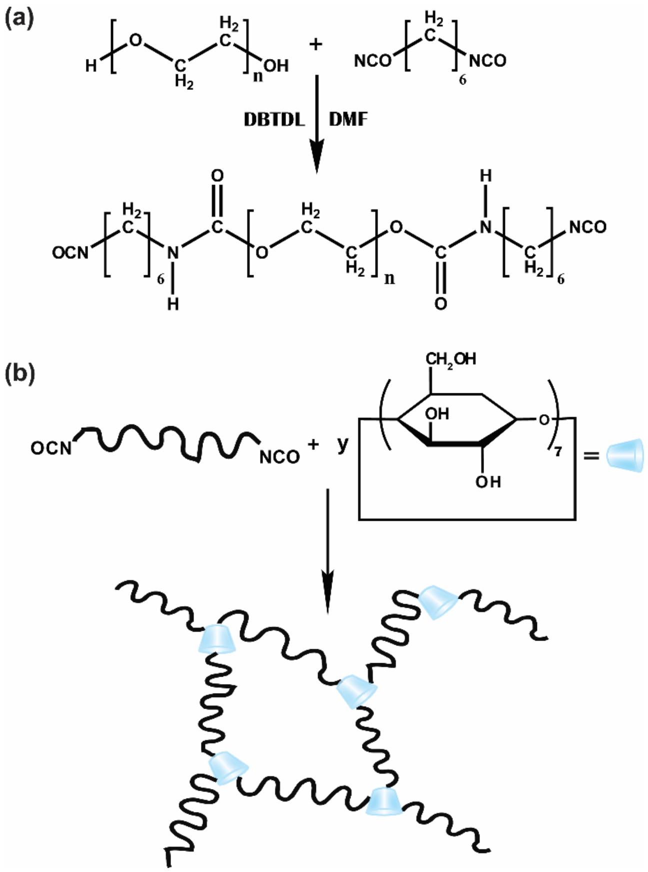

Figure 3.10. (a) End-capping process of PEG with HDMI, (b) Reaction among the end-capped PEG with isocyanate groups and the β-CD, together with an idealized outline of the structure of the gel.

First, two solutions of PEG and HDMI in DMF in a molar ratio of 1:2 are allowed to react in a two-neck round bottom flask initially purged with dry N2 at 55 °C. The reactor contains 0.01 wt % of the catalyst (DBTDL) compared to the total weight of the reagents and the overall concentration of reagents is 25 wt %. The product is poly(ethylene glycol) chains where terminal hydroxyl groups were substituted by isocyanate groups by an end-capped method in which each molecule of HDMI utilizes one of its two isocyanate groups to react with the hydroxyl group of PEG through the formation of a urethane group. The first step of the resulting reaction is shown in Figure 3.10 (a). Second, the solution of β-CD in dimethylformamide (16.5 wt %) was added into the flask for 60 minutes to achieve the desired composition in the gel. After keeping the system in agitation for 30 minutes, the reactive mixture was transferred to the test tube, capped with septa under N2 maintained at75 °C for 7 days. The resulting reaction is described in Figure 3.10 (b). After that the gel was collected and washed repeatedly, first with DMF and then with DI water, at room temperature, to remove water-soluble β-CD until less than 1 ppm monomer was found in the wash solution. Synthesized gel has been characterized by FTIR. It can be noted that the gel spectrum reveals the presence of bands at 1094 cm-1 and 1031 cm-1, corresponding to PEG and β-CD. Amide I (1700 cm-1) and amide II (1561 cm-1), which confirm the chemical structure, are two simple bands corresponding to the existence of urethane groups as shown in Figure 3.11.

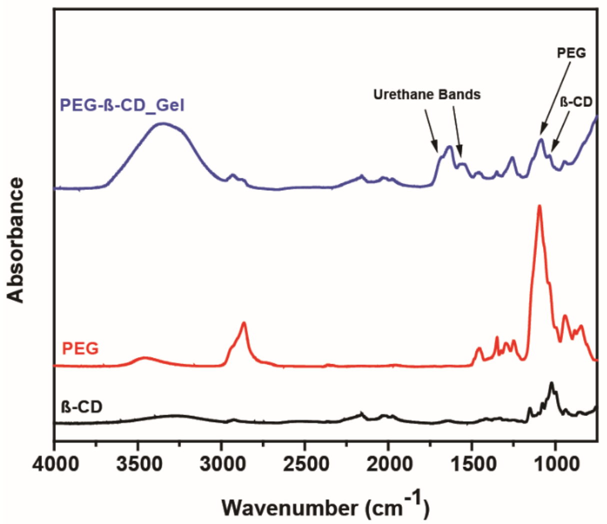

Figure 3.11. FTIR Spectra of PEG, β-CD, and a β-CD-PEG gel

3.4.4 Isothermal Titration Calorimetry

The thermodynamic parameters of cyclodextrin/benzimidazole molecular recognition were measured in aqueous at pH 7.4 using the Malvern MicroCal PEAQ-ITC at 25.0 °C (298.15 K). The ITC experiment included 39 consecutive 0.5 µL injections of BzI solution (10.0 mM) with the use of a syringe into the calorimeter sample cell containing β-cyclodextrin (200 µM) at an interval of 150s with the constant rate of 750 rpm. Control experiment involved similar injections into an aqueous solution under same conditions at 25.0 °C. Benzimidazole titration into an aqueous β- cyclodextrin solution resulted in an exothermic isotherm, which fitted to a 1:1 complexation model after heat of dilution corrections. For the disassembly of β-CD/BzI complex, the solution of acidic water (pH3) in the syringe was titrated into the pre-assembled β-CD/BzI solution in the calorimetric cell involved 19 sequential 2µl injections. It resulted into an endothermic isotherm.

3.4.5 UV-Vis Study of BzI Soaked β-CD Gel

A small piece of "host" gel was soaked in an aqueous solution for 12 hours and then dialyzed for 24 hours to remove any loosely bound “guest” molecules. To measure the absorbance of “host-guest” assembled gel, a small piece of the gel was placed between two quartz slides and the absorbance of the gel demonstrated a characteristic absorption of benzimidazole. No characteristic absorption was observed for “host” gel only. A small piece of gel pre-assembled with BzI was placed inside a cuvette. Upon addition of acidic aqueous solution (pH<6) to the cuvette, the dissociation of BzI from β-CD cavity occurred and the release was monitored by measuring the absorbance of BzI. It is observed that the rate of release is higher at lower pH.

Note: The permission has been granted by authors and corresponding author of the published paper prior to its adoption in the present thesis. The publication associated with this work is:

Mujeeb Alam, Rohit Varshney, Chinmayee Agashe, Arshdeep Kaur Gill and Debabrata Patra. Valveless flow reversal by a pH responsive supramolecular micropump**. *Chem. Commun.***, 2021, **57**, 4584-4587.

3.5 References

1. J. Khandurina, T. E. McKnight, S. C. Jacobson, L. C. Waters, R. S. Foote and J. M. Ramsey, *Anal. Chem.*, 2000, **72**, 2995–3000.
2. A. T. Woolley, D. Hadley, P. Landre, A. J. deMello, R. A. Mathies and M. A. Northrup, *Anal. Chem.*, 1996, **68**, 4081–4086.
3. Lian Zhang, Jae-Mo Koo, Linan Jiang, M. Asheghi, K. E. Goodson, J. G. Santiago and T. W. Kenny, *J. Microelectromech. Syst.*, 2002, **11**, 12–19.
4. T. A. Franke and A. Wixforth, *ChemPhysChem*, 2008, **9**, 2140–2156.
5. R. Zengerle, J. Ulrich, S. Kluge, M. Richter and A. Richter, *Sens. Actuators, A*, 1995, **50**, 81–86.
6. P. Lisowski and P. K. Zarzyski, *Chromatographia*, 2013, **76**, 1201–1214.
7. M. Zdblick, Proc. of Tech. Dig. *Solid-state Sensors and Actuators Workshop*, 1994, 251–255.
8. S. Yufeng, C. Wenyuan, C. Feng and Z. Weiping, *Int. J. Adv. Des. Manuf. Technol.*, 2006, **30**, 215–220.

9. W. Wang, T.-Y. Chiang, D. Velegol and T. E. Mallouk, *J. Am. Chem. Soc.*, 2013, **135**, 10557–10565.
10. L. Liu, Y. Dong, Y. Sun, M. Liu, Y. Su, H. Zhang and B. Dong, *Nano Res.*, 2016, **9**, 1310–1318.
11. X. Lin, T. Si, Z. Wu and Q. He, *Phys. Chem. Chem. Phys.*, 2017, **19**, 23606–23613.
12. M. J. Esplandiu, A. A. Farniya and A. Bachtold, *ACS Nano*, 2015, **9**, 11234–11240.
13. D. Patra, S. Sengupta, W. Duan, H. Zhang, R. Pavlick and A. Sen, *Nanoscale*, 2013, **5**, 1273–1283.
14. Y. Wang, R. M. Hernandez, D. J. Bartlett, J. M. Bingham, T. R. Kline, A. Sen and T. E. Mallouk, *Langmuir*, 2006, **22**, 10451–10456.
15. T. R. Kline, W. F. Paxton, Y. Wang, D. Velegol, T. E. Mallouk and A. Sen, *J. Am. Chem. Soc.*, 2005, **127**, 17150–17151.
16. S. Sengupta, D. Patra, I. Ortiz-Rivera, A. Agrawal, S. Shklyaev, K. K. Dey, U. Co´rdova-Figueroa, T. E. Mallouk and A. Sen, *Nat. Chem.*, 2014, **6**, 415–422.
17. R. Varshney, M. Alam, C. Agashe, R. Joseph and D. Patra, *Chem. Commun.*, 2020, **56**, 9284–9287.
18. Y. Tu, F. Peng, J. M. Heuvelmans, S. Liu, R. J. M. Nolte and D. A. Wilson, *Angew. Chem., Int. Ed.*, 2019, **58**, 8687–8691.
19. M.-O. M. Piepenbrock, G. O. Lloyd, N. Clarke and J. W. Steed, *Chem. Rev.*, 2010, **110**, 1960–2004.
20. D. A. Uhlenheuer, K. Petkau and L. Brunsveld, *Chem. Soc. Rev.*, 2010, **39**, 2817–2826.
21. G. Sinawang, M. Osaki, Y. Takashima, H. Yamaguchi and A. Harada, *Polym. J.*, 2020, **52**, 839–859.
22. M. Cheng and F. Shi, *Chem. – Eur. J.*, 2020, **26**, 15763–15778.
23. H.-J. Schneider, *Angew. Chem., Int. Ed.*, 2009, **48**, 3924–3977.
24. A. L. K. L. Koner, I. G. Ghosh, N. S. Saleh and W. M. N. M. Nau, *Can. J. Chem.*, 2011, **89**, 139–147.
25. M. Xue, X. Zhong, Z. Shaposhnik, Y. Qu, F. Tamanoi, X. Duan and J. I. Zink, J. Am. *Chem. Soc.*, 2011, **133**, 8798–8801.
26. T. Wang, M. Wang, C. Ding and J. Fu, *Chem. Commun.*, 2014, **50**, 12469–12472.
27. M. Alam, A. K. Gill, R. Varshney, C. Miglani, N. Tiwari, D. Patra, *Soft Matter*, 2022, **18**, 5605-5614.
28. L. C. Cesteros, C. A. Ramírez, A. Peciña and I. Katime, *J. Appl. Polym. Sci.,* 2006, **102**, 1162–1166.

Chapter 4

Macroscopic Discrimination of Isomers on Supramolecular Interfaces by Autonomous Fluid Flow

4.1 Introduction

Chiral and structural isomers have comparable structures but there is a marked difference in their bioactivity and pharmacological activity.[1-4] For example, amino acids exist in both D- and L- isomeric form. L-amino acids are used in the synthesis of proteins, while D-amino acids do not participate in this process or even generate adverse reaction to living organisms.[5-7] Similarly, the structural isomers such as nitroaromatics have key role in dyes, pesticides and fine chemicals manufacturing.[8,9] However, the highly stable residues of nitroaromatics that remained in the environment are listed as health hazards and the toxicity of these isomers are different from each other.[10-11] Thus, rapid discrimination between isomers is of utmost importance in pharmaceuticals and chemical industries.

Several approaches have been widely used to recognize chiral and structural isomers including chromatographic methods,[12-15] electroanalytical,[16-19] spectrophotometry,[20-23] voltametric,[24-27] and capillary electrophoresis.[28-31] However, their practical application is limited due to complexity, high cost and time-consuming analysis. Another increasingly explored approach is the designing of supramolecular interfaces that uses "host-guest" interaction in recognizing both chiral and structural isomers. Usually "host-guest" recognition is the cumulative effort of multiple noncovalent interactions which can be fine-tuned to attain selective isomers recognitions.[32-34] Macrocyclic "host" such as cyclodextrins, cucurbit[n]urils, pillar[n]arenes and calix[n]arenes functionalized interfaces proved to be suitable candidates for isomers specific "host-guest" recognition where the output signals are typically either optical signals or electric signals.[34-37] Efforts have been made to amplify these weak molecular signals into visible outputs that could provide a gateway to the macroscopic world. Pioneer work by Harada[38,39] *et al* demonstrated macroscopic self-assembly via molecular recognition where the supramolecular motifs were seeded into hydrogel and the recognition was amplified to the macroscopic scale for visual comparison. In another approach, Li and coworkers have developed supramolecular interfaces via surface functionalization of macrocyclic "host" molecules that can be used to distinguish the chiral "guest" molecules by macroscopic contact angle shift.[6,40] However, for practical applications like point-of-care devices or lab-on-chip based technology, more attentions are required to develop a strategy with macroscopic readout of the information present at molecular level.

In view to amplify the weak molecular interactions into macroscopic signals, herein, we have developed a supramolecular interface that distinguishes the isomers by self-generated fluid flow. In this approach, multilayer films comprising of macrocyclic "host" molecules was constructed that triggered an autonomous fluid flow in response to "guest" isomers due to "host-guest" molecular recognition. First example demonstrated the discrimination of chiral Tryptophan (Trp) isomers using β-CD based interface that yielded higher fluid flow velocity in case of L-Trp compared to D-Trp. The analytical modelling predicted that the observed fluid flows were predominantly driven by solutal buoyancy and the higher velocity output of L-Trp indicated its higher affinity as compared to D-Trp for the "host" site due to favourable molecular orientation. To extend the scope of this approach, pillar[5]arene based interface was used to discriminate the structural isomers of nitrophenol. The fluid flow was observed only in case of p-nitrophenol whereas o-nitrophenol did not produce any fluid flow because of cavity size mismatch with pillar[5]arene.

4.2 Results and Discussions

4.2.1 Fabrication of Supramolecular Interface and Discrimination of Chiral Isomers

To construct the supramolecular interfaces for autonomous fluid flow, the "host" multilayer films consisting of β-CD was constructed via LbL assembly as shown in Figure 4.1(a) (see experimental section for film fabrication method). β-CD grafted polyethyleneimine (PEI-β-CD) (see experimental section for synthesis) and polyacrylic acid (PAA) were used as polyelectrolyte pair to fabricate the multilayer films and the growth of the films was monitored using ellipsometer. A liner growth of the film was observed depositing 18 nm per bilayer (BL = 1 layer of PEI-β-CD and 1 layer of PAA) as shown in Figure 4.1b. To investigate the fluid flow generated by these "host" multilayer films, a circular pattern of the films was constructed in the middle of a glass slide and it was then covered by a sealed chamber ((l= 1 cm, b= 1 cm, h = 1.8 mm). In chiral isomer discrimination study, aqueous solutions of D-Trp and L-Trp were separately prepared along with along with 5 μm sulfate functionalized polystyrene microbeads. These beads were employed as tracer particles to analyse the flow direction and flow velocity. Next, the freshly prepared amino acid solutions were injected into two different chambers and the flow pattern was analysed under the microscope for further analysis. In both cases, an inward flow of

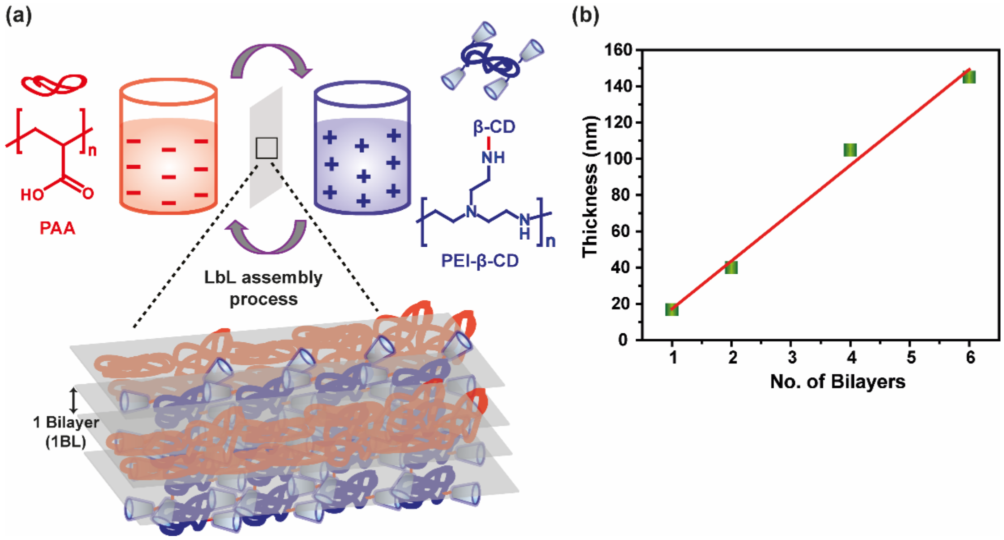

Figure 4.1. (a) Schematic of layer-by-layer (LbL) assembly using PAA and PEI-β-CD, (b) Thickness profile of the polymer multilayer film grown on a silicon wafer (dry state).

tracer particles towards the pattern were observed when viewed at the bottom layer of the chamber as shown in Figure 4.2a, b and c. To validate our findings, we performed two control experiments – (i) the “host” multilayer film (PAA/PEI-β-CD)$_{1BL}$ was treated with DI water (ii) D-/L-Trp solutions were injected into a chamber containing (PEI/PAA)$_{1BL}$ film; without any "host" functionality. No directional flow was observed concluding “host-guest” recognition between β-CD and Trp was the key to trigger the fluid flow (Figure 4.3a and b). In earlier report it was established that the chemical reaction generating a density gradient caused the fluid flow. To validate the origin of flow, the flow chamber was inverted and was observed under the microscope. In each case, the flow direction was reversed i.e., the tracer particles were moving away from the coating confirming the density driven flow caused by “host-guest” molecular recognition.

To understand the role of “guest” concentration on fluid velocity, three different concentrations (1 mM, 10 mM and 40 mM) of Trp enantiomers were chosen for the study using 1 BL of PEI-β-CD/PAA films in which PEI-β-CD was the outer most layer. In case of D-Trp, the velocity was increased from 0.50±0.08 μm/s (1mM) to 1.54±0.07 μm/s (40mM) whereas the fluid velocity was 2.6 times higher at 1 mM (1.33±0.06 μm/s) concentration and 3.5 times higher at 40 mM (5.52±0.11 μm/s) concentration of L-Trp (Figure 4.3c). From these results, it can be predicted that β-CD:L-Trp complexation causing a higher density change inside fluid chamber probably due to higher affinity of L-Trp towards β-CD than D-Trp.

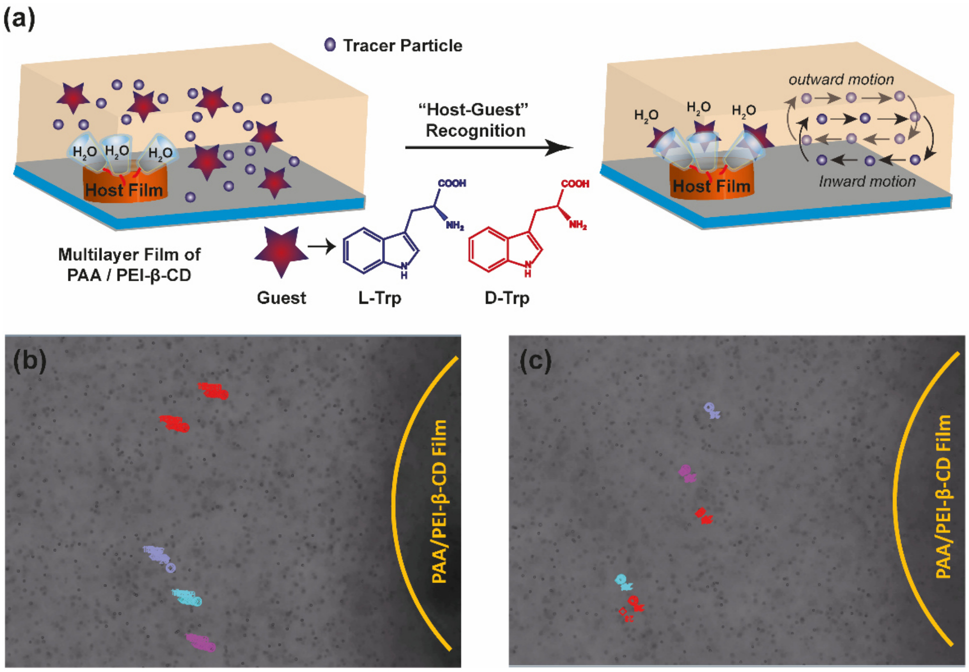

Figure 4.2. (a) Schematic of fluid pumping as a result of "host-guest" complex formation. Tracer particles trajectories: (b) directional flow as a result of "host-guest" recognition between. (b) L-Trp and β-CD, and (c) D-Trp and β-CD.

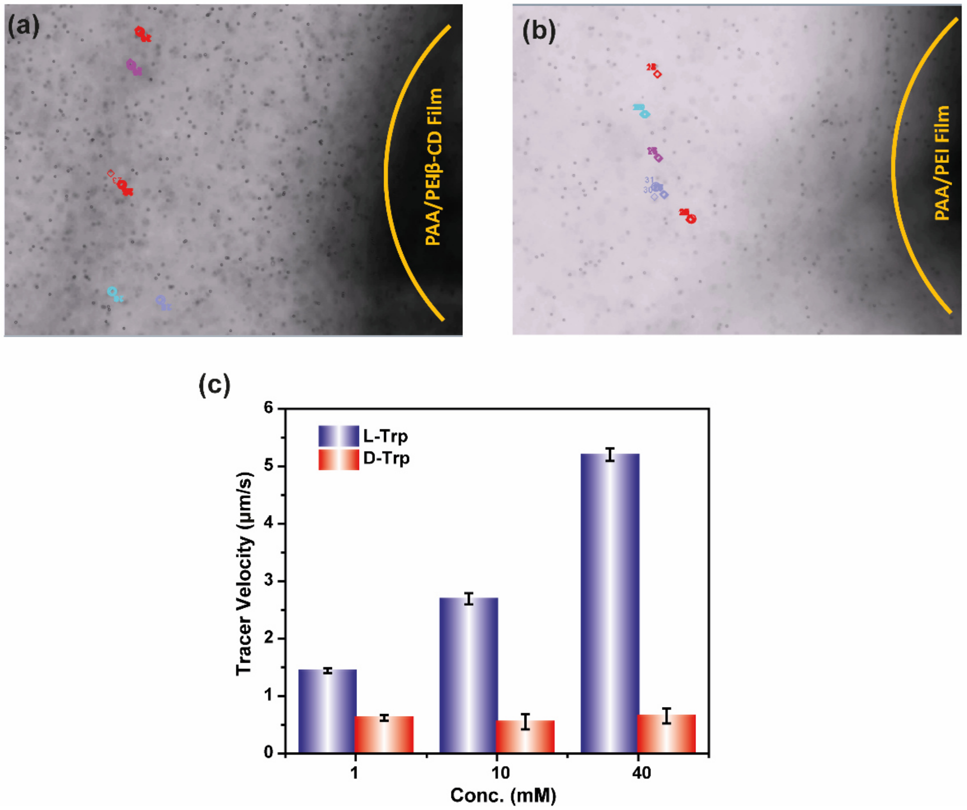

Figure 4.3. Tracer particles trajectories: No flow on injecting (a) water into the chamber containing PAA/PEI-β-CD film, and (b) Trp into the chamber containing PAA/PEI film. (c) variation of fluid pumping velocity with concentration.

4.2.2 Investigation of "Host-Guest" Complexation.

Both L- and D-Trp form inclusion complexes with β-CD. The aromatic part of the Trp enters the hydrophobic cavity of β-CD while leaving the polar part outside. Now, the favourability of hydrogen bond formation between the polar part of the Trp with the hydroxyl group of β-CD dictates the chiral recognition. In such condition, L-Trp favours the formation of hydrogen bond with β-CD. The thermodynamic parameters (K_a, ΔG, ΔH, ΔS) of β-CD and Trp (D- and L-) complexation was determined by Isothermal Titration Calorimetry (ITC) at 298K (Figure 4.4a and b). The ITC results showed that the binding constant of β-CD:L-Trp complex (666 M^{-1}) was higher than β-CD:D-Trp (37 M^{-1}) complex indicating β-CD formed a more stable complex with L-Trp than D-Trp. The "host-guest" molecular recognition between β-CD and Trp were further studied using ^1H NMR spectroscopy as shown in Figure 4.5 and 4.6. The signal for aromatic protons H1, H2, H3, H4 and H5 (L-Trp) were shifted upfield by 0.005, 0.01, 0.01, 0.01 and 0.015 ppm in the L-Trp:β-CD complex respectively. While in the case of D-Trp:β-CD complex, the chemical shift of the protons was insignificant. The results suggested that β-CD would selectively interact with L-Trp, and form more stable complex with L-Trp as compared to D-Trp.

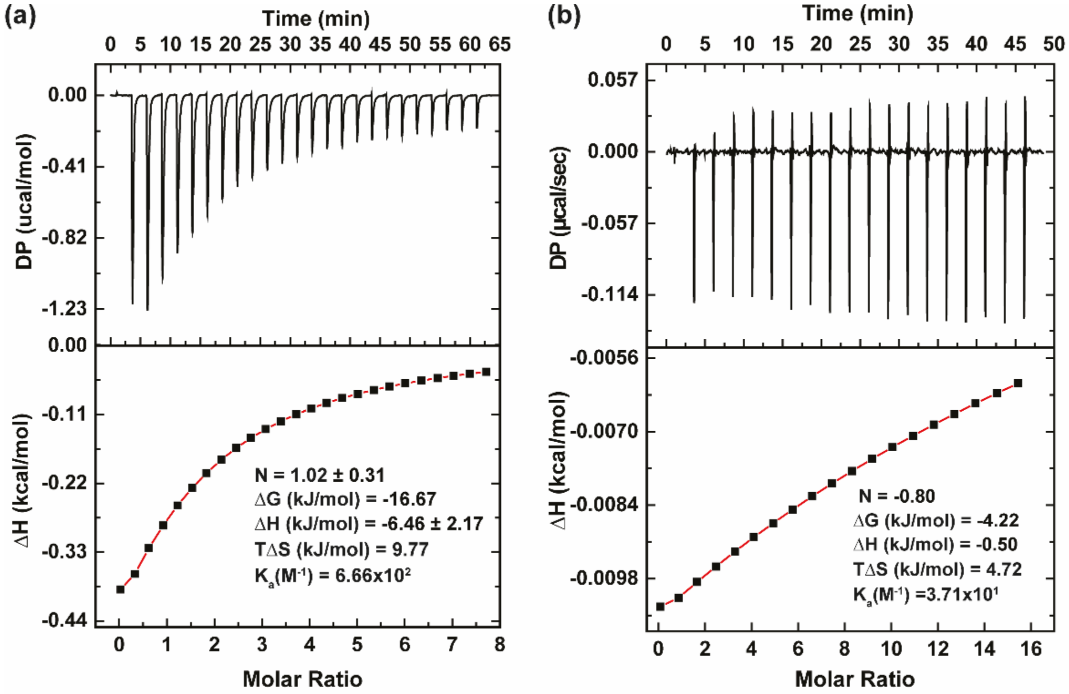

Figure 4.4. Isothermal Titration Calorimetry (ITC) isotherm of (a) L-Trp (20 mM), and (b) D-Trp with β-CD (250μM) at 25 °C.

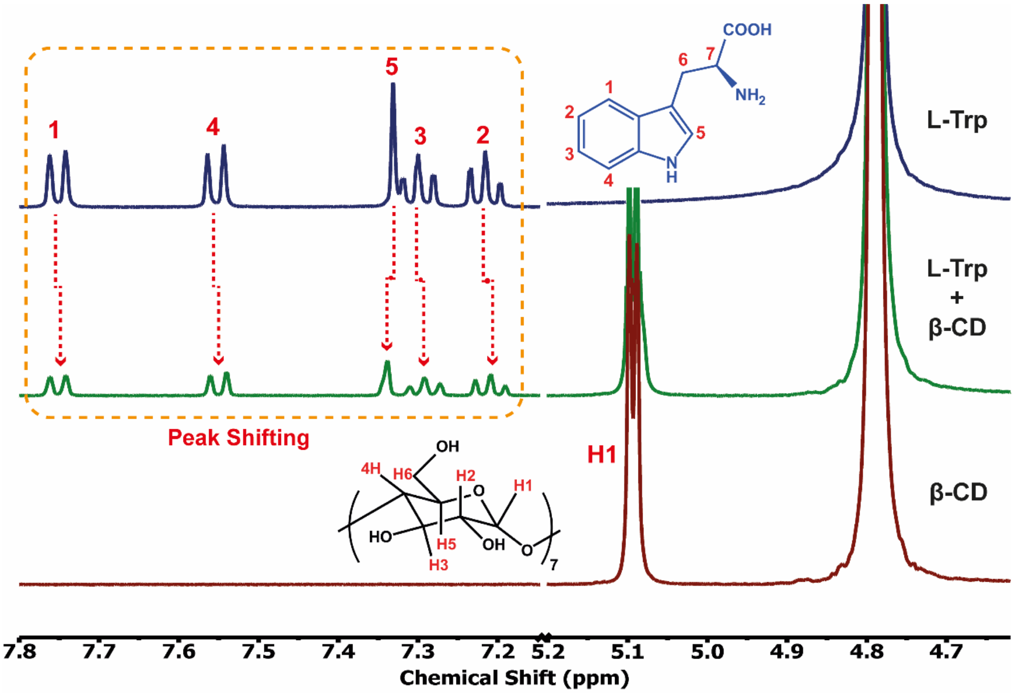

Figure 4.5. 400 MHz ^{1}HNMR spectra of β-CD with L-Trp. The concentration for each component was 5 mM.

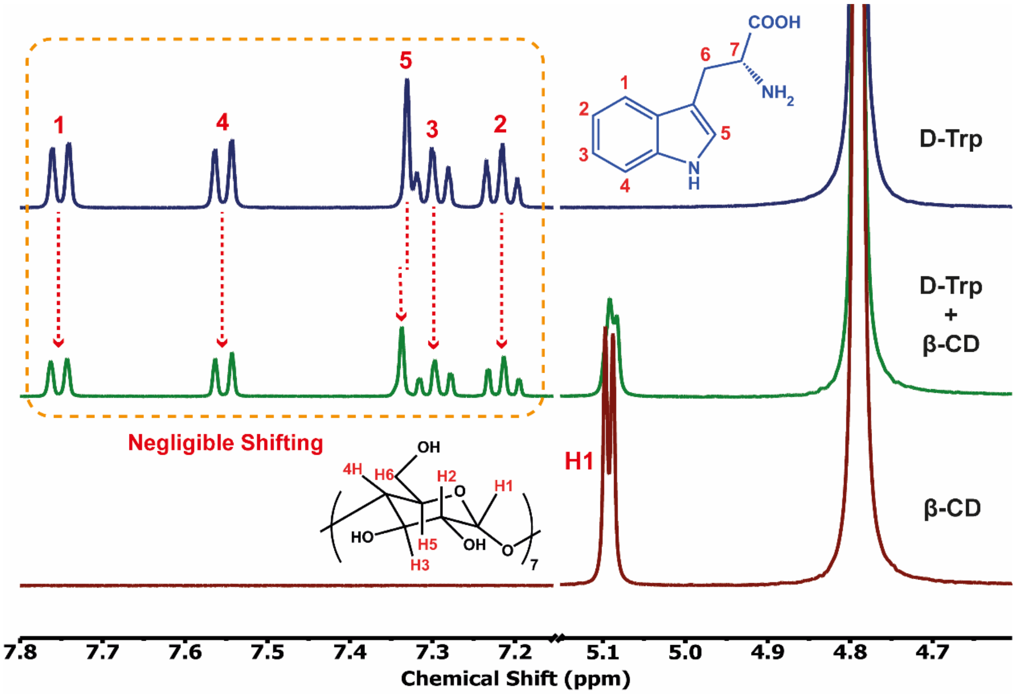

Figure 4.6. 400 MHz ^{1}HNMR spectra of β-CD with D-Trp. The concentration for each component was 5 mM.

4.2.3 Competitive Binding Effects on Pumping Velocity

The competitive binding is quite common in “host-guest” system and it depends on the binding constant of a particular “host-guest” pair. “Guest” molecules with higher binding constant tends to occupy the cavity of β-CD molecules and it could potentially replace the pre-existing “guest” molecules with a lower binding constant. The effect of competitive binding on fluid pumping was studied using a 1BL multilayer film pre-soaked with D-Trp. Upon addition of higher affinity “guest” molecules i.e., L-Trp (10 mM), an inward fluid flow with a velocity of 2.57±0.09 μm/s towards the coating was observed as shown in Figure 4.7a and b. The solutal buoyancy originated from the substitution reaction may be the prime reason for fluid motion. In a control experiment, a 1 BL film soaked with L-Trp guest molecules was treated with D-Trp (10mM). No directional motion was observed confirming that L-Trp-β-CD complex was not disrupted by D-Trp due to lower binding affinity of the later as shown in Figure 4.7c.

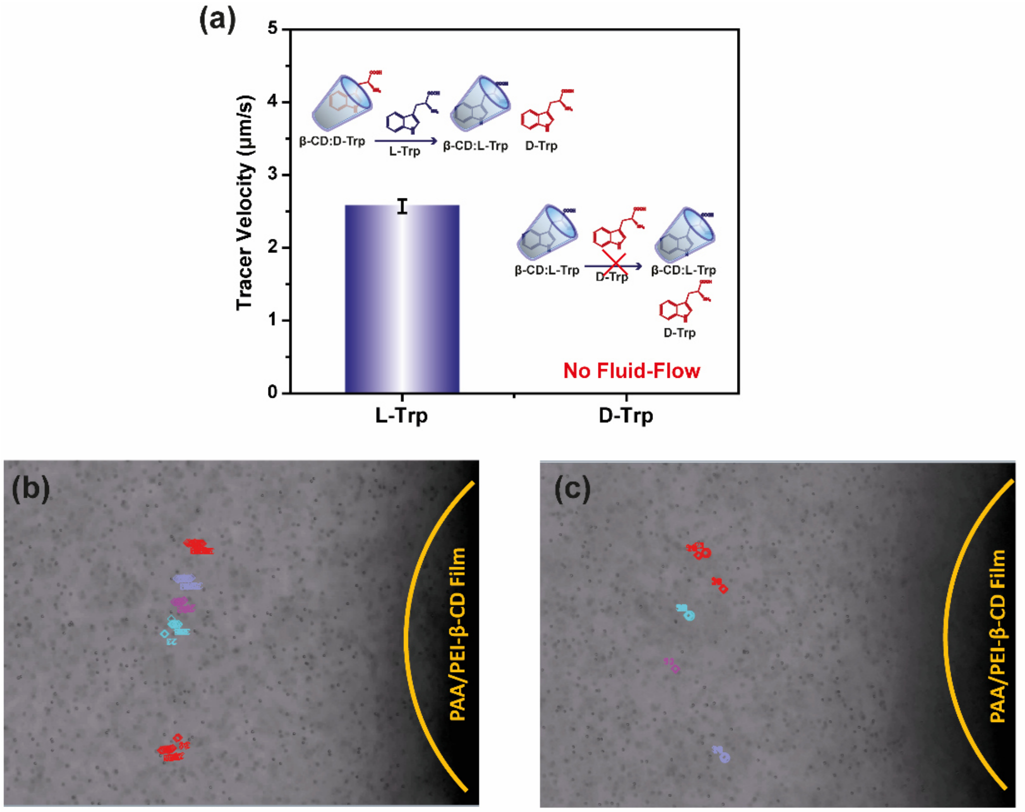

Figure 4.7. (a) Tracer velocity of competitive binding between L-Trp and D-Trp. Tracer particle trajectories: (b) directional flow for L-Trp, and (c) no flow for D-Trp.

4.2.4 Theoretical Investigation of Density Driven Flow

Theoretical modeling was used to get a better understanding of how solutal and thermal buoyancy impact fluid velocity. Thermal mechanisms were previously assumed to adequately explain the direction and approximate amplitude of the observed pumping, however the results of the numerical modelling revealed that the observed fluid flows were predominantly driven by solutal buoyancy.

We consider a 2-dimensional axisymmetric geometry (Figure 4.8a), with height of 1.8 mm, width of 10 mm. A circular patch of radius r = 2.4 mm, which is considered as the reaction zone, is placed at the center. We now solve for the radial velocity (u) and axial velocity (w) as a function of space coordinates (r and z) and time (t). The flow is governed by the continuity equation:

$$\frac{\partial u}{\partial r}+\frac{\partial w}{\partial z}=0$$

and the momentum balance equations in radial and axial directions, respectively:

$$\rho_0\left(\frac{\partial u}{\partial t}+u\frac{\partial u}{\partial r}+w\frac{\partial u}{\partial z}\right)=-\frac{\partial P}{\partial r}+\mu\left(\frac{1}{r}\frac{\partial}{\partial r}\left(r\frac{\partial u}{\partial r}\right)+\frac{\partial^2 u}{\partial z^2}\right)$$

$$\rho_0\left(\frac{\partial w}{\partial t}+u\frac{\partial w}{\partial r}+w\frac{\partial w}{\partial z}\right)=-\frac{\partial P}{\partial z}-\rho_0 g\;-\rho_0 g\beta_c(c-c_0)+\;\mu\left(\frac{1}{r}\frac{\partial}{\partial r}\left(r\frac{\partial w}{\partial r}\right)+\frac{\partial^2 w}{\partial z^2}\right)$$

where, P is the local pressure. In the above equation, we have applied the Boussinesq approximation to consider the solutal buoyancy effect, where the density variation is assumed to affect the gravity term only and ρ_0 is the fluid density at reference concentration c_0. β_c is the expansion coefficients due to solute concentration. No-slip condition is imposed at all the solid surfaces in the geometry. Due to the presence of the buoyancy terms in the momentum equation, it is coupled to the solute transport equation,

$$\frac{\partial c}{\partial t}+u\frac{\partial c}{\partial r}+w\frac{\partial c}{\partial z}=D\left(\frac{1}{r}\frac{\partial}{\partial r}\left(r\frac{\partial c}{\partial r}\right)+\frac{\partial^2 c}{\partial z^2}\right)$$

The bulk diffusivity of the guest molecule in water, D, is assumed to be O (10^{-7} m/s^2). The solute is getting consumed at the reaction patch. The boundary condition at the patch is written as

$$D\frac{\partial c}{\partial z}=-kce^{-\gamma t}$$

indicating that the diffusive flux at the patch is balanced by the consumption due to the reaction. At all other surfaces of the domain, it is assumed that no flux can pass through. In the reaction kinetics term, the apparent rate constant k includes the resistance due to the

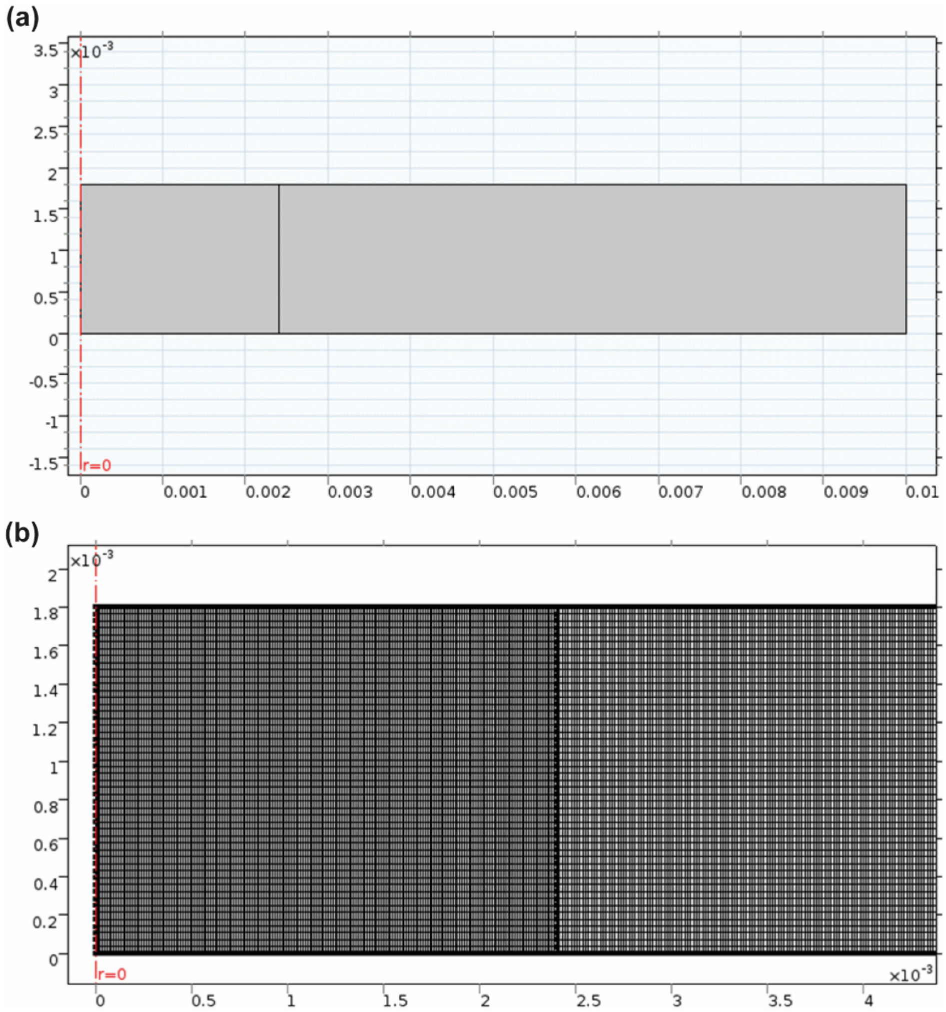

Figure 4.8. (a) Domain, and (b) Mesh used in the numerical study

polymer layer, and the binding constant of the “host -guest” molecule. The exponentially decaying terms accounts for the fact that as the “guest” molecules gradually occupy the cavity, the probability of finding a favourable site decreases. This form of the surface reaction has been proposed based on the experimental observations. The value of γ seems to be independent of the initial concentration of the “guest” molecule. Also, the apparent rate constant k may decrease with increase in the initial concentration, possibly due to the steric hindrance at the polymeric layer. The values of these constants seem to depend upon the relative orientation of the “guest” molecule with respect to the cavity of the β-CD. If the orientation is such that the insertion is not favored, then k can achieve a low value leading to smaller peak velocity. Also, once the sites get filled-up, the probability of finding another favourable site reduces drastically for D-Trp molecules indicated by a larger value of γ. This behaviour may help in sorting the chiral molecules.

The thermal contribution in the buoyancy is ignored due to the ratio of the Rayleigh numbers is small,

$$\frac{Ra_T}{Ra_s} = \frac{\beta_T \Delta H_{rxn}/\alpha}{\beta_s C_p \rho_0 / D} \sim O(10^{-3})$$

For this calculation, thermophysical properties of water were considered. Also, the enthalpy values presented earlier were used to estimate the order of magnitudes of ΔH_{rxn}. The change in density with concentration is simply given by, $\beta_s = M_w$ (molecular weight of the molecule), which is the same for the chiral molecules considered here. The mesh for the computations is shown in figure 4.8 (b). A mesh sensitivity test was done and a uniform mesh consisting of 50x1000 grids was found sufficient for the computations. Linear elements were used in the finite element method employed to solve the system of equations numerically. The velocity contours are shown in Figure 4.9a for 40 mM L-Trp at time, t = 1 minute and at for time t = 11 minutes in Figure 4.9b. The effective rate parameters for the "guest" molecules are listed in Table 4.1. The lower values of *k* for D-Trp indicate its lower affinity as compared to L-Trp for the “host” site supporting the preferential binding effect hypothesis due to favourable molecular orientation.

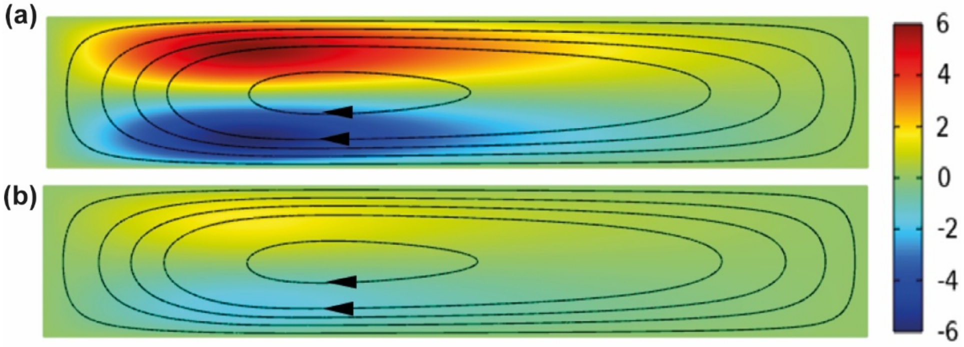

Figure 4.9. (a) Velocity contour and streamlines for 40 mM L-Trp at t=1 minute. The arrows indicate the direction of the flow, (b) Velocity contour and streamlines for 40 mM L-Trp at t=11 minutes. The arrows indicate the direction of the flow.

Conc.(mM)	***k* (L-Trp)**	***k* (D-Trp)**	***γ (L-Trp)***	***γ (D-Trp)***
1	$2x10^{-8}$	$1.3x10^{-8}$	0.0015	0.0015
10	$4.3X10^{-9}$	$1.8x10^{-9}$	0.002	0.002
40	$2.1 X 10^{-9}$	$1.3 X 10^{-9}$	0.0022	0.004

Table 4.1. Values of k and γ (effective rate parameters) used in the calculations of various cases of L-Trp and D-Trp molecule.

4.2.5 Temporal Changes in Pumping

The temporal velocity was investigated for both D-Trp and L- Trp at 1mM and 10mM with 1 BL of PEI-β-CD/PAA films. As the "host" binding sites inside the multilayer films were expected to be gradually occupied by "guest" molecules over time, the rate of the “host-guest” reaction was affected and it was reflected in tracer velocity. Figure 4.10 (a &b) revealed that the tracer velocity decreased from 2.57±0.09µm/s to 0.88±0.09µm/s for L-Trp and from 0.55±0.05µm/s to 0.13±0.06µm/s for D-Trp at 10 mM concentration. The fluid movement came to a complete halt after 17 minutes and 8 minutes in case of L-Trp and for D-Trp, respectively. The fluid flow of D-Trp stopped very quickly as compared to L-Trp, this is because of the lower affinity of D-Trp with β-CD than L-Trp. The results of the experiments illustrated in Figure 4.10 are very comparable to those obtained through theoretical modeling

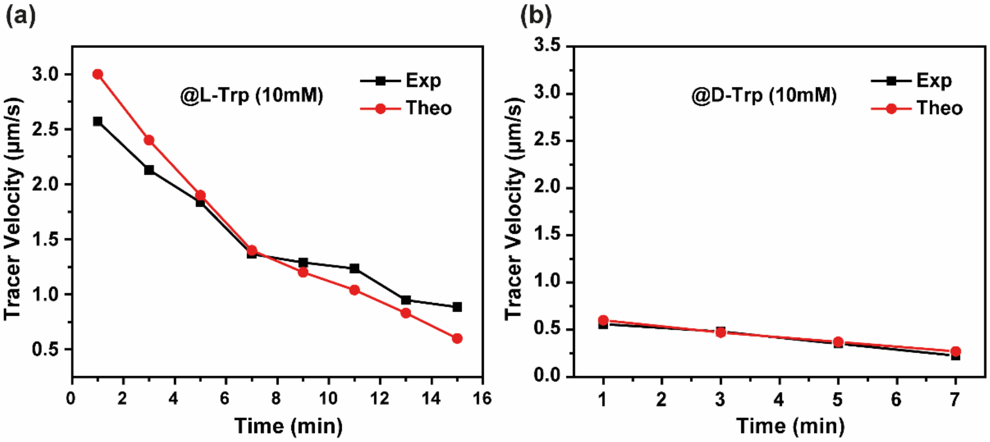

Figure 4.10. The temporal variation of fluid pumping in case of (a) L-Trp (1mM), (b) D-Trp (10mM).

4.2.6 Recognition of Nitrophenol Isomers by Pillar[5]arene Multilayer Films

After validating the chiral recognition of D-/L- Trp with β-CD functionalized multilayer film, we intended to extend this approach with a different macrocycle that can discriminate the structural isomers of nitrophenols. In this case, pillar[5]arene found to be the suitable candidate for selective recognition of o-and p- nitrophenol by “host-guest” molecular recognition.[47] To fabricate the supramolecular interface, the multilayer films were constructed using polyacrylic acid (PAA) and cationic pillar[5]arene (CP[5]A) as shown in Figure 4.11 (see experimental section for synthesis). Next, an aqueous solution of o-/p-nitrophenol (1 mM) along with 5 µm sulfate functionalized polystyrene microspheres were injected separately into the chambers containing CP[5]A multilayer film as shown in Figure 4.11. In case of p-nitrophenol, the tracer particles were moving towards the film at the bottom layer with a velocity of 2.48±0.12μm/s (Figure 4.12a and c). While in case of o-nitrophenol, no directional movement of tracer particles was observed (Figure 4.12b and c).

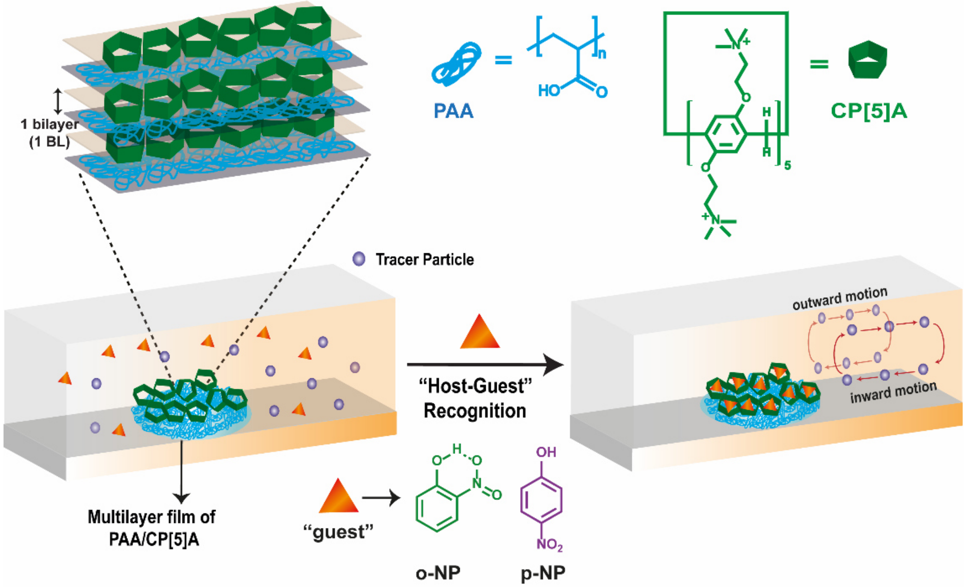

Figure 4.11. Schematic of layer-by-layer (LbL) assembly using cationic and anionic P[n]As.

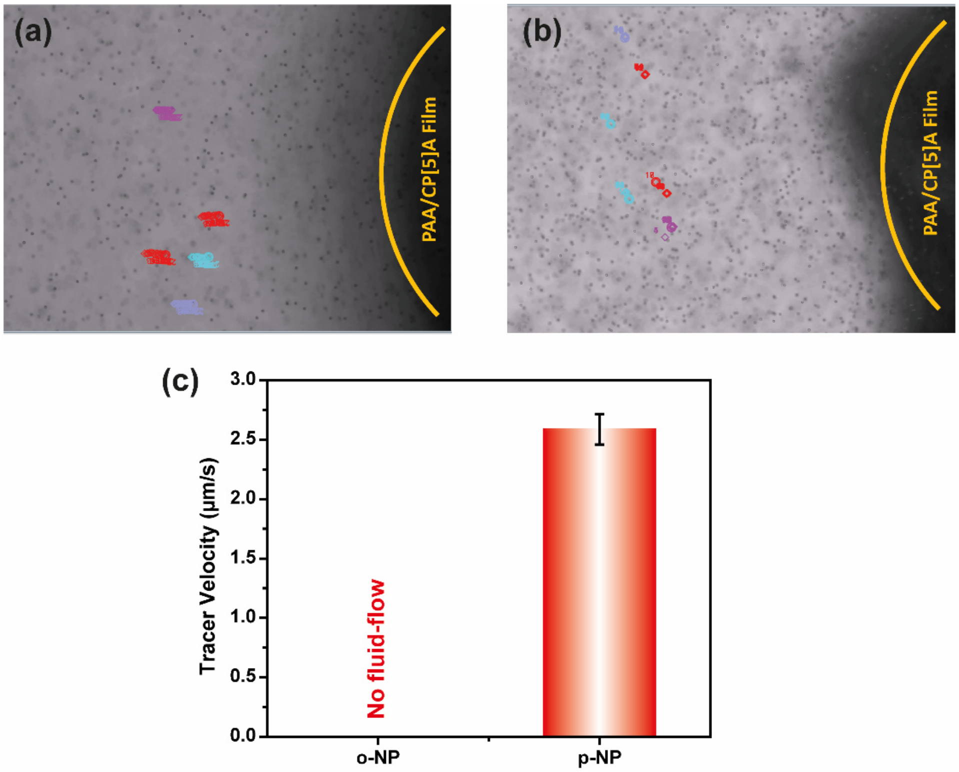

Figure 12. Tracer particle trajectories: (a) directional flow for p-NP, (b) no flow for o-NP, and (c) variation of fluid pumping velocity of isomers of nitrophenol at 1mM.

4.2.7 Investigation of "Host-Guest" Complexation.

To understand the different response of o-/p- nitrophenols with CP[5]A, the "host-guest" complexation was further was studied by ^{1}H NMR spectroscopy. In the presence of CP[5]A, the protons signal of p-NP disappeared and the signal of H_b protons was shifted upfield with a peak broadening effect. Similarly, an upfield shift of the CP[5]A aromatic proton was also observed upon "host-guest" complexation (Figure 4.13). However, the protons H_a, H_b, H_c, and H_d of o-NP showed insignificant chemical shift compared to free o-nitrophenol suggesting no complex formation (Figure 4.14). It was assumed that o-nitrophenol formed an intramolecular hydrogen bonding between adjacent nitro and hydroxyl group. As a result, the effective dimension of the molecule was increased and it was unable to enter into the cavity of CP[5]A. Meanwhile, p-nitrophenol formed an inclusion complex with CP[5]A due to the deficient-rich electron effect, electrostatic interaction, and size match of the "host-guest" molecules.

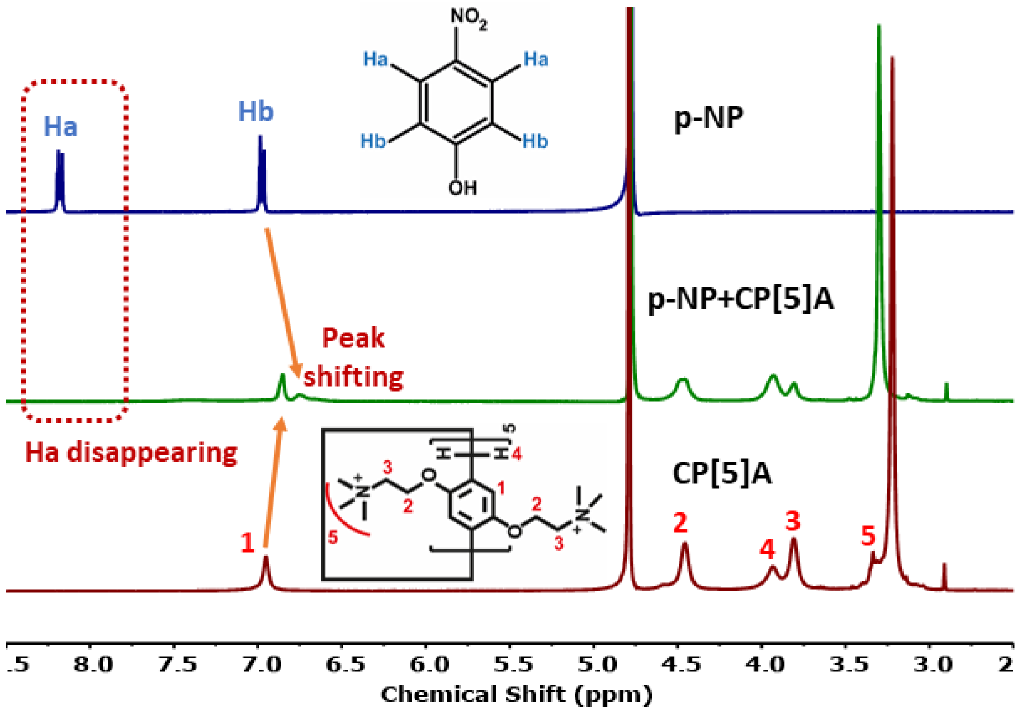

Figure 13. 400 MHz ^{1}H NMR spectra of (a) p-NP, CP[5]A + p-NP, and CP[5]A. The concentration for each component was 10 mM.

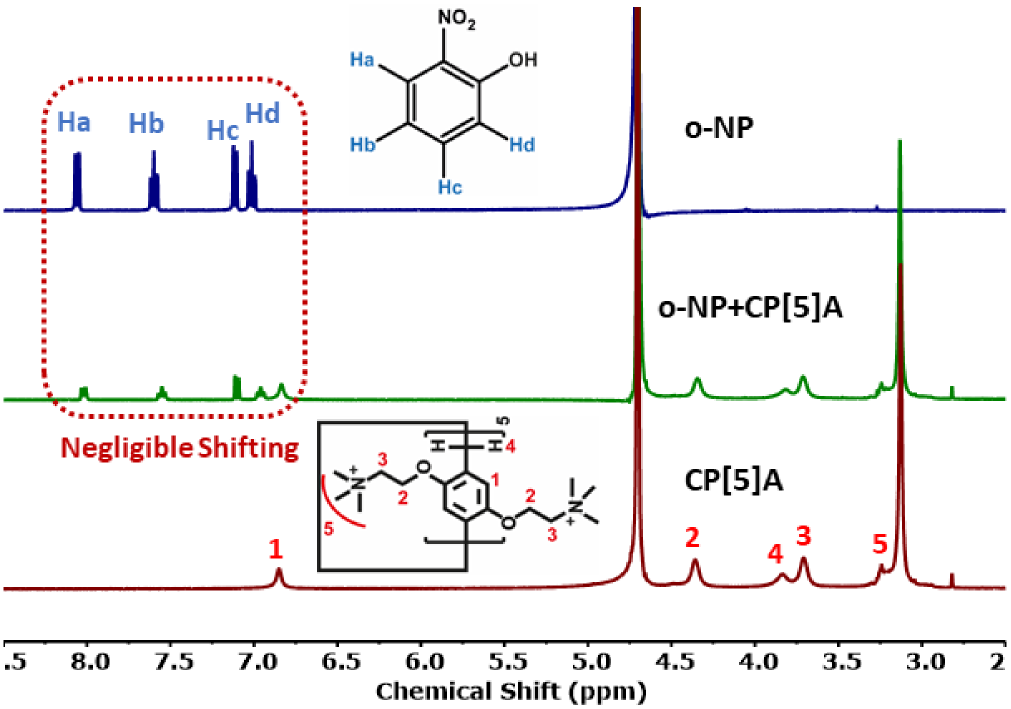

Figure 14. 400 MHz ^{1}H NMR spectra of (a) o-NP, CP[5]A + o-NP, and CP[5]A. The concentration for each component was 10 mM.

4.3 Conclusions

In summary, we have successfully demonstrated the amplification of weak molecular signals into macroscopic motion. The supramolecular interfaces fabricated by LbL assembly were used as a platform for molecular recognition and the resultant fluid flows originated from "host-guest" recognition were able to distinguish the isomers. The discrimination of Trp enantiomers on β-CD interface was achieved and the output flow velocity was ~ 3.5 times higher for L-Trp compared to D-Trp. Similarly, CP[5]A interfaces were able to distinguish o-/p- nitrophenols where only p-NP triggered the fluid flow. No flow was observed upon addition of o-NP to the analysis chamber. The fluid flow-based detection of isomers will pave the way for developing point-of-care devices for the detection of drug, pesticides or biologically relevant molecules.

4.4 Experimental Section

4.4.1 Reagents and Materials

Boron trifluoride diethyl etherate ($BF_3{\cdot}(OC_2H_5)_2$, Branched polyethyleneimine (bPEI, 25kDa), polyacrylicacid (PAA 100kDa, 35 wt%), p-toluenesulfonyl chloride (TsCl), L-tryptophan, and sulfate latex particles (5μm in diameter) were purchased from Sigma-

Aldrich. 1,4-bis(2-hydroxyethoxy)benzene, paraformaldehyde, trimethylamine, ortho-nitrophenol, meta-nitrophenol, para-nitrophenol, β-CD and D-tryptophan were obtained from TCI chemicals. Acetonitrile, 1,2-dichloroethane, hexane, dichloromethane, methanol, ethanol, dimethyl sulfoxide (DMSO), hydrochloric acid and sodium hydroxide were purchased from Merck. DC/GEN/184 SYLGARD (PDMS Elastomer KIT) was supplied by from Kevin Electrochem. Millipore water (18.2 MΩ•cm at 25 °C) was used in all experiments.

4.4.2 Characterization

A 400 MHz Bruker AvanceII spectrometer was used to record ^{1}H nuclear magnetic resonance (NMR) spectra of the products in DMSO-d_6 and D_2O. Based on proton integration, the grafting level of CD was estimated using the ^{1}H NMR spectra. Spectroscopic Ellipsometer (Angstrom Sun Technology Inc. USA) was used to measure the thickness of the host multilayer films. The binding of the "host-guest" molecules were determined by isothermal titration calorimetry (Malvern MicroCal PEAQ-ITC). Optical microscope (OLYMPUS IX73) with a high resolution coloured cooled camera (DP74) and X-Cite 120 LED Boost were used to record all the videos at 15 frames per second. In each experiment, 20 tracer particles were monitored over a 15 second time interval using Tracker software (Motion Analysis Software) to determine fluid pumping velocity.

4.4.3 Synthesis of PEI-β-CD

The following two-step reaction was used to synthesize PEI-β-CD according to the reported procedure (Figure 4.15).

4.4.3.1 Synthesis of Mono-6-(p-Tolylsulfonyl)-β-Cyclodextrin (Ts-*O*-β-CD)

Ts-O-β-CD was synthesized using a previously described method.[48] At room temperature, 5 g of β-CD was dissolved in 240 mL of deionized water and 550mg of NaOH in 2ml deionized water was added to the mixed solution, the suspension turned to be homogenous. 21.26 g of p-toluenesulfonyl chloride in 2.5ml of acetonitrile was gently added into the β-CD aqueous solution under magnetic stirring to ensure that substitution occurred only at the C6 position. The solution was stirred for 2 hours at 25°C after white precipitation appeared. The suspension was then cooled at 4°C overnight. The precipitate was then obtained using vacuum filtering The precipitate was recrystallized three times at 60°C to eliminate any remaining unreacted β-CD and p-TsCl. The product was obtained after vacuum drying at

50°C. ^{1}H NMR (DMSO-d_6) δ: 2.44 (s, 3H, CH_3), 3.41-3.74 (m, H-3,5,6) overlap with HOD, 4.21-4.53 (m, 6H, C6-OH), 4.80 (s, 7H, H-1 of CD), 7.43-7.77 (dd, 4H, aromatic tosyl) (Figure 4.16).

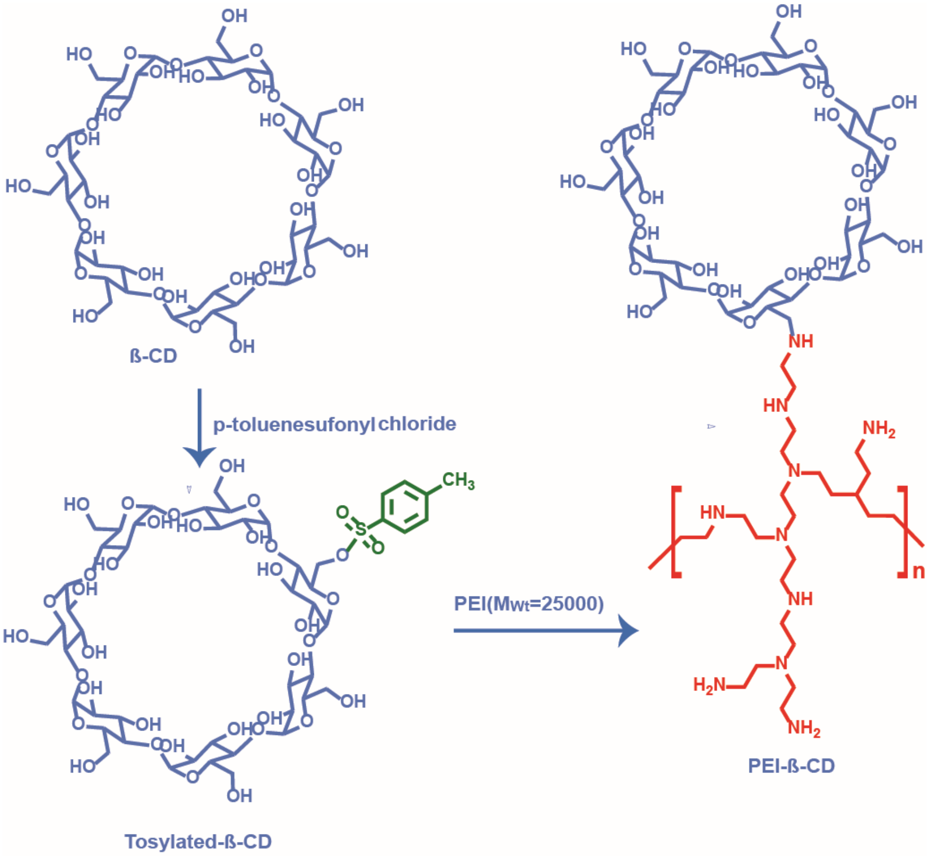

Figure 4.15. Synthesis of cyclodextrin functionalized polyethyleneimine (PEI-β-CD).

4.4.3.2 Synthesis of PEI-β-CD

The PEI-CD was prepared in accordance with the previous report.[49] Briefly, 0.25 g of PEI was reacted with 1.9 g of Ts-O-β-CD synthesized as mentioned above in 10 mL dimethyl sulfoxide (DMSO). For 3 days, the solution was stirred in a nitrogen atmosphere at 70°C. After that, the product was dialyzed in water for 3 days with a MWCO 12kDa membrane. After 3 days of freeze drying, the light-yellow powder was obtained. According to ^{1}H NMR (D_2O), the β-CD grafting level per PEI chain estimated to be approximately 8.0%. δ: 4.99 (s,7H, H(e) of CD), 3.81 (m, 28H, H(a), H(c), H(f) of CD), 3.58 (m, 14H, H(b) and H(d) of CD), 2.33-2.76 (m, 78, methylene of $–CH_2CH_2-$) (Figure 4.17). From the integrated area of (S1) of H1 of β-CD and the integrated peak area (S2) of PEI from 2.76 to 2.33, the degree of β-CD substitution (DS) to PEI was calculated according to the following formula[50]:

DS = (S1/7) [(S2-4S1)]

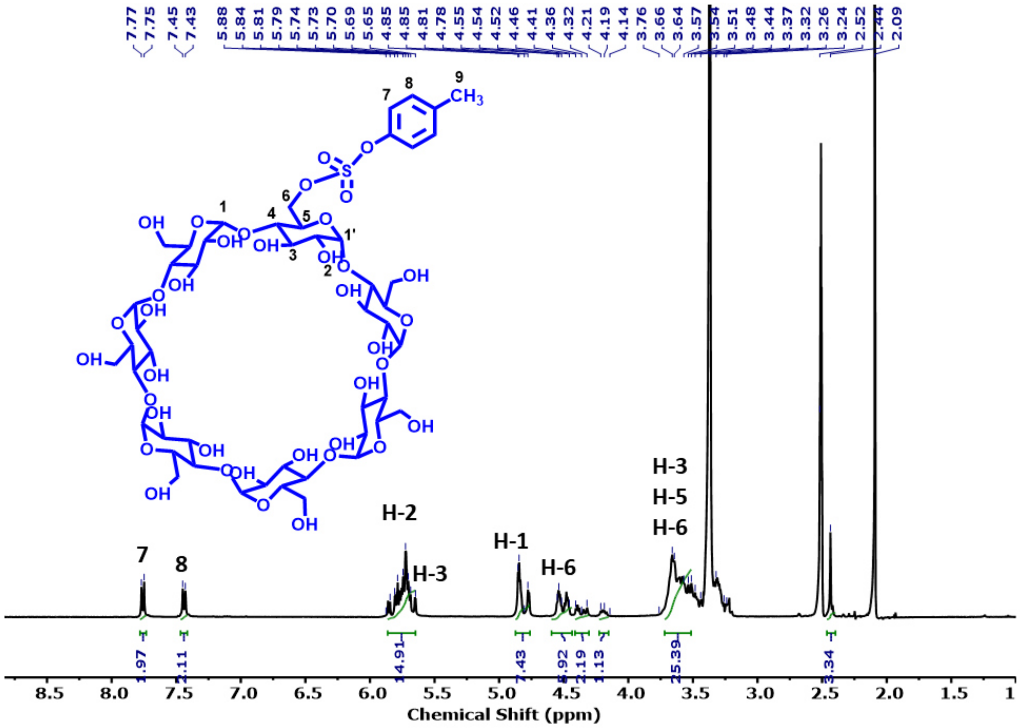

Figure 4.16. 400 MHz 1H NMR spectra Tosyl-β-CD in DMSO-d_6

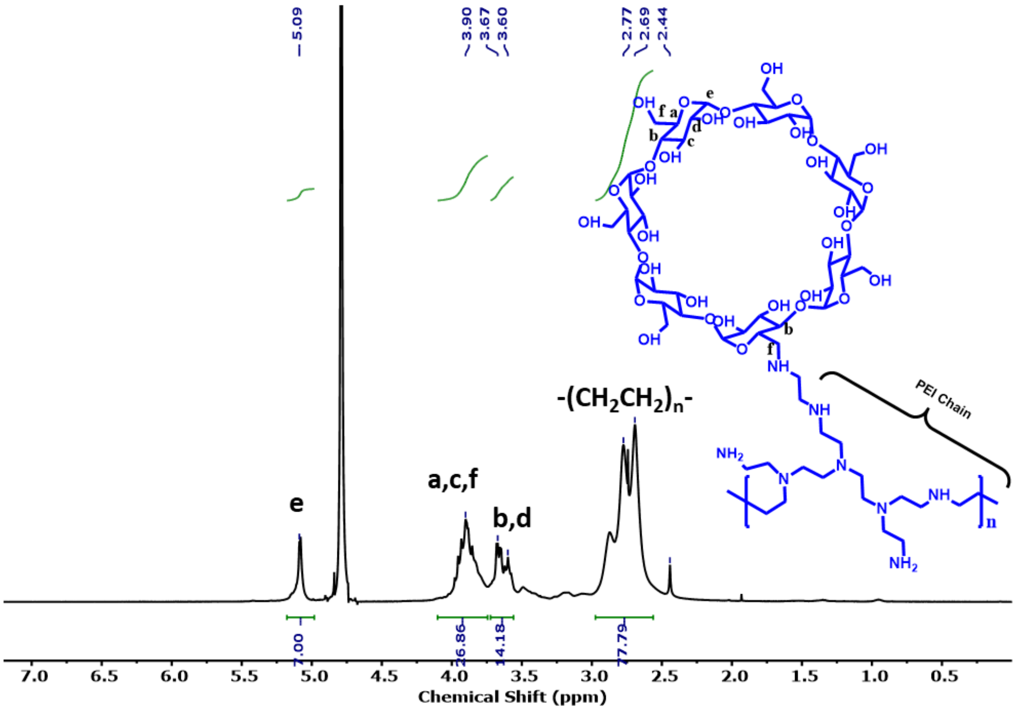

Figure 4.17. 400 MHz 1H NMR spectra Tosyl-β-CD in DMSO-d_6

4.4.4 Synthesis of Cationic Pillar[5]arene (CP[5]A)

The following three-step reaction was used to synthesize cationic pillar[5]arene according to the reported procedure (Figure 4.18).[51]

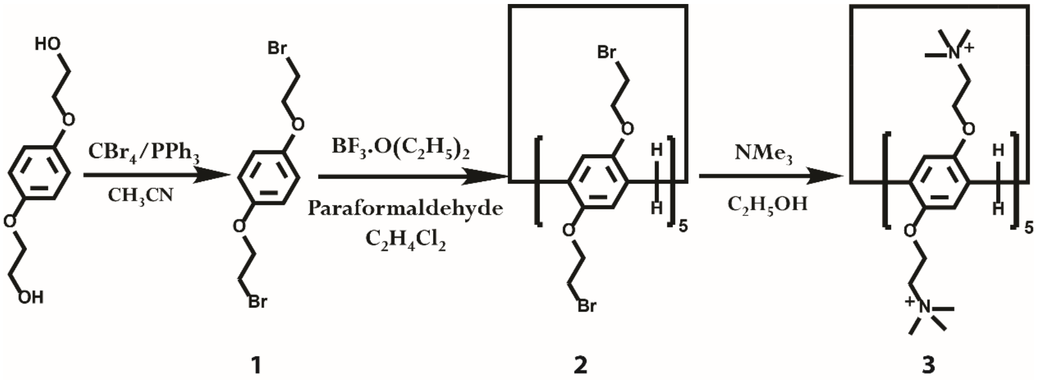

Figure 4.18. Synthesis of cationic Pillar[5]arene (CP[5]A).

4.4.4.1 Synthesis of 1

Carbon tetrabromide (39.8 g, 120 mmol) was gradually added in small amounts to a solution of 1,4-bis(2-hydroxyethoxy)benzene (10.0 g, 50.4 mmol) and triphenylphosphine (31.5 g, 120 mmol) in 300 mL dry acetonitrile at 0°C with stirring. After allowing the reaction mixture to cool to ambient temperature, the clear solution was stirred for further 4 hours under N_2. Product 1 precipitated as a white solid when 200 mL of cold water was added to the reaction mixture. Vacuum filtration was used to collect the product, which was then completely cleaned in a 60:40 methanol/water solution before being recrystallized from methanol. High vacuum was used to dry the white flake-like crystals (13.8 g, 85 %). Figure 4.19 shows the ^{1}H NMR spectra of 1. ^{1}H NMR (400 MHz, $CHCl_3$-d, r): δ (ppm): 6.79 (s, 4H), 4.27 (t, J=6.3 Hz, 4H), 3.64 (t, J=6.3Hz, 4H).

4.4.4.2 Synthesis of 2

Paraformaldehyde (0.349 g, 11.5 mmol) was added to a solution of 1 (3.37 g, 11.5 mmol) in 1, 2-dichloroethane (200 mL) under nitrogen atmosphere. The solution was then mixed with boron trifluoride diethyl etherate ($BF_3(OC_2H_5)_2$, 1.63 g, 11.5 mmol), and the mixture was stirred at room temperature for 3 hours. A green solution was obtained. The obtained solid was purified by column chromatography on silica gel with hexane/dichloromethane (1:2 v/v) as the eluent after the solvent was removed, yielding a white powder (1.6 g, 41%). ^{1}H NMR spectra of 2 is shown in Figure 4.20. ^{1}H NMR (400 MHz) δ (ppm): 6.83 (s, 10H), 4.15 (t, J=5.7Hz, 20H), 3.77 (s, 10H), 3.56 (t, j=5.7 Hz, 20H).

4.4.4.3 Synthesis of 3

Compound 3 (1.00 g, 0.595 mmol) and trimethylamine (33 % in ethanol, 6.43 mL, 23.8 mmol) were added to ethanol (50 mL). The mixture was refluxed overnight. The solvent was then evaporated, and deionized water (20 mL) was poured. A clear solution was obtained after filtration. The water was then evaporated completely to yield 1 as a colourless solid (1.28 g, 95 %). Figure 4.21 depicts the ^{1}H NMR spectrum of 3. ^{1}H NMR(400 MHz) δ (ppm): 6.94 (s, 10H), 4.44 (s, 20H), 3.93 (s, 10H), 3.80 (s, 20H), 3.22 (s, 90H).

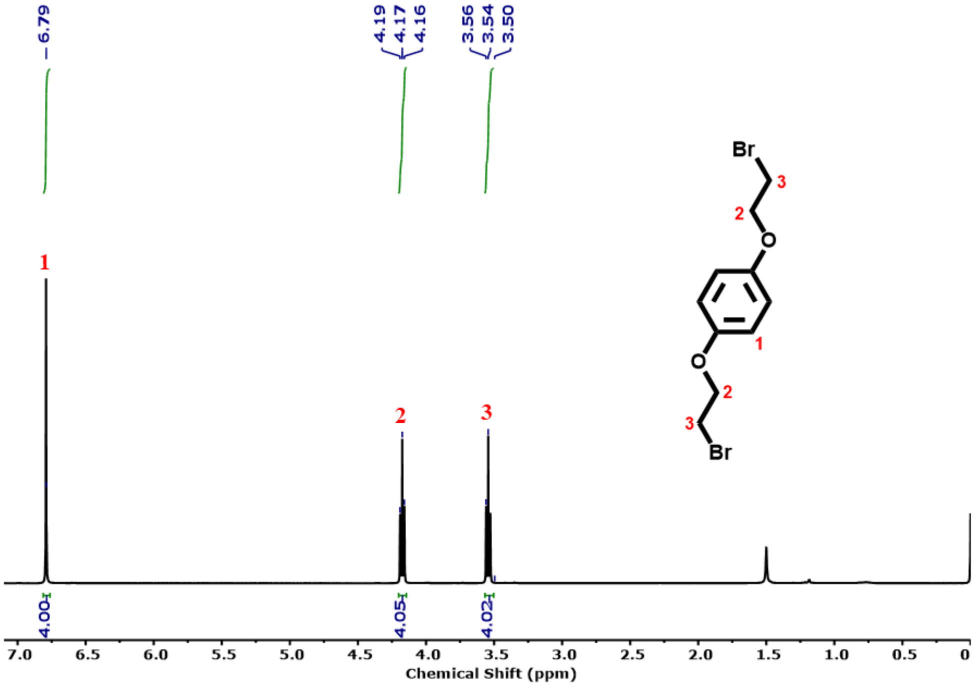

Figure 4.19. 400 MHz ^{1}H NMR spectra 1 in $CDCl_3$.

4.4.5 Substrate

The multilayer films were made on glass slides and silicon wafers. The thickness of the film was measured using silicon wafers as a substrate. Sylgard 184 was mixed with curing agent in a 10:1 weight ratio and cast onto a plastic petri plate to make PDMS elastomer. In a convection oven at 70°C, the prepolymer PDMS is allowed to settle for 2 hours. The piranha solution was used to clean all of the glass slides and silicon wafers. Glass slides were soaked for 45 minutes in a solution of H_2SO_4/H_2O_2 at a ratio of 7:3 (v/v), then rinsed with deionized water and dried for 5 minutes using nitrogen jet. *Beware! Piranha solution reacts aggressively to organic compounds and must be handled with caution*.

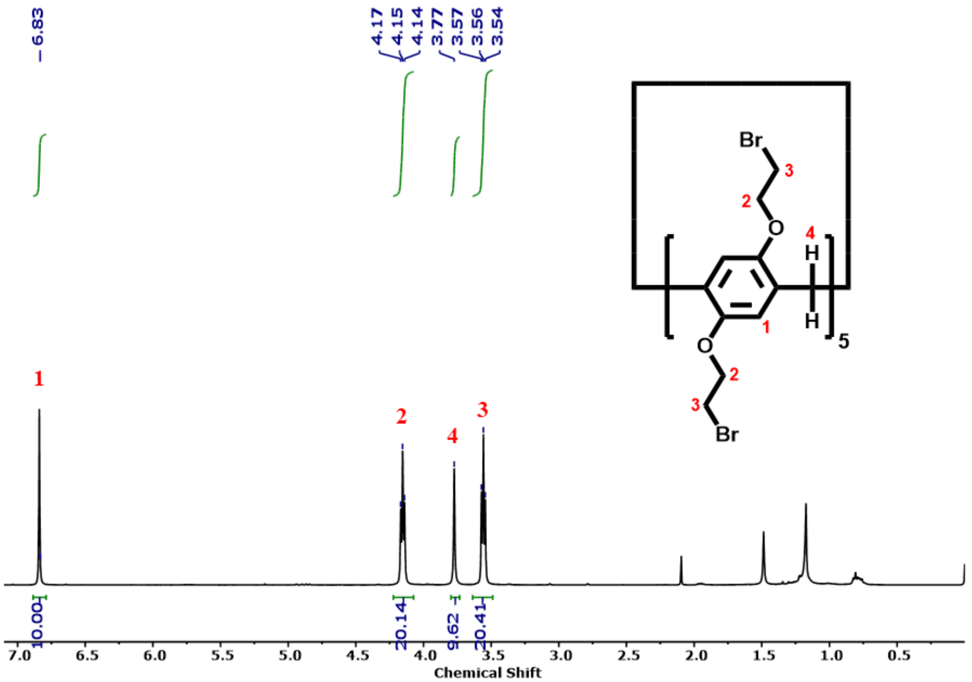

Figure 4.20: 400 MHz ^{1}H NMR spectra 2 in $CDCl_3$.

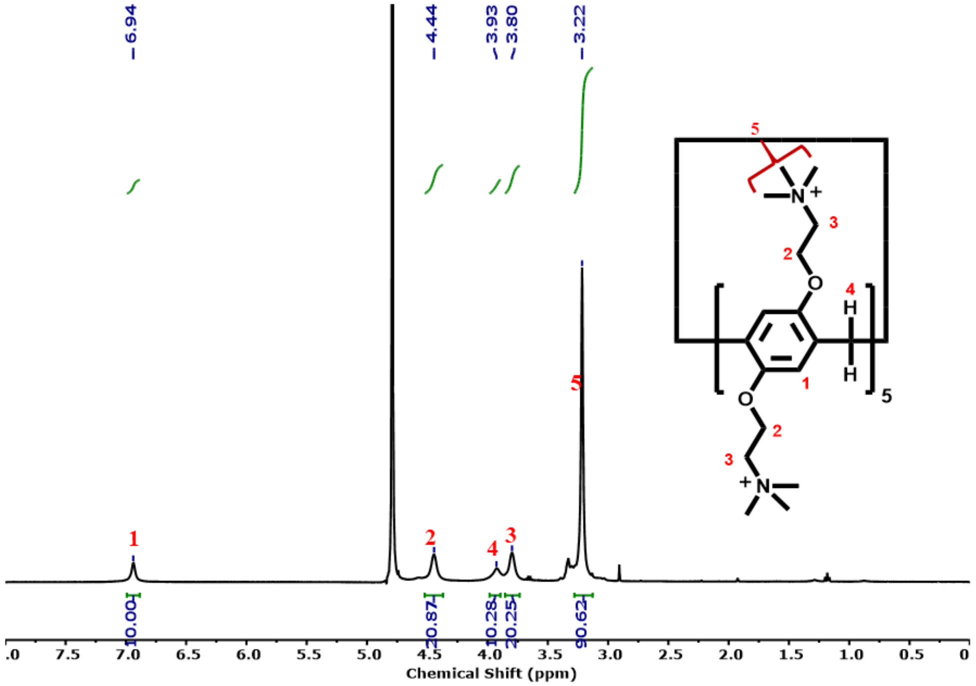

Figure 4.21: 400 MHz ^{1}H NMR spectra 3 in D_2O.

4.4.6 Multilayer Film Pattern and Tracking Fluid Flow

A thin layer of PDMS sheet with a small circular aperture in the centre (d=4.6mm) was first made and put on the glass slide in such a manner that the circular opening remained in the middle of the slide. Then the same glass slide with PDMS sheet was employed as a substrate for LbL deposition for required number of cycles. The PDMS sheet was peeled off to leave the film pattern after acquiring desired bilayers, maintaining the covered region untreated. The surface was carefully cleaned with water and sprayed with nitrogen gas. After that, an airtight imaging chamber (l= 1 cm, b= 1 cm, h = 1.8 mm) was used to cover the pattern, and an aqueous suspension of guest molecules was loaded into the chamber, along with 5 μm diameter neutral charged non-interacting polystyrene particles (tracer particles). Under an optical microscope, the complete setup was analysed, and movies were recorded for subsequent study. In each experiment, 20 tracer particles were monitored over a 15 second time interval using Tracker software to calculate fluid pumping velocity.

4.4.7 Fabrication of Multilayer Film

The multilayer films were made with a polyelectrolyte pair of PEI-β-CD and polyacrylic acid (PAA). An automated rotatory Dip Coater was used to fabricate the PAA/PEI-β-CD (host multilayer films) on microscope glass slides. Figure 1 depicts the full deposition process for making multilayer films using LbL assembly. The formation of the films was predominantly governed by electrostatic interaction between the pairs. Prior to multilayer deposition, a cleaned substrate was first treated with a priming solution (1 wt% branched PEI solution; pH 10) for 5 minutes. Next, the multilayer films were prepared by dipping the primer coated substrate in a PAA (0.2 wt%; pH 4) solution for 5 minute and then washing it with MilliQ water; the substrates were then dipped in PEI (0.1 wt%; pH 10) solution for 5 minutes before being washed with MilliQ water once more. The assembly of one PAA/PEI-β-CD double layer is described in this procedure. These steps with 1 minute dipping and washing in each solution were repeated until the desired number of bilayers have been deposited on the glass substrate. In the same way, the $(PAA/CP[5]A)_{2BLs}$ were made with a layer by layer assembly with consecutive adsorption of CP[5]A, and PAA. The primer coated substrate was immersed in an aqueous solution of PAA (0.2 wt%; pH 4) for 5 minutes and then immersed in CP[5]A (0.5 wt%) for 30 minutes with an intermediate steps of rinsing with water. By repeating the alternate immersion processes in PAA and CP[5]A solutions, multilayer films (nL, n being the number of deposited layers) were obtained.

4.4.8 Isothermal Titration Calorimetry (ITC)

The thermodynamic parameters of L- and D-Trp with β-CD complexations were measured at 25°C in phosphate buffer (pH 5.9) using a Malvern MicroCal PEAQ-ITC. The

20 mM of L- and D-Trp (pH 5.9) solution in the syringe was titrated into the 250μM β-CD in the calorimeter cell with 25 (1.5μL) and 19 (1.5μL) consecutive injections every 150 seconds intervals rsepectively. The same injections into aqueous under the same conditions were used in all control experiments (for the heat of dilution). The curve fitting was done on the ITC instrument using a one-site model fitting based on the thermal effect per injection.

Note: The permission has been granted by authors and corresponding author of the published paper prior to its adoption in the present thesis. The publication associated with this work is:

Mujeeb Alam, Chinmayee Agashe, Arshdeep Kaur Gill, Rohit Varshney, Naveen Tiwari and Debabrata Patra. Discrimination of enantiomers and constitutional isomers by self-generated macroscopic fluid flow. ***Chem. Commun.,*** 2023, **59**, 434-437.

4.5 References

1. E. Rubenstein, W. A. Bonner, H. P. Noyes, G. S. Brown, *Nature*, 1983, **306**, 118-118.
2. C. Han, X. Hou, H. Zhang, W. Guo, H. Li, L. Jiang, *J. Am. Chem. Soc.*, 2011, **133**, 7644-7647.
3. X. Gu, Y. Tao, Y. Pan, L. Deng, L. Bao, Y. Kong, *Anal. Chem.*, 2015, **87**, 9481-9486.
4. K. C. Honeychurch, J. P. Hart, *Electroanalysis: An International Journal Devoted to Fundamental and Practical Aspects of Electroanalysis*, 2007, **19**, 2176-2184.
5. V. M. Gumerov, E. P. Andrianova, M. A. Matilla, K. M. Page, E. Monteagudo-Cascales, A. C. Dolphin, T. Krell, I. B. Zhulin, *Proc. Natl. Acad. Sci.*, 2022, **119**, e2110415119.
6. J. Ma, H. Yan, J. Quan, J. Bi, D. Tian, H. Li, *ACS appl. Mater. Interfaces*, 2018, **11**, 1665-1671.
7. S. Zhuo, X. Wang, L. Li, S. Yang, Y. Ji, *ACS Appl. Mater. Interfaces*, 2021, **13**, 31059-31065.
8. R. Meulenberg, M. Pepi, J. A. de Bont, *Biodegradation*, 1996, **7**, 303-311.
9. Y.-Q. Wang, Q.-H. Tan, H.-T. Liu, Z.-L. Liu, *RSC adv.*, 2015, **5**, 86614-86619.
10. K. Asadpour-Zeynali, P. Najafi-Marandi, *Electroanalysis*, 2011, **23**, 2241-2247.
11. K. Wang, L. Wang, W. Jiang, J. Hu, *Talanta*, 2011, **84**, 400-405.
12. R.-P. Liang, C.-M. Liu, X.-Y. Meng, J.-W. Wang, J.-D. Qiu, *J. Chromatr. A*, 2012, **1266**, 95-102.
13. R. Pandey, M. Collins, X. Lu, S. R. Sweeney, J. Chiou, A. Lodi, S. Tiziani, *Ana. Chem.*, 2021, **93**, 5805-5814.

14. J. Yu, S. Di, H. Yu, T. Ning, H. Yang, S. Zhu, *J. Chromatr. A*, 2021, **1637**, 461822.
15. D. N. Shurpik, Y. I. Aleksandrova, A. A. Rodionov, E. A. Razina, M. R. Gafurov, I. R. Vakhitov, V. G. Evtugyn, A. V. Gerasimov, Y. I. Kuzin, G. A. Evtugyn, *Langmuir*, 2021, **37**, 2942-2953.
16. L. Dong, Y. Zhang, X. Duan, X. Zhu, H. Sun, J. Xu, *Anal. Chem.*, 2017, **89**, 9695-9702.
17. X. Niu, S. Yan, J. Chen, H. Li, K. Wang, *Electrochim. Acta*, 2022, **405**, 139809.
18. F. Li, K. Jiang, Q. Wu, Z. Li, G. Chen, *Electroanalysis*, **2022**.
19. Y. Fang, D. Wang, X. Lv, X. Xu, H. Zhou, P. Liu, B. Cui, L. Wang, *Sens. Actuators B: Chem.l*, 2021, **333**, 129568.
20. J. Fu, S. Zhou, P. Zhao, X. Wu, S. Tang, S. Chen, Z. Yang, Z. Zhang, *Biosens. Bioelectron.*, 2022, **198**, 113848.
21. H. Zhu, Q. Li, Z. Gao, H. Wang, B. Shi, Y. Wu, L. Shangguan, X. Hong, F. Wang, F. Huang, *Angew. Chem. Int. Ed.*, 2020, **59**, 10868-10872.
22. J. Ji, Y. Li, C. Xiao, G. Cheng, K. Luo, Q. Gong, D. Zhou, J. J. Chruma, W. Wu, C. Yang, *Chem. Comm.*, 2020, **56**, 161-164.
23. X. Zhu, J. Zhao, F. Dai, W. Xu, L. Chen, X. Xiao, Z. Tao, C. Zhang, *Spectrochim. Acta A: Mol. Biomol. Spectrosc.*, 2021, **250**, 119381.
24. B. Kaur Billing, *ChemistrySelect*, 2021, **6**, 9571-9590.
25. A. Dinu, C. Apetrei, *Int. J. Mol. Sci.*, 2022, **23**, 1218.
26. K. S. Babu, A. Padmanaban, V. Narayanan, *Inorg. Chem. Comm.*, 2022, **139**, 109400.
27. L. Cong, Z. Ding, T. Lan, M. Guo, F. Yan, J. Zhao, *Carbohydr. Polym.*, 2021, **271**, 118446.
28. G. A. H. D. Banni, R. Nasreddine, S. Fayad, P. Cao-Ngoc, J.-C. Rossi, L. Leclercq, H. Cottet, A. Marchal, R. Nehmé, *Analyst*, 2021, 146, 1386-1401.
29. M. Wang, Q. Gong, W. Liu, S. Tan, J. Xiao, C. Chen, *J. Sep. Sci.*, 2022, 38, 8296-8303.
30. K. Zamuruyev, M. S. Ferreira Santos, M. F. Mora, E. A. Kurfman, A. C. Noell, P. A. Willis, *Anal. Chem.*, 2021, **93**, 9647-9655.
31. M. De Silva, P. M. Opallage, R. C. Dunn, *Anal. Methods*, 2021, **13**, 1340-1348.
32. Z. Liu, X. Li, H. Masai, X. Huang, S. Tsuda, J. Terao, J. Yang, X. Guo, *Sci. Adv.*, 2021, 7, eabe4365.
33. P. Dominique, M. Schnurr, B. Lewandowski, *Chem. Comm.*, 2021, **57**, 3476-3479.
34. S. Ohtani, K. Kato, S. Fa, T. Ogoshi, *Coord. Chem. Rev.*, 2022, **462**, 214503.
35. R. W. Pow, Z. L. Sinclair, N. L. Bell, N. Watfa, Y. M. Abul-Haija, D. L. Long, L. Cronin, *Chem. Euro. J.*, 2021, **27**, 12327-12334.

36. Y. Liu, H. Wang, L. Shangguan, P. Liu, B. Shi, X. Hong, F. Huang, *J. Am. Chem. Soc.*, 2021, **143**, 3081-3085.
37. D. S. Hassan, A. Zeus, K. G. Brady, S. Murkli, L. Isaacs, C. Wolf, *Org. Biomol. Chem.* **2021**, *19*, 4248-4253.
38. Y. Zheng, Y. Kobayashi, T. Sekine, Y. Takashima, A. Hashidzume, H. Yamaguchi, A. Harada, *Commun. Chem.*, 2018, **4**, 1-7.
39. A. Harada, R. Kobayashi, Y. Takashima, A. Hashidzume, H. Yamaguchi, *Nat. chem.*, 2011, **3**, 34-37.
40. L. Luo, G. Nie, D. Tian, H. Deng, L. Jiang, H. Li, *Angew. Chem. Int. Ed.*, 2016, **55**, 12713-12716.
41. R. Varshney, M. Alam, C. Agashe, R. Joseph, D. Patra, *Chem. Comm.*, 2020, **56**, 9284-9287.
42. M. Alam, R. Varshney, C. Agashe, A. K. Gill, D. Patra, *Chem. Comm.*, 2021, **57**, 4584-4587.
43. R. Varshney, A. K. Gill, M. Alam, C. Agashe, D. Patra, *Lab Chip*, 2021, **21**, 4352-4356.
44. M. Alam, A. K. Gill, R. Varshney, C. Miglani, N. Tiwari, D. Patra, *Soft Matter*, 2022, **18**, 5605-5614.
45. G. Xie, W. Tian, L. Wen, K. Xiao, Z. Zhang, Q. Liu, G. Hou, P. Li, Y. Tian, L. Jiang, *Chem. Comm.*, 2015, **51**, 3135-3138.
46. L. Zhu, H. Yan, C. Y. Ang, K. T. Nguyen, M. Li, Y. Zhao, *Chem. Euro. J.*, 2012, **18**, 13979-13983.
47. X. Tan, G. Zhao, X. Zhou, T. Li, H. Lei, G. Du, L. Yang, *Anal. Chim. Acta*, 2018, **1036**, 49-57.
48. R. C. Petter, J. S. Salek, C. T. Sikorski, G. Kumaravel, F. T. Lin, *J. AM. Chem. Soc.* 1990, **112**, 3860-3868.
49. S. H. Pun, N. C. Bellocq, A. Liu, G. Jensen, T. Machemer, E. Quijano, T. Schluep, S. Wen, H. Engler, J. Heidel, M. E. Davis, *Bioconjug. Chem.* 2004, **15**, 831–840.
50. J. Wan, *Polymers* **2012**, *4*, 1084–1108.
51. Y. Ma, X. Ji, F. Xiang, X. Chi, C. Han, J. He, Z. Abliz, W. Chen, F. Huang, *Chem. Commun.*, 2011, **47**, 12340-12342.

Chapter 5

Cavity Shape Dependent Self-Sorting of Pillar[n]arenes via Macroscopic Fluid Flow

5.1 Introduction

Supramolecular chemistry has risen to prominence in recent decades, emulating some of nature's most fundamental aspects, such as self-assembly, molecular recognition, self-sorting, multivalency, complementarity, etc.[1–6] Supramolecular chemists have used concepts like self-assembly,[7,8] templating[9] to construct supramolecular structures for more than 20 years, but the strategy of self-sorting remains scarce. Self-sorting is the ability to recognise the difference between "self" and "non-self" in a mixture of related components.[3,10,11] It is a fundamental aspect of natural and biological systems and has been observed less commonly in synthetic supramolecular systems.[12–14] Consider for example, how fish form schools with members of their own species, how some compounds spontaneously resolve upon crystallisation to form conglomerates,[3] formation of DNA double helix: four bases (adenine (A), thymine (T), guanine (G), and cytosine (C)) automatically self-sort to form two base pairs (AT and GC).[15,16] During cell growth, carbohydrates, peptides, and fatty acids also self-sort.[3,17] Self-sorting requires components to have a stronger interaction with themselves than with other components, as specified by the binding affinities between all possible pairings. It's a promising way to make supramolecular assemblies with precise architectures and integrated functionalities.[12,18,19]

The majority of self-sorting systems rely on geometric matching of global shapes or alignment of local interactions. The challenge of developing a successful self-sorting algorithm is directly proportional to the similarity of the individual components. This is because structural variations on which discrimination should be based become smaller and smaller. To build complicated supramolecular systems, supramolecular self-assembly of µm-to-mm sized components is required. However, at this length scale, selective assembly to construct defined structures is difficult because short-range molecular recognition cannot drive the assembly of macroscopic components. As a result, it is challenging to monitor self-sorting at the molecular level using spectroscopic techniques such as NMR, mass spectroscopy, FTIR spectroscopy, etc. Attempts have been made to explore this uncommon self-sorting and convert them into observable outputs that could work as a doorway to the macroscopic domain. In this regard, the fluid-flow-based self-sorting achieved by micropump proves to be a promising novel approach owing to its capability to convert weak signals into macroscopic observations. The autonomous fluid flow in chemical micropumps results from the harvesting of chemical free energy from the surrounding environment, which can be used to convert weak signals into macroscopic observation.[20–23] In this work, we uncovered surprising self-sorting behaviour governed by geometrical complementarity by the shape of pillar[n]arenes on a surface via macroscopic fluid flow. Pillar[n]arenes possess exceptionally symmetrical polygonal tube architectures; pentagonal and hexagonal molecules, respectively, are examples of pillar[5]arene (P[5]A) and pillar[6]arene (P[6]A).[24–27] The fluid-flow based self-sorting in the area of micropump technology is very uncommon. It has not been recognized till now and should be given more attention.

Herein, layer-by-layer (LbL) deposition was used to fabricate a multilayer thin film composed of anionic pillar[n]arenes (anionic pillar[5]arene and pillar[6]arene) and cationic pillar[n]arenes (cationic pillar[5]arene and pillar[6]arene) as electrolyte pairs to develop the micropump. Using a concept of geometrical complementarity by shape, we demonstrated fluid-flow-based self-sorting behaviour during our study of the layer-by-layer assembly of pillar[5]arenes and pillar[6]arenes on a substrate. These multilayer films were placed inside a microchamber and employed as a scaffold to demonstrate their practical value through fluid flow study. Ionic pillar[5]arenes shows fluid flow toward layers created by oppositely charged pillar[5]arenes, whereas ionic pillar[6]arenes were not. Similarly, fluid flow toward layers made from oppositely charged pillar[6]arenes was observed for the reverse combination of ionic pillar[6]arenes, but not for ionic pillar[5]arenes. This behaviour is caused by the surface forming distinct assembly patterns based on the ring shape of the pillar[n]arenes.

5.2 Results and Discussions

5.2.1 Fabrication of Multilayer Films

The anionic and cationic pair of pillar[n]arenes (see experimental section for synthesis) were used to make the multilayer films via layer-by-layer (LbL) deposition technique, and the electrostatic interactions between the pairs regulated the formation of the multilayer films. The substrate was first dipped in an aqueous solution of polyethyleneimine (1 wt%, pH 10) for 10 minutes for priming, followed by washing with water for 2 minutes and drying in air for 2 minutes. To grow the multilayer film of oppositely charged pillar[5]arenes, the primer-coated substrate was dipped in an aqueous solution of anionic pillar[5]arenes (AP[5]A, 0.5 wt%, pH ~12) and cationic pillar[5]arenes (CP[5]A, 0.5 wt %, pH~6) alternately for 30 minutes each with intermediate steps of rinsing in water for 2 minutes and drying in air for 2 minutes. The process was performed until the required number of bilayers (BLs) was obtained (Figure 5.1). In a similar way, the multilayer films of anionic pillar[6]arenes (AP[6]A, 0.5 wt%, pH ~12) and cationic pillar[6]arenes (CP[6]A, 0.5 wt %, pH~6) were fabricated at the same conditions (Figure 5.1). 5BLs in the case when cationic pillar arene was on the top layer, while 5.5 BLs when anionic pillar arene was on the top layer were grown for all experiments.

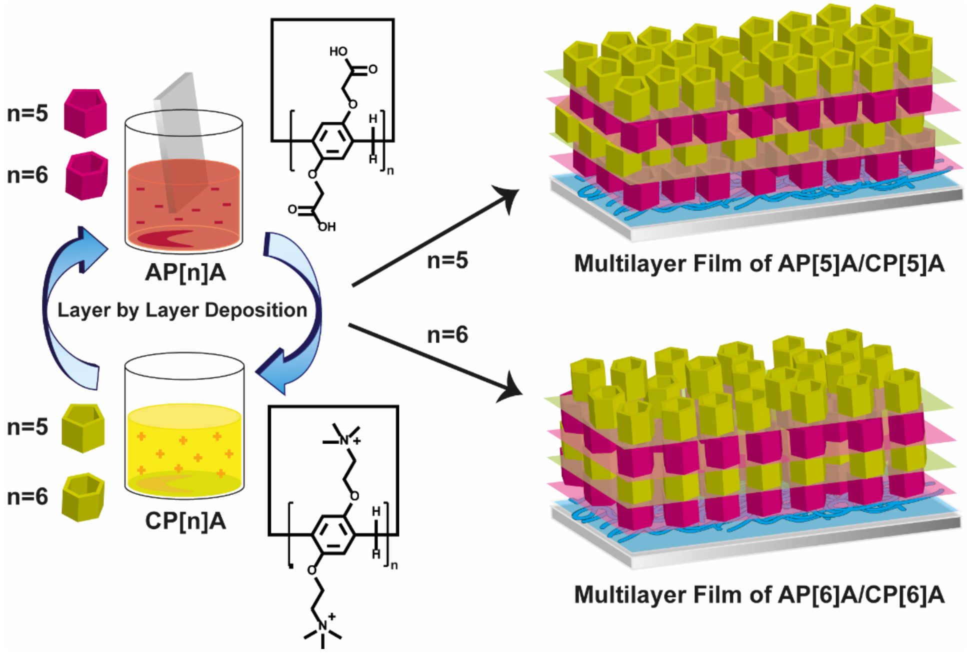

Figure 5.1. Schematic of layer-by-layer (LbL) assembly of cationic and anionic P[n]As.

5.2.2 Self-Sorting on a Surface Based on Shape (Fluid-Pumping Study)

To examine the shape-dependent self-sorting on a surface, the micropump was made by placing multilayer film in a disc shape over the centre of a glass slide (4.6 mm diameter). To track the fluid flow around the coating, sulphate latex particles (5 µm in diameter) suspended in an aqueous solution a of substrate (pillar[5]arenes and pillar[6]arenes) were injected as tracers into the chamber and closed with an imaging chamber. On observing under the microscope, fluid flow toward coatings generated within the chamber from oppositely charged pillar[5]arenes was observed on injecting an aqueous solution of ionic pillar[5]arenes, but not in the case of ionic pillar[6]arenes (Figure 5.2a, c, and d). Similarly, ionic pillar[6]arenes showed fluid flow toward coatings created from oppositely charged pillar[6]arenes in the reverse combination, whereas ionic pillar[5]arenes did not show any fluid flow (Figure 5.2b). The assemblies formed by the electrostatic cationic-anionic interactions are strong non-directional physical interactions; therefore, they are not self-sorting by nature. However, successful self-sorting is realized through geometrical complementarity by shape. The fluid flow of oppositely charged pillar[n]arenes with the same shape was observed due to the self-sorting of same shape and oppositely charged pillar[n]arenes. This behaviour is caused by forming different assembly patterns on the surface depending on the shape of pillar[n]arenes ring. All studies were carried out with 5 bilayers (BLs) of each set-in case when cationic pillar[n]arene was on the top layer ((AP[5]A/CP[5]A)$_{5BLs}$, (AP[6]A/CP[6]A)$_{5BLs}$), and 5.5BLs when anionic pillar[n]arene was on the top layer ((CP[5]A/AP[5]A)$_{5.5BLs}$, and (CP[6]A/AP[6]A)$_{5.5BLs}$). Figure 5.3 depicts the pumping velocity profile for all cases in the presence of their corresponding substrates.

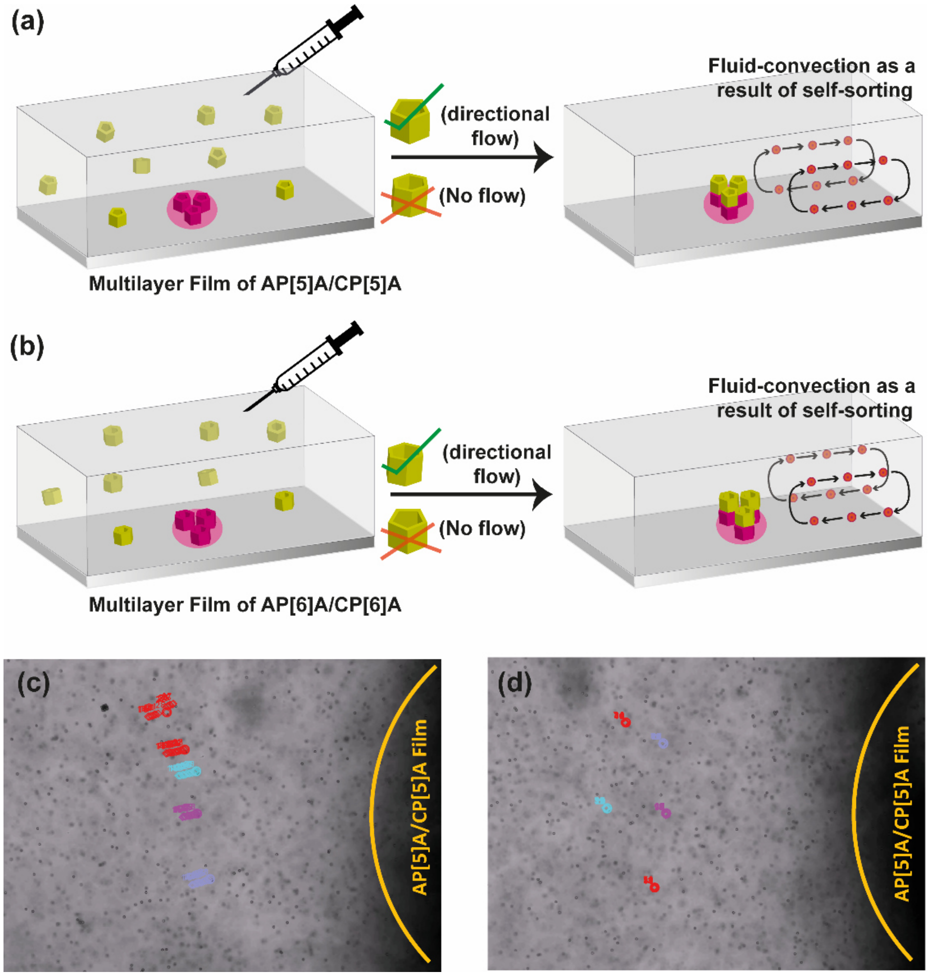

Figure 5.2. Schematics of fluid pimping as a result of self-sorting of (a) ionic pillar[5]arenes, and pillar[6]arenes. Tracer particles trajectories: (c) directional flow as a result of self-sorting between same shape and oppositely charged pillar[n]arenes, and (d) non-directional flow as a result of no self-sorting between different shape and oppositely charged pillar[n]arenes.

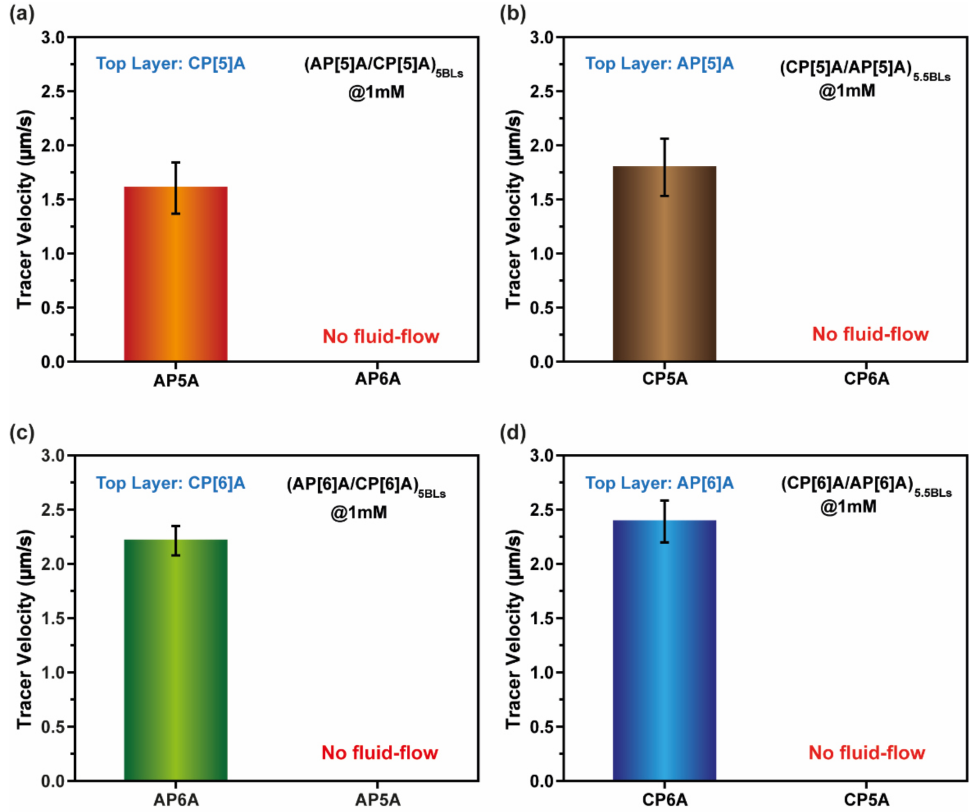

Figure 5.3. Tracer velocity for (a) (AP[5]A/CP[5]A)$_{5BLs}$, (b) (CP[5]A/AP[5]A)$_{5.5BLs}$, (C) (AP[6]A/CP[6]A)$_{5BLs}$, and (d) (CP[6]A/AP[6]A)$_{5.5BLs}$ film in the presence of their corresponding substrates (AP[5]A, CP[5]A, AP[6]A, and CP[6]A).

5.2.3 Effects of Substrate Concentration on Fluid Velocity

Three sets of concentrations (1, 2, and 3 mM) were utilized to demonstrate the change in fluid velocity with substrate concentration. All experiments were performed with 5 and 5.5 bilayers (BLs) of each set, as above mentioned. We predicted that as the substrate concentration increases, the pumping velocity would increase due to an increase in the degree of self-sorting, which in turn causes a higher density change in the fluid. As a result, more assembly patterns occurred on increasing the substrate concentration within the chamber. This will directly affect the solutal buoyancy, which enhances the tracer velocity. The hypothesis was validated, and the pumping behaviour was investigated using all sets of multilayer films. According to the plots shown in Figure 5.4, the pumping velocity increased as the substrate concentration increased. We observed that the tracer velocity increases from 1.60±0.23µm/s (1mM) to 2.96±0.15µm/s (3mM) for (AP[5]A/CP[5]A)$_{5BLs}$, 1.79±0.26µm/s (1mM) to 2.94±0.21µm/s (3mM) for (CP[5]A/AP[5]A)$_{5.5BLs}$, 2.39±0.19µm/s (1mM) to 3.44±0.28µm/s (3mM) for (AP[6]A/CP[6]A)$_{5BLs}$, and 2.21±0.13µm/s (1mM) to

3.41±0.26μm/s (3mM) for $(CP[6]A/AP[6]A)_{5.5BLs}$ as shown in Figure 5.4a, b, c, and d, respectively. It is important to mention that the tracer velocity for pillar[6]arenes coating was always higher than pillar[5]arenes at any given substrate concentration. The higher tracer velocity in the case of pillar[6]arenes was the result of the greater symmetry of pillar[6]arenes due to its hexagonal shape as compared to pentagonal pillar[5]arenes.

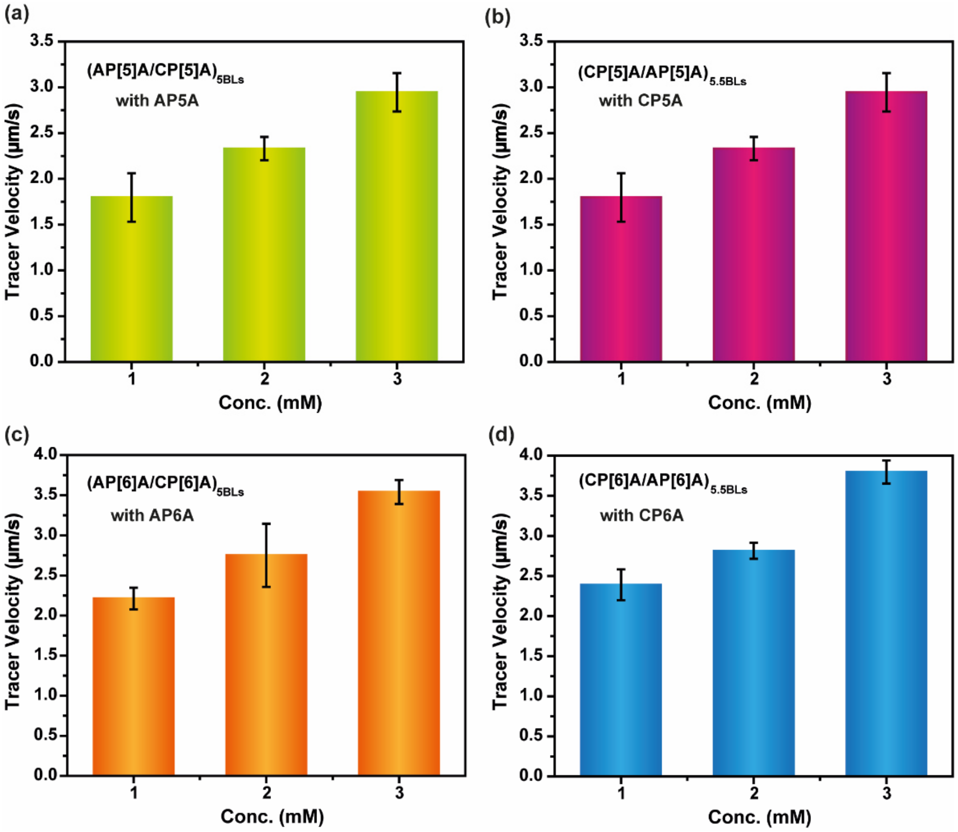

Figure 5.4. Tracer velocity with varying concentration of corresponding substrate (a) $(AP[5]A/CP[5]A)_{5BLs}$ with AP[5]A, (b) $(CP[5]A/AP[5]A)_{5.5BLs}$ with CP[5]A, (c) $(AP[6]A/CP[6]A)_{5BLs}$ with AP[6]A, and (d) $(CP[6]A/AP[6]A)_{5.5BLs}$ with CP[6]A.

Next, we investigated the variation in fluid pumping velocity by injecting the solution of AP[5]A/AP[6]A mixture (molar ratio 1:1) to the corresponding multilayer films of $(AP[5]A/CP[5]A)_{5BLs}$ and $(AP[6]A/CP[6]A)_{5BLs}$), and the solution of CP[5]A/CP[6]A mixture (molar ratio 1:1) to the corresponding bilayers of each set of $((CP[5]A/AP[5]A)_{5.5BLs}$ and $(CP[6]A/AP[6]A)_{5.5BLs}$. The concentration of the mixture was maintained at 6mM for all experiments. Figure 5.5 showed that the pumping velocity was slightly lower than the velocity of the solution having a concentration of 3mM. The presence of both pillararenes (P[5]As and P[6]As) in the same solution creates a hindrance within the chamber, which in turn results in a small decrease in tracer velocity as shown in Figure 5.5.

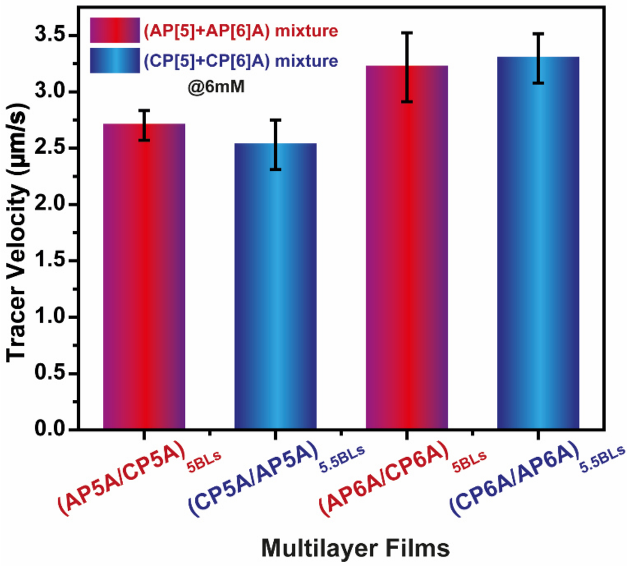

Figure 5.5. Tracer velocity on adding mixture of (AP[5]A+AP[6]A) and (CP[5]A+C[6]A) solution (6mM) to the corresponding multilayer films.

5.2.4 Self-Sorting Analysis by UV-Vis Absorption Spectra

The cavity-shape-dependent self-sorting was further confirmed by ultraviolet-visible (UV-Vis) spectroscopy. To check the absorbance of each layer, quartz slides were used to fabricate the multilayer films. The absorbance at 293 nm increased linearly as the number of coated layers, corresponding to the absorption of 1,4-dialkoxybenzene groups in pillar[5]arene (Figure 5.6a). A similar pattern was seen in multilayer films composed of CP[6]A and AP[6]A, which indicates that the multilayer films were made by alternately dipping a substrate in cationic and anionic solutions of pillar[6]arenes repeatedly, with the same shape and geometry (Figure 5.6b). The plot shown in figure 5.6c suggested that the absorbance intensity of pillar[6]arenes multilayer films increased at a faster rate than pillar[5]arenes multilayer films at 293 nm, implying that the pillar[6]arenes has a greater density on the substrate than pillar[5]arenes. Molecular tiling utilises hexagonal molecules packed tightly together to create high-density supramolecular structures. The greater symmetry of hexagonal pillar[6]arenes compared to pentagonal pillar[5]arenes might be a possible factor for the higher density of pillar[6]arenes on the substrate than pillar[5]arenes. The higher absorption intensity of P[6]A as compared to P[5]A is in good agreement with the higher tracer velocity in the case of P[6]A multilayer films, as discussed earlier in the section 5.2.3.

Further, we have also checked the self-sorting of bilayer formation by deposition of cationic P[6]A on anionic P[5]A monolayer to create microporous films with different

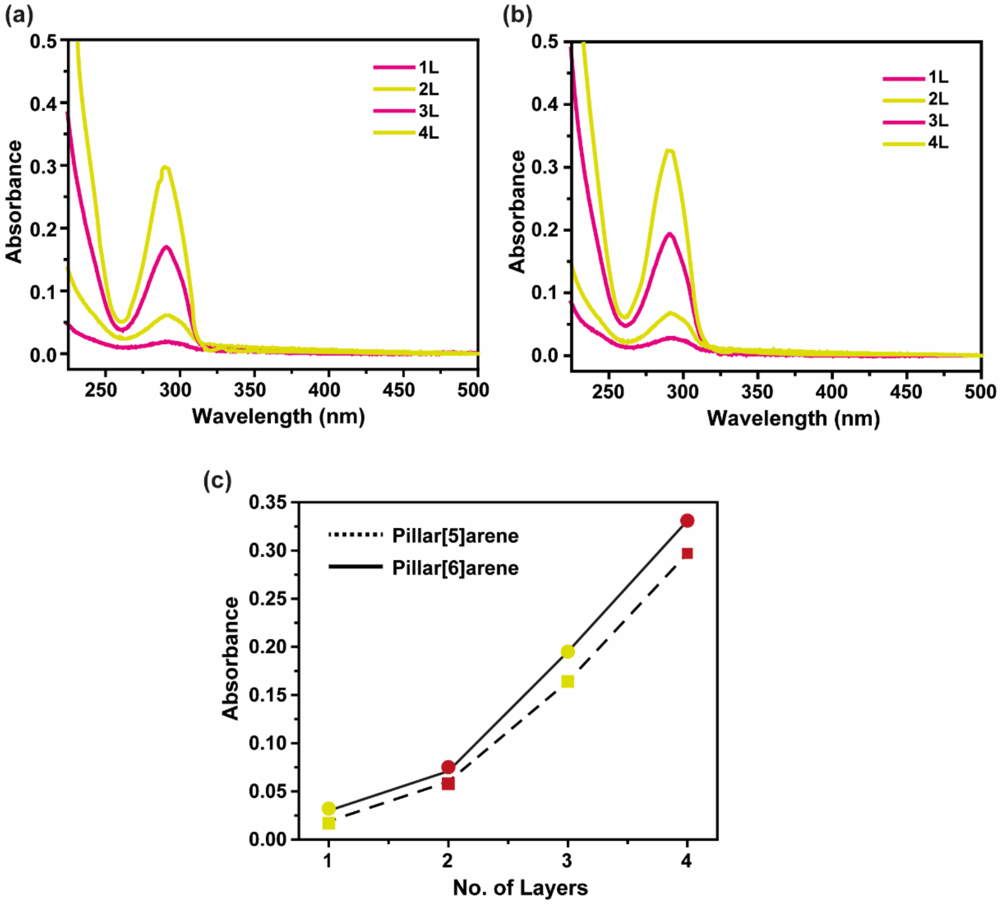

Figure 5.6. UV-vis absorption spectra of the film fabricated by repeated adsorption of (a) AP[5]A and CP[5]A, (b) AP[6]A and CP[6]A (c) cationic and anionic P[5]As (dotted line), and (b) cationic and anionic P[6]As (solid line).

porosity. Despite our predictions, there was no increase in absorption after dipping the monolayer of P[5]A with an anionic surface in an aqueous solution of cationic P[6]A (Figure 5.7a). It shows that no P[6]A molecules were deposited on the cationic monolayer of P[5]A. In a similar way, after dipping monolayer of P[6]A with an anionic surface in an aqueous solution of cationic P[5]A, the absorption of the cationic P[5]A monolayer did not change (Figure 5.7b). As aforementioned, multilayer films can only be made utilising pillar[n]arenes which have the same ring shape; that is, homo-assembly of ionic pillar[5]arenes CP[5]A and AP[5]A or ionic pillar[6]arenes CP[6]A and AP[6]A. Therefore, ring shape-dependent self-sorting was used to assemble ionic pillar[5]arenes as well as pillar[6]arenes on a surface. These results supported the control experiments of adding ionic pillar[n]arenes into the multilayer films containing oppositely charged pillar[n]arenes of different shapes which showed no fluid flow as discussed earlier in the fluid pumping study (section 5.2.2).

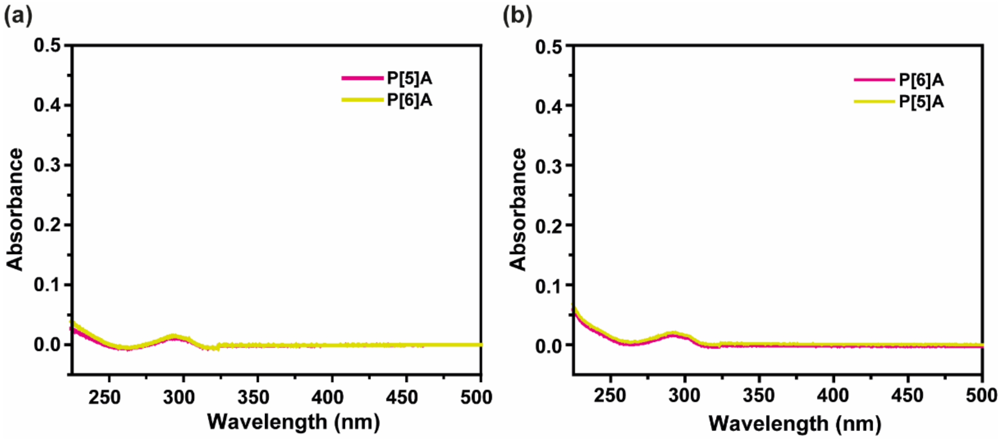

Figure 5.7. UV-vis absorption spectra of the film fabricated by repeated adsorption of (a) AP[5]A and CP[6]A, and (b) AP[6]A and CP[5]A.

5.2.5 Effect of Adding Guest Molecule on Fluid Pumping

Methyl viologen (MV) was used as a complementary guest molecule to check the self-sorting in the presence of the guest molecule. According to the previous studies, MV forms a stable complex with pillar[5]arenes with a binding constant of 2.5 x 10^4 M^{-1}.[28] To investigate the pumping behaviour of self-sorting in the presence of guest molecule, coatings obtained from ionic charged pillar[5]arenes were dipped in an aqueous solution of methyl viologen for 30 minutes to form the "host-guest" complex between AP[5]A and MV. Before usage, any physically trapped or unwanted guest molecules were removed by washing with water and drying with a nitrogen stream. To show the pumping behaviour, an imaging chamber was put on the pre-soaked host multilayer film (AP[5]A/MV film). Next, upon the addition of an aqueous solution of anionic pillar[5]arene into the chamber, an inward motion of the tracer particles towards the coating was observed with the tracer velocity of 0.50 µm/s. While in another case, the solution of 1 mM AP[5]A was mixed with 1 mM MV solution for 30 min to form AP[5]A/MV complex. To demonstrate the pumping behaviour, multilayer film obtained from ionic charged pillar[5]arenes was covered with an imaging chamber. Next, upon the addition of a pre-assembled solution of AP[5]A/MV complex into the chamber, an inward flow was observed towards the coating with the velocity of 0.55 µm/s. This is because of the fact that the available sites on the host multilayer film were gradually occupied upon the addition of MV. Therefore, the binding sites available for self-sorting decrease due to an increase in repulsion between the injected solution (CP[5]A) and MV encapsulated in the AP[5]A, which in turn decreased the tracer velocity.

5.2.6 Self-sorting in Microchannel

Here, we expanded the capabilities of these self-driving pumps by investigating a self-sorting of pillar[n]arenes for transferring fluids over large distances via complex microchannels. A dumbbell-shaped channel was fabricated by soft lithography[29] to show flow over a long distance. The goal of using this kind of channel was to determine whether or not self-sorting would take place through the inlet and output of the channel. To show the fluid flow inside the microchannel, a dumbbell-shaped microchannel was put on the multilayer films in such a way that the chamber C1 was on $(AP[6]A/CP[6]A)_{5BLs}$ coating and chamber C2 was on $(AP[5]A/CP[5]A)_{5BLs}$ coating as shown in Figure 5.8. The channel was composed of two circular chambers of 1 cm diameter (C1 and C2) that were interconnected by 400 µm long and 200 µm deep connector denoted as L.

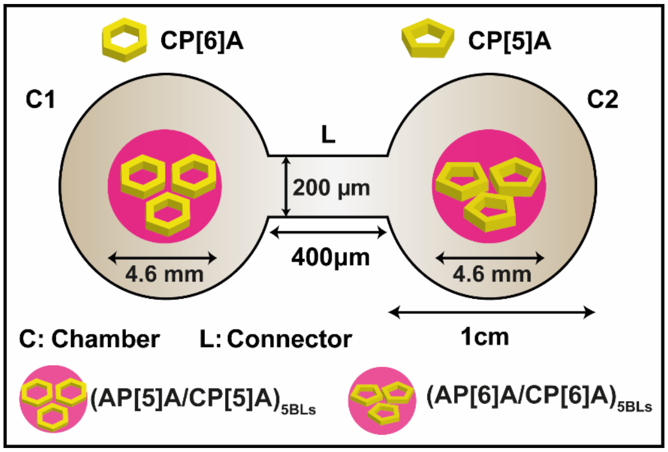

Figure 5.8. Schematic representation of a channel to demonstrate self-sorting over long distances.

In the fluid pumping experiment, mixture of (AP[5]A:AP[6]A) aqueous solution were prepared separately at three different ratios (1:0, 1:0.25 and 1:1 and vice versa) along with 5 µm sulphate functionalized polystyrene microbeads. The freshly prepared mixture of AP[5]A and AP[6]A were then injected into two separate chambers, and the flow pattern was examined under a microscope for further investigation. On injecting a mixture of AP[5]A and AP[6]A solution at two different ratios (AP[5]A:AP[6]A=1:0 and 1:0.25), an inward flow of tracer particles was observed from chamber C1 to chamber C2 via connector L towards the CP[5]A coating when viewed at the bottom layer of the chamber. While on injecting the reverse ratio (0:1 and 0.25:1) of the same solution (AP[5]A and AP[6]A) a reverse flow from C2 to C1 via L towards CP[6]A coating was observed. The tracer velocity was higher in case of 1:0 ratio than 1:0.25 for both experiments as shown in Table 5.1. The decrease in tracer velocity at a 1:0.25 ratio is because of the counter-effect of adding both pillar arenes in the same chamber, which results in a reduction in tracer velocity. The decrease in tracer velocity was observed as the distance from the reaction centre to the connector increased (Table 1). This spatial decrease in tracer velocity was caused by the reduction in solutal gradient on moving away from the source multilayer film. Further, on adding the solutions of AP[5]A and AP[6]A at a 1:1 ratio, no flow was observed in the chamber at both junctions. This is due to the cancellation effect of adding both pillar arenes at the same ratio.

Table 5.1. Tracer particles velocity at different junctions of microchannel.

Junction	**AP[5]A : AP[6]A Velocity (µm/s)**		**AP[6]A : AP[5]A Velocity (µm/s)**	
	1:0	**1:0.25**	**1:0**	**1:0.25**
C1-L	1.41±0.19	1.20±0.28	2.66±0.11	2.09±0.16
C2-L	2.16±0.21	1.85±0.17	1.90±0.12	1.29±0.12

5.3 Conclusions

We have successfully showed flow-based self-sorting of pillar[n]arenes utilising a concept of geometrical complementarity by shape. To develop the micropump, layer-by-layer (LbL) deposition method was used to construct a multilayer thin film comprised of anionic and cationic pillar[n]arenes. The multilayer films were employed as a platform for molecular recognition, and the resulting fluid flows were able to demonstrate the self-sorting of pillar[n]arenes.

5.4 Experimental Section

5.4.1 Reagents and Materials

Boron trifluoride diethyl etherate ($BF_3 \cdot (OC_2H_5)_2$, Branched polyethyleneimine (bPEI, 25kDa), methy viologen, ferrocene carboxylicacid and sulfate latex particles (5µm in diameter) were purchased from Sigma-Aldrich. 1,4-bis(2-hydroxyethoxy)benzene, paraformaldehyde, trimethylamine, were obtained from TCI chemicals. Acetonitrile, 1,2-dichloroethane, hexane, dichloromethane, chloroform, tetrahydrfuran, potassium carbonate, methanol, ethanol, dimethyl sulfoxide (DMSO), hydrochloric acid and sodium hydroxide were purchased from Merck. DC/GEN/184 SYLGARD (PDMS Elastomer KIT) was supplied by from Kevin Electrochem. Millipore water (18.2 MΩ•cm at 25°C) was used in all experiments.

5.4.2 Characterization

The chemical structures of all synthesized compounds were characterized by ^1H nuclear magnetic resonance (^1H NMR) spectra on a 400 MHz Bruker AvanceII, and D_2O, DMSO-d_6, $CDCl_3$ as the solvents. Isothermal Titration Calorimetric measurements were performed by Malvern MicroCal PEAQ-ITC. Videos were recorded using an inverted optical microscope (OLYMPUS IX73) with an X-Cite 120 LED Boost, via a 10X objective (CPLN10XPH), excitation light was focused on the sample. Emission light was captured by the objective, passed through interference filters and eventually recorded at 15 frames per second by a high resolution coloured cooled camera (DP74). Videos were recorded with DP74 camera connected to an optical microscope at 20X. To measure fluid-pumping velocity in each experiment, 20 tracer particles were tracked for a 30 second time interval using Tracker software (Motion Analysis Software).

5.4.3 Synthesis of Pillar[n]arenes

5.4.3.1 Synthesis of Cationic Pillar[5]arene (CP[5]A)

The cationic pillar[5]arene was synthesized according to the following reaction procedure (Figure 5.9).[30]

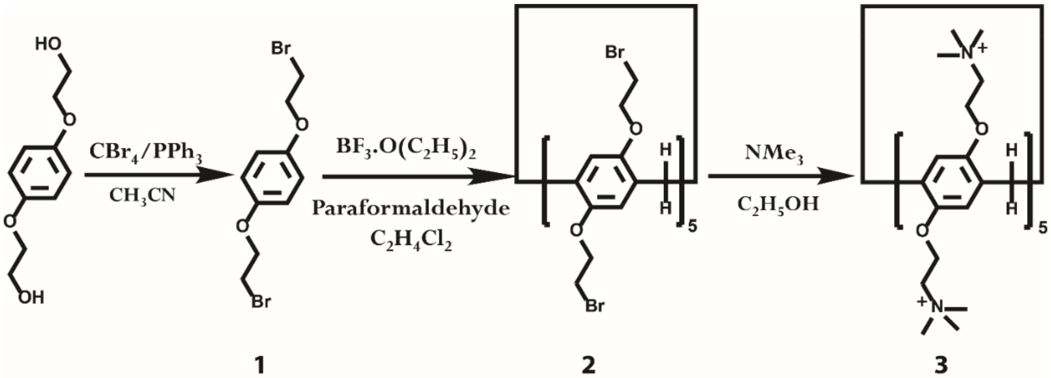

Figure 5.9. Synthesis of cationic pillar[5]arene (CP[5]A)

5.4.3.1.1 Synthesis of 1

Carbon tetrabromide (39.8 g, 120 mmol) was gradually added in minute amounts to a 300 mL dry acetonitrile solution containing 1,4-bis(2-hydroxyethoxy)benzene (10.0 g, 50.4 mmol) and triphenylphosphine (31.5 g, 120 mmol) at 0°C with stirring. The resulting solution was stirred for 4 hours under N_2 once the reaction mixture had cooled to room temperature. After 200 mL of cold water was added to the reaction mixture, product 1 precipitated as a white solid. The product was collected using vacuum filtration and then thoroughly cleaned in a 60:40 methanol/water solution before being recrystallized from methanol. The white flake-like crystals were dried using a high vacuum.

5.4.3.1.2 Synthesis of 2

Paraformaldehyde (0.698 g, 23 mmol) was added to a solution of 1 (6.74 g, 23 mmol) in 1, 2-dichloroethane (400 mL) under N_2 atmosphere. The solution was then stirred at room temperature for 3 hours with boron trifluoride diethyl etherate ($BF_3(OC_2H_5)_2$, 3.26 g, 23 mmol). A green product was prepared. The solvent was removed, and then the solid was purified by column chromatography on silica gel with hexane/dichloromethane (1:2 v/v) as the eluent, obtaining a white powder.

5.4.3.1.3 Synthesis of 3

Compound 3 (0.50 g, 0.298 mmol) and trimethylamine (33% in ethanol, 3.22 mL, 11.9 mmol) were added to ethanol (25 mL). Overnight, the mixture was refluxed. The solvent was then evaporated, and 10 mL of deionized water was added. Following filtering, a clear solution was recovered. The water was then entirely evaporated, yielding 3 as a colourless

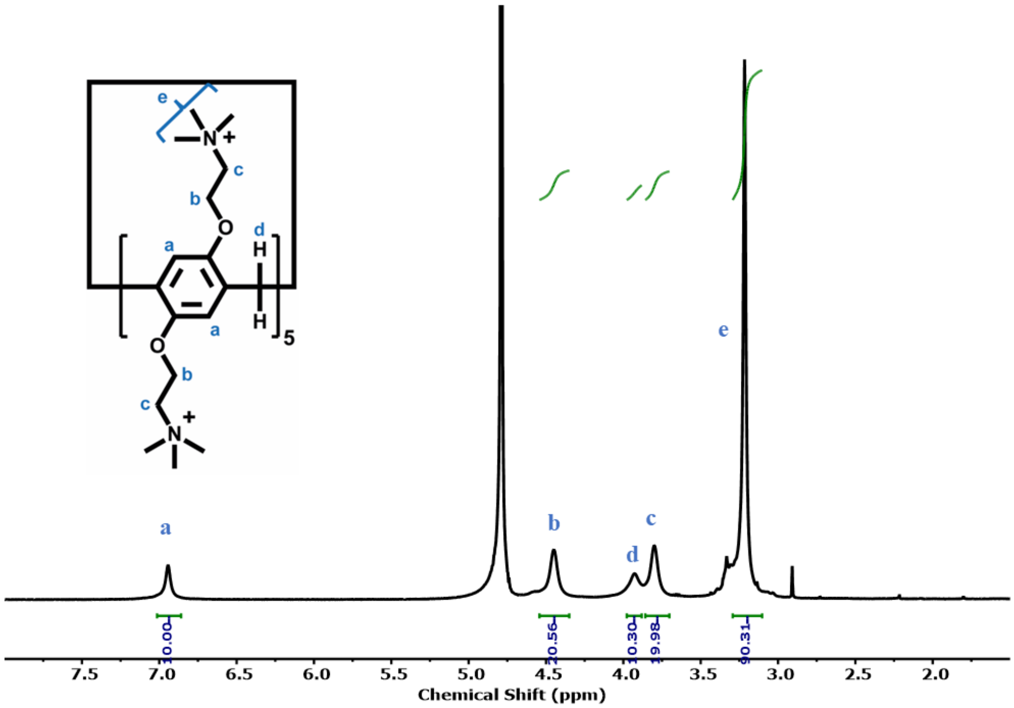

Figure 5.10. 400 MHz ^1H NMR spectra 3 in D_2O

solid (0.64 g, 95 percent). Figure 5.10 depicts the ^{1}H NMR spectrum of 3. ^{1}H NMR (400 MHz) δ (ppm): 6.94 (s, 10H), 4.44 (s, 20H), 3.93 (s, 10H), 3.80 (s, 20H), 3.22 (s, 90H).

5.4.3.2 Synthesis of Cationic Pillar[6]arene (CP[6]A)

The cationic pillar[6]arene was prepared using the following reaction procedure (Figure 5.11).[31]

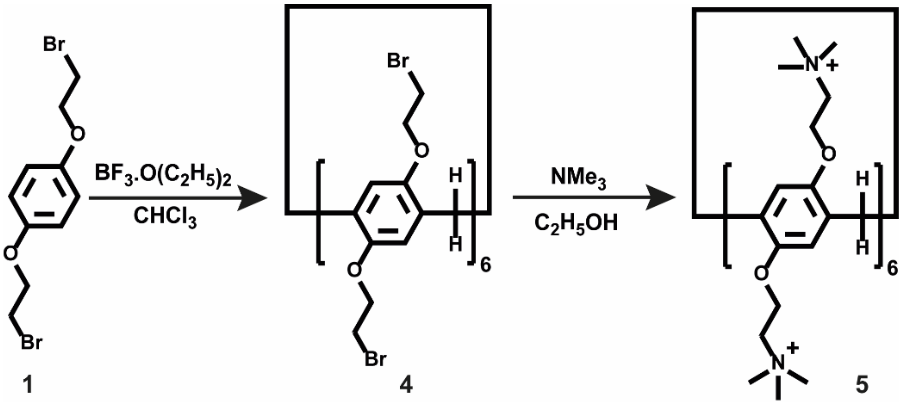

Figure 5.11. Synthesis of cationic pillar[6]arene (CP[6]A).

5.4.3.2.1 Synthesis of 4

Paraformaldehyde (0.698 g, 23 mmol) was added to a solution of 1 (6.74 g, 23 mmol) in 1, chloroform (400 mL) under N_2 atmosphere. The solution was then stirred at room temperature for 3 hours with boron trifluoride diethyl etherate ($BF_3(OC_2H_5)_2$, 3.26 g, 23 mmol). A green product was prepared. After the solvent was removed, the solid was purified by column chromatography on silica gel with hexane/dichloromethane (1:2 v/v) as the eluent, obtaining a white powder.

5.4.3.2.2 Synthesis of 5

Compound 4 (0.50 g, 0.298 mmol) and trimethylamine (33% in ethanol, 3.22 mL, 11.9 mmol) were added to ethanol (25 mL). Overnight, the mixture was refluxed. The solvent was then evaporated, and 20 mL of deionized water was added. Following filtering, a clear solution was recovered. The water was then entirely evaporated, yielding 3 as a colourless solid (0.64 g, 95 %). Figure 5.12 depicts the ^{1}H NMR spectrum of 5. ^{1}H NMR (400 MHz) δ (ppm): 6.94 (s, 12H), 4.54 (s, 24H), 3.97 (s, 12H), 3.78 (s, 24H), 3.24 (s, 108H).

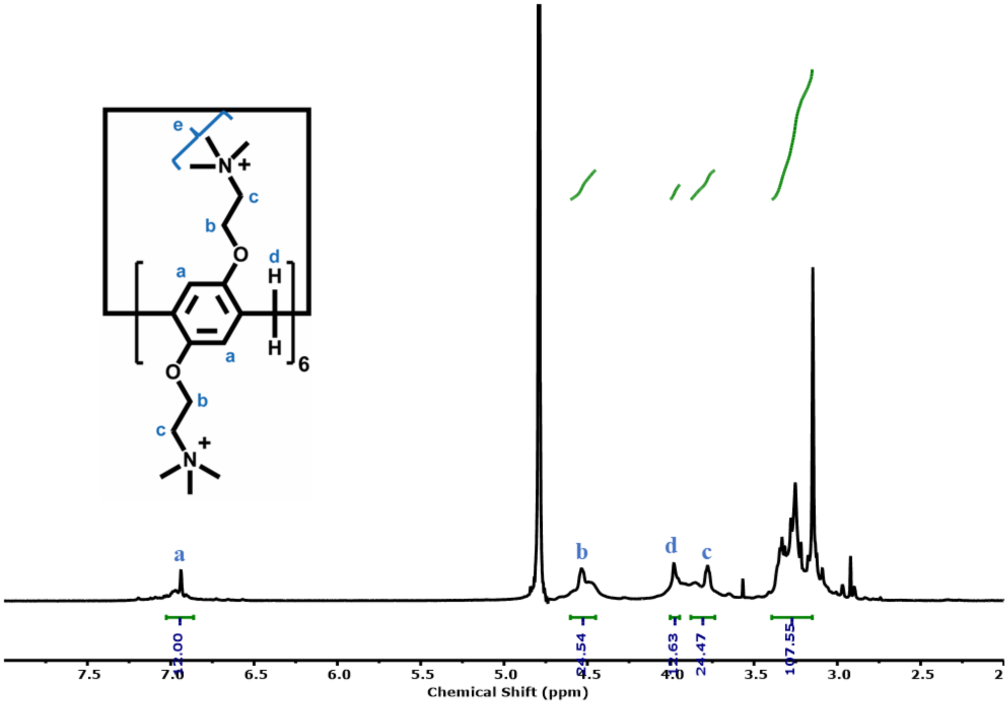

Figure 5.12. 400 MHz ^{1}H NMR spectra 5 in D_2O.

5.4.3.3 Synthesis of Anionic Pillar[5]arene (AP[5]A)

The anionic pillar[6]arene was prepared using the following reaction procedure (Figure 5.13).[32]

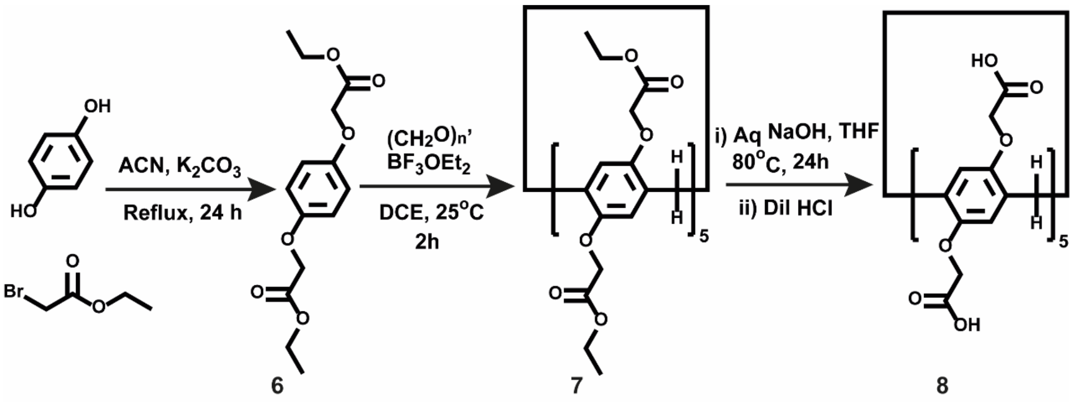

Figure 5.13. Synthesis of anionic pillar[5]arene (CP[5]A).

5.4.3.3.1 Synthesis of 6

Hydroquinone (5.5 g, 50 mmol) and ethyl bromoacetate (300 mmol) were dissolved in acetone (300 ml) under a nitrogen atmosphere, followed by the addition of K_2CO_3. The reaction mixture was refluxed for one day. The cooled reaction mixture was then filtered and washed with DCM. To get a white powder, the residue was purified using column chromatography on silica gel (hexane/ethyl acetate, 4:1).

5.4.3.3.2 Synthesis of 7

Paraformaldehyde was added to a solution of compound 6 (676 mg, 2 mmol) in 1,2 dichloroethane (10 mL) (186 mg, 6 mmol). The solution was then treated with 0.25 mL (2 mmol) boron trifluoride diethyletherate BF_3Et_2O and stirred at room temperature for 2 hours. After quenching with water, the organic layer was washed with water, saturated aqueous $NaHCO_3$ solution, and brine, dried over Na_2SO_4, and concentrated. The residue was purified by column chromatography on silica gel (hexane/ethyl acetate, 4:1→ 2:1) to yield a white powder.

5.4.3.3.3 Synthesis of 8

Compound 7 (0.30 g, 0.204 mmol), NaOH (0.60 g), ethanol (30 mL), water (30 mL), and THF (30 mL) were refluxed for 24 hours. Diluted aqueous HCl was added to the solution. Filtration was used to collect the precipitated solid. The solid was washed repeatedly with water and dried under reduced pressure. Figure 5.14 depicts the ^1H NMR spectrum of 8. ^1H NMR (400 MHz) δ (ppm): 6.67 (s, 10H), 4.23 (s, 20H), 3.93 (s, 10H).

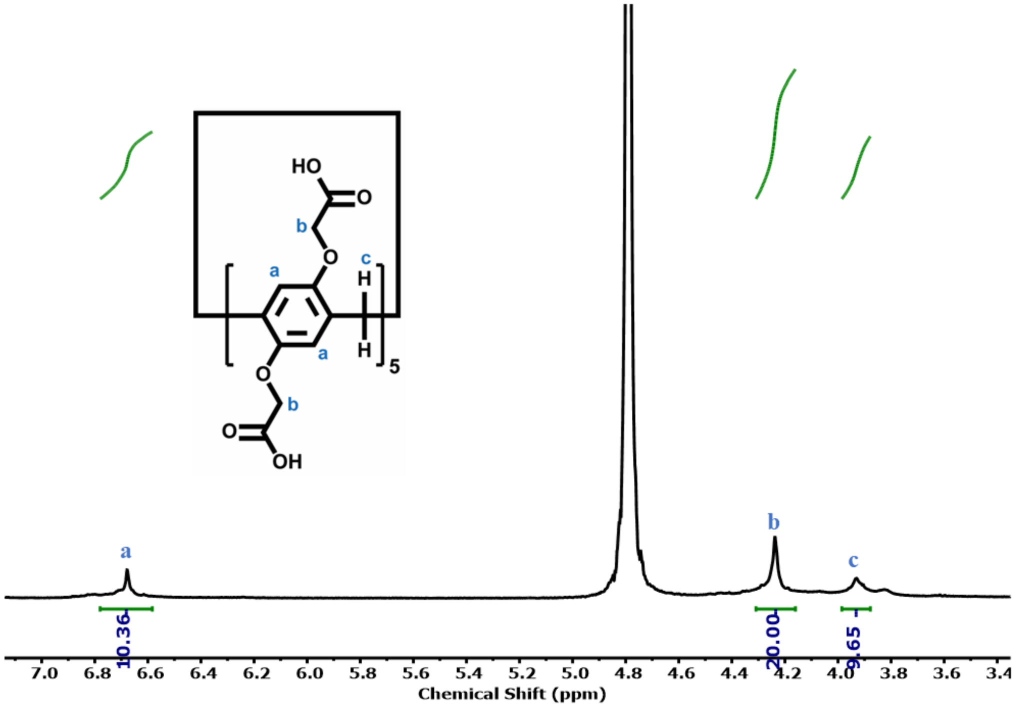

Figure 5.14. 400 MHz ^1H NMR spectra 8 in DMSO-d_6.

5.4.3.4 Synthesis of Anionic Pillar[6]arene (AP[6]A)

The anionic pillar[6]arene was prepared using the following reaction procedure (Figure 4.15).[33]

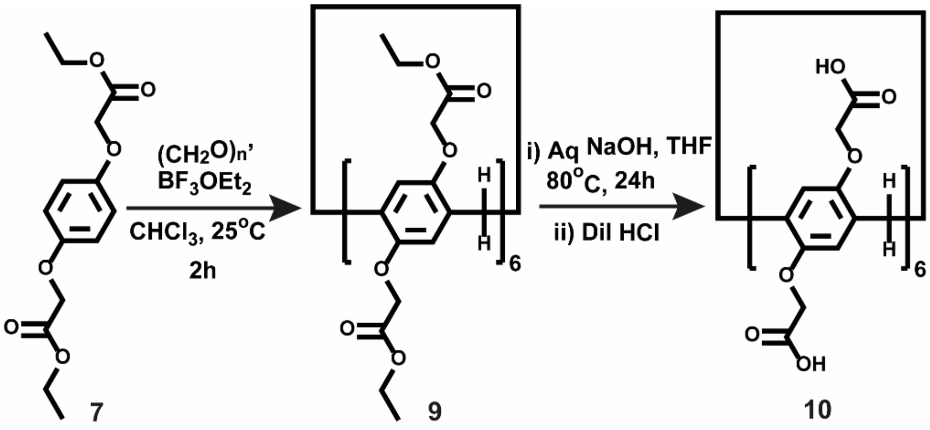

Figure 5.15. Synthesis of anionic pillar[6]arene (AP[6]A)

5.4.3.4.1 Synthesis of 9

Paraformaldehyde was added to a solution of compound 6 (676 mg, 2 mmol) in chloroform (10 mL) (186 mg, 6 mmol). The solution was then treated with 0.25 mL (2 mmol) boron trifluoride diethyletherate BF_3Et_2O and stirred at room temperature for 2 hours. After quenching with water, the organic layer was washed with water, saturated aqueous $NaHCO_3$ solution, and brine, dried over Na_2SO_4, and concentrated. The residue was purified by column chromatography on silica gel (hexane/ethyl acetate, 4:1→ 2:1) to yield a white powder.

5.4.3.4.2 Synthesis of 10

Compound 7 (0.30 g, 0.204 mmol), NaOH (0.60 g), ethanol (30 mL), water (30 mL), and THF (30 mL) were refluxed for 24 hours. Diluted aqueous HCl was added to the solution. Filtration was used to collect the precipitated solid. The solid was washed repeatedly with water and dried under reduced pressure. Figure 5.16 depicts the ^{1}H NMR spectrum of 10. ^{1}H NMR (400 MHz) δ (ppm): 7.60 (s, 10H), 4.86 (s, 12H, b), 4.41 (s, 12H, b'), 4.18 (s, 12H, c).

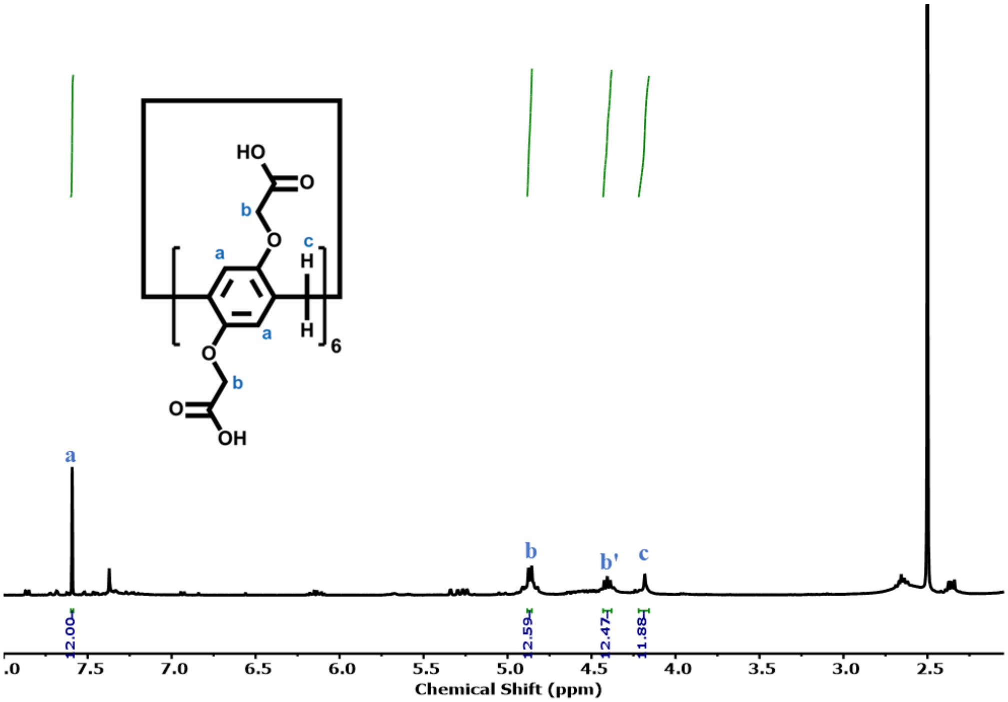

Figure 5.16. 400 MHz ^{1}H NMR spectra 10 in DMSO-d_6.

5.4.4 Substrate

The multilayer films were constructed using glass slides as a substrate. PDMS elastomer was made by blending Sylgard 184 in a 10:1 oligomeric base to curing agent weight ratio and casting onto a plastic Petri plate. Allow the prepolymer PDMS to settle for 2 hours in a convection oven set to 70 ° C. Before deposition, all glass slides were cleaned with piranha solution for 45 minutes and then washed with DI water. *Beware! Piranha solution reacts severely to organic materials and must be handled with caution.*

5.4.5 Multilayer Film Pattern and Fluid Flow Tracking

Initially, a thin layer of PDMS sheet with a 4.6mm diameter circular aperture in the centre was manufactured and deposited on the glass surface such that the circular opening remained in the middle of the slide. The same slide was utilised as a substrate for the desired number of cycles of LbL deposition. As LbL deposition resulted in conformal coating, the layer was applied to the whole slide. Following the formation of the desired bilayers, the PDMS sheet was peeled away to expose the film pattern, leaving the covered portion uncoated. The surface was properly cleansed with water before being blown with nitrogen gas. After that, an air-tight imaging chamber (r= 0.5 cm, h = 0.8 cm) was placed over the pattern, and an aqueous solution of substrates together with 5 m diameter neutral charged non-interacting polystyrene particles (tracer particles) was introduced into the chamber. The complete setup was observed using an optical microscope, and videos were recorded for later analysis in Tracker software. The flow velocity was determined by analysing the motion of tracer particles captured using digital cameras, which is the usual measuring approach in fluid dynamics research. In each experiment, 20 tracer particles were monitored for 30 seconds using Tracker software to measure fluid-pumping velocity.

5.5 References

1. D. Phlip, *Adv. Mater.*, 1996, **8**, 866–868.
2. I. P. Parkin, *Appl. Organomet. Chem.*, 2001, **15**, 236–236.
3. P. Mukhopadhyay, A. Wu and L. Isaacs, *J. Org. Chem.*, 2004, **69**, 6157–6164.
4. T. Ogoshi, S. Takashima and T. Yamagishi, *J. Am. Chem. Soc.*, 2015, **137**, 10962–10964.
5. X. Ji, M. Ahmed, L. Long, N. M. Khashab, F. Huang and J. L. Sessler, *Chem. Soc. Rev.*, 2019, **48**, 2682–2697.
6. G. Ju, Q. Zhang, F. Guo, P. Xie, M. Cheng and F. Shi, *J. Mater. Chem. B*, 2019, **7**, 1684–1689.
7. G. M. Whitesides, J. P. Mathias and C. T. Seto, *Science*, 1991, **254**, 1312–1319.
8. D. Philp and J. F. Stoddart, *Angew. Chem. Int. Ed.*, 1996, **35**, 1154–1196.
9. F. Diederich and P. J. Stang, *Templated Organic Synthesis*, Wiley-VCH, Weinheim/Germany, 2000.
10. A. Wu and L. Isaacs, *J. Am. Chem. Soc.*, 2003, **125**, 4831–4835.
11. M. L. Saha and M. Schmittel, *Org. Biomol. Chem.*, 2012, **10**, 4651–4684.
12. M. M. Safont-Sempere, G. Fernández and F. Würthner, *Chem. Rev.*, 2011, **111**, 5784–5814.
13. D. Kaizerman-Kane, M. Hadar, E. Granot, F. Patolsky, Y. Zafrani and Y. Cohen, *Org. Chem. Front.*, 2019, **6**, 3348–3354.
14. Z. Zhang, Y. Liu, J. Zhao and X. Yan, *Polym. Chem.*, 2020, **11**, 367–374.
15. D. Voet and J. G. Voet, *Biochemistry*, Wiley, New York, 1995
16. W. Jiang and C. A. Schalley, *Proc. Natl. Acad. Sci. U.S.A.*, 2009, **106**, 10425–10429.
17. Lubert Stryer, *Biochemistry (4th edition)*, W H Freeman & Co (Sd), New York, 1998.
18. H. Shigemitsu, T. Fujisaku, W. Tanaka, R. Kubota, S. Minami, K. Urayama and I. Hamachi, *Nat. Nanotechnol.*, 2018, **13**, 165–172.
19. J. R. Nitschke, *Acc. Chem. Res.*, 2007, **40**, 103–112.

20. R. K. Manna, K. Gentile, O. E. Shklyaev, A. Sen and A. C. Balazs, *Langmuir*, 2022, **38**, 1432–1439.

21. M. Alam, A. K. Gill, R. Varshney, C. Miglani, N. Tiwari and D. Patra, *Soft Matter*, 2022, **18**, 5605–5614.

22. M. Alam, R. Varshney, C. Agashe, A. K. Gill and D. Patra, *Chem. Commun.*, 2021, **57**, 4584–4587.

23. C. Agashe, M. Alam, A. K. Gill, R. Varshney, R. Joseph, N. Tiwari and D. Patra, *ChemNanoMat*, e202200277.

24. T. Ogoshi, S. Kanai, S. Fujinami, T. Yamagishi and Y. Nakamoto, *J Am Chem Soc*, 2008, **130**, 5022–5023.

25. T. Ogoshi, K. Saito, R. Sueto, R. Kojima, Y. Hamada, S. Akine, A. M. P. Moeljadi, H. Hirao, T. Kakuta and T.-A. Yamagishi, *Angew. Chem. Int. Ed. Engl.*, 2018, **57**, 1592–1595.

26. T. Kakuta, T.-A. Yamagishi and T. Ogoshi, *Acc Chem Res*, 2018, **51**, 1656–1666.

27. H. Zhang, Z. Liu and Y. Zhao, *Chem Soc Rev*, 2018, **47**, 5491–5528.

28. R. Varshney, M. Alam, C. Agashe, R. Joseph and D. Patra, *Chem. Commun.*, 2020, **56**, 9284–9287.

29. J. Wan, Polymers, 2012, 4, 1084–1108.

30. Y. Ma, X. Ji, F. Xiang, X. Chi, C. Han, J. He, Z. Abliz, W. Chen and F. Huang, *Chem. Commun. (Camb)*, 2011, **47**, 12340–12342.

31. G. Yu, J. Zhou, J. Shen, G. Tang and F. Huang, *Chem. Sci.*, 2016, **7**, 4073–4078.

32. T. Ogoshi, M. Hashizume, T. Yamagishi and Y. Nakamoto, *Chem Commun. (Camb)*, 2010, **46**, 3708–3710.

33. G. Yu, M. Xue, Z. Zhang, J. Li, C. Han and F. Huang, *J. Am. Chem. Soc.*, 2012, **134**, 13248–13251.

List of Publications

Included in thesis

1. **M. Alam**, R. Varshney, C. Agashe, A. K. Gill and D. Patra, Valveless flow reversal by a pH responsive supramolecular micropump, *Chem. Commun*., 2021, **57**, 4584-4587.
2. **M. Alam**, A. K. Gill, R. Varshney, C. Miglani, and D. Patra, Polymer multilayer films regulate macroscopic fluid flow and power microfluidic devices *via* supramolecular interactions, *Soft Matter,* 2022, **18**, 5605-5614.
3. **M. Alam**, C. Agashe, A. K. Gill, R. Varshney, N. Tiwari and D. Patra, Discrimination of enantiomers and constitutional isomers by self-generated macroscopic fluid flow, *Chem. Commun.,* 2023, **59**, 434-437.
4. **M. Alam**, R. Sangwan, A. K. Gill, C. Agashe and D. Patra, Cavity Shape Dependent Self-Sorting of Pillar[n]arenes via Macroscopic Fluid Flow *(submitted).*

Not a part of the thesis

1. A. K. Gill, S. Riyajuddin, **M. Alam**, K. Ghosh and D. Patra, Mussel-inspired UV protective organic coatings via layer-by-layer assembly, *Eur. Polym. J. 2020*, **124**, 109455.
2. R. Varshney, **M. Alam**, C. Agashe, R. Joseph and D. Patra, Pillar[5]arene microcapsules turn on fluid flow in the presence of paraquat, *Chem. Commun*., 2020, **56**, 9284-9287.
3. R. Varshney, A. K. Gill, **M. Alam**, C. Agashe and D. Patra, Fluid actuation and buoyancy driven oscillation by enzyme immobilized microfluidic microcapsules, *Lab on a chip*, 2021, **21**, 4352-4356.
4. R. Varshney, C. Agashe, A. K. Gill, **M. Alam**, R. Joseph and D. Patra, Modulation of liquid structure and controlling molecular diffusion using supramolecular constructs, *Chem. Commun*., 2021, **57**, 10604-10607.
5. A. K. Gill, R. Varshney, **M. Alam**, C. Agashe and D. Patra, Maneuvering fluid motion and flow-induced detection of toxins by enzyme multilayer films, *ACS Appl. Bio Mater*., 2021, **8**, 6203-6208.
6. C. Agashe, R. Varshney, R. Sangwan, A.K. Gill, **M. Alam** and D. Patra, Anisotropic compartmentalization of the liquid–liquid interface using dynamic imine chemistry, *Langmuir.,* 2022, **27**, 8296–8303.

7. C. Agashe, **M. Alam**, A.K. Gill, R. Varshney, R. Joseph, N. Tiwari and D. Patra, Flow-based detection of micropollutants using Pillar[5]arene multilayer film, *ChemNanoMat.,* 2022.

Workshop and Conferences Attended

1. Oral presentation on “Macroscopic Fluid-Flow Based on Molecular Recognition”, *2nd Research Scholar Day*, 31th March – 1st April, 2022, Institute of Nano Science and Technology, Mohali Punjab, India.
2. Oral presentation on "Flow Reversal in pH Responsive Self-powered Supramolecular Micropump” *International e-Conference on Recent Advancements in Chemical Sciences: Health, Environment and Society (ICRACS-2022)* 8th – 9th April 2022, Department of Chemistry, Deshbandhu College, University of Delhi, Delhi, India.
3. Poster presentation on “Polymer Multilayer Films Trigger Autonomous Fluid-Flow and Power Microfluidic Device” *International Conference on Nanotechnology for Better Living (NBL-2021),* 7th – 11th November, 2021, Department of Physics, National Institute of Technology, Srinagar, Kashmir, India.
4. Participated in *International Conference on Chemical Science for Drug Discovery and Therapy (CSDDT-2020),* 22th – 26th July, 2020, Department of Chemistry, VNIT Nagpur, India.

Permissions from Journals for reuse of content in Thesis

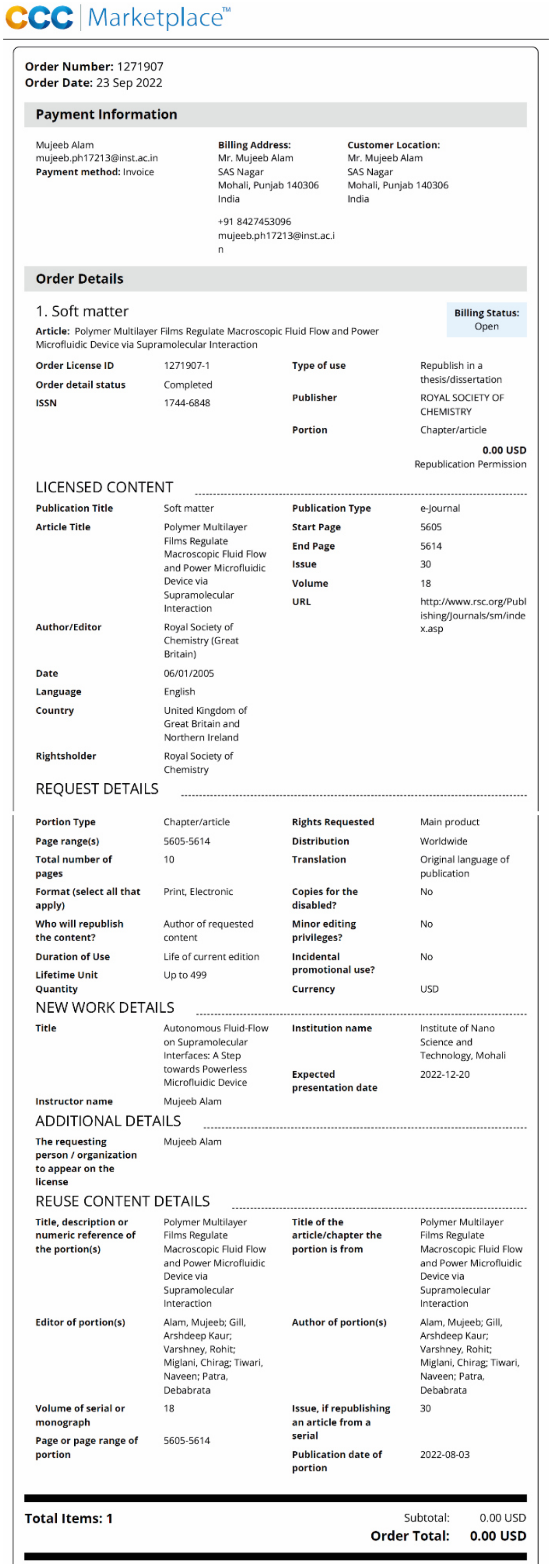

Order Number: 1271907
Order Date: 23 Sep 2022

Payment Information

Mujeeb Alam mujeeb.ph17213@inst.ac.in **Payment method:** Invoice	**Billing Address:** Mr. Mujeeb Alam SAS Nagar Mohali, Punjab 140306 India +91 8427453096 mujeeb.ph17213@inst.ac.in	**Customer Location:** Mr. Mujeeb Alam SAS Nagar Mohali, Punjab 140306 India

Order Details

1. Soft matter

Article: Polymer Multilayer Films Regulate Macroscopic Fluid Flow and Power Microfluidic Device via Supramolecular Interaction

Billing Status: Open

Order License ID	1271907-1	**Type of use**	Republish in a thesis/dissertation
Order detail status	Completed	**Publisher**	ROYAL SOCIETY OF CHEMISTRY
ISSN	1744-6848	**Portion**	Chapter/article

0.00 USD
Republication Permission

LICENSED CONTENT

Publication Title	Soft matter	**Publication Type**	e-Journal
Article Title	Polymer Multilayer Films Regulate Macroscopic Fluid Flow and Power Microfluidic Device via Supramolecular Interaction	**Start Page**	5605
		End Page	5614
		Issue	30
		Volume	18
		URL	http://www.rsc.org/Publishing/Journals/sm/index.asp
Author/Editor	Royal Society of Chemistry (Great Britain)		
Date	06/01/2005		
Language	English		
Country	United Kingdom of Great Britain and Northern Ireland		
Rightsholder	Royal Society of Chemistry		

REQUEST DETAILS

Portion Type	Chapter/article	**Rights Requested**	Main product
Page range(s)	5605-5614	**Distribution**	Worldwide
Total number of pages	10	**Translation**	Original language of publication
Format (select all that apply)	Print, Electronic	**Copies for the disabled?**	No
Who will republish the content?	Author of requested content	**Minor editing privileges?**	No
Duration of Use	Life of current edition	**Incidental promotional use?**	No
Lifetime Unit Quantity	Up to 499	**Currency**	USD

NEW WORK DETAILS

Title	Autonomous Fluid-Flow on Supramolecular Interfaces: A Step towards Powerless Microfluidic Device	**Institution name**	Institute of Nano Science and Technology, Mohali
		Expected presentation date	2022-12-20
Instructor name	Mujeeb Alam		

ADDITIONAL DETAILS

The requesting person / organization to appear on the license	Mujeeb Alam

REUSE CONTENT DETAILS

Title, description or numeric reference of the portion(s)	Polymer Multilayer Films Regulate Macroscopic Fluid Flow and Power Microfluidic Device via Supramolecular Interaction	**Title of the article/chapter the portion is from**	Polymer Multilayer Films Regulate Macroscopic Fluid Flow and Power Microfluidic Device via Supramolecular Interaction
Editor of portion(s)	Alam, Mujeeb; Gill, Arshdeep Kaur; Varshney, Rohit; Miglani, Chirag; Tiwari, Naveen; Patra, Debabrata	**Author of portion(s)**	Alam, Mujeeb; Gill, Arshdeep Kaur; Varshney, Rohit; Miglani, Chirag; Tiwari, Naveen; Patra, Debabrata
Volume of serial or monograph	18	**Issue, if republishing an article from a serial**	30
Page or page range of portion	5605-5614	**Publication date of portion**	2022-08-03

Total Items: 1

Subtotal: 0.00 USD
Order Total: 0.00 USD

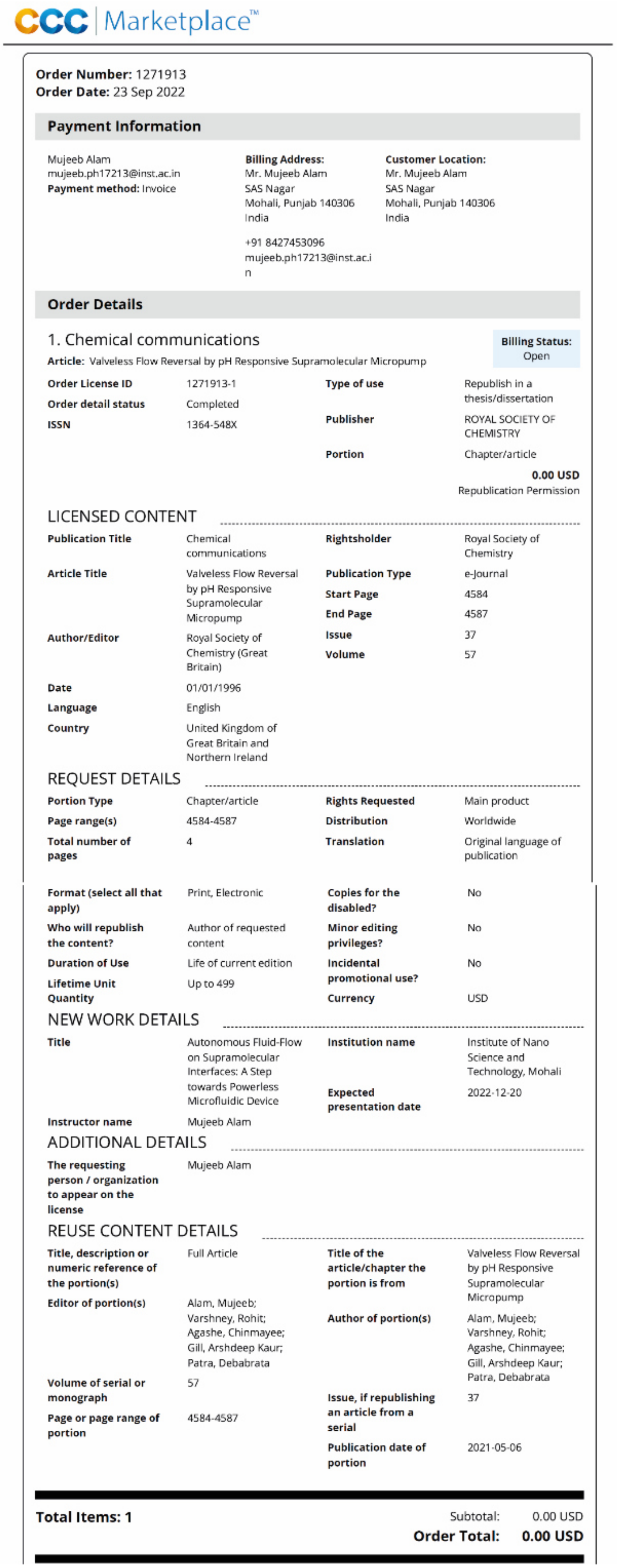

Order Number: 1271913
Order Date: 23 Sep 2022

Payment Information

Mujeeb Alam mujeeb.ph17213@inst.ac.in **Payment method:** Invoice	**Billing Address:** Mr. Mujeeb Alam SAS Nagar Mohali, Punjab 140306 India +91 8427453096 mujeeb.ph17213@inst.ac.in	**Customer Location:** Mr. Mujeeb Alam SAS Nagar Mohali, Punjab 140306 India

Order Details

1. Chemical communications

Billing Status: Open

Article: Valveless Flow Reversal by pH Responsive Supramolecular Micropump

Order License ID	1271913-1	**Type of use**	Republish in a thesis/dissertation
Order detail status	Completed	**Publisher**	ROYAL SOCIETY OF CHEMISTRY
ISSN	1364-548X	**Portion**	Chapter/article

0.00 USD
Republication Permission

LICENSED CONTENT

Publication Title	Chemical communications	**Rightsholder**	Royal Society of Chemistry
Article Title	Valveless Flow Reversal by pH Responsive Supramolecular Micropump	**Publication Type**	e-Journal
		Start Page	4584
		End Page	4587
Author/Editor	Royal Society of Chemistry (Great Britain)	**Issue**	37
		Volume	57
Date	01/01/1996		
Language	English		
Country	United Kingdom of Great Britain and Northern Ireland		

REQUEST DETAILS

Portion Type	Chapter/article	**Rights Requested**	Main product
Page range(s)	4584-4587	**Distribution**	Worldwide
Total number of pages	4	**Translation**	Original language of publication
Format (select all that apply)	Print, Electronic	**Copies for the disabled?**	No
Who will republish the content?	Author of requested content	**Minor editing privileges?**	No
Duration of Use	Life of current edition	**Incidental promotional use?**	No
Lifetime Unit Quantity	Up to 499	**Currency**	USD

NEW WORK DETAILS

Title	Autonomous Fluid-Flow on Supramolecular Interfaces: A Step towards Powerless Microfluidic Device	**Institution name**	Institute of Nano Science and Technology, Mohali
		Expected presentation date	2022-12-20
Instructor name	Mujeeb Alam		

ADDITIONAL DETAILS

The requesting person / organization to appear on the license	Mujeeb Alam

REUSE CONTENT DETAILS

Title, description or numeric reference of the portion(s)	Full Article	**Title of the article/chapter the portion is from**	Valveless Flow Reversal by pH Responsive Supramolecular Micropump
Editor of portion(s)	Alam, Mujeeb; Varshney, Rohit; Agashe, Chinmayee; Gill, Arshdeep Kaur; Patra, Debabrata	**Author of portion(s)**	Alam, Mujeeb; Varshney, Rohit; Agashe, Chinmayee; Gill, Arshdeep Kaur; Patra, Debabrata
Volume of serial or monograph	57	**Issue, if republishing an article from a serial**	37
Page or page range of portion	4584-4587	**Publication date of portion**	2021-05-06

Total Items: 1

Subtotal: 0.00 USD
Order Total: 0.00 USD